Genetic and Phenotypic characterisation of a novel *Efl1* mutant mouse model of Shwachman Diamond Syndrome





Angela Hoslin (BSc)

Department of Biochemistry, Wolfson College

Mammalian Genetics Unit, Medical Research Council, Harwell

A thesis submitted for the degree of Doctor of Philosophy

October 2016

Declaration

I, Angela Hoslin confirm that the work presented in this thesis is my own. Where information has been derived from other sources, I confirm that this has been indicated in the thesis.

Abstract

A novel mouse mutant was identified through an ENU (*N*-ethyl-*N*-nitrosourea) mutagenesis screen due to an abnormal gait. Next generation sequencing revealed the causative mutation to be in the gene *Efl1* (K983R). The protein EFL1 is involved in ribosome maturation, a cellular process that is defective in diseases collectively known as ribosomopathies. More specifically, EFL1 is critical for the release of anti-association factor eIF6 from the 60S subunit, which allows subsequent joining with the 40S subunit to form a translationally active particle. Shwachman-Diamond syndrome (SDS) is a ribosomopathy in which this process is known to be defective.

SDS is an autosomal recessive disorder typified by bone marrow failure, pancreatic insufficiency and various anaemias. 90% of patients with SDS have missense mutations in the gene *SBDS.* The protein SBDS, together with EFL1, binds to the 60S subunit and causes the release of the anti-association factor eIF6. Both SBDS and EFL1 are needed for this process to occur correctly. In patients with SDS, eIF6 release is impaired due to a deficiency of functional SBDS, thus causing a ribosomal joining defect. Current research into SDS focuses on yeast models or conditional knockout/embryonic mouse models. However, this gives a limited view of the disorder as it does not reflect the multi-system nature or temporal aspects of SDS.

In depth phenotypic characterisation of the *Efl1*-K983R mouse-line has revealed many phenotypes that reflect human SDS symptoms, such as small size, various haematological abnormalities, reduced bone mass density, deafness secondary to otitis media and behavioural deviations. At the molecular level, impaired eIF6 release has been demonstrated in mouse embryonic fibroblasts and liver. Multiple tissues from mutant mice show severe EFL-1 deficiency, suggesting that these symptoms may be reflective of the SBDS deficiency seen in SDS patients. Approximately 10% of SDS patients do not have *SBDS* mutations, and these patients are referred to as having 'genetically undefined' SDS. The cause of patients symptoms in these cases are unclear, and no causative gene has been found.

Here we present data that suggests that *Efl1* may be a candidate gene for 'genetically undefined' SDS. The data presented here also suggests that this mouse represents an opportunity to study SDS-like processes in a long lived, multi-system mammalian model, which is otherwise unavailable for *Sbds* mutants.

Acknowledgements

A large number of people have contributed to the work undertaken during my DPhil. Firstly I would like to thank Abraham Acevedo-Arozena for welcoming me into his group and for his unceasing help and patience with my project, and for the many interesting discussions about *Efl1*, Shwachman Diamond Syndrome, and ribosomopathies in general.

I am grateful to all members of my lab, both past and present. In particular I would like to thank Silvia Corrochano who taught me many lab techniques. I would also like to thank Michelle Stewart for all her help and advice regarding mouse phenotyping and breeding.

The core services of MRC Harwell have been very helpful and I would like to acknowledge Chris Esapa and Helen Hilton of proteomics, everyone in the genotyping service, especially Debbie Williams and Anne Southwell, Jeremy Sanderson from microscopy, and everyone in the histology team.

All mice were housed in the Mary Lyon Centre and I am grateful to the entire staff in ward 6, in particular Michelle Stewart, Elizabeth Joynson and Jackie Harrison for looking after the mice and being available to help me at my request. Their patience and hard work has been crucial to the work presented in this thesis.

I would also like to give a big thanks to Alan Warren and all of his lab, particularly Felix Weis, in Cambridge at the CIMR. They taught me the technique of polysome profiling, allowed me to use their equipment and consumables, and also allowed me to visit again and again to repeat experiments.

I would also like to thank Kelvin Cain and Carolyn Jones of the MRC Toxicology Unit in Leicester, for helping me with the liver polysome profiling. Carolyn in particular was dedicated to helping me and I am very grateful for her hard work and efficiency in this work.

I would lastly like to thanks the Medical Research Council and the University of Oxford for generous funding.

Contents

Declaration ii

Abstract iii

Acknowledgements iv

Contents v

Figures xii

List of Abbreviations xvi

1. Introduction 2

1.1. ENU mutagenesis 2

1.1.1. Model organisms in genetic research 2

1.1.2. The molecular mechanism of ENU mutagenesis 4

1.1.3. ENU treatment and breeding strategies 6

1.1.4. Phenotypic screens 10

1.1.5. The Harwell Ageing Screen 10

1.2. The ribosome structure and function 13

1.2.1. Ribosome structure 13

1.2.2. The ribosome in translation 16

1.2.2.1. Initiation 16

1.2.2.2. Elongation 19

1.2.2.3. Termination 22

1.3. Ribosomal maturation 23

1.3.1. Nucleolar ribosome biogenesis and nuclear export 23

1.3.2. Cytoplasmic maturation of the 40S subunit 26

1.3.3. Cytoplasmic maturation of the 60S subunit 27

1.3.4. Mechanism of release of eIF6 (Tif6) from the pre-60S subunit 30

1.3.5. Energy consumption in ribosome biogenesis 35

1.4. Ribosomopathies 37
1.4.1. Diamond-Blackfan Anaemia and 5q syndrome 39
1.4.2. Treacher Collins Syndrome 40
1.4.3. Dyskerotosis Congenita 41
1.4.4. Cartilage Hair Hypoplasia 41
1.4.5. Roberts Syndrome 42
1.4.6. Shwachman-Diamond Syndrome 42
1.4.7. Other ribosomopathies 44
1.4.8. The genetics of Shwachman-Diamond Syndrome 44
1.4.8.1. Class A mutations: Protein stability 44
1.4.8.2. Class B mutations: Surface epitopes and interactivity 45
1.4.9. SDS model systems 47
1.4.9.1. Yeast and *D. discoidium* models 47
1.4.9.2. Conditional Knockout and Embryonic Mouse Models 48
1.4.9.3. Haematopoietic Stem Cells 49
1.4.9.4. SDS patients 50
1.4.10. Proposed mechanism underlying ribosomopathies 50
1.4.10.1. Differential mRNA translation 50
1.4.10.2. p53 in ribosomopathies 51
1.4.10.3. Ribosomal dysfunction and cancer 53
1.5. EFL1 biology 56
1.5.1. GTPase biology 56
1.5.2. EFL1 structure and function 58
1.5.3. Modelling *Efl1* mutations in the mouse 61
1.6. Aims of the thesis 62
2. Materials and Methods 64
2.1. Mouse generation and mutation discovery 64
2.1.1. Mouse generation 64

2.1.2. Mutation discovery 65
2.1.3. Rederivation of the *Efl-1*K98R mouse line 66
2.1.4. Mouse genotyping 66
2.2. Phenotyping 67
2.2.1. License 67
2.2.2. SHIRPA (SmithKline Beecham, Harwell, Imperial College and Royal London Hospital Phenotype Assessment 68
2.2.3. Social Dominance test 69
2.2.4. Resident Intruder Test 69
2.2.5. Crack-it home cage video tracking 70
2.2.6. Intraperitoneal Glucose Tolerance Test (IPGTT) 72
2.2.7. Dual-energy X-ray Absorptiometry 73
2.2.8. Locotronic 73
2.2.9. Grip Strength 73
2.2.10. Wheel running activity cages 74
2.2.11. Open Field 74
2.2.12. Auditory Brainstem Response 74
2.2.13. Contextual and cued fear conditioning 76
2.2.14. Novel Object Test 77
2.2.15. Y-Maze spontaneous alternation test 78
2.2.16. Acoustic Startle Response and Pre-Pulse Inhibition (PPI) test 79
2.2.17. Haematological analysis 80
2.3. Histological staining 81
2.3.1. Muscle pathology 81
2.3.2. p21 Immunostaining of tibiae 81
2.3.3. Oil Red O staining of pancreas 81
2.3.4. H&E staining of middle ear sections 81
2.4. Cell culture and cell-based assays 82

2.4.1. Mouse Embryonic Fibroblast Culture 82
2.4.2. Mouse embryonic fibroblast freezing 82
2.4.3. Mouse Embryonic Fibroblast Growth Assay 82
2.4.4. Bradford Assay 83
2.4.5. Western Blot Analysis in Mouse Embryonic Fibroblasts 83
2.4.6. Quantitative PCR in Mouse Embryonic Fibroblasts 84
2.5. Translation Assays 85
2.5.1. Radioactive Methionine Assay in mouse embryonic fibroblasts 85
2.5.2. SUnSET western blot analysis in mouse embryonic fibroblasts 86
2.6. Polysome Profile Analysis 86
2.6.1. Polysome profiles in Mouse Embryonic Fibroblasts 86
2.6.2. Polysome profiles in liver 87
2.6.3. Quantitative PCR in liver polysome fractions 87
3. Genetic characterisation of the *Efl1*-K983R mouse line 90
3.1. Positional cloning of mouse chromosome seven 90
3.2. Identification of causative mutation via Next-generation sequencing 92
3.3. Validation of Next-generation sequencing 93
3.4. Possible functional consequences of the *Efl1*-K983R mutation 97
4. Phenotypic characterisation of the *Efl1* K983R mouse line 100
4.1. Longevity and Viability 100
4.1.1. Life span is not affected by the *Efl1* K983R mutation 100
4.1.2. *Efl1*$^{K983R/K983R}$ mice are smaller and weigh significantly less than littermates 104
4.1.3. Pancreatic structure is normal in *Efl1*$^{K983R/K983R}$ mice 109
4.1.4. Glucose tolerance is unimpaired in *Efl1*$^{K983R/K983R}$ mice 111
4.1.5. Longevity and viability conclusions 111
4.2. Gait abnormality and motor impairment 113
4.2.1. Gait abnormalities are present in *Efl1*$^{K983R/K983R}$ mice 113
4.2.2. *Efl1*$^{K983R/K983R}$ mice show increased rear leg errors in locotronic tests 115

4.2.3. *Efl1*$^{K983R/K983R}$ mice display weaker grip strength 117
4.2.4. Muscle histology is normal in *Efl1*$^{K983R/K983R}$ mice 119
4.2.5. *Efl1*$^{K983R/K983R}$ mice display reduced activity on running wheels 121
4.2.6. Open field activity in *Efl1*$^{K983R/K983R}$ mice is normal 123
4.2.7. Gait and motor conclusions 125
5. Behavioural Phenotyping 128
5.1. Behavioural phenotyping 128
5.1.1. Social and behavioural abnormalities are present in *Efl1*$^{K983R/K983R}$ mice 128
5.1.2. Balance issues were present in *Efl1*$^{K983R/K983R}$ mice 131
5.1.3. Startle reflex and pre-pulse inhibition is unimpaired in *Efl1*$^{K983R/K983R}$ mice 132
5.1.4. Behavioural conclusions 135
5.2. Learning and memory 136
5.2.1. *Efl1*$^{K983R/K983R}$ mice show contextual fear conditioning defect 136
5.2.2. *Efl1*$^{K983R/K983R}$ mice show an attention deficit in novel object recognition 140
5.2.3. *Efl1*$^{K983R/K983R}$ mice display abnormal Y maze behaviour 141
5.2.4. Learning and memory conclusions 144
5.3. Deafness and Otitis Media 145
5.3.1. *Efl1*$^{K983R/K983R}$ mice display elevated hearing thresholds 145
5.3.2. *Efl1*$^{K983R/K983R}$ mice have otitis media 145
6. Bone and Haematological Characterisation 151
6.1. Bone and Haematological Abnormalities 151
6.1.1. *Efl1*$^{K983R/K983R}$ mice show features of macrocytic anaemia 151
6.1.2. *Efl1*$^{K983R/K983R}$ mice show features of thrombocytopenia 152
6.1.3. *Efl1*$^{K983R/K983R}$ mice have white blood cell variations 155
6.2. Bone Abnormalities 159
6.2.1. *Efl1*$^{K983R/K983R}$ mice have lower bone mass density 159
6.2.2. Bone cellularity appears normal in *Efl1*$^{K983R/K983R}$ mice 163
6.2.3. Bone and Haematological conclusions 164

7. In vitro characterisation of the *Efl1*-K983R mutation 167

7.1. Molecular pathways in the *Efl1*-K983R mouse line 167

7.1.1. EFL1 protein levels are dramatically reduced in *Efl1*$^{K983R/K983R}$ mice 167

7.1.1. EFL1 transcript levels are unaffected by the *Efl1*-K983R mutation 172

7.1.2. p53 signalling is unaffected by the *Efl1*-K983R mutation 174

7.1.3. mTOR signalling is unaffected by the *Efl1*-K983R mutation 176

7.1.4. *In vitro* characterisation conclusions 179

7.2. Ribosome biogenesis and translation in *Efl1*-K983R mutants 180

7.2.1. Growth is reduced in *Efl1*$^{K983R/K983R}$ in mouse embryonic fibroblast 180

7.2.2. Mouse embryonic fibroblast polysome profiles indicate defective eIF6 release and subunit joining defect 181

7.2.3. eIF6 accumulates in the cytoplasm in *Efl1*$^{K983R/K983R}$ mouse embryonic fibroblasts 184

7.2.4. Liver polysome profiles show mislocalisation of eIF6 in the cytoplasm 186

7.2.5. Translation is unaffected by the *Efl1*-K983R mutation in MEFs..... 188

7.2.6. Ribosome biogenesis conclusions 191

8. Discussion 194

8.1. The relevance of *Efl1*$^{K983R/K983R}$ for EFL1 function 194

8.2. The relevance of *Efl1*$^{K983R/K983R}$ for SDS 197

8.3. The relevance of *Efl1*$^{K983R/K983R}$ for studying cognitive symptoms in SDS patients 202

8.4. The effects of the *Efl1*-K983R mutation on translation 203

8.5. *Efl1* could be candidate for genetically undefined SDS 206

8.6. EFL1 and ribosome biogenesis in cancer 207

8.7. p53 signalling in ribosomopathies and the *Efl1*$^{K983R/K983R}$ mice 209

8.8. The ribosomopathy phenomenon: tissue-specific disease from a universal process 210

8.9. Concluding remarks 212

8.10. Future work 216

Bibliography 218

List of Figures

Figure 1 Diagram of the breeding scheme for an ENU-driven G1 screen for dominant mutations. 8
Figure 2 Diagram of the breeding scheme for an ENU-driven G3 recessive screen. 9
Figure 3 Crystal structures of the *Thermus thermophillus* 70S ribosome. 14
Figure 4 Pathway of translation initiation in eukaryotes. 18
Figure 5 Schematic of translating an mRNA molecule. 21
Figure 6 Schematic of the eukaryotic translation elongation pathway. 22
Figure 7 Diagram of nuclear rRNA processing in *S. cerevisiae*. 24
Figure 8 Structure of the yeast 60S ribosomal subunit. 27
Figure 9 Cryo-EM maps of 60S-SBDS-eIF6 complexes. 32
Figure 10 Dynamic rotation of domains I and III of SBDS. 34
Figure 11 Schematic of locations of SDS-associated mutations within SBDS protein. 47
Figure 12 Schematic diagram of the universal switch mechanism present in GTPases. 58
Figure 13 EFL1 domains and structure with comparison to EF2. 59
Figure 14 Photo of SHIRPA apparatus. 69
Figure 15 Resident Intruder Offensive Aggressive Behaviours. 70
Figure 16 Illustration of Home Cage Analysis Rig setup, with main components highlighted. 72
Figure 17 Schematic of subdermal electrode placement. 75
Figure 18 Schematic of home cage with different objects during the novel object recognition test. 78
Figure 19 The different type of trials of the acoustic startle & pre-pulse inhibition test. 80
Figure 20 Schematic of SNP sequencing in critical region. 91
Figure 21 Sanger sequencing of four other SNVs to validate Next Generation Sequencing. 94
Figure 22 Sanger sequencing of the missense variant indicated by the Next Generation Sequencing results at position 7:82763352. 96
Figure 23 Computer generated ribbon models of EFL1. 98
Figure 24 Survival curves of male and female mice. 102
Figure 25 Average body weight of male and female mice between 3 and 52 weeks of age. 105
Figure 26 E18.5 day post coitum embryo weights. 106
Figure 27 Fat and lean mass percentage for male and female mice. 107
Figure 28 Body weight and individual organ weights. 108
Figure 29 Oil Red O Staining of Pancreas. 109

Figure 30 Intraperitoneal glucose tolerance test (IPGTT) glucose clearance for male and females. 110
Figure 31 Average male and female gait scoring from monthly SHIRPA tests. 114
Figure 32 Average number of leg errors made on locotronic apparatus. 116
Figure 33 Average grip strength at 2, 6 and 14 months of age. 118
Figure 34 Skeletal muscle histology. 120
Figure 35 Free wheel running activity analysis. 122
Figure 36 Open field arena analysis. 124
Figure 37 Startle and pre-pulse inhibition sensorimotor gating test in males and females. 133
Figure 38 Fear conditioning freezing behaviour in male and females. 138
Figure 39 Novel object recognition test. 141
Figure 40 Y maze working memory test. 143
Figure 41 ABR thresholds for male and female mice at varying frequencies. 147
Figure 42 Electron Microscopy images of apical, mid and basal regions of the cochlea, showing inner hair cells. 148
Figure 43 H&E staining and width measurements of middle ear epithelial lining. 149
Figure 44 Red blood cell phenotypes in male and female mice. 153
Figure 45 Platelet counts and plateletcrit for males and females. 154
Figure 46 White blood cell counts for males and females. 156
Figure 47 White blood subpopulation counts for male and females. 158
Figure 48 Bone Mass Density and Bone Mineral Concentration. 161
Figure 49 p21 immunostaining of tibiae sections. 163
Figure 50 Mouse embryonic fibroblast (MEF) protein levels. 169
Figure 51 Mouse embryonic fibroblast (MEF) protein levels, using alternative antibody. 170
Figure 51 Adult tissue EFL1 protein levels. 171
Figure 52 Relative quantification of MEF *Efl1* transcript levels. 172
Figure 53 Relative quantification of liver polysome *Efl1* transcript levels. 173
Figure 55 p53 and p21 protein levels in mouse embryonic fibroblasts. 175
Figure 56 mTOR signalling markers; eIF2α and S6K protein levels. 178
Figure 57 Mouse embryonic fibroblast growth assay. 181
Figure 58 Mouse embryonic fibroblast polysome profiles and western blot analysis. 183
Figure 59 Nuclear and cytoplasmic eIF6 levels in MEFs. 185
Figure 62 Liver Polysome Profiles and Western Blot Analysis. 187
Figure 60 S^{35}-Methionine incorporation assay in MEFs. 189

Figure 61 SUnSET translation assay with MEFs.....190

List of Tables

Table 1 Ageing screen phenotyping pipeline. 12

Table 2 Summary of known and suspected ribosomopathies with details about clinical characteristics, cancer risk, and diagnosis. 38

Table 3 Next generation sequencing results indicated 9 high confidence single nucleotide variations with the region of interest. 92

Table 4 Experimental cohort mice details, including age and reason for death. 103

Table 5 Number of mice that sustained fight wounds. 128

Table 6 Social dominance in male and female mice. 129

Table 7 Resident intruder test results. 129

Table 8 Swim test results. 131

Table 9 Summary of parallels and differences of the *Efl1*$^{K983R/K983R}$ mice and Shwachman-Diamond Syndrome. 215

List of Abbreviations

4E-BP – eIF4E-bind protein

ABR – Auditory Brainstem Response

AML – acute myleloid leukaemia

Cas – CRISPR-associated

CMP – common myeloid progenitor

CRISPR - Clustered Regularly Interspaced Short Palindromic Repeats

crRNA – CRISPR RNA

DBA - Diamond Blackfam Anaemia

DEXA – Dual-Energy X-ray Analysis

DNA – Deoxyribonucleic Acid

ECG – Echocardiogram

eEF – eukaryotic elongation factor

EF – Elongation factor

eIF – eukaryotic initiation factor

EM – Electron Micrscopy

ENU – N-ethyl-N-Nitrosourea

GAP – GTPase-activing protein

GDS – Guanine nucleotide dissociation stimulator

GEF – Guanine exchange factor

GMP – granulocyte/monocyte progenitor

GSF – GTP stabilising factor

HSC- haematopoietic stem cell

IF – Initiation factor

IPGTT – Intraperitoneal Glucose Tolerance Test

IPGTT – Intraperitoneal Glucose Tolerance Test

IRES – internal ribosome entry site

IVC – individually-ventilated cages

LRS – Leucine RNA synthetase

MDS – myelodysplastic syndrome

NDP – nucleotide diphosphate

NGD – No Go Decay

NOR – Nucleolar Organising Region

NPC – Nuclear Pore Complex

NTP – nucleotide triphosphate

ORF – open reading frame

PIC – preinitiation complex

Pol I – RNA Polymerase I

rDNA – Ribosomal DNA

RF – release factor

RNA – Ribonucleic Acid

RNAi – RNA interference

RPL – Ribosomal protein large

r-proteins – Ribosomal Proteins

RPS – Ribosomal protein small

r-RNA – Ribosomal RNA

SBDS – Shwachman-Bodian-Diamond syndrome

SDS – Shwachman-Diamond Syndrome

sgRNA – single guide RNA

SHIRPA – Smith Kline Beecham, Harwell, Imperial College, Royal London Hospital phenotype assessment

SL – stable-stem loop

snoRNP – small nucleolar ribonucleoprotein

SNP – single nucleotide polymorphism

SRL – Sarcin-rich loop

T-ALL – T-cell lymphoblastic leukaemia

TCS - Treacher Collins Syndrome

tRNA – Transfer RNA

uORF – upstream open reading frame

UTR – Untranslated Region

Chapter 1
Introduction

1. Introduction

The work presented in this thesis characterises a novel *N*-ethyl-*N*-Nitrosourea (ENU) mouse mutant with a missense mutation in the gene *Efl1*. The protein is encoded by this gene is Elongation Factor Like GTPase 1 (EFL1), which is involved in the maturation of the 60S subunit of the ribosome. This mouse was derived from the Harwell ageing screen, and was originally identified due to the presentation of an abnormal gait phenotype. Detailed genetic and phenotypic characterisation has revealed multiple additional, affecting numerous tissues. To our knowledge, this is the first *Efl1* mouse model to be described. This thesis herein contains details of the genetic and molecular characterisation, phenotypes present in the *Efl1* mouse line, and the ramification of these findings.

1.1. ENU mutagenesis

1.1.1. Model organisms in genetic research

The study of model organisms with genetic mutations has been fundamental to research into human disease. Various species have been utilised in this area, ranging from eukaryote models such as yeast, to more complex mammalian species such as the mouse. Whilst each species has its merits, mammalian systems tend to be more translational to human disease processes due to their comparable anatomy and closely analogous genetic makeup. One of the most powerful advantages of using the mouse as a model system for disease is that the pathological consequences of genetic manipulation parallel human disease states due to their comparable anatomy and physiology. Also, mouse behaviours can, to an extent, be comparable to human behaviours, allowing the study not only of physical diseases, but psychological disorders as well (Silver 1995)

Mice have played a role in genetic research ever since the discovery of Mendel's laws the 1900, when they were chosen as a species in which to investigate if the laws of Mendelian inheritance applied to mammals as well as plants (Silver 1995). One of the challenges in translating Mendel's findings to mammals was that mammalian traits are far more complex than the 'either/or' forms of phenotype that Mendel chose to focus on in plants. It was therefore necessary to choose a species in which numerous variants had been derived and were readily available within pure-breeding lines. And thus began the marriage between the fancy mice and experimental genetics. Evidence for the applicability of Mendel's laws to mammals — and by implication, to humans — came quickly, with a series of papers published

by the French geneticist Cuénot on the inheritance of the various coat colour phenotypes. Not only did these studies confirm the simple dominant and recessive inheritance patterns expected from "Mendelism", they also brought to light additional phenomena such as the existence of more than two alleles at a locus, recessive lethal alleles, and epistatic interactions among unlinked genes. A significant contributor to early mouse genetics was William Ernest Castle, who brought the fancy mouse into his laboratory in 1902, and began a systematic analysis of inheritance and genetic variation in this species. The Castle group developed the first inbred mouse strain termed DBA (so called because it carries mutant alleles at three coat colour loci — dilute (D), brown (B), and non-agouti (A)) in response to the need for development of inbred genetically homogeneous lines of mice. One of Castle's students, Little, went on to produce many other inbred strains commonly used today: C57BL6, C57BL10, C3H/HeJ, CBA, and BALB/c. Although an original reason for the development of these lines was to demonstrate the genetic basis for cancer, these inbred lines have played a crucial role in all areas of mouse genetics by allowing independent researchers to perform experiments on the same genetic material. This made the mouse an extremely powerful research tool, and this pioneering work paved the way for much of today's research using mouse models (Silver 1995)

The genetic purity of mouse lines has allowed frequent use of this species to model many human diseases. There are also many other factors that make the mouse a useful model organism. Firstly, mice are relatively easy to breed, with short regeneration times compared to higher mammals. Also, their genetic makeup has been studied intensively and the complete mouse genome sequence is now readily available (Asif T. Chinwalla 2002). In addition, there are many tools available to alter the mouse genome. These range from random mutagenesis programs to more specific alterations, such as those using genetically altered mouse embryonic stem (ES) cells to breed genetic chimeras carrying specific mutations. Targeted gene alteration is a sought after mutagenesis approach within human disease research, as they allow the mutation of specific-disease associated genes. One of the major advantages of using mice in genetic research is the ability to manipulate ES cells genetically, and then transfer them back to the mouse to generate mutant offspring (Southon and Tessarollo 2009). ES cells are capable of self-renewal and are pluripotent, meaning they are capable of differentiation into any cell type. ES cells can be maintained in culture in the totipotent, undifferentiated state, under strict growth conditions. When injected into a blastocyst, ES cells can contribute to the somatic and germ cell lineages of the resulting chimeric mouse. If germline transmission occurs, an offspring of the chimeric mouse can be

produced that was derived from the injected ES cell clone. The ability to pass on germline transmission means that a mouse can be generated from ES cells that are genetically manipulated in culture (Limaye, Hall et al. 2009).

The recently developed CRISPR/Cas9 method of genome-editing represented a huge leap in genetic engineering and generated considerable excitement, as it represented an efficient and reliable way to make precise, targeted changes to the genome. CRISPR (Clustered Regularly Interspaced Short Palindromic Repeats) and CRISPR-associated (Cas) genes are essential in adaptive immunity in select bacteria and archaea. Their potential for gene editing was realized in 2012 when Doudna and Charpentier developed a system using a synthetic single guide RNA (sgRNA) (Doudna and Charpentier 2014) designed to guide the CRISPR/Cas9 machinery to a specific point in the genome based on sequence complementarity. Here site-specific cleavage of double-stranded DNA occurs, resulting in the activation of the double-strand break (DSB) repair machinery. DSBs can be repaired by 1) the Non-Homologous End Joining (NHEJ) pathway, resulting in insertions and/or deletions (indels) which disrupt the targeted locus, or 2) the homology-directed repair (HDR) pathway, which allows for precise replacement mutations during the DSB repair, if a donor template with homology to the targeted locus is supplied (Reis 2014).

While targeted gene alteration is desired for learning more about known disease-associated mutations, the discovery of novel genes associated with disease states is also crucial in modern research into human diseases. For this to be achieved, random mutagenesis programs and forward genetics screens are implemented that aim to identify mutants based on phenotype alone, with no presumptions about genetic aetiology. ENU is a popular mutagen for random mutagenesis screens, and will be the focus of this project.

1.1.2. The molecular mechanism of ENU mutagenesis

N-ethyl-*N*-Nitrosourea (ENU) is a potent mutagen that was first discovered by Bill Russell in the 1970's (Russell, Kelly et al. 1979). The work by Russell et al. was ground breaking for mutagenesis techniques as it identified ENU as the most effective mutagen for creating new genetic models, stating it as "clearly the mutagen of choice for the production of any kind of desired new gene mutation". ENU is now used to generate mutations to create model organisms, ranging from zebrafish to *Mus musculus*. The stochastic nature in which ENU generates point mutations in the genome makes it an excellent tool for forward genetic screens.

ENU causes a high incidence of point mutations by acting as an alkylating agent, transferring its ethyl group to nucleophilic nitrogen or oxygen radicals in any of the four DNA bases. This alkylation of the bases causes mispairing, which leads to base pair substitution if not rectified by the cells' repair mechanisms. DNA repair constitutes a large part of the ENU mutagenesis system, and ENU is relatively ineffective at low doses due to compensation by various repair mechanisms. Once these systems are saturated however, the mutation rate increases in a dose-dependent manner. ENU mutagenesis is therefore a balancing act of dosage, with a dose that is too low being ineffectual due DNA repair and a dose that is too high detrimentally affecting either the fertility (spermatogonial cells) or health (somatic cells) of the animal (Justice, Noveroske et al. 1999, Acevedo-Arozena, Wells et al. 2008).

Pre-meiotic spermatogonial stem cells accumulate ENU-induced mutations at a particularly high rate, acquiring them at a rate of 1 mutation every 1-1.5Mb, depending on the dose regime and mouse strain used (Justice, Noveroske et al. 1999, Acevedo-Arozena, Wells et al. 2008). This initially depletes the spermatogonial stem cells, causing temporary sterility. Surviving stem cells repopulate the spermatogonial stem cell pool by mitosis, and subsequently produce sperm cells by meiosis, rendering the animal fertile once more. The result is mature gametes with ENU-induced point mutations spread throughout the genome, with each individual sperm cell carrying a unique array of mutations. This allows efficient transfer of ENU-induced mutations to the next generation (after the temporary sterility caused by the ENU dosage has subsided). The sterility period is often an indicator as to the effectiveness of the ENU treatment. Because of the unique array of mutations in individual sperm cells, this mutagenesis regime results in each individual offspring harbouring a potentially unique set of mutations.

Many potential outcomes of these mutations are possible, depending on their location within the genome. If the mutation is within a coding region of DNA, missense mutations may occur, whereby a change in amino acid results in a loss or gain of function effect on the protein encoded. Alternatively, nonsense mutations may occur, whereby the resultant protein will be truncated due to a premature stop codon being generated. In addition, synonymous mutations can be generated, whereby the amino acid is not changed even though the codon is mutated, due to the degenerate nature of codons. Mutations in non-coding regions can also affect gene function, by altering promoter/suppressor activity or by causing alternative splicing of a gene. It has also been reported that small deletions can occur through ENU mutagenesis, however this is rare. ENU has a strong bias towards causing point mutations at A-T base pair sites, with 70-85% of ENU-induced point mutations estimated to be A-T to T-A transversions or A-T to G-C

transitions. In contrast, G-C to C-G transversions are rarely seen. Approximately 70% of ENU-induced point mutations result in nonsynonymous amino acid substitution, and 65% of these cases are estimated to be due to missense mutations (with nonsense and splice mutations making up the remainder). The strong tendency to induce point mutations at A-T base pair sites may, in time, become a limiting factor of ENU mutagenesis, as certain genes will be mutated more often than others based on their G-C content.

1.1.3. ENU treatment and breeding strategies

ENU is administered in adult male mice via a series of intraperitoneal injections. The most effective dosage regimes vary depending on the mouse strain being used, and optimal regimes have been elucidated for many different inbred strains (Justice, Carpenter et al. 2000, Weber, Salinger et al. 2000). A typical dosage of ENU might be 80-100mg/kg of body weight, in two or three injections spaced a week apart (Acevedo-Arozena, Wells et al. 2008). Breeding schemes for propagation of ENU-induced mutations can vary depending on whether dominant or recessive alleles are of interest. The breeding schemes are normally carried out using two strains of mice, one that is mutagenized and one that is used as a 'clean' background on to which to backcross. Using two different strains allows for easy detection of mutagenised regions of the genome in resultant offspring by the mapping of informative single nucleotide polymorphisms (SNPs). In both dominant and recessive breeding schemes, a G0 mutagenised male mouse (of one particular strain) is crossed to a wildtype female (of a different strain). The G1 offspring of this cross can be screened for dominant mutations. If recessive alleles are of interest further steps are required as follows. There are two methods of homozygosing mutations from the cross described above. One option is to intercross the offspring of the G1 mice (G2 individuals) or alternatively, the G2 females can be backcrossed to the G1 father to produce G3 individuals.

G1, G2 or G3 individuals can then be put through phenotyping pipelines to identify any detrimental effects of the mutations they carry. However, because of the stochastic nature of ENU, each individual pedigree will carry multiple mutations, with a G1 mouse estimated to carry between 30-50 potentially functional mutations that could confound findings in phenotypic screens (Quwailid, Hugill et al. 2004). Some of these mutations could be passed on to further generations even when bred by selecting for a particular phenotype, albeit at a much lower rate (a reduction of approximately 50% of mutations will occur in each subsequent generation). This is because crossing over occurs at sites all along the chromosomes in the genome. The farther apart two loci are from each other, the more likely it is that a crossover event will occur somewhere within the length of chromosome that lies

between them. Thus, the frequency of recombination provides a relative estimate of genetic distance. Genetic distances are measured in centimorgans (cM) with one centimorgan defined as the distance between two loci that recombine with a frequency of 1% (Silver 1995). In order to ensure the correct mutation is being selected and is causative of the phenotypes seen, mapping is carried out to narrow the region of interest down to approximately 5Mb. It is unlikely for two mutations to occur is such close proximity in the genome (probability <0.05) (Keays, Clark et al. 2006), and so by selecting for this region through multiple backcrosses other potentially confounding mutations can be reduced to near elimination.

With the advent of next generation sequencing (NGS), it is no longer necessary to narrow the region of interest down to as little as 5Mb. Once a region of interest has been identified in affected mice NGS is carried out, and protein-coding and non-protein-coding mutations with this region are identified. Mice can then be genotyped for a specific mutation in a gene to allow for accurate selection. Other mutations in the region will also have been identified by NGS and can be reduced by subsequent backcrossing. By using certain assumptions, the number of backcrosses required to eliminate other mutations in a critical region can be calculated. It has been shown that ENU mutations occur at a rate of 1 in 1.82Mb (Quwailid, Hugill et al. 2004). To use an example, take a region of interest of 5Mb, of which 115kb is coding (approximately 2.3% of the mouse genome is coding). The likelihood of there being another coding mutation within this region is 0.002, in other words very unlikely. However, if there is a larger region, this probaibilty increases. Using these same assumptions it can be calculated how many mutatiosn are likely to be within any region of interest, and therefore how many backcrosses are required to eliminate those mutations (mutation load reduces by half in each backcross) (Keays, Clark et al. 2006).

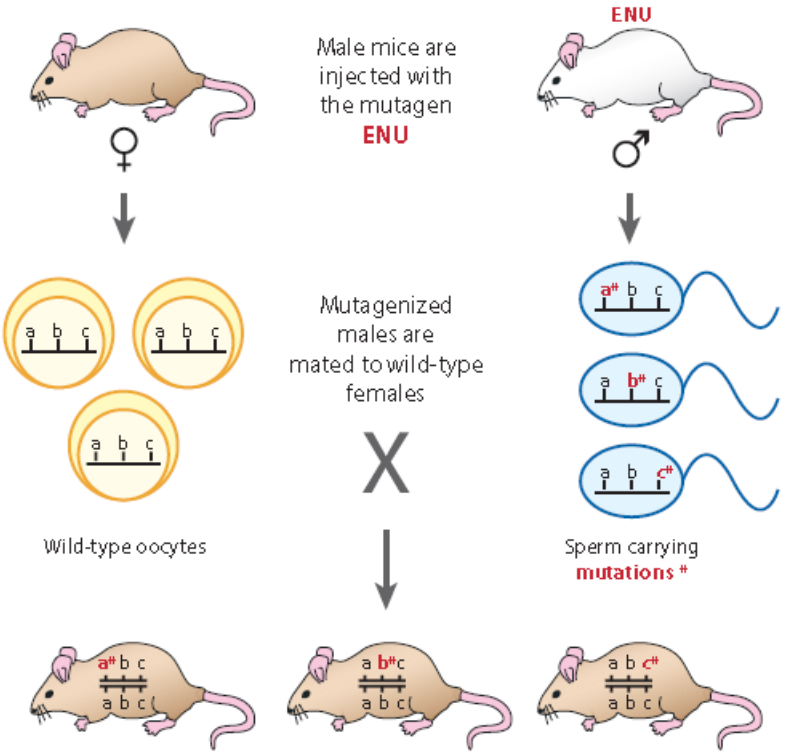


Figure 1 Diagram of the breeding scheme for an ENU-driven G1 screen for dominant mutations. Male mice are mutagenised with ENU, and after a period of sterility, are mated to wildtype females (of a different selected inbred strain, as stressed in the figure by different coat colours). The point mutations that were induced by ENU treatment are carried by the spermatogonial cells and are therefore transferred to the next generation in a Mendelian fashion. Each individual G1 offspring will carry a unique array of mutations, and they are subsequently screened for any abnormal phenotypes. (Acevedo-Arozena, Wells et al. 2008)

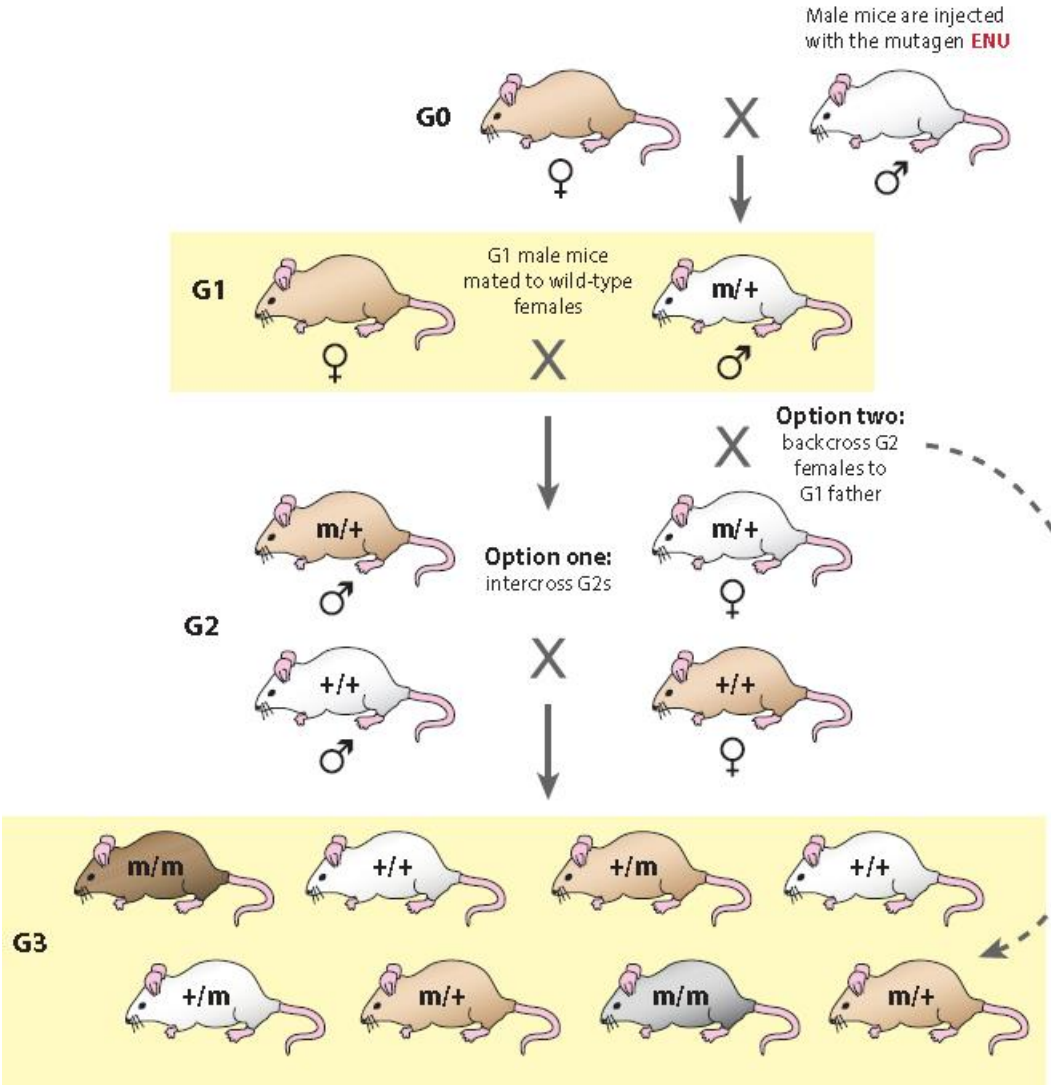


Figure 2 Diagram of the breeding scheme for an ENU-driven G3 recessive screen. As above , a male is mutagenized by injection of ENU and, following a period of sterility, is mated to a wildtype female (of a selected inbred strain, as stressed in the figure by different coat colours). Mutations harboured in the mutagenised male genome will be passed onto the offspring in a Mendelian fashion. Each G1 offspring will harbour a unique array of mutations. Each G1 male will be carried on into its own breeding scheme to generate a specific mouse line. The G1 male is crossed with a wildtype female to produce G2 offspring. By intercrossing the G2 mice, or by crossing G2 females back to the G1 father, a mixture of homozygous, heterozygous and wildtype G3 offspring are produced. (Acevedo-Arozena, Wells et al. 2008).

Phenotypic screens

Phenotypic screens of ENU-mutagenised mice are a form of forward genetics that allow for the discovery of novel disease models via a phenotype-driven approach. Because mice are only detected based on the phenotypes they express, no assumptions are made about the genetic aetiology or molecular pathways involved. This can lead to novel association of genes with disease states or pathways that were previously unknown. This is a very powerful technique for discovering new mouse models of diseases and for furthering knowledge of gene function. Due to the promiscuous nature of ENU, it is possible to identify models of any given disease or pathogenic pathway. Phenotypic screening have become increasing sophisticated over the years, with early studies merely focusing on visible phenotypes, such as coat colour, or lethality as indictors of potentially significant mutations. Modern screens comprise intricate and coordinated pipelines of phenotyping tests that look at multiple aspects of a mouse' health. Phenotyping tests included in these types of screens may include regular weighing, behavioural tests, metabolic tests such as glucose tolerance, hearing and visions screens, bone morphology scans and even higher executive function tests. Many ENU mutants have been generated over the years, with a variety of novel gene mutations and phenotypes associated. Some examples include a seizure mouse model (*Kcnq1*), a motor neuron degeneration model (*Dync1b1*), a circadian mutant (*Clock*), a retinal degeneration model (*Pde6b*), an age-related hearing loss model (*Slc4a10*), a hypertrophic cardiomyopathy model (*Ecsit*) to name a few (Acevedo-Arozena, Wells et al. 2008, Potter, Bowl et al. 2016). ENU mutagenesis screens have also generated models with non-protein-coding mutations. For example, a novel deafness model was identified with a mutation in *Protein tyrosine phosphatase, receptor type, Q* (*Ptprq)* that resulted in a donor splice site mutation (Potter, Bowl et al. 2016). In conjunction with this, a novel ENU mutant with a mutation in the gene for the mircoRNA *Mirn96*, also shows progressive hearing loss. This non-coding mutant was shown to have reduced Prptq protein levels as a result of the non-coding mutation (Lewis, Quint et al. 2009).

1.1.5. The Harwell Ageing Screen

One example of a phenotypic screen is the ageing screen at MRC Harwell, UK. The aim of this screen is to identify age-related phenotypes that may not present until later stages of life in the mouse. It consists of a large-scale, 18 month phenotyping pipeline aiming to identify novel phenotypes induced by ENU-induced mutations. The screen is recessive, recurrently testing G3 mice for phenotypic abnormalities, and thus allows for the identification of recessive as well as dominant and semi-dominant mutations. The screen is designed to identify mice harbouring

mutations that cause late-onset phenotypes, and encompasses phenotyping tools that focus on a wide variety of disease areas. For the ageing screen, C57Bl/6N mice are mutagenised using three weekly intraperitoneal ENU injections, with a dosage of 80-100mg/kg. Subsequent breeding is carried out with an un-mutagenised C3H.Pde background. This strain is based on the C3H/HeJ strain, but does not carry the *rd1* mutation in the *Pde6b* gene (*Pde6b*^{rd1}), which causes a rapid degeneration of photoreceptors in the retina in the C3H/HeJ mice (Banks, Heise et al. 2015). Tests included in the ageing screen are as follows; Echo Cardiogram (ECG), Smith Kline Beecham, Harwell, Imperial College, Royal London Hospital phenotype assessment (SHIRPA), grip strength, opthalmoscope and optokinetic drum (vision tests), click box and auditory brainstem response (ABR), Echo-MRI, Dual-Energy X-ray Analysis (DEXA) and X-ray, pupillometry, sleep tracking, clinical chemistry of blood, fasted blood test, fasted insulin tolerance test and intraperitoneal glucose tolerance test (IPGTT) (Table 1). These tests look at multiple different somatic systems; heart function, behaviour, muscular strength, vision, hearing, body composition, bone morphology, reflexes, circadian rhythm, blood chemistry and metabolism, respectively. This is an example of a comprehensive phenotyping pipeline that is employed as a standardised, uniform practice. Subsequent to this initial screen, mutants of potential interest can undergo secondary screening of more specialist tests to further elucidate the phenotypes present.

To conclude, ENU mutagenesis represents a powerful, hypothesis generating approach that has resulted in many novel gene functions being discovered over the years. It is being employed in unique and detailed phenotypic screens to investigate complex disease areas, such as age-related disease, and is beneficial not only in assigning novel function to genes, but also in generating new mouse models of disease (Potter, Bowl et al. 2016).

Table 1 Ageing screen phenotyping pipeline. Various phenotyping platforms are employed to assess multiplepenotpic areas, including cardiac function, hearing, neurological, neurobehaviour, muscoloskeletal, vision, growth/body composition, metabolism and pathology. Mouse lines of interest are rederived and pursued in more detail after the screen. ECG, electrocardiogram; DEXA, dual energy X-ray analysis; IPGTT, intraperitoneal glucose tolerance test; MRI, magnetic resonance imaging; SHIRPA, SmithKline Beecham, Harwell, Imperial College and Royal London Hospital phenotype assessment. (Potter, Bowl et al. 2016).

Test	Phenotypic Area	Age (weeks)
ECG	Cardiac	12
SHIRPA	Neurological	13, 66
Grip strength	Musculoskeletal/neurological	13, 66
Slit lamp/opthalmoscope	Vision	15, 49, 65, (73)
Optokinetic drum	Vision/neurological	15, 49, 65, (73)
Click box	Hearing	14, 26, 39, 50
Auditory brainstem response + click stimulus	Hearing	14, 39
Echo-MRI	Growth/body composition	16, 27, 51, 71
DEXA	Musculoskeletal/body composition	16, 51,
X-ray	Musculoskeletal	16, 51, 74
Pupillometry	Vision/neurobehaviour	18, 68
Sleep tracking	Neurobehaviour	18, 68
Clinical chemistry	Pathology	28, 53, 80
Fasted bleed	Diabetes/metabolism	17, 28, 52, 80
Fasted insulin	Diabetes/metabolism	33, 57, 72
IPGTT	Diabetes/metabolism	33, 57, 72

1.2. The ribosome structure and function

1.2.1. Ribosome structure

In all living cells, the ribosome is responsible for the last stage of converting genetic information into functional proteins. The ribosome is universal to all nucleated cells, and is critical for life. The average human body contains ~10^{14} cells, each containing ~1 billion proteins, which are constantly being synthesised and degraded. For this to occur, the ribosomes within the cell must be functioning at an extremely high rate, with a high level of efficiency. It is estimated that the typical mammalian cell contains around 1 million ribosomes (Bashan and Yonath 2008). Therefore, to keep this highly demanding system afloat, ribosome biogenesis needs to occur continuously and in an accurate manner.

The ribosome is made of two subunits, each of which has a complex assemblage process and maturation pathway to follow. The subunits are made up of ribosomal RNA (rRNA) and are distinct from each other in many ways, the most obvious of which is size. The two subunits are referred to as the large 60S subunit (50S in prokaryotes) and the small 40S subunit (30S in prokaryotes), with the former being approximately twice the size of the latter. Despite the size difference between prokaryotes and eukaryotes, ribosomes from all kingdoms of life are functionally conserved, with the functional domains having the highest level of sequence conservation (Yusupova and Yusupov 2015).

Remarkable progress has been made in the field of ribosome structure and function research in recent decades. From the initial visualisation of the ribosome from negative staining of various rat and chicken tissues (Palade 1955) to the highly sophisticated Cryo-electronmicroscopy (Cryo-EM) structures obtained recently (Ben-Shem, Garreau de Loubresse et al. 2011, Weis, Giudice et al. 2015), we have now been able to elucidate the structure of the ribosomal subunits in various functional states, including their interaction with each other (Bashan and Yonath 2008). The atomic structures of an archaeal 50S subunit from *Haloarcula marismortui* (Ban, Nissen et al. 2000) and a bacterial 30S subunit from *Thermus thermophilus* (Wimberly, Brodersen et al. 2000) published in 2000 were the basis for elucidating every subsequent structure of the ribosome or its individual subunits. Such structures include low-resolution structures of the 70S ribosome by crystallography (Yusupov, Yusupova et al. 2001) and cryoEM (Gao, Sengupta et al. 2003), the structure of a bacterial 50S subunit (Harms, Schluenzen et al. 2001), and more recent high-resolution structures of the 70S ribosome (Selmer, Dunham et al. 2006). Also, mobile elements of the 50S subunit such as the L1 (Nikulin,

Eliseikina et al. 2003) or L7/L12 stalks (Diaconu, Kothe et al. 2005), which are mostly disordered in most high-resolution structures of the ribosome, have been solved in isolation.

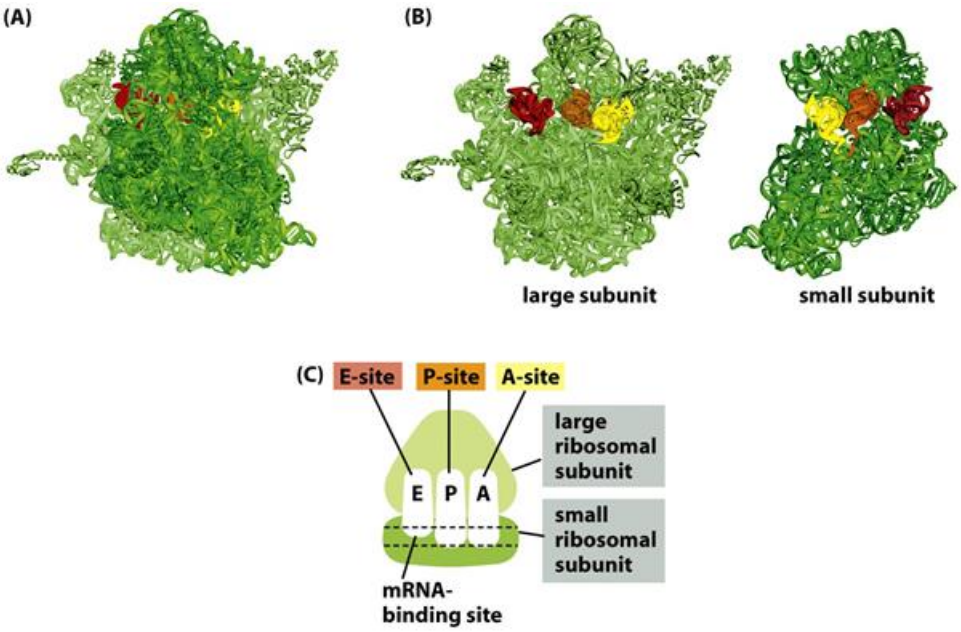


Figure 3 Crystal structures of the *Thermus thermophillus* 70S ribosome. *Thermus thermophillus* 70S ribosome with 30S subunit in front (dark green) and 50S subunit behind (light green). Transfer RNAs (tRNAs) are shown bound in the E site (red), P site (orange) and A site (yellow). Note: although three tRNAs are shown, in the process of translation only two sites are thought to be occupied at any one time. B) *Thermus thermophillus* 50S and 30S subunit alone, with tRNA in E site (red), P site (orange) and A site (yellow). C) Simplified schematic representation of the E site, P site and A site in the core of the ribosome (conserved between prokaryotic and eukaryotic ribosomes). Adapted from (Alberts 2007).

The ribosome core is universally conserved and has been described in detail by structures of prokaryotic ribosomes. However, eukaryotes and prokaryotes differ markedly in translation processes such as initiation, termination, and regulation, and eukaryotic ribosomes play a central role in many eukaryote-specific cellular processes. Accordingly, eukaryotic ribosomes are at least 40% larger than their bacterial counterparts as a result of additional rRNA elements called expansion segments and extra protein moieties. As mentioned above, all ribosomes are composed of two subunits. The large 60*S* subunit of the eukaryotic ribosome consists of three rRNA molecules (25*S*, 5.8*S*, and 5*S*) and 46 proteins, whereas the small 40*S* subunit includes one rRNA chain (18*S*) and 33 proteins. Of the 79 proteins, 32 have no bacterial or archaeal homologues, and those that do have homologues usually harbour large eukaryote-specific extensions. Apart from variability in certain rRNA expansion segments, all eukaryotic ribosomes, from yeast to human, are highly similar. The crystal structure of the 80*S* ribosome from the yeast *Saccharomyces cerevisiae has been solved almost in its entirety, with ~90.5% of the ribosomal proteins and ~95.5% of the rRNA present. T*he final model consists of

all 44 proteins specific to eukaryotes and all 35 universally conserved proteins, with the exception of the highly mobile L1, regions within the P-stalk proteins, and residues located in disordered loops or tails (Ben-Shem, Garreau de Loubresse et al. 2011).

More recently, the human 80S ribosome structure has been elucidated using single-particle Cryo-EM. The overall strcture of the human ribosome contains the common hallmarks of the 60S and 40S subunit that are seen in yeast, including the central protuberance, P stalk, L1 stalk of the 60S subunit, and the beak, platform and head of the 40S subunit. One difference of the human ribosome compared to yeast is the presence of an additional r-protein – RPL28. It also two additional intersubunit bridges contacts, termed B15 and B16. There are also missing intersubunit bridges in the human ribosome structure compared to the yeast ribosome, and other contacts are mediated by different r-proteins in the two species. These intersubunit bridges may affect the rotation of the subunit relative to each other during translocation. Overall however, the structure of the human and yeast ribosomes are highly similar, with the universal core behaving in the same manner in both species (Khatter, Myasnikov et al. 2015).

The structure also revealed the types of movement the human ribosome makes from the pre-translocation state to the post-translocation state. In the human 80S structures, a tRNA is present in the E site. In the pre-translocation state, The L1 stalk rRNA interacts with the tRNA close to the elbow region, as observed for the 70S ribosome in bacteria. The 40S subunit head shows a swivel movement away from the 60S, which leads to a partial closure of the latch region, which has not been seen in previous structures. However, this could be due to the fact that the mRNA channel is empty, in contrast with previous yeast and human ribosome structures (Khatter, Myasnikov et al. 2015).

The detailed structures of the ribosome, in many different species, have made it possible to study in detail the function of the ribosome and it is now known that there is a distinct division of labour between the two subunits, with the small subunit carrying out the decoding of the messenger RNA (mRNA) into amino acid sequence by recognising codons on the mRNA molecule, and the large subunit carrying out peptide bond formation and polypeptide chain assembly. The transfer RNA (tRNA) sites that are formed when the two ribosomal subunits come together are key to ribosomal function. There are three tRNA sites in total, that reside in the highly conserved ‘common core’ and span both subunits, but are predominantly made up of small subunit rRNA. These three sites accommodate tRNAs in a chain-like reaction whereby cognate tRNA molecules enter the A site, move to the P site for peptide bond

formation and leave via the E site, producing a polypeptide chain in the process. This process will be discussed in more detail in 1.2.2.

1.2.2. The ribosome in translation

Translation is the final step of decoding the genetic material of a cell and results in protein synthesis. Translation involves three phases; initiation, elongation and termination. Initiation refers to the assembly of a translation-competent ribosome at the AUG start codon on an mRNA molecule; elongation is the codon-dependent assembly of a polypeptide chain; and termination involves the release of the completed protein when the ribosome reaches a stop codon. These three steps are facilitated by trans-acting proteins that are referred to as eukaryotic initiation factors (eIF), elongation factors (eEF) and release factors (eRF).

1.2.2.1. Initiation

Translation initiation involves the detection of a start codon (AUG) in the 5'-untranslated region (UTR) of an mRNA molecule. In eukaryotes this involves a scanning mechanism in which the 40S subunit, preloaded with a Methionyl-$tRNA_i$ (Met-$tRNA_i$), binds to the mRNA target and moves downstream until a start codon is recognised. The Met-tRNA is loaded onto the 40S subunit by the initiation factor eIF2 – a GTPase with no bacterial counterpart. GTP-bound eIF2 (known as the binary complex) binds to Met–$tRNA_i$, to become the ternary complex (TC) and associates with the 40S ribosomal subunit. The scanning mechanism is promoted by eIF1, eIF1A, eIF5 and the multi-subunit eIF3, and these factors together with the 40S subunit constitute the 43S preinitiation complex (PIC). The 43S PIC attaches to the free 5' end of the mRNA, and the 5'-UTR is scanned base by base for a complementary codon for the Met-$tRNA_i$ as successive codons enter the P site of the 40S subunit. Thus the first AUG codon in the 5'-UTR is favoured as the start codon, and AUG codons inserted upstream of this will replace the primary initiation site leading to an elongated protein product. Conversely, mutation of the primary initiation site leads to initiation from a downstream AUG codon (Klann and Dever 2004, Sokabe and Fraser 2014).

In addition to the AUG start codon, the 5'-7-methyl-GTP (m^7GTP) cap and the 3'-poly(A) tail on mRNAs are also important in translation initiation (Klann and Dever 2004, Hinnebusch 2014).The binding of the 43S PIC to an mRNA is facilitated by the eIF4 family of translation factors. The m^7G-cap at the 5' end of eukaryotic mRNAs is a feature that facilitates the scanning mechanism by binding the eIF4F complex which attaches to the cap to activate the mRNA for 43S PIC attachment, resulting in 48S complex formation. The eIF4F complex comprises the cap-binding protein eIF4E, the scaffold protein eIF4G, and the RNA helicase

eIF4A. eIF4G contains binding domains for mRNA, eIF4E, eIF4A, poly(A)-binding protein (PABP), eIF3 (in mammals), and eIF1 and eIF5 (in budding yeast). The binding domains for eIF4E, PABP, and mRNA in eIF4G results in a bridging of the 5’ and 3’ ends of the mRNA, enabling assembly of a highly stable, circular mRNA–protein complex—the closed-loop structure. The eIF4A-binding domain of eIF4G allows it to activate eIF4A allosterically. This allows the unwinding of secondary structures at the 5' end of mRNAs by eIF4A, with the initiation factor eIF4B. . Energy is required for the unwinding of the secondary structure of the mRNA as the eIF4F complex scans the nucleotide sequence. This energy is provided by ATP hydrolysis by eIF4A. Recognition of a start codon triggers hydrolysis of GTP by eIF2 in the TC, which leads to the release of factors from the 48S complex and allows eIF5B- and GTP-dependent joining of the large ribosomal subunit (Klann and Dever 2004, Hinnebusch 2014).

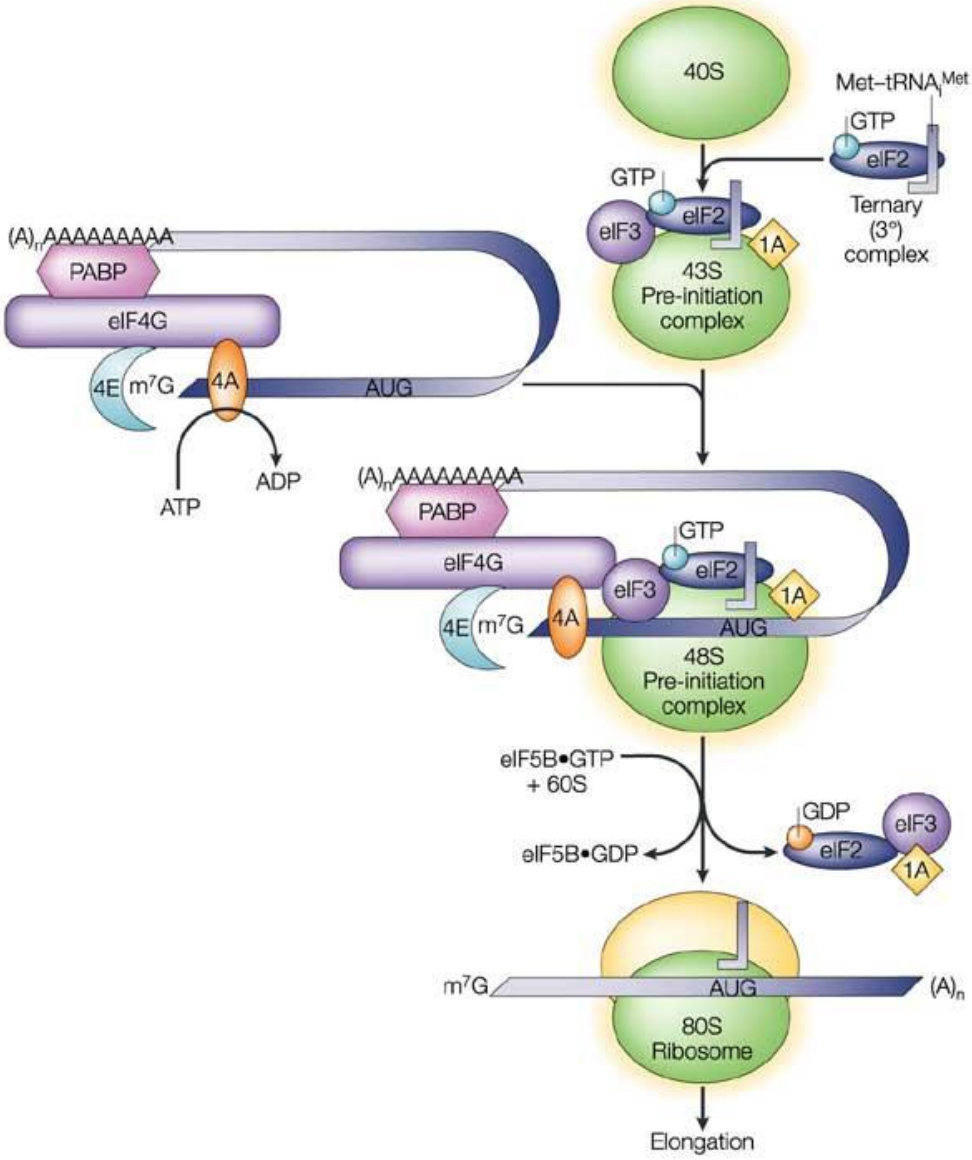


Figure 4 Pathway of translation initiation in eukaryotes. A binary complex of eukaryotic translation initiation factor 2 (eIF2) and GTP binds to methionyl–transfer RNA (Met–tRNA$_i^{Met}$), and associates with the 40S ribosomal subunit, forming the ternary complex. The association of additional factors, such as eIF3 and eIF1A (1A), with the 40S subunit promotes ternary complex binding and generates a 43S pre-initiation complex. The cap-binding complex, which consists of eIF4E (4E), eIF4G and eIF4A (4A), binds to the 7-methyl-GTP (m^{7}GTP) cap structure at the 5' end of a messenger RNA (mRNA). eIF4G also binds to the poly(A)-binding protein (PABP), thereby bridging the 5' and 3' ends of the mRNA. This mRNA circularization and the ATP-dependent helicase activity of eIF4A are thought to promote the binding of the 43S pre-initiation complex to the mRNA, which produces a 48S pre-initiation complex. Following scanning of the ribosome to the AUG start codon, GTP is hydrolysed by eIF2, which triggers the dissociation of factors from the 48S complex and allows the eIF5B- and GTP-dependent binding of the large, 60S ribosomal subunit. Adapted from (Klann and Dever 2004).

1.2.2.2. Elongation

At the heart of translation is the elongation cycle, which consists of sequential additions of amino acids to the growing polypeptide chain directed by the mRNA codons. This process is catalysed by two GTPases, elongation factor 1A (eEF1A) and elongation factor 2 (eEF2) (EF-Tu and EF-G in bacteria, respectively). As mentioned above, the 80S ribosome shows a division of labour between its two subunits. The 40S subunit is responsible for decoding the mRNA message, whereas the 60S subunit contains the peptidyl transfer centre (PTC) and is responsible for constructing the polypeptide chain. tRNAs form a bridge between the functions of the two ribosomal subunits. Their anticodon loop contacts the small ribosomal subunit, thereby allowing the decoding of the mRNA message, while the 3' end, which carries the corresponding amino acid, provides the large subunit's PTC withthe next amino acid. The ribosome contains three distinct binding sites for tRNAs, which span both subunits: the A-site accepts the incoming aminoacyl-tRNA (AA-tRNA) and matches the mRNA codon and tRNA anticodon with one another; the P-site holds the peptidyl-tRNA and catalyses the formation of new peptide bonds; and finally the E-site holds the deacylated tRNA after peptidyl transfer (Dever and Green 2012).

The mechanism of translation elongation is well conserved between eukaryotes and bacteria. In eukaryotes, the 80S ribosome is poised on an mRNA with the anticodon of a Met-tRNA$_i$ in the peptidyl (P) site base-paired with the start codon after the initiation phase of translation. The adjacent acceptor (A) site of the ribosome sits over the next codon of the open reading frame (ORF) awaiting a cognate tRNA. eEF1A (the orthologue of bacterial EF-Tu) binds an AA-tRNA in a GTP-dependent manner and directs it to the A site of the ribosome. Cognate codon recognition by the tRNA triggers GTP hydrolysis by eEF1A, releasing the factor and enabling the AA-tRNA to be fully accommodated into the A site. Following accommodation of the AA-tRNA into the A site, peptide bond formation with the amino acid on the P-site peptidyl-tRNA occurs. The PTC, consisting primarily of conserved rRNA elements on the 60S subunit, positions the substrates for catalysis. Recent crystal structures of the *Saccharomyces cerevisiae* 80S ribosome and the *T. thermophila* 60S subunit revealed that the rRNA structure of the PTC is nearly superimposable between the eukaryotic and bacterial ribosomes. Following GTP hydrolysis eEF1A is released from the ribosome in a GDP-bound state. The spontaneous rate of GDP dissociation from these factors is slow, and the GEF eEF1B is required to recycle the inactive GDP-bound factor to its active GTP-bound state (Dever and Green 2012).

Following peptide bond formation, a ratchet-like mechanism of the ribosomal subunits occurs, whereby the two subunits move independently of one another in a 3' direction along the mRNA molecule. This triggers movement of the tRNAs into the so-called hybrid P/E and A/P states, with the acceptor ends of the tRNAs in the E and P-sites and the anticodon loops remaining in the P and A sites, respectively. Full translocation of the tRNAs to the E and P sites requires the eEF2. Binding of the GTP-bound eEF2 is thought to stabilize the hybrid state and promote rapid hydrolysis of GTP. This results in conformational changes in eEF2 and this, with P_i release, is thought to 'unlock' the ribosome from the original codon on the mRNA, allowing tRNA and mRNA movement and then 'lock' the subunits in the post-translocation state. P_i release is also coupled to release of the factor from the ribosome. In the post-translocation state, a deacylated tRNA occupies the E site of the ribosome and the peptidyl-tRNA occupies the P site. The A site is vacant and available for binding of the next AA-tRNA in complex with eEF1A. Release of the deacylated tRNA is thought to be coupled to the binding of the next AA-tRNA in the A site (Dever and Green 2012).

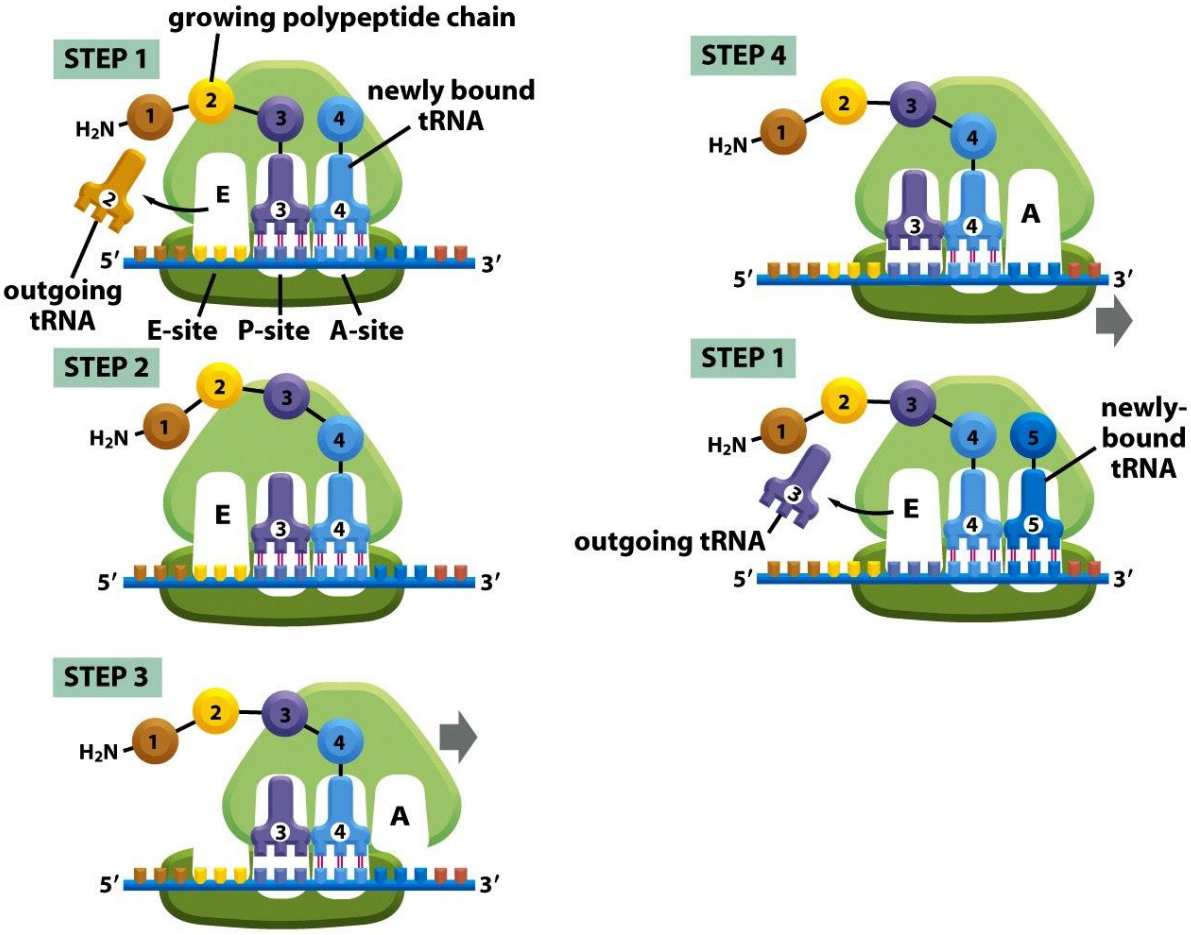


Figure 5 Schematic of translating an mRNA molecule. In step 1, an aminoacyl-tRNA (AA-tRNA) molecule binds in the vacant A site, and a deacylated tRNA molecule dissociates from the E site. In step 2, a new peptide bond is formed between the AA-tRNAs in the P site and the A site. In step 3, the large subunit translocates relative to the small subunit along the mRNA, leaving the two tRNAs in a hybrid state: P site on the large subunit but A site on the small subunit for one, and E site on the large subunit but P site on the small subunit for the other. In step 4, the small subunit translocates along the mRNA and catches up to the large subunit. This translocation travels the ribosome a total of three nucleotides in the 3' direction along the mRNA, leaving a new codon in the vacant A site, allowing the process to repeat again. (Alberts 2007)

Termination

Translation termination occurs when a stop codon (UAA, UGA or UAG) on the mRNA is reached. As the ribosome moves along the mRNA, one of these stop codons will eventually occupy the A site, and this causes translation to stop and the dissociation of the 80S ribosome from the mRNA. Termination in eukaryotes is catalysed by two protein factors, eRF1 and eRF3. eRF1 is responsible for high-fidelity stop codon recognition and peptidyl-tRNA hydrolysis. eRF1 is a tRNA-shaped protein composed of three domains. The amino-terminal domain is thought to be responsible for codon recognition and contains a distal loop with a highly conserved NIKS motif that has been proposed to decode stop codons through codon:anticodon-like interactions. The middle (M) domain of eRF1 is functionally analogous to the tRNA acceptor stem and as such extends into the PTC and is thought to promote peptide release. The carboxyl terminus of eRF1 is involved in facilitating interactions with eRF3. eRF3 itself has a variable amino terminus but a relatively conserved carboxyl terminus that is directly involved in interactions with the M and C domains of eRF1 (Dever and Green 2012)

eRF3 both facilitates peptide release and increases termination efficiency at stop codons in a GTP-dependent manner. Dissociation of GTP from eRF3 is slowed by eRF1 binding off the ribosome and as such eRF1 has been proposed to play the role of a GTP dissociation inhibitor. The ternary complex of eRF1-eRF3-GTP then engages the ribosome, triggering GTP hydrolysis, ultimately leading to the deposition of the M domain of eRF1 in the PTC. In this scenario, eRF3 is playing a role similar to that of EF-Tu (the bacterial eIF1A orthologue to which it is closely related) in controlling delivery of a tRNA-like molecule into the PTC. (Dever and Green 2012).

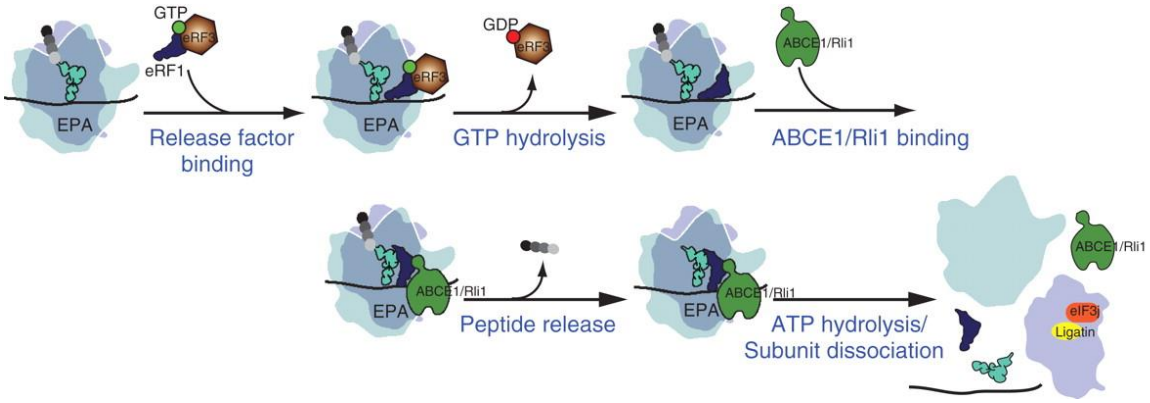


Figure 6 Schematic of the eukaryotic translation elongation pathway. On recognition of a stop codon, the eRF1-eRF3-GTP ternary complex binds to the A site of the ribosome, GTP hydrolysis occurs, and eRF3 is released. ABCE1/Rli1 binds and facilitates the accommodation of eRF1 into an optimally active configuration. (Dever and Green 2012).

1.3. Ribosomal maturation

The production of ribosomes takes up a vast portion of a cells energy. It has been estimated that in a rapidly growing yeast cell, the majority of transcription is devoted to ribosomal RNA (rRNA) and about half of RNA polymerase II transcription to ribosomal proteins (r-proteins) (Robledo, Idol et al. 2008). Eukaryotic ribosome maturation is a highly complex and concerted process that requires the amalgamated action of several accessory proteins, called trans-acting factors. These are non-ribosomal factors that associate transiently with the precursor ribosome in the maturation process, but are not ultimately part of the mature ribosome particle. Ribosome biogenesis consumes a vast portion of the cells energy and occupies considerable nuclear space before its final maturation in the cytoplasm, reflecting its criticality for cell homeostasis (Henras, Plisson-Chastang et al. 2015).

1.3.1. Nucleolar ribosome biogenesis and nuclear export

Eukaryotic ribosome biogenesis begins in the nucleolus, where ribosomal DNA (rDNA) is transcribed into rRNA, which undergoes co-transcriptional folding and modifications, and amalgamation with ribosomal proteins (r-proteins). In contrast to bacterial ribosome biogenesis, which requires as little as ~25 accessory proteins, eukaryotic ribosome biogenesis requires the amalgamated action of over ~80 r-proteins, 150 other proteins and 70 snoRNAs (Robledo, Idol et al. 2008).

The 40S subunit (40S) is made from the 18S rRNA assembled with 33 r-proteins (RPSs) and the 60S subunit is made from three rRNA molecules (5S, 5.8S, and 25S/28S rRNAs (25S in yeast, 28S in mammals)) associated with 46 r-proteins (RPLs). The 18S, 5.8S, and 25S/28S rRNAs are produced as a long pre-rRNA molecule, called the 35S rRNA in yeast and the 47S rRNA in humans, which is transcribed by RNA polymerase I (Pol I). This pre-rRNA also contains an externally transcribed spacer (ETS) and two internally transcribed spacers (ITS1 and ITS2). The 5S rRNA is transcribed independently by RNA polymerase III (Pol III) (Bashan and Yonath 2008, Steitz 2008). The pre-rRNA assembles, co-transcriptionally, with accessory factors and a subset of r-proteins. This facilitates the formation of a secondary structure necessary for the correct folding, modification and cleavage of pre-rRNA (Greber 2016).

The nascent 35S transcript assembles with the U3 small nucleolar ribonucleoprotein (U3 snoRNP), additional box C/D and H/ACA snoRNPs, 40S subunit assembly factors, and early-

binding ribosomal proteins to produce the first pre-ribosomal particle, which is termed the SSU processome, and sediments at 90S (Greber 2016).

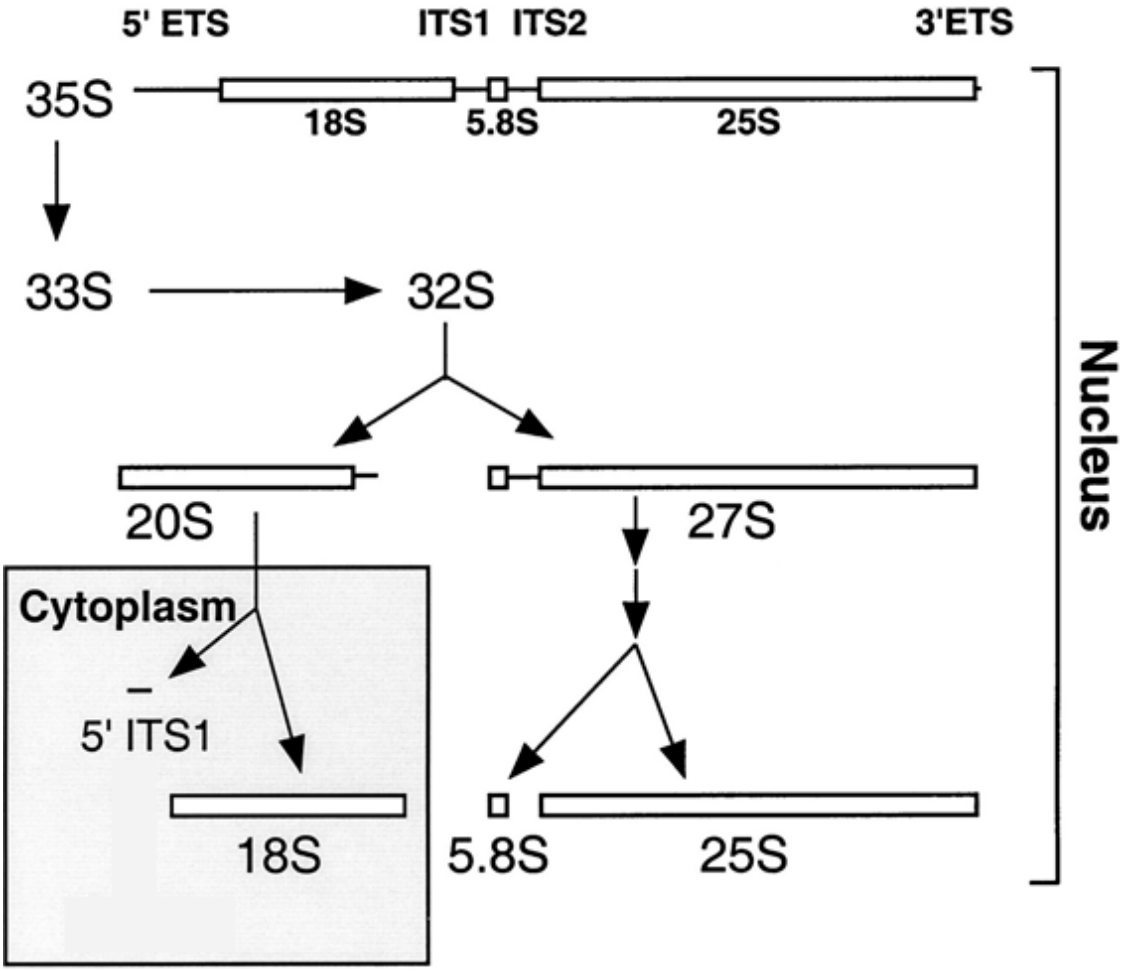


Figure 7 Diagram of nuclear rRNA processing in *S. cerevisiae*. 18S, 5.8S, and 25S rRNAs are transcribed as a 35S pre-rRNA in the nucleolus. The mature forms of the rRNAs are depicted as open bars and the external transcribed spacers (ETSs) and ITSs are depicted as lines. The series of endonucleolytic changes are depicted in sequence to generate the pre-40S and pre-60S partciles. Adapted from (Steitz 2008).

The resultant rRNA-protein assemblage is known as the 90S particle, which was first described in the early 1970s by Planta and Warner. They identified this as the main pre-ribosomal rRNA molecule in yeast that is transported from the nucleolus to the nucleoplasm for processing (Trapman, Retel et al. 1975). Internally and extrernally transcribed spacers (ETS/ITS) are removed during this process through a series of endonucleolytic and exonucleolytic cleavages. The U3 snoRNP in the SSU processome is important for pre-rRNA cleavage at site A_2 in the internal transcribed spacer 1 (ITS1). This occurs co-transcriptionally in yeast. A_2-cleavage leads to the 90S particle being broken down into smaller rRNA molecules – the 66S (20S rRNA) and 43S (27S rRNA) particles – the precursors for the two ribosomal subunits (Trapman, Retel et al. 1975). Cleavage of the ITS1 spacer releases the 18S rRNA from the 35S rRNA, leaving the 5.8S and 25S/28S rRNA joined. The biogenesis pathways of the two ribosomal subunits diverge from this point on, and the pre-ribosomes are then actively exported to the cytoplasm (Steitz 2008, Panse and Johnson 2010). Additionally, several pre-rRNA cleavage steps, including the removal of ITS2, which is inserted between the sequences for the mature 25S and 5.8S rRNAs in the 27S pre-rRNA species, are required to generate the mature large subunit rRNAs.

While the nascent 40S subunits are rapidly exported to the cytoplasm, the biogenesis of the 60S ribosomal subunit progresses through several nucleolar and nucleoplasmic assembly and maturation steps that give rise to defined pre-ribosomal particles. These are characterized by the arrival and departure of certain sets of assembly factors and energy-consuming enzymes as well as the accompanying structural transitions of the nascent 60S particle (Greber 2016).

Perturbations in the rRNA processing pathway can lead to various phenotypes. Depletion of specific r-proteins can stall rRNA processing at specific points, with different r-protins resulting in different processing defects. Approximately half of r-proteins from the 40S ribosomal subunit, including RPS24 and RPS7, associate with the 5’ end of the nascent pre-rRNA and are required for the initiation of cleavages at the 5’ETS and ITS1. The other half of r-proteins, which includes RPS19 and RPS17, is not required for 5’ETS removal but is necessary for ITS1 cleavage. Correspondingly, depletion of RPS24 or RPS7 in yeast and human cells results in the failure of maturation of the 5’ end of 18S rRNA, whereas, in the absence of RPS19 or RPS17, the 3’ end of the 18S rRNA cannot mature. In all cases, pre-40S particles that contain non-cleaved pre-rRNA cannot be exported and accumulate in the nucleus. Similarly, deficiency of most r-proteins that are mutated in DBA, both from the small and the large ribosomal subunits, affects pre-rRNA processing in a unique way, leading to the accumulation of different

rRNA precursors and disruption of ribosome biogenesis at different steps (Robledo, Idol et al. 2008, Danilova and Gazda 2015)

Human rRNA processing differs slightly from that of yeast. Unique strategies are adopted by human cells and distinct *trans*-acting factors are recruited to carry out essential processing steps. These differences have implications for understanding ribosomopathies at the molecular level and developing effective therapeutic agents. A study conducted in HeLa cells found 286 proteins that are required for rRNA processing, and of these proteins 153 have a yeast homolog known to be a ribosome biogenesis factor, 59 have a yeast homolog not directly linked to ribosome synthesis, and 74 have no obvious yeast homolog. Approximately 73% (83 genes) of the human proteins have a function similar to that of their yeast homolog, while the rest have either additional (13.5%) or alternative (13.5%) functions. Strikingly, many of the human genes (109/286 genes, 38%) identified in the screen as ribosome assembly factors are also known disease biomarkers, notably in cancer (Tafforeau, Zorbas et al. 2013). Nuclear export of pre-ribosomal subunits is conducted through the nuclear pore complex (NPC). *In vivo* export assay using large and small subunit reporters (Rpl25-GFP and Rps2-GFP, respectively) revealed various export factors that are needed for export of both subunits. Although the small and large subunit are exported independently of each other, they both require an export receptor known as CRM1 that directly recognises nuclear export signals (NES) on cargo molecules (Panse and Johnson 2010). The pre-60S subunit has only one known Crm1 adaptor, called Nmd3, whereas the pre-40S subunit has up to three NES-containing trans-acting factors; Ltv1, DIM2 and RIO2 (Seiser, Sundberg et al. 2006, Zemp, Wild et al. 2009). Ltv1 has been shown to be non-essential for nuclear export of the pre-40S subunit, suggesting redundancy in the 40S export factors. The pre-60S employs additional export molecules that interact directly with the NPC to facilitate export. This may be required due to the larger size of the pre-60S subunit, as it is known that efficient transport of larger cargo molecules requires multiple receptors (Ribbeck and Gorlich 2002). These adaptors for pre-60S export include the trans-acting factor Arx1 and the export factor Mtr2-Mex67 (Bradatsch, Katahira et al. 2007, Yao, Roser et al. 2007).

1.3.2. Cytoplasmic maturation of the 40S subunit

The pre-40S subunit is accompanied into the cytoplasm by several r-proteins that either have export function or function in later steps of maturation. It is thought that the pre-40S particle is converted into a functional subunit relatively quickly, as detection of intermediates have been challenging. It is thought that the cytoplasmic steps of maturation of the 40S subunit can be broken down into two stages; 1) a conformational rearrangement that forms a 'beak'

structure, and 2) a final endonucleolytic cleavage to yield the mature 18S rRNA. Details of this process will not be discussed here, as more focus will be given to the more relevant 60S subunit.

1.3.3. Cytoplasmic maturation of the 60S subunit

The large subunit harbors a number of important functional centers, including the polypeptide exit tunnel, which provides the exit path for the newly synthesized protein, a binding platform for nascent chain targeting, processing, and folding factors at the exit of the tunnel and the GTPase-activating centre between the P-stalk and the sarcin-ricin loop (SRL), where translational GTPases are recruited and activated. The L1 stalk and the 5S rRNA-containing central protuberance (CP) are additional landmark features of the 60S subunit (Figure 8) (Greber 2016).

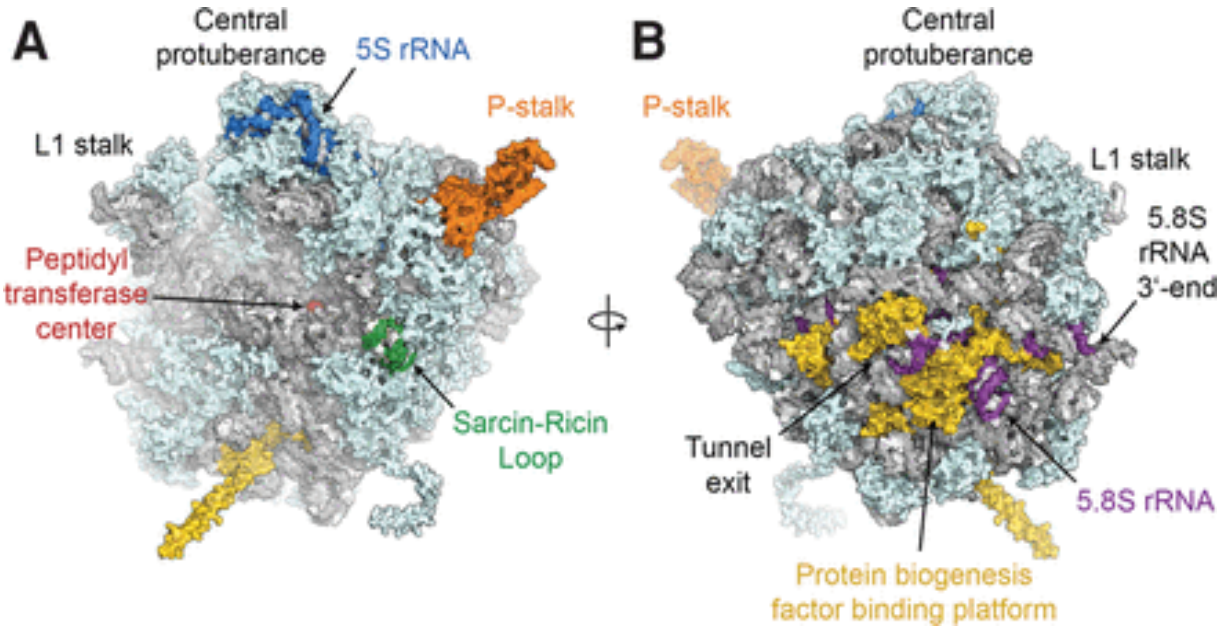


Figure 8 Structure of the yeast 60S ribosomal subunit. *A.* View of the 60S subunit from the interface side. *B.* View of the 60S subunit from the solvent side. Structural and functional hallmarks of the 60S subunit discussed in the text are colored: blue – 5S rRNA, orange – P-stalk, green – Sarcin-Ricin Loop, purple, 5.8S rRNA, yellow – protein biogenesis factor binding platform, red – peptidyl-tramnsferase centre. (Greber 2016)

While the high-resolution structures of the 40S and 60S subunits as well as the 80S ribosome of both lower and higher eukaryotes have provided detailed insight into the molecular

architecture of eukaryotic ribosomes, much remains to be learned about how these particles are made. Ribosome assembly has been investigated extensively in yeast as well as in the human system. Many aspects of human ribosome biogenesis are conserved in yeast, and therefore yeast have served as a model system in which much of the research on ribosome biogenesis has been conducted.

Cytoplasmic maturation of the pre-60S particle is extensive, with the trans-acting factors it acquires in the nucleolus and nucleoplasm are released by specialised cytoplasmic trans-acting factors at distinct stages. The first such stage, upon arrival into the cytoplasm, involves the AAA-ATPase Drg1, which is thought to release Rlp24 from the pre-60S particle. This allows Rpl24, an r-protein that is closely related to Rlp24, to bind to the site previously occupied by the latter. Rpl24 then recruits the zinc-finger protein Rei1, which acts to release Arx1. Based on the sequence and structural similarities between Arx1 and methionyl amino peptidases it is predicted that they bind to the same site on the ribosome. Methionyl amino peptidases are a family of proteins that remove the N-terminal methionine residue from nascent peptide chains in the mature ribosome, and are crucial for proper translation. It is also known that Arx1 binds in close proximity to Rpl25, which is located near the exit tunnel on the ribosome, adding weight to the hypothesis that methionyl amino peptidase bind to the Arx1 site when it is vacated, bringing the pre-60S particle one step closer to its mature state (Panse and Johnson 2010).

The pre-60S particle also contains the trans-acting factor Tif6 upon entering the cytoplasm. This protein is required for the export of the 60S subunit from the nucleus into the cytoplasm. It also acts as an anti-association factor, bound to the pre-60S particle at the 40S-60S interface, preventing the premature joining of the two subunits. More specifically, Tif6 is bound to the intersubunit bridge B6 and makes contact with the sarcin-ricin loop (SRL), Rpl23 and Rpl24 (see Figure 9c). The yeast GTPase Elongation factor-like 1 (Efl1) and Sdo1 are required to release Tif6 before the two subunits can join to make a fully functional ribosome (Panse and Johnson 2010). Tif6 is then recycled back to the nucleus to take part in further export of pre-60S subunits. Deletion of *Efl-1* in yeast results in severe growth defects and reduction of cytoplasmic 60S subunits (Senger, Lafontaine et al. 2001, Menne, Goyenechea et al. 2007). In mammals, this process is largely the same as in yeast. The anti-association factor eIF6 (orthologue of Tif6) is removed from the B6 intersubunit bridge of the pre-60S subunit by the GTPase EFL1 (orthologue of Efl1) and Shwachman-Bodian-Diamond Syndrome (SBDS (orthologue of Sdo1)). However, eIF6 is not required for the export of the pre-60S particle

from the nucleus to the cytoplasm in mammals. The release of eIF6 is discussed in more detail in 1.3.4.

The pre-60S particle is also exported to the cytoplasm with the nuclear export adaptor Nmd3. This must be removed and recycled to the nucleus for further rRNA export. This is achieved by the cytoplasmic GTPase Lsg1 and Rpl10. It is thought that Lsg1 induces conformational changes in Rpl10 that stabilises its place in the pre-60S subunit, which in turn triggers Nmd3 release (Panse and Johnson 2010). Rpl10 has recently been shown to be involved in quality control of the ribosome, and has also been implicated in the release of Tif6 in yeast (Bussiere, Hashem et al. 2012). Another protein involved in Nmd3 recycling in yeast is Sqt1, which forms a complex with free Rpl10 and may serve as an Rpl10 chaperone required for loading of Rpl10 onto the subunit. A dominant *Lsg1* mutation leads to accumulation of Sqt1 on pre-60S particles, indicating that the presence of Lsg1 is necessary for correct loading of Rpl10 onto the subunit and subsequent release of Sqt1. Thus, Nmd3 release seems to be coupled directly to loading of Rpl10 onto the maturing 60S subunit (Zemp and Kutay 2007).

The assembly of the ribosomal stalk is one of the last processing events in the cytoplasm. The ribosomal stalk is required for recruitment of translation factors, such as elongation factors, and is therefore essential for ribosome functionality. The stalk consists of three proteins; P0 and the heterodimer P1 and P2. When the pre-60S particle enters the cytoplasm, Mrt4 is in place of P0, preventing stalk assembly. The removal of Mrt4 is thought to require the protein Yvh1, which, in a series of linear events, binds to the pre-60S particle causing the removal of Mrt4. This then allows P0 to load onto the pre-60S particle, at which point Yvh1 is released (Panse and Johnson 2010). Tif6 becomes mislocalised to the cytoplasm in Yvh1 mutants in which stalk assembly is prevented. This suggests a role for stalk assembly in the release of Tif6.

All of these processes are essential for ribosome functionality, and mutations in any of the required trans-acting factors can potentially have an effect on the maturation of the ribosome, and therefore translation. Out of all there-proteins required for ribosome biogenesis (~80), only a few are dispensable, including RPS25 (Rps25p in yeast) and RPL26 (Rpl26p in yeast). Mutations in the majority of r-proteins, however, result in a group of extremely varied diseases called ribosomopathies (discussed in 1.3.5) (Henras, Plisson-Chastang et al. 2015).

1.3.4. Mechanism of release of eIF6 (Tif6) from the pre-60S subunit

The mechanism of eIF6 release has been pieced together by many researchers. However, none show the mechanism as clearly as the recent single-particle cryo-EM structures obtained by Weis et al in 2015, using *Dictyostelium discoidium* 60S subunits, with and without endogenous eIF6 bound, and human SBDS and EFL1 proteins. The high conservation of the 60S subunit and its associated protein factors allows for inter-species substitution in these pathways, meaning that human SBDS and EFL1 can be combined with *Dictyostelium* (or other species) 60S subunits and still retain their functionality, and vice versa.

As mentioned above, Sdo1 (SBDS) and Efl1 (EFL1) work cooperatively to release Tif6 (eIF6) from the intersubunit face of the 60S ribosomal subunit. X-ray crystallography and solution NMR spectroscopy have revealed the conserved tripartite architecture of the SBDS protein. SBDS comprises three domains; domain I is comprised of a FYSH domain (residues 2–96), domain II is comprised of residues D97–A170 and domain III is comprised of residues H171–E250 (see Figure 11). Domain I of SBDS has been shown to interact with rRNA (de Oliveira, Sforca et al. 2010). Interestingly, there is a ferredoxin-like fold in domain III of SBDS that is most closely related to domain V of EF-2, and is also found in EFL1. EFL1 is homologous to the ribosomal translocase EF-G in prokaryotes and to elongation factor 2 (eEF-2) in eukaryotes, and like eEF-2 and other GTPases, has a five-domain structure. Domain I of EFL1 contains the G1–G5 motifs seen in other GTPases that bind and hydrolyse GTP (Weis, Giudice et al. 2015). The presence of an insertion of variable length within domain II distinguishes EFL1 from other ribosomal translocases, such as eEF-2, however this appears to be dispensable for EFL1 function (Weis, Giudice et al. 2015).

3D cryo-EM maps of the 60S–eIF6–SBDS complex, at 3.3-Å resolution (Figure 9a), show that SBDS domain I occupies the P site of the 60S ribosomal subunit, sitting between the P loop (helix 80), helix 69 and the conserved internal loop of Rpl10 (known as the P-site loop). Rpl10, as mentioned above, is required for the release of export adapter Nmd3 from the pre-60S subunit. Rpl10 (L16 in bacteria) has been shown to reside in a cleft between the central protuberance and the P0/P1/P2 ribosomal stalk (L10/L7/L12 in bacteria). High-resolution crystal structures of the bacterial ribosome show that L16 has a loop that extends towards the P-site of the 60S subunit, together with bacterial protein L27, and makes contact with the P-site tRNA. Archaeons and eukaryotes do not have an orthologue of L27, but instead have an extended Rpl10 loop. Cryo-EM studies have shown the Rpl10 loop makes contact with the acceptor stem of tRNA molecules in the P-site (Armache, Jarasch et al. 2010). Crystal structures show that one side of the β-hairpin loop of Rpl10 (residue R98) is likely to make

electrostatic interactions with helix 39 of the 60S subunit. On the other side of this hairpin loop, residue Q123 lies in proximity to domain I of SBDS (Figure 9d), suggesting that the interaction of SBDS with the 60S subunit may be linked to Rpl10's position. Residues 2-15 of SBDS domain I interact with the peptidyl transferase centre (the 6 N-terminal residues at the entrance of the peptide exit tunnel) (Figure 9b). SBDS domain III contacts the SRL and the P-stalk base (P0) (Figure 9c-e), as do eEF-2 and EF-G when bound to the 60S subunit. This data suggests that SBDS is shielding the critical catalytic components of the 60S subunit from premature association with translational GTPases (Weis, Giudice et al. 2015).

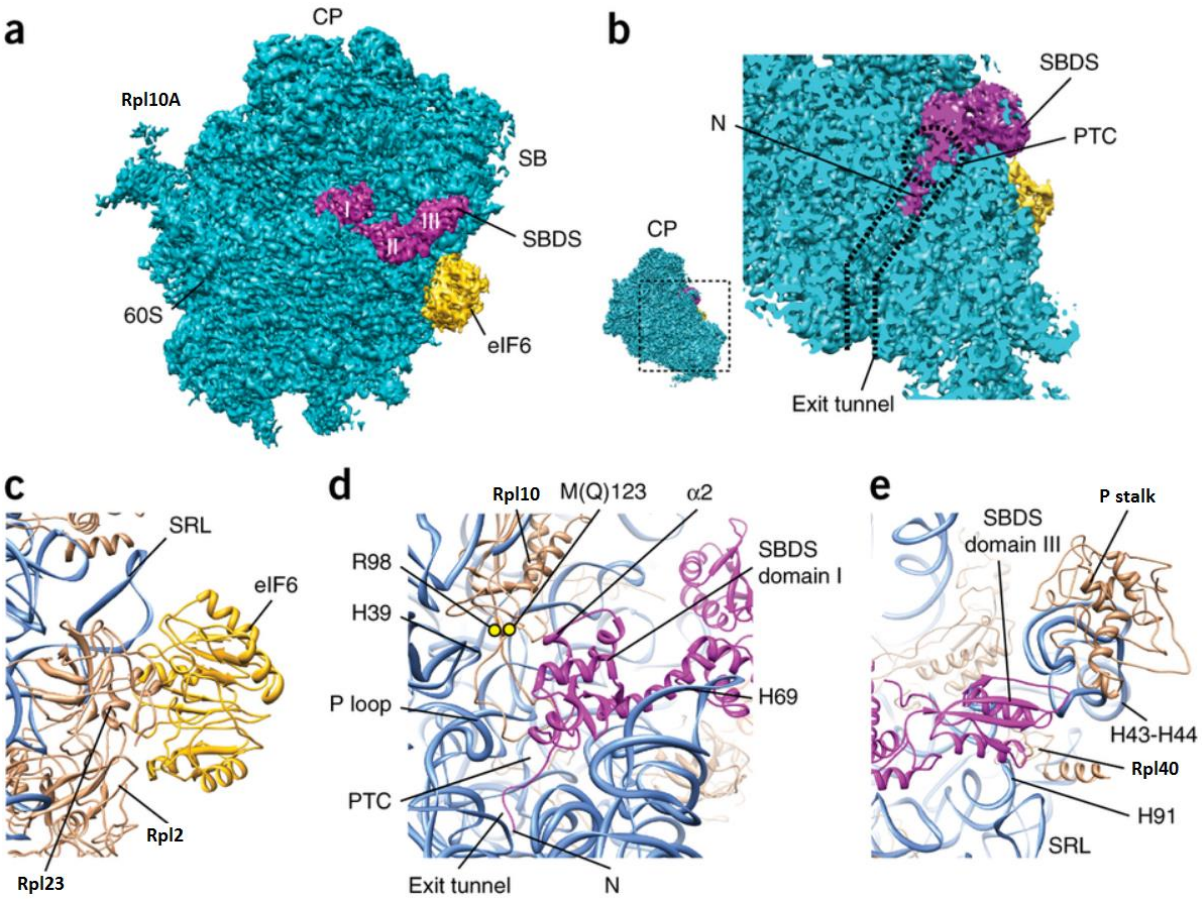


Figure 9 Cryo-EM maps of 60S-SBDS-eIF6 complexes. **(a,b)** Crown view **(a)** and transverse section **(b)** of the cryo-EM map of the 60S–eIF6–SBDS complex, filtered to 4 Å. The 60S ribosomal subunit is shown in cyan, eIF6 in yellow and SBDS in magenta. CP, central protuberance; SB, stalk base; PTC, peptidyl transferase centre; N, N terminus. **(c–e)** Atomic models of the interface between the 60S ribosomal subunit and eIF6 **(c)**, SBDS domain I **(d)** and SBDS domain III **(e)**. 26S rRNA is shown in blue, ribosomal proteins in beige, eIF6 in yellow and SBDS in magenta. Residues R98 and M123 (Q123 in humans) of human RPL10 that are mutated in T-ALL are indicated. SRL, sarcin-ricin loop. R-protein name shown are for *Dictyostelium discoidium.* Adapted from (Weiss, Mason et al. 2012)

It is thought that there is no direct contact between SBDS and eIF6 on the surface of the 60S subunit, and there is now evidence to suggest that EFL1 acts as a bridge between the two, relaying structural changes in a three-way conformational switch. Like its homologue EF-2, EFL1 occupies the canonical GTPase centre on the 60S subunit, which as mentioned above is in close proximity to the binding site of SBDS. Cryo-EM maps of complexes containing 60S, SBDS and EFL1, with and without eIF6, with an overall resolution of 4-2-4.3Å, show the positions of these proteins on the 60S surface. It was found that EFL1 adopts two conformations. Firstly, an initial conformation in the 60S-eIF6-SBDS-EFL1 complex with 13.5% of the buried surface area of EFL1 making contact with rRNA, and the remainder binding SBDS (33%), eIF6 (40%) and the ribosomal stalks proteins P0 and P2 (1.5% and 12%, respectively). The second conformation has been termed the 'accommodated' conformation, in reference to EFL1 undergoing a conformational change upon recognition of a cognate (in this case its binding site on the 60S subunit near the SRL) and securing a stronger interaction on the subunit. The 'accommodated' conformation is achieved by an 'arc-like' large-scale domain rotation of domains I and II, and domain IV pivoting around the relatively fixed axis of domains III and V. This results in EFL1 occupying a position in the 60S-SBDS-EFL1 complex, with eIF6 being released. In this 'accommodated' state, EFL has more extensive interactions with the rRNA (24% of the buried surface area of EFL1), ribosomal proteins (34%) and SBDS (42%). The release of eIF6 is caused by EFL1 outcompeting eIF6 for an overlapping binding site on the SRL of the 60S subunit during the 'accommodation', as in the 'accommodated' state, simultaneous EFL1 and eIF6 binding is incompatible (Weis, Giudice et al. 2015).

Upon EFL1 binding SBDS undergoes dynamic domain rotations, and therefore also exists in two conformations: 'open' and 'closed'. Without EFL1 bound to the 60S, SBDS exists in the 'closed' conformation. Upon EFL1 binding, SBDS domain III undergoes a 180° rotation, away from the P stalk and towards helix 69. Domain II also undergoes a smaller rotation of 60°, pivoting about the N terminus of helix α5. The resultant conformation is called the 'open' conformation and displacement of domain III from the P stalk site allows EFL1 to bind to the 60S subunit. These overlapping binding sites of SBDS and EFL1 explain the structural homology between EFL1 domain V and the ferrodoxin-like domain in domain III of SBDS (Weis, Giudice et al. 2015). The common binding site in the proximity of the P stalk may explain why Yvh1 mutants, which are defective in stalk assembly, have Tif6 release impairment (as mentioned in 1.3.3) (Panse and Johnson 2010).

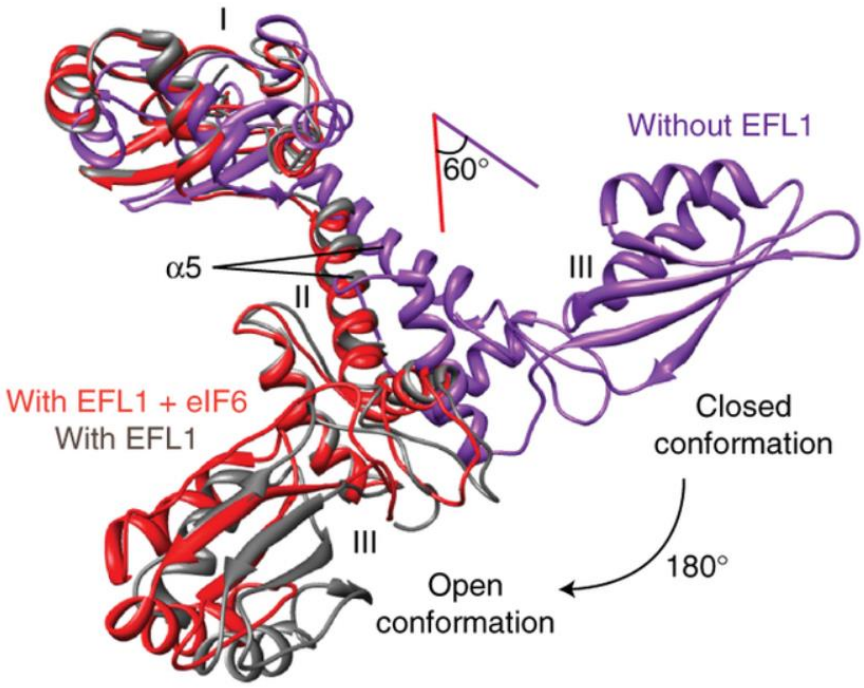


Figure 10 Dynamic rotation of domains I and III of SBDS. Upon EFL1 binding domain III of SBDS rotates 180°, away from the P stalk and towards helix 69 of the 60S subunit. Domain I simultaneously rotates 60°, pivoting around the N terminus of helix α5 of SBDS. This structural rearrangement from the 'closed' to the 'open' conformation results in EFL1 binding to the 60S subunit, which consequently allows the accommodation of EFL1 and the outcompeting of eIF6 from the binding site near the SRL (Weis, Giudice et al. 2015).

In summary, these cryo-EM maps provide a comprehensive view of the release mechanism of eIF6, and the authors propose the following sequence of events. Firstly, EFL1 binds to the GTPase centre, in direct contact with SBDS and eIF6, in a low-affinity, GTP-bound state. Competition with SBDS for an overlapping binding site by EFL1 domain V triggers a 180° rotational displacement of SBDS domain III away from the P-stalk base (closed state) toward helix 69 (open state). The resultant conformation of SBDS is likely to be stabilized by interactions between residues K151 and R218 and helix 69 of the 60S subunit. In the open state, SBDS then drives GTP-bound EFL1 toward an active, high-affinity ('accommodated') SRL-bound conformation that effectively competes with eIF6 for an overlapping binding site on the SRL and promotes eIF6 displacement from the 60S subunit (Weis, Giudice et al. 2015).

The exact role of GTP hydrolysis by EFL1, and its timing in this mechanism, is yet to be confirmed. However, it is hypothesised that the interaction of EFL1 with the SRL promotes GTP hydrolysis, causing a shift of EFL1 from a high- to a low-affinity conformation. This weakened affinity for the ribosome subsequently promotes dissociation of both EFL1 and SBDS from the 60S subunit (Weis, Giudice et al. 2015). It has also been suggested that SBDS acts as a guanine-nucleotide exchange factor (GEF), stabilising the GTP-bound form of EFL1 (Gijsbers, Garcia-Marquez et al. 2013).

1.3.5. Energy consumption in ribosome biogenesis

Among the non-ribosomal factors involved in ribosome biogenesis are several ATP- or GTP-consuming enzymes; DExD/H-box ATPases, GTPases, AAA-ATPases, kinases and ABC proteins. These enzymes provide energy to drive ribosome biogenesis in one direction. While DExD/H-box proteins are involved in early stages of rRNA processing, AAA-ATPases and GTPases act predominantly at later stages. The DExD/H-box proteins act as energy-consuming chaperones that aid the folding of rRNA and RNP structures. They are also involved in the biogenesis of the pre-40S and 60S subunits, predominantly by remodelling RNA:RNA, RNA:protein and protein:protein interactions. The general function of DExD/H-box proteins in ribosome biogenesis is to promote structural rearrangements, presumable by rejecting unfavourable substrates and promoting correct conformations which may be further stabilised by downstream factors. This is an energy-requiring stabilisation of intermediates that is crucial for correct timing of ribosome biogenesis (Kressler, Hurt et al. 2010).

AAA-ATPases are required for the release of non-ribosomal factors during ribosome biogenesis. Three AAA-ATPases are essential for 60S biogenesis; Rix7, Rea1 and Drg1. As mentioned above Drg1 is required for the release of Rlp24, and subsequently Arx1. Rix7 is

required for Nsa1 in the nucleus, prior to nuclear export. Rea 1 is required for 60S subunit formation and ITS2 processing. All of these enzymes are essential for proper 60S formation, and mutants in these genes shown severe accumulations of later factors due to their not being released (Kressler, Hurt et al. 2010).

GTPases are key regulators of many cellular processes. To date, 6 GTPases have been identified as required for ribosome biogenesis; Bms1, Efl1, Lsg1, Nog1, Nog2, Nug1. Bms1 is essential for 40S biogenesis by mediating the incorporation of Rcl1 into 90S particles. The other five GTPases are involved in different aspects of ribosome biogenesis. Efl1 is involved in the release of Tif6 (see 1.3.4). Nog1 interacts with Rlp24, and directly after export, both Nog1 and Rlp245 are released from the pre-60S subunit in a Drg1-dependent manner. However, it is still not clear what the role of Nog1 is in this stage of ribosome biogenesis. Nog2, Nug1 and Lsg1 belong to a specific group of GTPases, called circularly permutated GTPases (cpGTPases). These are required for the incorporation of various r-proteins, and mutations that disrupt the GTPase activity of these enzymes result in biogenesis defects in yeast (Kressler, Hurt et al. 2010).

In conclusion, energy is a crucial part of ribosome biogenesis. These energy-consuming enzymes are critical for the forward directionality if ribosome biogenesis, and mutations in these enzymes often result in biogenesis defects.

1.4. Ribosomopathies

Ribosomopathies account for a growing plethora of human pathologies. There currently 19 ribosomopathies defined, however new revelations may encumber reclassification of known disorders to ribosomopathies, and so the group of diseases continues to grow. It is perhaps unsurprising given the number of trans-acting factors involved in ribosomal maturation, and the complexity of the process, that consequences of defects in this pathway can result in extremely varied disorders. Ribosomopathy is an umbrella-term given to any disease associated with defects in ribosome production. All aspects of cell growth require protein synthesis, and therefore deficits in this process would be expected to have wide-spread, systemic effects with reduced growth and proliferative capacity. This is typified by the *Drosophila minutes*, originally identified by their small size, which are now known to harbour mutations in genes encoding r-proteins (Marygold, Roote et al. 2007).

The majority of these diseases are inherited through mutations in genes affecting ribosome biogenesis, such as Diamond-Blackfan Anaemia (DBA), Shwachman-Diamond Syndrome (SDS) and Treacher Collins Syndrome (TCS). However, the ribosomopathy 5q-syndrome, a sub-type of myelodysplastic syndrome, is a result of acquired somatic deletion of the 5q chromosome. Some of these diseases are discussed below, and they can also be found in Table 2.

Ribosomopathies are infamous for their clinical heterogeneity, varying greatly in severity and clinical features. However, some symptoms are common to most, if not all. One such symptom is cytopenia, with the majority of ribosomopathies resulting in anaemias of the blood, such as neutropenia, thrombocytopenia or erythroblastopenia. Additionally, many ribosomopathies are cancer predisposition syndromes, most frequently haematological malignancies, but solid tumours have also been reported (Tourlakis, Zhang et al. 2015). It is also worth noting that r-protein mutations have been found in cancer cell lines, providing a link between ribosome biogenesis and cancer. Bone marrow failure syndromes and craniofacial or other skeletal defects are also common symptoms of ribosomopathies (Narla and Ebert 2010). Short stature is also a common feature due to delayed growth (Armistead and Triggs-Raine 2014).

Table 2 Summary of known and suspected ribosomopathies with details about clinical characteristics, cancer risk, and diagnosis. (Narla and Ebert 2010).

Disease	Gene Defect	Clinical Features	Cancer Risk	Diagnosis
Diamond Blackfan anemia	RPS19, RPS24, RPS17, RPL35A, RPL5, RPL11, RPS7, RPL36, RPS15, RPS27A	Macrocytic anemia Short stature Craniofacial defects Thumb abnormalities	?osteosarcoma ?MDS	RPS19/RPS24 Sequencing Elevated ADA Elevated Hgb F levels
5q-syndrome	RPS14	Macrocytic anemia Hypolobulated micromegakaryocytes	10% progression to AML	Bone marrow aspiration/biopsy with karyotype
Shwachman-Diamond syndrome	SBDS	Neutropenia/infections Pancreatic insufficiency Short stature	MDS and AML	SBDS gene testing
X-linked dyskeratosis congenita	DKC1	Cytopenias Skin hyperpigmentation Nail dystrophy Oral leukoplakia	AML Head+neck tumors	Telomere length analysis
Cartilage hair hypoplasia	RMRP	Hypoplastic anemia Short limbed dwarfism Hypoplastic hair	Non-Hodgkin lymphoma Basal cell carcinoma	RMRP sequencing
Treacher Collins syndrome	TCOF1	Craniofacial abnormalities	None reported	Physical exam (imaging if needed)

1.4.1. Diamond-Blackfan Anaemia and 5q syndrome

In 1938, Louis Diamond and Kenneth Blackfan described a congenital anaemia with hypoplasia of red cell precursors in infancy. This syndrome is now known as Diamond Blackfan Anaemia (DBA) and it affects 4-5 cases in 1 million live births, and the male to female ratio is approximately 1-1.3:1 (Handin 2003, Greer 2013). Patients are usually diagnosed in the first year of life, with pallor and lethargy being the most common presenting symptoms. There is often a family history of the disease, and approximately 45% of cases are thought to be autosomal dominant. In 1997, Dahl et al identified a child with DBA with an X:19 chromosomal translocation. This lead to a positon on chromosome 19 being linked to DBA in a proportion of other multiplex families, and positional cloning lead to the discovery that the causative mutation was in *RPS19*, which encodes an r-protein of the 40S subunit (Draptchinskaia, Gustavsson et al. 1999). Subsequently, *RPS19* mutations were discovered in approximately 25% of DBA patients. Since the initial discovery of *RPS19* mutations, many other mutations in ribosomal proteins have been found in DBA patients. Mutations in *RPS19*, *RPS24*, *RPS17*, and *RPL35A* have been identified in approximately one-third of patients with DBA. More recently, Gazda et al identified mutations in *RPL5* and *RPL11* in an additional 11.4% of patients and noted that mutations in *RPL5* were associated with a higher frequency of physical abnormalities, including cleft lip and/or palate, whereas mutations in *RPL11* had more isolated thumb abnormalities compared with patients with mutations in *RPS19*. This may indicate that mutations in different ribosomal protein genes lead to distinct clinical phenotypes. Currently, 50-70% of patients with DBA are known to have mutations in 1 of 10 ribosomal protein genes (Narla and Ebert 2010, Weiss, Mason et al. 2012). RPL5 and RPL11 have also been implicated in p53 stabilisation through binding to MDM2 (see 1.4.10.2 for more details).

Mouse models of DBA have been generated, usually focusing on the *Rps19* gene, as this is the most common genetic abnormality seen in patients. Homozygous *Rps19* deletion is lethal in mice, and heterozygotes do not show a phenotype. *Rps19* knockdowns have been achieved in zebrafish, and these recapitulate the DBA phenotype. One DBA mouse model is the novel *Rps19*^{Dsk} mouse, which recapitulates the DBA phenotype in terms of anaemia and growth retardation (Luft 2010).

5q-syndrome is another ribosomopathy, and its clinical features are often similar to that of DBA. The 5q− syndrome was first described in 1974 by van Den Berghe as refractory anaemia with an interstitial deletion of the long arm of chromosome 5. Patients with the 5q− syndrome are classed as an independent subtype of myelodysplastic syndrome (MDS) patients

in the World Health Organization classification system, in which del(5q) is the sole cytogenetic abnormality. Patients characteristically have a severe macrocytic anaemia, normal or elevated platelet levels and a relatively low rate of progression to acute myeloid leukaemia (AML) compared with other types of MDS. *RPS14* was identified as a causative gene in 5q− syndrome. In patients with the 5q− syndrome, 1 allele of *RPS14* is deleted, and haploinsufficient expression of *RPS14* has been confirmed in patient samples. This may explain the similarity in symptoms with DBA patients. A murine model has been developed for 5q-syndrome, in which deletion of the loci commonly deleted region of the 5q− syndrome, including haploinsufficiency for *Rps14*, recapitulates the macrocytic anaemia seen in patients.

1.4.2. Treacher Collins Syndrome

Treacher Collins Syndrome (TCS) is an autosomal dominant condition that was first descried in 1900 by ophthalmologist Edward Treacher Collins. It has an estimated incidence of 1 case in 50,000 live births. The main symptoms of TCS are craniofacial abnormalities that arise from symmetrically and bilaterally diminished growth of the structures derived from the first and second pharyngeal arch, groove, and pouch. Complications often arise in these patients due to the craniofacial abnormalities, which can include issues with airway, swallowing, brain development, and hearing.

TCOF1 was identified in 1996 as the gene responsible for TCS. *TCOF1* encodes a protein known as TREACLE, which colocalises with upstream binding factor (UBF) and RNA polymerase I (pol I) in the nucleolus and is a constituent of one of the pre-ribosomal ribonucleoprotein (pre-RNP) complexes. It has also been shown that treacle is required for rDNA transcription. There is evidence that Treacle protein is also involved in snoRNA-mediated rRNA methylation of the 18S rRNA. Treacle does this by directly interacting with human NOP56, a component of the ribonucloprotein complex that 2'-O-methylates pre-rRNA during early phases of rRNA processing (Gonzales, Henning et al. 2005, Jones, Lynn et al. 2008).

Tcof1 haploinsufficient mice have been generated and show diminished production of ribosomes and decreased proliferation of both neural ectoderm and neural crest cells, and display craniofacial defects. The craniofacial defects in TCS are highly similar to those seen in some cases of DBA, and there is a suggestion of a ribosomal basis for this pathophysiology. However, there are no haematological abnormalities associated with TCS. This adds another level of complexity to ribosomopathies, and TCS is one of the only ribosomopathies without an associated anaemia of some kind.

p53 has been implicated in the pathogenesis of TCS. It has been shown that neural crest cells from *Tcof1* haploinsufficient mice have elevated levels of p53 activation and cell cycle arrest. In addition to these findings, inhibition of p53 has been shown to rescue the craniofacial abnormalities seen in *Tcof1* haploinsufficient mice, and reduce apoptosis in the neuroepithelial cells (Jones, Lynn et al. 2008)

1.4.3. Dyskerotosis Congenita

Dyskerotosis Congenita (DC) is a highly heterogeneous disorder, classically associated with mucocutaneous abnormalities, pulmonary fibrosis, bone marrow failure and predisposition to cancer. Mutations in approximately 10 genes have been associated with DC, each of which is associated with telomerase function and telomere integrity. Hoyeraal-Hreidarsson syndrome, a severe variant of DC, has recently been shown to be to caused by mutations in the regulator of the telomere elongation helicase *Rte1*.

Because of the clear role of telomere defects in DC, it is usually grouped with other telomere shortening disorders, such as Bloom syndrome and Fanconi anaemia. Indeed, the clinical phenotypes of DC include premature ageing and loss of cells in high turnover tissues.

X-linked DC is caused by mutations in the gene *DKCG1*, which encodes the dyskerin protein. This protein is not only found in the telomerase complex, but also in H/ACA ribonucleoprotein (RNP) complexes, where it is involved in rRNA pseudourylation. There is evidence to suggest that this ribosomal defect results in decreased translational fidelity and impaired control of IRES-mediated translation. This may contribute to the susceptibility of these patients to cancer (nakhoul 2014).

1.4.4. Cartilage Hair Hypoplasia

Cartilage Hair Hypoplasia (CHH) is an autosomal recessive disorder most commonly observed in the Old Order Amish population. It is clinically characterised by short stature, hair growth abnormalities and bone deformities. Anaemia and immunodeficiency can also occur. There is also an increased risk of cancer, particularly non-Hodgkin lymphoma and basal cell carcinoma. A spectrum of related disorders has been described, ranging from least to most severe; metaphyseal dysplasia without hypertrichosis, CHH and anauxetic dysplasia (AD). Disorders on this spectrum are caused by mutations in the untranslated gene *RMRP*, which encodes the RNA component the RNase mitochondrial RNA-processing (MRP) complex. This particular RNA is classified as a snoRNA, and plays multiple roles in the cell. It is unclear how mutations in this gene result in the disorders seen. *Nme1*, the yeast homologue of *RMRP*, is involved in RNA processing. IN mammalian cells, RNase MRP RNA forms complexes with the catalytic

subunit of the telomerase reverse transcriptase (one of the genes mutated in DC) to produce double stranded RNA that can be processed into small interfering RNAs (siRNA). Targets of these siRNAs includes genes involved in skeletal and hair development, suggesting disturbed siRNA production may be the primary pathogenic mechanism underlying CHH (Nakhoul 2014).

1.4.5. Roberts Syndrome

Roberts syndrome (RBS) is characterized by pre- and post-natal growth retardation, bilateral symmetric limb reduction, and craniofacial abnormalities. RBS is an autosomal recessive disorder that is caused by mutations in the ESCO2 gene, which is involved in the production of rRNA. ESCO2, Establishment of Cohesion 1 Homolog 2 (Eco1 in yeast), is an acetyl transferase important in assembly of Cohesin. Cohesin is a complex of proteins which binds chromosomes and holds sister chromatids together from DNA replication to cell division. However, Cohesin also has other cellular roles including binding genes with paused RNA Polymerase, facilitating DNA looping to bring together enhancers and promoters, and in DNA repair.

Studies in yeast and human cell lines revealed that *eco1/ECO1* mutants exhibited defects in ribosome biogenesis including reduced protein translation. More specifically, production of the methylated 25S and 18S rRNA transcripts was diminished. In line with this, fibroblasts from RBS patients showed diminished rRNA production and protein synthesis. This suggests a similar dysregulation of ribosome biogenesis underlies the pathogenesis of TCS, DBA and RBS. Therefore, similar to TCS and DBA, it seems likely that the RBS phenotype may be related, at least in part, to increased cell death and death of neural crest precursors. However, in contrast to TCS and DBA, the cell death in *esco2* mutants is p53 independent.

Cohesin proteins may therefore also facilitate production of rRNA and protein translation. Although RBS is classically considered a cohesinopathy, it can also be classified as a ribosomopathy given the diminished ribosome biogenesis described above (Trainor and Merrill 2014).

1.4.6. Shwachman-Diamond Syndrome

Shwachman-Diamond Syndrome (SDS) is a rare (frequency of 1:76,000) autosomal recessive disorder caused by (in 90% of cases) biallelic loss-of-function mutations in the gene *SBDS* (Boocock, Morrison et al. 2003). It was originally described by Shwachman and Diamond in 1964 as a new entity characterized by pancreatic insufficiency and bone marrow hypoplasia (Shwachman, Diamond et al. 1964). The disease is now known to be a consequence of expression of hypomorphic *SBDS* alleles (complete loss of *SBDS* function is lethal). Symptoms typical of SDS include exocrine pancreatic dysfunction, skeletal abnormalities and bone

marrow failure, predisposition to cancer and various anaemias, most commonly neutropenia. SDS patients are at risk of developing severe infections due to insufficiency in white blood cell number and function, bone marrow failure and leukaemic transformation of B cells, malnutrition and failure to thrive due to pancreatic dysfunction and in severe cases infant death due to skeletal defects of the rib cage (costochondral thickening) causing breathing difficulties.

Cognitive impairment is also a common feature of SDS, with approximately 20% of children with SDS meeting the criteria for intellectual disability. Other neurobehavioral and social concerns such as attention deficits and anti-social behaviours are prominent in children with SDS (Kerr, Ellis et al. 2010). Autism-spectrum disorders have also been reported in SDS patients (Perobelli, Alessandrini et al. 2015). Neurological problems in SDS patients are becoming increasingly apparent in the SDS research field, and this is one of the primary complaints from patients and their families.

SBDS is a highly conserved gene , with yeast, human and even *Dictyostelium* orthologues of the protein being interchangeable with no effect on functionality in ribosome biogenesis (Wong, Traynor et al. 2011). Targeted deletion of S*bds* in mice leads to embryonic lethality at or before E6.5 (Zhang, Shi et al. 2006). Accordingly, homozygosity for null alleles of *SBDS* has not been reported in humans, indicating that *SBDS* is essential for life (Ball, Zhang et al. 2009). Targeted deletion of the yeast orthologue of *SBDS*, *Sdo1*, severely impairs growth in *S. cerevisiae*, and results in Tif6 (yeast orthologue of eIF6) being mislocalised to the cytoplasm (Wong, Traynor et al. 2011).

1.4.7. Other ribosomopathies

Several other diseases exist in which ribosomal dysfunction is thought to be the main contributing factor. Approximately 19 ribosomopathies have so far been identifies, with more being added to the list as disease mechanisms are elucidated. Bowen-Conradi syndrome is an extremely rare disease that causes severe growth retardation and death in early childhood. It is cause by mutations in *EMG1*, which encodes a pseudouridine methyltransferase involved in ribosome biogenesis. North American Indian childhood cirrhosis, which affects children in a small population in North-western Quebec, is caused by mutations in hUTP/Cirhin, which is involved in synthesis of the 18S rRNA. This has recently been shown to result in haploinsufficiency of ribosomal protein SA, a component of the 40S subunit.

In addition to these classified diseases, other diseases may have ribosomal factors associated. For example, mutations in eukaryotic initiation factors have been discovered in vanishing white matter disease, and in some cases of autism. Mutations in many r-proteins and other ribosomal factors have been identified in various cancers, which is discussed below (1.4.10.3).

1.4.8. The genetics of Shwachman-Diamond Syndrome

Most SDS patients have at least one allele of *SBDS* that prematurely truncates the protein, while 25% of patients have mutations of missense, nonsense, splice or indel nature located anywhere within the coding region of the gene. These mutations usually result in a reduction in protein stability or are predicted to inhibit surface electrostatic interactions with other factors. However, functional relevance of many SDS-related mutations has not been assigned. Mutations in the *SBDS* gene often arise from gene conversion, caused by recombination between *SBDS* and a pseudogene that lies 5.8Mb upstream. SDS-associated mutations can be categorized into two main groups; 1) mutations that are predicted to destabilize the protein and 2) mutations that are predicted to modify surface epitopes and interactivity, referred to as class A and B, respectively. All three domains of SBDS are required for function *in vivo*. Yeast strains that have *Sdo1* deleted are severely deficient in growth. Various yeast *Sdo1* suppressor strains have been used to study the effect of disease-associated mutations on *Sdo1* (and *SBDS* in humans due to high conservation between species) function.

1.4.8.1. Class A mutations: Protein stability

Converted gene segments consistently include at least one of two pseudogene-like sequence changes that are predicted to result in SBDS protein truncation; 1) the *SBDS* dinucleotide mutation 183-184TA → CT introduces an in-frame stop codon (K62X) and 2) the 258 + 2T → C mutation is predicted to result in premature truncation of the SBDS protein by frameshift (C84fs3). These mutations fall into the first category of common mutations. The majority of

SDS patients carry one of these common conversion mutations, and 50% are compound heterozygotes with respect to the K62X and C84Cfs mutations. There have been no reports of homozygotes for the K62X mutation, indicating that this mutation may be lethal. Alleles from affected individuals who do not have the common conversion mutations carry additional frameshift and missense mutations in the *SBDS* coding region.

The N-terminal (FYSH) domain, so called because of its homology with the fungal protein Yhr087wp, which is involved in RNA metabolism (Fungal, *Y*hr087wp, Shwachman Domain) is the most frequent target for disease mutations. The FYSH domain (Asp5-Ile87) has a mixed αβ topology, comprising four β-strands and four α-helices arranged as a three stranded anti-parallel β-sheet broken by the insertion of a hydrogen-bonded water molecule between strands β3 and β4. Mutagenesis studies showed that the disease-associated K62X mutation truncates the SBDS protein within the β4-α3 loop of the FYSH domain, whereas the C84fs3 frameshift mutation is predicted to result in truncation within helix α4, and these mutations might therefore be expected to result in loss of protein function. Three examples of other residues that fall into this category of SDS mutations have also been attributed to disease; C31W, L71P, and I87S, which map to the hydrophobic core of the FYSH domain are predicted to result in loss or reduction of protein stability.

1.4.8.2. Class B mutations: Surface epitopes and interactivity

A great number of mutations that fall into the second category have been identified: R19Q, K33E, N34I, E44G, K67E, K118N, R126T, S143L, K148R, Q153R, R169C, and R169L are expected to alter surface epitopes but are not expected to disrupt the overall fold of the protein (Shammas, Menne et al. 2005). Cryo-EM mapping has shown that many disease-related SBDS variants target rRNA contacts that are critical for 60S binding and the stabilization of functionally important conformational states. Mutations in domain I of SBDS show that this domain is necessary, but not sufficient, for 60S binding. The disease-associated missense mutation F57L causes a disruption of the ferrodoxin-like in domain I, but does not affect structure of domains II and III, and the resultant yeast strain was impaired in 60S binding assays. Cryo-EM maps have also shown that the disease-associated residue K67 (N67 in yeast), potentially makes an electrostatic interaction with the P loop of the 60S subunit. If this residue is mutated in yeast (N67E) severe growth deficiencies are seen. These data show that a specific interaction between Sdo1 domain I and the 60S subunit is required for yeast cell fitness (Weis, Giudice et al. 2015).

R126T is a disease-associated mutation found in SDS, and is known to be a functional hypomorph *in vivo*. Residue R126 lies on the surface of the α5–α6 loop at the interface between domains II and III of SBDS. R126T mutants display impaired GTP hydrolysis by EFL1 compared to wildtype SBDS protein, despite showing no impairment in 60S binding. As might be expected, R126T variants were severely defective in eIF6 release assays *in vitro* (Finch, Hilcenko et al. 2011).

Certain mutations in SBDS are thought to affect the conformation of SBDS upon EFL1 binding. The highly conserved residues K151 and R218 (yeast R224) in domain II and III of SBDS potentially make electrostatic interactions with the tip of helix 69 of the 60S subunit. Mutations in the flexible linker region of SBDS, between domain I and II (residues 90-200), such as K151, which resides on a basic patch on helix α7 on the surface of domain II, may affect the stability of SBDS's interaction with 60S subunit, by inducing order in helix 69, which is intrinsically disordered in the absence of SBDS. Mutations in this region in yeast (i.e. deletion of residues 94-95 or deletion/insertion of EVQVS between residues 97-98 in Sdo1) cause impaired cell fitness. This loss of flexibility is likely to hinder the dynamic rotations that are required from SBDS for interaction with EFL1 and the release of eIF6 (Finch, Hilcenko et al. 2011, Weis, Giudice et al. 2015).

One disease-associated mutation, S134L in domain II, has been attributed to inhibiting the interaction between EFL1 and SBDS. This has been hypothesised to reduce the GEF-like activity of SBDS on EFL1, and reduce GTP hydrolysis. This disease-associated mutation may therefore cause SDS by indirectly reducing the functionality of EFL1. However, on the surface of the 60S subunit, it is debateable that these two proteins have any contact at all, and so these data may suggest a role for SBDS and EFL1 in the cytoplasm when not bound to the 60S subunit. These mutations exemplify the wide range of mutations that can affect eIF6 release, and may reflect the heterogeneity of SDS.

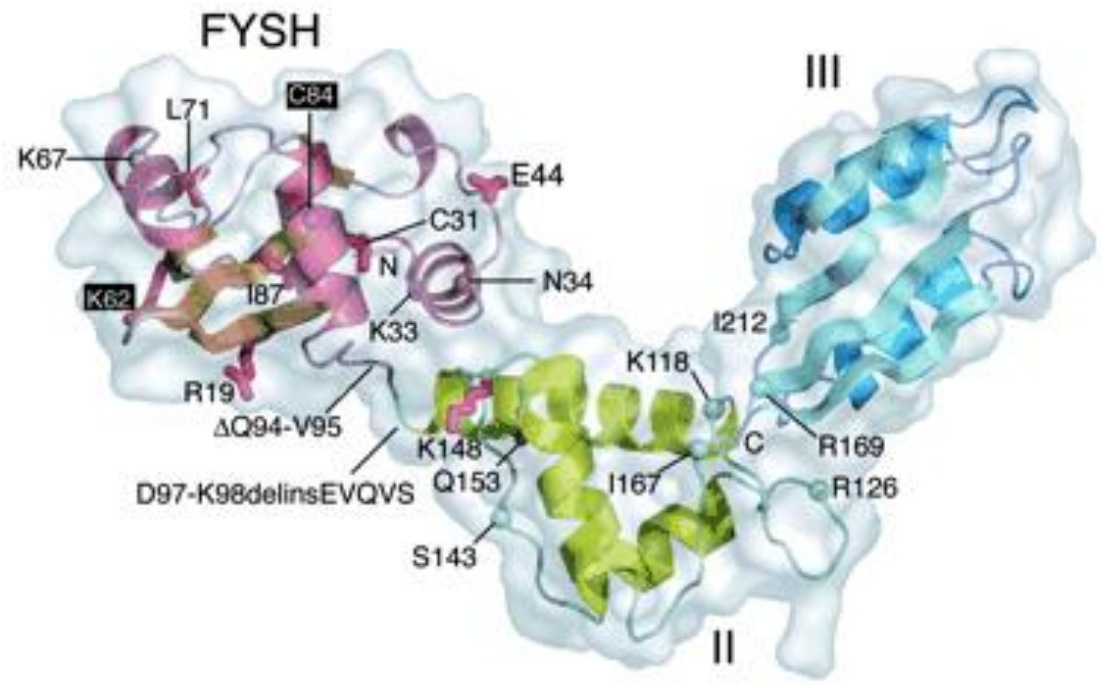


Figure 11 Schematic of locations of SDS-associated mutations within SBDS protein. Mutations listed in the text are shown with their location in the protein. Of note are the C84Cfs and K62X mutations (in black boxes). Adapted from (Shammas2005).

1.4.9. SDS model systems

1.4.9.1. Yeast and *D. discoidium* models

Various genetic studies have shown ribosomal joining defects in *SBDS* mutants. Yeast have been utilised to model *Sdo1* mutations and their impact on growth and ribosome biogenesis. Deletion of either *Sdo1* or *Efl1* in yeast results in severe growth defects, accumulation of Tif6 in the cytoplasm, and defective nuclear export of the pre-60S subunit as a result (Tif6 is required for nuclear export of the pre-60S subunit). As a result, fewer 60S subunits are available for 80S formation, and polysome profiles show a reduction in the 80S peak and reduced polysomes (Senger, Lafontaine et al. 2001, Menne, Goyenechea et al. 2007).

Conditional *SbdS*-knockout *Dictyostelium discoidium* models have been generated by introducing a temperature sensitive intein into the *SbdS* gene. At the restrictive temperature, SbdS protein was barely detectable in these cells. Polysome profiles in the *SbdS*-deleted *D. discoidium* showed increased 40S and 60S peaks in polysome profiles, which suggests an impairment of their joining to form the 80S subunit. Also detected in the polysome profiles of these conditional knockouts were halfmers (40S subunits attached to mRNA in the absence of the 60S subunit) and an accumulation of eIF6 in the cytoplasm due it's not being released from the pre-60S subunit and recycled back to the nucleus (Wong, Traynor et al. 2011). This model was also used to demonstrate that SBDS and EFL1 are required for the release of eIF6.

1.4.9.2. Conditional Knockout and Embryonic Mouse Models

SBDS is essential for life, as demonstrated in S*bds*-null mouse models. Mouse embryos that are either homozygous for the disease-associated allele R126T (*Sbds*$^{R126T/R126T}$) or null allele (S*bds*$^{R126T/-}$) do not survive birth. These embryos show severe growth defects compared with littermate controls, with the S*bds*$^{R126T/-}$ embryos showing more severe growth defects that the *Sbds*$^{R126T/R126T}$ embryos. Heterozygous carriers of either the null or the missense mutations alleles (*Sbds*$^{+/-}$or *Sbds*$^{R126T/+}$ *respectively)* were indistinguishable from wildtype, consistent with a recessive mode of inheritance for SDS. Although they did not survive to birth, the homozygous mutant embryo models recapitulated certain disease aspects. The foetal liver (the primary site of haematopoiesis during development) showed decreased granulocytes and myeloid progenitor cells. Hypocellularity in the bone marrow was also observed, presumably due to the foetal liver abnormalities. Delayed ossification and bone growth of the metacarpals was also observed, although no gross skeletal abnormalities were present. Increased cell death and decreased cell proliferation was seen in the developing cortices of these embryos, and necrotic regions were detected at E18.5. Additionally, polysome profiles of foetal pancreas showed a decrease in the 80S peak.

Conditional knockout mice have been utilised as SDS models to circumvent embryonic lethality, and allow the study of SBDS loss in adult tissues. One such model was created using a conditional knockout allele (CKO) in conjunction with a pancreas-specific Cre driver (*Ptfla*^{Cre}). Mice with biallelic loss-of-function mutations in the pancreas showed 47% reduction in adult pancreas size with severe atrophy of the acinar cell component. Additionally, this phenotype was accompanied by depletion of zymogen granules (the specialised vesicles that produce digestive enzymes). However, in contrast to the embryonic brain, poor pancreatic growth was not due to apoptosis, but to senescence. This senescent phenotype in the pancreas was shown to be p53 dependent, and rescue of the phenotype was achieved by crossing with a *p53*-null mouse line (Tourlakis, Zhang et al. 2015).

A conditional knockout mouse has also been generated with *Sbds*-deleted livers. This was achieved by generating *Sbds*-conditional knockout mice, with lox-P sites flanking exon 2, and crossing them with a Cre-*Mx1* transgenic line for deletion of *Sbds* in the liver only. Histological abnormalities were observed in the livers of *Sbds*-deleted mice. The livers showed a disordered architecture and a range of degenerative hepatocyte appearances such as necrosis and apoptosis, as well as degeneration of nuclei and nuclear cavitation. Nucleolar abnormalities were also observed, with nuclei becoming large and ring-shaped with

eosinophilic centres. *Sbds*-deleted mouse hepatocytes show accumulation of cytoplasmic 40S and 60S subunits in polysome profiles, as well as halfmers, with no significant difference between the ratio of 40S and 60S peaks. This is suggestive of a ribosomal subunit joining defect, or rather an incompleteness of 60S maturation, whci results in an inability of the two subunits to join. Accumulation of eIF6 in the cytoplasmic 60S subunit fraction of the polysome profiles of *Sbds*-deleted hepatocytes was also observed. This suggests that eIF6 is not being released efficiently in the *Sbds*-deleted livers, and this was deemed to be the cause of the ribosomal subunit joining defect. This mouse model was used as the first demonstration that SDS is caused by an impairment of eIF6 release and a subunit joining defect. This mouse model also demonstrated for the first time that both SBDS and EFL1 are required for eIF6 release, and that SBDS stimulates 60S-depepndent GTP hydrolysis by EFL1, and that accurate cooperativity between the two proteins is essential (Finch, Hilcenko et al. 2011).

1.4.9.3. Haematopoietic Stem Cells

A mouse model with SBDS loss in the haematopoietic stem cells (HSCs) has also been generated. This was achieved by crossing *Sbds*-conditional knockout mice, with lox-P sites flanking exon 2 of *Sbds*, with *Cebpa*$^{Cre/+}$ R26 EYFP mice. C/EBPα (CCAAT/Enhancer-Binding Protein α) is a leucine zipper transcription factor expressed in a fraction of HSCs and throughout the myeloid lineages. Resultant offspring of this cross did not include mice that were homozygous for the *Sbds* knockout, suggesting that deficiency of *Sbds* in *Cepba*-expressing cells is lethal in mice. An alternative approach was used, whereby irradiated wildtype mice were transplanted with foetal *Sbds*-deficient liver cells. These reconstituted mice developed profound neutropenia, as seen in SDS patients, and accordingly the bone marrow was hypocellular.

More specifically, the hypocellularity resulted mostly from a marked reduction in neutrophils. A reduction in other cell types (lymphoid and erythroid progenitors) was also seen to a lesser extent. However, *Sbds* deficiency did not result in a reduction of haematopoietic progenitor numbers along the myeloid lineage. Interestingly, granulocyte/monocyte progenitors (GMPs) were found to be dramatically increased in transplanted mice, and it is thought that this is a compensatory mechanism for the neutropenia seen. The neutropenia was shown to arise due to a cell-cycle-exit arrest preventing myelocytes differentiating into metamyelocytes (the final precursor before the mature neutrophil) (Zambetti, Bindels et al. 2015). Activation of the p53 pathway was observed in metamyelocytes from transplanted mice. In line with this, an increased expression of pro-apoptotic genes was also detected in these cells (Zambetti, Bindels et al. 2015).

1.4.9.4. SDS patients

SDS is a very rare disease, and as such sample sizes are small and access to patient tissues is limited. Various SDS patient registries are set up all over the world, i.e. the North American SDS Registry. These registries aim to collect extensive information about a patient's genetics and disease pathogenesis and aim to follow them throughout their lives. However, these do not constitute tissue banks, and therefore studying SDS in patients is extremely difficult, hence the need for model systems. However, some work has been done with patient-derived cells.

SDS patient lymphoblasts have shown a dramatic decrease in SBDS levels, between 1 and 48% that of wildtype lymphoblast levels. Polysome profiles show increased 60S peaks, and immunoblotting shows accumulation of eIF6 in the 60S fractions specifically. The severity of joining defect correlated with the level of SBDS protein in the patient cells, indicating a strong link between SBDS protein activity and eIF6 release. Interestingly, the levels of eIF6 and NMD3 protein were increased, perhaps as a compensatory mechanism. Components of the 60S subunit (RPL11 and ROK23) were unaffected, nor were assembly factors EFL1 or EBP1 (the mammalian orthologue or Arx1) (Wong, Traynor et al. 2011). p53 protein levels have been shown to be increased in the bone marrow of SDS patients, and this was specific to SDS patients, and not seen in patients with acquired hematologic disorders with variable risk levels for leukaemia, including acquired aplastic anaemia, refractory anaemia and various other acquired cytopenias (Elghetany and Alter 2002).

1.4.10. Proposed mechanism underlying ribosomopathies

Ribosomopathies are a heterogeneous class of diseases, and although they all involve ribosomal dysfunction of some kind, the mechanisms underlying their clinical presentations differ significantly between diseases. These different mechanisms have clinical relevance as the potential treatments for ribosomopathies would depend on the underlying pathogenesis mechanism.

1.4.10.1. Differential mRNA translation

Translational defects, both global and at specific mRNA levels, have been proposed as the cause of certain ribosomopathy symptoms. For example, global protein synthesis rates are reduced in SDS and RS patients cells (Wong, Traynor et al. 2011, Yelick and Trainor 2015). However, this does not explain the tissue specific phenotypes seen in all ribosomopathies.

Although ribosome biogenesis is a global process that occurs in all cells, a growing body of literature has revealed that certain mutations in r-proteins can result in tissue specific defects. In this way r-proteins selectively regulate the expression of specific mRNAs, an idea known as

the ribosome filter hypothesis. In 2011, it was shown that skeletal patterning defects in the tail-short mouse were caused by loss-of-function in the Rpl38 gene, which resulted in decreased translation in a subset of homeobox proteins. Other r-proteins can regulate extra-ribosomal mechanisms. One examples of this is Rpl26, which induces translation of p53 by binding to the 5' and 3' UTRs of the p53 mRNA (Nakhoul, Ke et al. 2014).

Given the ubiquity of r-proteins, a paradoxical feature of ribosomopathies is the variety of their phenotypic effects. This variety is explained by the emerging concept of 'specialised' ribosomes, in which tissue-specific variations in ribosome structure or function confer regulatory specificity in translation. These variations include expression of r-protein paralogues in different tissues, heterogeneity of r-protein expression in different tissues, heterogeneity of post-translational modifications of r-proteins, to name a few. Ribosomal composition can even vary within the same cell. An example of this is in neurons, where certain r-proteins and RNAs are selectively enriched either in the axon or the dendrites relative to the soma. These variations can in turn affect the translation of specific mRNAs (Nakhoul, Ke et al. 2014).

The ribosome plays a unique role in the maintenance of the species, translating mRNAs into functional proteins. Moreover, it is known that the affinity of the translational apparatus for any single mRNA species is unique. Therefore, given that there is an excess in the number of mRNA transcripts to ribosomes, a decrease in ribosome number would impinge not only on the rates of translation, but also on the patterns of translation. This is because as the number of ribosomes to mRNA transcripts decreases, those mRNAs for which the translational apparatus has high affinity, or 'strong' mRNAS, will continue to be translated, whereas the translation of those mRNAs for which the protein synthetic apparatus has low affinity, or 'weak' mRNAs will decrease (Yelick and Trainor 2015). This could in theory lead to certain genes being under expressed, with potentially pathogenic consequences.

1.4.10.2. p53 in ribosomopathies

Ribosomal biogenesis is a highly energy-consuming process that is coupled to cell growth and requires tight regulation. It is controlled by the TOR pathway, which regulates the synthesis of ribosomal components in response to growth factors and nutrient availability. Various cellular stresses such as hypoxia or DNA damage decrease ribosome biogenesis, mostly by inhibition of PolI transcription of rRNA. Shutting down ribosome biogenesis during stress preserves cellular homeostasis and ensures that enough cellular resources can be relocated to a response to stress (Danilova and Gazda 2015).

The transcription factor p53, a key tumour suppressor and regulator of cell fate, is particularly involved in ribosomal function. p53 can activate or repress transcriptional targets, such as p21, to induce cell-cycle arrest or apoptosis. One of the first indications that p53 is involved in controlling the fidelity of ribosome biogenesis came from the finding that a mutation in *Bop1*, which is involved in maturation of rRNAs, leads to p53-dependent cell cycle arrest in mouse cells and that *RPS6*-gene haploinsufficiency activates p53 in mouse embryos and T cells (Danilova and Gazda 2015). Subsequent studies have established p53 activation as a general response to r-protein deficiency in various systems, including mouse, zebrafish and human cells, with specific reference to DBA. The presiding hypothesis as to why defects in rRNA processing and ribosome biogenesis affect p53 pathways comes from the observation that various r-proteins have been shown to bind MDM2 (mouse double minute 2 homolog, which is a negative regulator of p53) and to inhibit its binding to p53, leading to p53 stabilization and to cell cycle arrest (Zhang and Lu 2009).

Many r-proteins of both the 40S subunit (RPS3, RPS7, RPS14, RPS15, RPS20, RPS25, RPS26, RPS27, RPS27L and RPS27a) and 60S subunit (RPL4, RPL5, RPL6, RPL11, RPL23, RPL26 and RPL37) have been shown to bind and block the activity of MDM2. This results in p53 not being directed to the proteasome for degradation, and thus its stabilisation within the cell. The initial model proposed that disruption of ribosome biogenesis leads to the accumulation of free r-proteins, which bind MDM2 and activate p53. However, almost all r-proteins are synthesized in excess and rapidly degraded making it unlikely they would be stable enough to interact with MDM2.

RPL5 and RPL11, together with the 5S rRNA, form the 5S RNP, a stable assembly intermediate of the 60S subunit. It is now thought that it is the 5S RNP, and not the individual r-proteins RPL5 and RPL11, binds and regulates MDM2 in unstressed cells. This interaction is enhanced after defects in ribosome production when the 5S RNP accumulates. PICT1 has recently been identified as a novel tumour suppressor that induces p53 and activates the PTEN pathway/ATM checkpoint in response to DNA damage. Interestingly, PICT1 has also been shown to retain RPL11 in the nucleolus in normal cells. However, under ribotoxic stress conditions, RPL11 and PICT1 relocalize to the nucleoplasm, where they activate p53 (Pelava, Schneider et al. 2016).

Activation of p53 has been proposed as a common mechanism in the pathogenesis of various different ribosomopathies, including SDS, DBA, Treacher Collins Syndrome and 5q-syndrome (Fumagalli and Thomas 2011). Elevated protein levels of p53 have been detected in the bone

marrow of SDS patients, supporting a potential role for p53 in the bone marrow-related symptoms of the disease. It could be postulated that increased levels of p53 due to the ribosomal stress caused by the *SBDS* mutations could cause cell death in the bone marrow population.

Sbds loss in the murine pancreas results in severe atrophy that is p53 dependent. This p53 dependence was not specific to the pancreas, as loss of p53 impacted many phenotypes of this embryonic SDS mouse model, in that it had a restorative effect on haematological progenitor levels in the *Sbds* null embryo and reduce apoptosis was seen in the foetal brain. Loss of p53 also lessened disturbances seen in polysome profiles of foetal livers of *Sbds* null embryos, with 80S levels increasing slightly, but still remaining below wildtype levels (Tourlakis, Zhang et al. 2015).

A role for p53 in the regulation of cellular metabolism has recently been identified by a mouse model carrying a cancer derived point mutation, C305F, in *Mdm2*. This mutation blocks the 5S RNP–MDM2 interaction and renders the mouse cells insensitive to p53 activation. In addition, this mutation also increases the rate the mice develop c-*myc*-induced lymphomas. Therefore, the Mdm2-C305F mouse model provides insights into the link between ribosome biogenesis and cancer. Interestingly, the *Mdm2*–C305F mutation also promotes fat accumulation in mice under normal conditions and hepatosteatosis under fasting conditions. It was further shown that ribosome biogenesis, and the 5S RNP–MDM2 pathway, is the sensor responsible for p53-mediated remodelling of lipid homoeostasis in the liver in response to restricted nutrients. These findings indicate that the regulation of ribosome production is a major nutrient sensor and critical for the correct response to changes in diet that affect liver function (Pelava, Schneider et al. 2016).

1.4.10.3. Ribosomal dysfunction and cancer

Susceptibility to cancer is a common symptom of ribosomopathies. This may not be surprising, as at the cellular level, dysregulation of translation has been shown to be a common pathway amongst cancers. Indeed, ribosome biogenesis is upregulated by the oncogene *c-Myc*, downregulated by the tumour suppressor $p14^{ARF}$, and is linked to the regulation of the tumour suppressor p53 (Pelava, Schneider et al. 2016). The mechanistic link between ribosomopathies and cancer however may seem paradoxical. Proliferation in tumours is generally associated with an increase in ribosomal biogenesis and translation, allowing for excessive growth of the cells. In fact, several cancers shown over production of r-proteins.

There are several steps in ribosome biogenesis, which, when deregulated, can contribute to increased tumorigenesis. The first step in ribosome production requires the synthesis of the 45S rRNA precursor. The transcription of this rRNA gene is negatively regulated by tumour suppressors such as p53 and retinoblastoma (RB). The accurate regulation of rRNA synthesis can be lost in cancer cells through inactivating mutations in tumour suppressors or upregulation of these kinases (Ruggero and Pandolfi 2003).

However, as discussed above, p53 is stabilised in some ribosomopathies, which should in theory suppress tumour transformation in these cells. It is thought that selective pressure on cells affected by ribosome biogenesis defects may result in spontaneous mutations that can circumvent tumour suppression mechanisms, and allow inappropriate cell growth. One example of this can be seen in SDS, where clonal chromosome abnormalities are seen in the bone marrow of patients, who have a predisposition to acute myeloid leukaemia (AML). Two clonal chromosome abnormalities are frequently detected in SDS patients; iso(7)q and del(20)q (Minelli, Maserati et al. 2009).

The del(20)q chromosomal abnormalities seen in the bone marrow of SDS patients is thought to include the deletion of the *eIF6* gene, thus providing a mechanism to circumvent to defect in ribosome biogenesis presented by the SBDS deficiency. The *SBDS* gene is located on 7q11, and thus bone marrow cells with the iso(7)(q) abnormality have three copies of the gene, of which two or three copies will contain SDS-associated mutations. The reason for the development of these clonal chromosome abnormalities is debateable. They are not restricted to SDS patients, and occur in many different bone marrow failure disorders (Minelli, Maserati et al. 2009). There may be a strong selective pressure, with the loss of SBDS for mutations, that can compensate and allow cells to escape growth arrest or apoptosis, predisposing them to genomic instability. In addition, SBDS has been shown to support the mitotic spindle, and so depletion of this protein may make cells prone to genomic instability (Ball, Zhang et al. 2009). This role for SBDS in genomic stability may explain the predisposition of SBDS-deficient patients to accumulate these clonal chromosome abnormalities.

Another step in ribosome biogenesis that maintains accurate cellular function involves the modification of rRNA. One type of modification, which is catalysed by an enzyme known as dyskerin, converts uridine into pseudouridine. Mutations in the gene encoding dyskerin, DKC1, are seen in DC (as mentioned in 1.4.3) result in increased tumour susceptibility. Animal models that have lost DKC1 function show a marked increase in tumour incidence associated with a decrease in rRNA processing (Ruggero and Pandolfi 2003).

The third step is ribosome assembly, which involves the association of rRNA with more than 70 r-proteins to form the two subunit of the ribosome. An increase in r-protein production and activity has been observed in many cancer types. Mutations in ribosomal proteins such as RPS19 have also been associated with DBA, which is associated with susceptibility to cancer.

Each of the steps highlighted here may have deleterious effects on the cell that could contribute to tumour initiation and cancer progression through aberrant regulation of protein synthesis. This can be manifested either by an increase in ribosome production, thereby leading to an upregulation in total translation, or by alterations in translation of specific mRNAs, which are involved in the regulation of cell proliferation. Furthermore, when key checkpoints in the cell that are important in coordinating ribosome production with accurate cell-cycle progression are lost, 'nucleolar stress' can result, and subsequently unrestrained cellular proliferation occurs (Ruggero and Pandolfi 2003).

1.5. EFL1 biology

1.5.1. GTPase biology

Many proteins bind and hydrolyse nucleoside triphosphates (NTPs). These can be broken down into two main categories, based on the type of NTP they bind; ATPases and GTPases. Adenine and guanine NTPs have distinct biological functions. ATP is mostly used to drive metabolic reactions and provide energy to be consumed by various cellular systems. GTP hydrolysis seems to be mainly used for regulation of guanine-nucleotide binding proteins (GNBPs), with a few exceptions. These enzymes cycle between active and inactive states, and act as molecular switches in the process, utilising energy from NTP hydrolysis to drive reactions in the cell. Activation requires dissociation of the nucleotide diphosphate (NDP) from the enzyme, which is an intrinsically slow process and usually involves guanine-nucleotide exchange factors (GEFs). In this process, GDP is switched for GTP. The deactivation process is entirely different, and involves hydrolysis of GTP to GDP, switching the molecular switch off as a result. This process is also intrinsically slow, and requires guanine activating proteins (GAPs).

All GTPases have a conserved G domain, comprised of five structural motifs G1-G5, which is responsible for binding the guanine nucleotides. The G1 motif binds to the α- and β-phosphate of the GTP molecule while the G4 and G5 regions contact the guanine moiety and the ribose ring. The ~20kDa G domain carries out the basic function of nucleotide binding and hydrolysis and has a universal structure and universal switch mechanism. The G domain consists of a mixed six-stranded β-sheet and five α-helices on both sides. The most important contributors to binding are: 1) the nucleotide base making contact with the X/TKXD motif (where X is any amino acid) and 2) the β- and γ-phosphates with the conserved P-loop (phosphate-binding loop) GXXXXGKS/T motif.

Conformational changes between GDP- and GTP-bound G domains have been described, and we can therefore define the molecular switch mechanism involved. Structural differences between the two conformations are restricted to two segments, first observed in RAS, called the 'switch' regions (switch I and II). The trigger for the molecular switch conformational change is likely to be universal. In the GTP-bound conformation, the oxygens on the γ-phosphate form two hydrogen bonds to the main chain NH groups of the invariant Thr and Gly residues in switch I and II respectively. The glycine is a conserved residue of the DXXG motif (which confers specificity to guanine nucleotides in rather than adenine nucleotides) and the threonine is involved in binding a Mg^{2+} ion that is crucial for GTP hydrolysis. The release of the

γ-phosphate after GTP hydrolysis severs these interactions of the nucleotide with the switch regions, allowing them to relax away from the GTP-bound conformation into the GDP-bound conformation. It is worth noting that GTP-bound conformations tend not to vary greatly between GTPases, but that there is great variation in GDP-bound conformations, suggesting this inactive state is a more lenient structure (Vetter and Wittinghofer 2001). The exact conformational changes vary between GTPases, and EF-G displays large conformational changes that have been determined by low resolution electron microscopy (Stark, Rodnina et al. 2000). EFL1 switch conformational changes have not been determined due to the lack of a crystal structure.

EFL1 uses GTP hydrolysis to regulate conformational changes in a protein complex context (Vetter and Wittinghofer 2001). As mentioned in 1.3.4, EFL1 has a five-domain structure, with domain I containing a conserved G domain. This domain undergoes large conformational changes and cycles between an inactive and active form. The inactive form of GTPases is the GDP-bound state, and the active form is GTP-bound. The apo-form of a GTPase refers to the enzyme an unbound state, with neither GTP nor GDP bound to it. In classical GTPases, the conformational switch is triggered simply by the binding of a nucleotide. Classical GTPases where this is the case include EF-Tu and p21 Ras. In non-canonical GTPases, the conformational switch between the active and inactive states is triggered by effector molecules. Examples of non-canonical GTPases are EF-G/EF-2 and EFL1. The functional cycle of these non-canonical GTPases is better explained by the terms GTP- or GDP-favouring conformations, rather than GTP- or GDP-bound. Effector molecules come in two forms; GTPases-activating proteins (GAPs) and guanine exchange factors (GEFs). GAPs increase the hydrolysis rate of GTP by a GTPase. In many cases of ribosomal GTPases, the relevant ribosomal subunit has been found to be the GAP. GEFs accelerate the exchange of GDP for GTP, and can be divided into two subgroups: Guanine nucleotide Dissociation Stimulators (GDS) and GTP stabilising factors (GSF). GDSs increase the rate of GDP dissociation from the GTPase, and GSFs increase the affinity of the GTPase for GTP by shifting the equilibrium of the apo-form to the GTP-favouring conformation. It has been suggested that SBDS acts as a GEF for EFL1 (Gijsbers, Garcia-Marquez et al. 2013).

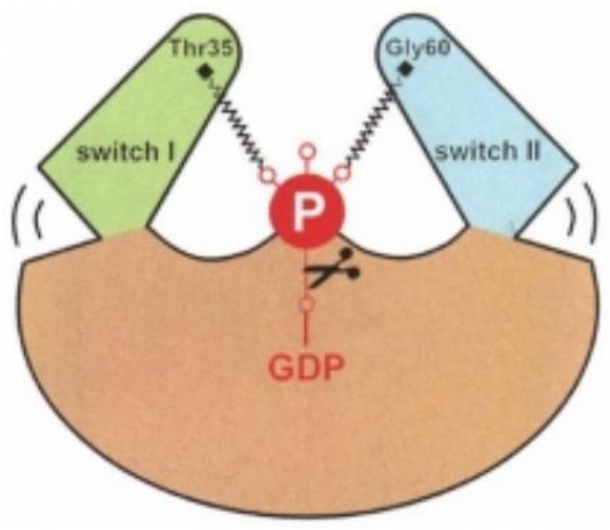


Figure 12 Schematic diagram of the universal switch mechanism present in GTPases. Switch I and II domains are bound to the γ-phosphate of GTP, in the active state of the GTPase, via hydrogen bonds to the main chain NH groups of two conserved residues; Thr in switch I and Gly in switch II. Thr35 and Gly60 are examples from the GTPase Ras. (Vetter and Wittinghofer 2001).

1.5.2. EFL1 structure and function

EFL1 is a GTPase with the five domain structure described in 1.3.4. EFL1 is a structural homologue of EF-2, the eukaryotic elongation factor, with 26.8% sequence identity between the two proteins. There is however a marked difference between these two proteins in the form of an insertion of variable length within domain II. This insertion domain has been hypothesised to mediate interactions between EFL1 and SBDS, along with domains II and III of EFL1. Circular dichroism spectroscopy showed that, in the absence of SBDS, the EFL1 insertion domain is a disordered structure but that upon binding with SBDS becomes a fixed conformation. Removal of the insertion domain abolishes any interaction with SBDS (Asano, Atsuumi et al. 2014).

EFL1 is a cytoplasmic GTPase that is expressed ubiquitously in all tissues, as might be expected for a protein involved in ribosome maturation. SBDS is also known to be expressed in all tissues, however there is evidence to suggest that it is more highly expressed in highly proliferative tissues, again unsurprisingly, given that tissue with high proliferative capacity will require higher levels of ribosome biogenesis. The only phenotype associated with *Efl1* is Glioma and cancer. *Efl1* expression was found to be increased in human glioma patient cells, and in glioma cell lines. However, expression of *Efl1* in the brain is wide spread, and not enriched in one particular area of the brain in the mouse, according the mouse Allen Brain Atlas. Other cancers have also now been associated with *Efl1* mutations, suggesting a link between EFL1, ribosome biogenesis and cancer.

Yeast *Efl1* suppressor strains have been employed to study the structure and function of EFL1. The homology models of Efl1 used in these yeast strains are based on EF-2 (Bussiere, Hashem et al. 2012, Weis, Giudice et al. 2015) due to the lack of a crystal structure for Efl1. It has been hypothesised that the insertion domain is critical for EFL1's ribosome biogenesis functionality by distinguishing it from EF-2. The transition of the disordered to fixed state may play a role in a dual functionality of EFL1; inhibiting EF-2 binding on the ribosome in the disordered, flexible state, and promoting Tif6 release in the fixed form (Asano, Atsuumi et al. 2014). However, the data that suggests a direct interaction of EFL1 and SBDS, via the EFL1 insertion domain, is taken out of context of the 60S subunit. These proteins may interact when in a non-ribosomal context, however in reality, the 60S subunit is likely to play a large role in the behaviour and binding profiles of EFL1 and SBDS. Further to this, it has been shown that EFL1 is still functional in ribosome biogenesis without the insertion domain (Weis, Giudice et al. 2015).

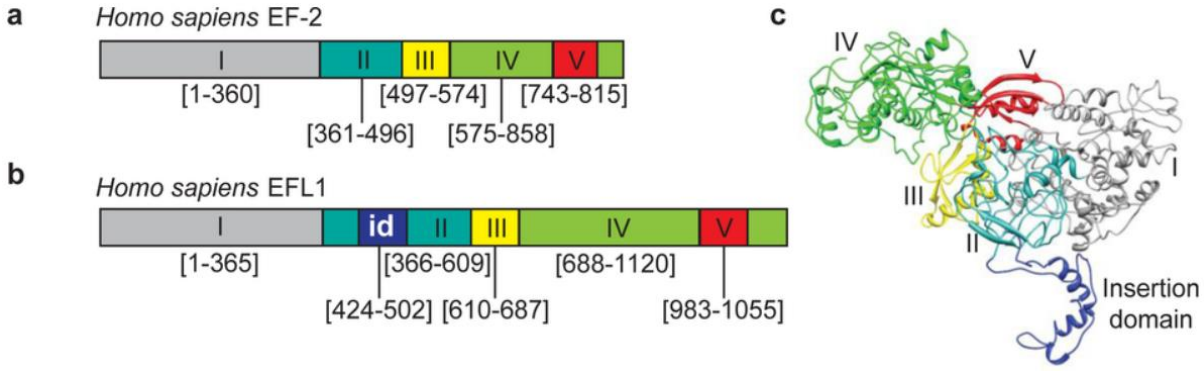


Figure 13 EFL1 domains and structure with comparison to EF2. A) Human EF2 domain schematic showing domains I (residues 1-360), II (361-496), III (497-574), IV (575-858) and V (743-815). B) Human EFL1 domain schematic showing domain I (residues 1-365), II (366-609), with insertion domain (424-502) with domain II, domain III (610-687), domain IV (688-1120) and V (983-1055). C) Ribbon representation of the atomic model of human EFL1 with the subdomain structure highlighted using the same colour scheme as (B). ((Weis, Giudice et al. 2015)

Weis et al showed that EFL1 occupies the canonical GTPase centre on the 60S subunit, which is in close proximity to the binding site of SBDS, and contacts with SBDS are made (33-44% contact between the two conformational states of EFL1, discussed in 1.3.4). However, the insertion domain is not involved in contacting SBDS in the 60S-SBDS-EFL1 complex, with or without eIF6. Instead, the insertion domain is in closer proximity to eIF6, and therefore may play a role in releasing eIF6 from the 60S subunit, distinguishing EFL1 activity from that of its homologue, and binding site competitor, EF-2, which has no insertion domain (Weis, Giudice et al. 2015).

As discussed in 1.3.4, EFL1 is crucial for eIF6 release from the 60S subunit, and for subsequent joining of the small and large ribosomal subunits. *Efl1*-deleted yeast strains show abnormal ribosome biogenesis as evidenced by polysome profiles that show reduced 60S subunits in the

cytoplasm and accumulation of Tif6 in the 60S fraction (Senger, Lafontaine et al. 2001). It is known that Tif6 release also requires the action of Sdo1, and possibly other factors such as Rpl10 (Bussiere, Hashem et al. 2012). Deletion of the Rpl10 P-site loop is lethal in yeast and blocks the recycling of Nmd3 (Hofer, Bussiere et al. 2007). Mutation of the P-site loop of Rpl10 in yeast resulted in not only an accumulation of Nmd3 in the cytoplasm, but also of Tif6, suggesting that Tif6 release is also dependent on the P-site loop. It is now thought that the supressed release of Nmd3 is an indirect effect of the suppression of Tif6 release, as Tif6 release is thought to be a prerequisite for Nmd3 release. P-site loop mutants show impaired growth and abnormal polysome profiles, including the presence of halfmers. These phenotypes can be rescued by Efl1 mutations. These Efl1 mutations were found to be in the domain interfaces, and are likely to disrupt conformational changes of Efl1, shifting the equilibrium of Efl1 conformations to an extended, and possibly constitutively active conformation. This shows a link between the P site of the 60S subunit and Efl1 function.

More work is required to assess the exact nature of this link, but it is possible that Efl1 functions as a quality control protein for the large subunit. P-site loop mutations in Rpl10 would likely disrupt translation by defective interaction with the tRNA in the P site. Communication of these flaws to Efl1 may be a mechanism to stop the maturation of the defunct 60S subunit, and therefore prevent defective ribosomes being released into the pool of translating ribosomes. The link between Rpl10 and Efl1 may be important in leukaemic transformation (Sulima, Patchett et al. 2014) Mutations in RPL10 have been found in patients with T cell acute lymphoblastic leukaemia. These mutations occurred almost exclusively in the invariant residue R98 of RPL10, with the exception of patient harbouring the Q123P mutation, which lies adjacent to the R98 residue in the tertiary structure of the protein. Both of these residues are at the base of a flexible P-site loop of RPL10, which, as mentioned above, is close the catalytic centre of the 60S subunit and is crucial for the late stages of 60S maturation. It has been shown that yeast models of this T-ALL mutation causes a failure of late-stage 60S maturation, and a shortage of mature 60S subunits. This subunit shortage in turn exerts pressure on cells to select for suppressors of the ribosome biogenesis defect, allowing them to re-establish normal levels of ribosome production. However, this leads to functionally defective ribosome being released into the pool of translating ribosomes, and as a result translation fidelity suffers and telomere length is affected (Sulima, Patchett et al. 2014). This shows that ribosome maturation is crucial for maintaining normal cellular function, and may provide insight into the mechanism by which cells with ribosomal defects can undergo transformation.

It is possible that Efl1 functions in other quality control pathways. It has been shown that Efl1 functions immediately after stalk assembly, a structure required for recruitment of other GTPases to the ribosome. Thus recruitment of Efl1 is a marker of stalk assembly, and if Efl1 does not bind or function correctly on the 60S subunit this may have implications for further recruitment of GTPases, such as EF2 seeing as the two share a ribosome binding site. Furthermore, activation of the catalytic activity of the GTPases of translation requires proper recognition of the SRL, whose presence repositions a critical histidine into the catalytic site of the GTPase. Hence, activation of Efl1 function also is likely to indicate the correct folding of the SRL (Bussiere, Hashem et al. 2012).

1.5.3. Modelling *Efl1* mutations in the mouse

EFL1 is known to be crucial for eIF6 release and proper ribosome biogenesis, and that its partnership with SBDS is also crucial for these processes. However, its intricate relationships with other ribosomal factors are not fully understood. There are no known mutations in *EFL1* in humans, suggesting it is crucial for life and that mutations are not tolerated. However, considering EFL1 is involved in the pathway that is defective in SDS, it may have implications in disease pathogenesis. There are currently no murine models for mutations in *Efl1*, and more models of SDS are needed to fully understand the disease. At present mouse models are limited to conditional knockouts or embryonic models, due to the lethality of *Sbds* knockout. However, SDS is a multisystem disorder in which a plethora of somatic systems are affected. Therefore, conditional knockouts cannot provide insight into the multi-tissue nature of the disease. Additionally, many symptoms of SDS develop over time after birth, such as anaemia and leukaemia. Embryonic models cannot provide insight into these temporal aspects of SDS as they do not survive birth. Therefore, there is a need for an adult mouse model, with SDS-like phenotypes in multiple tissues.

The *Efl1*$^{K983R/K983R}$ mouse line may provide such a model in which to study multi-tissue effects of SDS pathogenesis in a long lived organism. Mice homozygous for the K983R mutation in EFL1 recapitulates various phenotypes of an SDS-like nature, and polysome profiles show impaired eIF6 release. This mouse also allows the opportunity to study mammalian behavioural aspects of SDS-like symptoms, which form a major part of the disease in humans, but is not well studied.

1.6. Aims of the thesis

The main aims of the thesis were as follows:

- To identify the causative gene of the abnormal gait seen in the mice from the Harwell Ageing screen
- To fully characterise the mouse line phenotypically, to see if any other phenotypes are present, and what the progression of any identified phenotypes is like, i.e. is the gait phenotype age-related and progressive.
- To address the phenotypes of the mouse in terms of their association with ribosome biogenesis and ribosomopathies
- To investigate whether this mouse line parallels SDS, and whether it could be considered a model of this disease
- To assess whether this mouse line is a model of a unique ribosomal defect, or related to SDS (genetically undefined SDS)
- To determine the effect that the mutation has on the protein
- To investigate underlying biochemical pathways affected by the mutation in *Efl1*, such as ribosome maturation, mTORC1, p53 signalling and general protein synthesis

Chapter 2
Materials and Methods

2. Materials and Methods

2.1. Mouse generation and mutation discovery

2.1.1. Mouse generation

The *Efl1*-K983R mouse line was originally identified as part of the Harwell Ageing screen, a large-scale mouse screen for recessive mutations causing age-related disease incorporating an ENU mutagenesis and phenotype-driven approach. Large pedigrees of up to 100 G3 mice are screened for various phenotypes through an 18-month pipeline. This mouse was originally chosen for study due to an abnormal gait that presented in old age. This phenotype was deemed to warrant further investigation and as a result, the mouse line was rederived from archived sperm from the G1 founder of the ageing screen cohort.

For the Harwell Ageing screen, male C57BL6/J mice were mutagenised with ENU and mated to C3H.*Pde6bþ* (abbreviated to C3H.Pde from here on) mice to generate G1 founder males. G1 males were subsequently bred to C3H.Pde mice to generate G2 offspring. Next, large G3 pedigrees of at around 100 individuals were produced by two rounds of mating of the founder G1 male to ≥8 G2 female offspring. Large pedigrees ensured sufficient homozygous G3 individuals were available to map a phenotype directly from the G3 cohort. Each G3 pedigree was generated as two cohorts, 2–3 months apart. Across an entire G3 pedigree comprising some 100 mice, we might expect to identify on average 12 affected individuals homozygous for an individual recessive mutation inherited from the G1 founder male. The mixed genetic background assisted the mapping of mutations underlying the affected individuals identified in the G3 pedigrees (Potter, Bowl et al. 2016).

C3H.Pde mice were chosen for the breeding scheme because wild-type C3H strains exhibit retinal degeneration, due to a recessive mutation in the *Pde6b* gene (*Pde6brd1*). Therefore, the C3H.Pde6bþ11 line was employed as it is congenic for the BALB/c Q10 region encompassing *Pde6b* and which does not exhibit retinal degeneration, enabling screening for visual abnormalities.

C57BL6/J carries a recessive mutation in the *Cdh23* gene resulting in age-related hearing loss (*Cdh23ahl*). Therefore, in the ageing screen protocol G2 female mice were genotyped for the *Cdh23ahl* allele and only offspring from G2 females wild-type for *Cdh23* were used for auditory assessment (Potter, Bowl et al. 2016).

2.1.2. Mutation discovery

An Illumina medium density SNP array was carried out in the mice with the 'swimming' gait from the G3 cohort. The swimming gait was classified as a flat, low gait with the undercarriage of the mouse touching he floor as it walked and the legs being more wide spread than usual. The SNP array revealed a critical region, between ~68 and 95Mb on chromosome seven, identified by informative SNPs of the C57BL/6J strain. The G0 mutagenized strain used in the ageing screen is C57BL/6J, and so this block of homozygosity indicated the likely location of the causative mutation.

This ~27Mb region was subsequently narrowed down by SNP mapping to between ~71 and 84Mb. SNPs chosen were informative between C57BL6/J and C3H, and are as follows: rs31470929 (7:71012690), rs31275887 (7:75034769), rs3686423 (7:79583258), rs3023147 (7:84249894) and rs6317573 (7:90173202). These SNPs were genotyped using pyrosequencing. The pyrosequencing platform used was the Qiagen PyroMark Q96 MD, used according to manufacturer's instructions. PyroMark Q96 Gold Reagents kit (Qiagen cat# 972807) was used according to manufacturer's instructions. Biotinylated primers, plus a sequencing primer were designed for the SNPs. Primers as follows: rs31470929 F GTCCCTAAGCTCTGCTAGAGTGAT, R-Biot GCCTGACCAGAAAGGTAACTTCTA, Seq TGCATCCATAATTTAAAGAA, rs31275887 F CCCTCTATCTTCCTGGTGAGATGA, R-Biot AACACAAGCCACTGAACCAGAGAT, Seq TGAGATGATTCTTCCACTG, rs3686423 F ATCATGTCATGCGGGTAAC, R-Biot CTGCCCCATCCCTATAACT, Seq TCCAGCTGGGAAAAC, rs3023147 F CCCTGGACATGGCATCACCT, R-Biot NNNCCCCTTCCGAGCACACAGAT, Seq AAGCCAGGGCTGTG, rs6317573 F CAGTGCCAAGATGACCAG, R-Biot AAACAACCAACCCTCTTCA, Seq ACAACCAACCCTCTTC.

After SNP mapping, Next Generation Sequencing (NGS) of the G1 founder indicated a multitude of single nucleotide variations (SNVs) within the narrowed down region of interest. The only high confidence, coding SNV within the critical region was at position 7:82763352 and consisted of an A to G variation in the gene *Elongation factor Tu GTP binding domain containing 1* (*Eftud1)* or *Elongation factor-like 1 (Efl1)* (Ensembl Gene ENSMUSG00000038563), which resulted in a lysine to arginine change at position 983 in the protein (Ensembl transcript ENSMUST00000039881).

Sanger sequencing was carried out for four of the identified SNVs in the NGS, as well as the coding variant in *Efl1*, for validation. The SNVs validated were as follows: 7:71261407, 7:75326692, 7:79213370 and 7:83312171. Primers: SNV 7:71261407 – F

TGCTAGGAATCAACCTCTAGTCC, R AACCTAAAGGGAGACTATGAAA, SNV 7:75326692 – F CTAAATGCACCCTCCCTGAG, R CCAGGCATTGTTTCTCTCCT, SNV 7:79213370 – TCCTCACTGCCAAGCCTTAT, R TGGTGTGTGTGTATATGTGCTG, SNV 7:83312171 – F TTGGTTCAGAATTTGGTGTTTC, R CTAATTCTGTTTGGTCCAGCA. Primers for the *Efl1* coding variant at position 7:82763352 as follows: F – CACGTTGGAGATGAAAACCA, R – CTTTGACAGCACGGCATAGA.

2.1.3. Rederivation of the *Efl-1*K98R mouse line

The sperm from the G1 founders in the Harwell Ageing screen is frozen in order to rederive any lines that present with phenotypes of interest. The *Efl1*-K983R mice were rederived for further study, via an IVF with the G1 sperm and a wild-type C3H.Pde oocyte, which was subsequently implanted into a pseudo-pregnant CD1M female. The litter resulting from this IVF is the equivalent of the G2 offspring from the Ageing screen breeding scheme described 1.1.5. Not enough heterozygous mice were generated in the IVF litter, so an additional backcrossing step was carried out, crossing the G2 males to wildtype C3H.Pde females to generate G3 animals. Heterozygous G3 mice were then intercrossed to homozygose the mutation in the resultant G4 cohort.

Successive backcrossing of the C57BL6/J-C3H.Pde mice onto a C3H.Pde background was carried out to segregate ENU mutations elsewhere in the C57BL/6J genome. Each consecutive backcross results in a cumulative increase in the ratio of C3H.PDE genetic background to C57BL6/J. The mice described herein are of backcross 2-4.

2.1.4. Mouse genotyping

Once the K983R mutation in *Efl1* had been discovered, a LightScanner™ assay was developed to genotype the mice. The LightScanner™ (Idaho Technology) is a Hi-Res Melting™ genotyping and mutation scanning platform. High-resolution DNA melting is a method for genotyping and variant scanning that depends on the thermal stability of PCR-generated products. PCR is performed in the presence of the double stranded DNA binding dye LCGreen. After PCR, samples are heated on the LightScanner and the fluorescence emitted by bound LCGreen is monitored. As the DNA melts the LCGreen is released and so the fluorescence decreases until all the DNA has melted and all LCGreen is unbound. There are several different genotyping methods that can be used on the LightScanner.

Unlabelled probe genotyping is used to distinguish between different homozygote samples at a given SNP where scanning analysis may not have enough sensitivity. Here a 3’ blocked oligonucleotide (Probe) is designed that sits directly over the variant residue. Asymmetric

exhaustive PCR is performed using 5 times the amount of probe and opposite primer. This creates two products, one is the full PCR product between the normal primers and the other is the probe that is bound to the opposite strand. When the products are melted the probe melts at a lower temperature and by focussing analysis on this section, homozygote, heterozygote and wildtype samples can be resolved.

Mouse DNA was extracted from adult ear clips or embryonic tails by incubation overnight at 54°C with 200 µl TENS buffer (TENS: 10 mM Tris-HCl (pH 8), 1 mM EDTA, 150 mM NaOH, 0.5% SDS) and 20 µl proteinase K (Sigma Aldrich cat# 03115844001). The next day, samples were centrifuged at max speed for 5 minutes at 4°C in a microfuge. 200 µl isopropanol was added to precipitate the DNA, and samples were vortexed briefly before being centrifuged at maximum speed for 10 minutes at 4°C. TENS buffer and isopropanol were removed from DNA precipitate, and tubes were air dried. 50 µl TE buffer (TE: 10 mM Tris-HCl (pH 8), 1 mM EDTA) was then added and DNA was allowed to dissolve overnight. DNA was diluted 1:10 with ddH_2O before being used in the LightScanner assay.

Black 96 well plates with white wells were used for LightScanner genotyping (BioRad cat# HSP-9665). A 10 µl reaction mix was made using 5 µl HotShot master mix (Clent Life Siences, cat# HS002), 1 µl LCGreen (Biofire Diagnostics, cat# BCHM-ASY-0005), 0.5 µl *Efl1* Forward primer (stock concentration 20 ng/ul), 0.1 µl *Efl1* Reverse primer (stock concentration 20 ng/ul) 0.5 ul *Efl1* Probe (20 ng/ul), 0.9 µl ddH_2O, 2 µl DNA (stock 1:10 dilution). Primers: *Efl1* Forward GGTTATTGACTGCTATGGACCC, *Efl1* Reverse GTCTTCATCCTTCCCTCCTTAC, *Efl1* Probe (Reverse) GTTGAGGTCTCACCTGCAGAGCGTA.

2.2. Phenotyping

2.2.1. License

Phenotyping for all mice was conducted in accordance with conditions stated on Home Office Project License 30/2995, held by Dr Abraham Acevedo-Arozena, or 30/3015 for Auditory Brainstem Response testing, held by Professor Steven Brown. My personal license in completing this work is L359. Mice were maintained at MRC Harwell, following all Home Office conditions as specified in project and personal licenses. All mice deemed sick were assessed by the Named Animal Care and Welfare Officer (NACWO). All procedures were recorded for Home Office records. All behavioural tests were completed blind by the

experimenter. This was achieved through applying a numbering system for every mouse on the cage card where the genotype was hidden. This allowed staff to continue to maintain the colonies whilst simultaneously allowing the assessor to be blind to the genotype when completing tests. All tests were individually completed at approximately the same time of the day to minimise behavioural variation associated with circadian rhythms.

2.2.2. SHIRPA (SmithKline Beecham, Harwell, Imperial College and Royal London Hospital Phenotype Assessment

The purpose of the assessments is to examine mice for obvious physical characteristics, behaviours and morphological abnormalities. The mice were allowed to acclimatise to the phenotyping room for a period of 30 minutes prior to testing. Throughout the test any vocalisation, aggression, salivation or unexpected behaviours were noted. During this test, any unexpected dysmorphological characteristics (morphological irregularities are recorded by video sequences or photos) were noted. The mouse is placed in a clear cylinder over a wire grid and observed for activity and tremors. The mouse was then transferred to the arena by removing the metal grid and positioning it 30cm over the arena. The grid was removed abruptly, and the mouse was allowed to drop into the arena. Transfer arousal was recorded. Locomotor activity once in the new environment of the arena was recorded by the number of $10cm^2$ squares the mouse moved into in the first 30 seconds in the arena. The mouse was allowed to move freely around the arena whilst being observed for gait and tail elevation. The click box was held approximately 30cm above the arena and the button was pressed. The Preyer Reflex was recorded. The mouse was approached from the front with a bent finger, aiming to touch the mouse on the back of the neck. It was recorded whether the mouse moves away before the finger touches the mouse, when the finger touches the mouse or if the mouse does not move at all. The mouse was picked up by the tail and observed for limp grasping and trunk curl. Trunk curl must only be recorded if the mouse curled forward without twisting its body, bending to one side was not scored as a trunk curl. The mouse was placed in a small transparent tube. The tube was turned quickly so the mouse was fully upside down and it was recorded if the mouse rights itself (righting reflex). The mouse was placed on a vertical metal grid, and its downward climbing ability was recorded (negative geotaxis).



Figure 14 Photo of SHIRPA apparatus. Viewing jar, with mouse contained, is visible on right and arena if on the left. Negative geotaxis grid can be seen in foreground.

2.2.3. Social Dominance test

The Social Dominance Test is useful for identifying deficits in social interactions in strains of transgenic mice. Test apparatus comprised a 30-cm smooth, transparent acrylic tube with an internal diameter of 3.5 cm. Animals were placed at opposite ends of the tube and released simultaneously. Losers were scored as those animals that retreated from the tube; a full retreat was determined by the absence of any paws within the tube. Animals were weight matched as closely as possible. Due to the weight differences between *Efl1*$^{K983R/K983R}$ and *Efl1*$^{K983R/+}$ and wildtype mice, the heaviest *Efl1*$^{K983R/K983R}$ mice were paired with the heaviest of the *Efl1*$^{K983R/K983R}$/wildtype and so on. All genotype combinations were tested; *Efl1*$^{K983R/K983R}$ versus *Efl1*$^{K983R/+}$, *Efl1*$^{K983R/K983R}$ versus wildtype and *Efl1*$^{K983R/+}$ versus wildtype. Each animal pairing was tested three times consecutively. All mice paired were form separate cages, to ensure no previous cage hierarchy could interfere with the test. Any mice that were used in a repeated test, i.e. in the *Efl1*$^{K983R/K983R}$ versus wildtype and then the *Efl1*$^{K983R/+}$ versus wildtype trials, were tested with a minimum of one hour in between trials.

2.2.4. Resident Intruder Test

All animals tested were males. Each male (3 of each genotype) was socially isolated for 24 hours exactly. The socially isolated animals (residents) were confronted with the introduction of a weight matched, socially housed wild-type male of a different genetic background (C57BL/6JN) (intruders). Interactions and behaviours were closely monitored for 5 minute trials, and video recorded from a side and overhead view. Any aggressive interactions observed that lasted longer than 5 seconds were counted as fighting, upon which mice were promptly separated with the use of a soft-bristled brush. Offensive aggressive behaviours include: rearing, move towards, lateral threat, clinch attack and chase (Figure 15). Bite attack latency was also recorded to determine the violence tendency of the resident mouse. Clinch attacks, or other offensive aggressive behaviours deemed by the experimenter to be

detrimental to either mouse' health, lasting longer than 5 seconds were disrupted. Any biting episodes were immediately disrupted, and testing was aborted immediately in this case.



Figure 15 Resident Intruder Offensive Aggressive Behaviours. A. Rearing. B. Lateral threat. C. Clinch attack. D. Move towards. E. Chase. These were the behaviours being watched for during the resident intruder test. Any clinch attacks lasting longer than 5 second were to be disrupted. Any biting episodes were to be disrupted and testing was aborted immediately. (Adapted from (Koolhaas, Coppens et al. 2013))

2.2.5. Crack-it home cage video tracking

At 12 weeks of age, RFID microchips were injected subcutaneously in to the lower left or right quadrant of the abdomen of each mouse o be tested. These microchips were contained in standard ISO biocompatible glass capsules (11.5 × 2 mm, Peddy Mark Ltd, UK). The procedure was performed on sedated mice (Isoflo, Abbott, UK) after topical application of local anaesthetic cream on the injection site prior to the procedure (EMLA Cream 5%, Astra Zeneca, UK). In order to implant the chip, locally anesthetised and sedated mice were placed on their back to allow easy access to the site of implant, with the snout placed into the gas mask for

maintaining sedation. A section of abdominal skin from the lower left quadrant was lifted between the thumb and forefinger. The microchip was inserted using the implant device (a modified syringe) supplied by the RFID manufacturer (Peddy Mark Ltd, UK) subcutaneously into this fold of skin (no sutures were required). The mice were removed from the mask and placed into a recovery cage. Once the animals recovered and were mobile again, they were observed for any signs of distress or pain. Once full recovery was confirmed they were placed back into their home cage which was returned to its original position on the IVC rack. The animals were checked after 24 h for any signs of trauma or discomfort and to ensure that the microchips were still in place. The animals were allowed to recover from the microchip procedure for at least 1 week before placing them in the HCA rigs for collecting data.

The HCA (home cage analysis) system (Actual Analytics Ltd, UK), allows one to monitor a cage of mice, and has been designed to fit into two rack spaces of a standard IVC rack (Single sided seal safe rack, 1284 L holding 56 cages, Techniplast UK Ltd) (Figure 16). The animals were reared in a different room to the testing room so their cages, after cleaning, were placed in an IVC (individually ventilated cage) rack in the experimental room for the animals to acclimatize. For each recording, the cages were randomly assigned to an HCA rig. On the first day of recording, each cage was placed onto the ventilation system, within the rig, as would occur during the normal daily husbandry procedure. Animal welfare checks were carried out visually twice daily during testing. At the end of the recording period, the home cages were removed from the HCA rigs and returned to their original positions on the IVC racks.

The software package, Actual HCA-Capture (Actual Analytics Ltd, UK) was used to capture readings from the baseplate antennae as well as synchronized video for subsequent validation work. For each recording, the duration of the recording and the length of each recorded segment to be captured could be specified. Typically we used 30 min video segments with a matched series of antenna readings from the baseplate. Once initiated, the recording was allowed to proceed without user interference for the duration of the recording. Baseplate and video data for individual animals were recorded continuously in group-housed conditions for periods of up to 7 days.

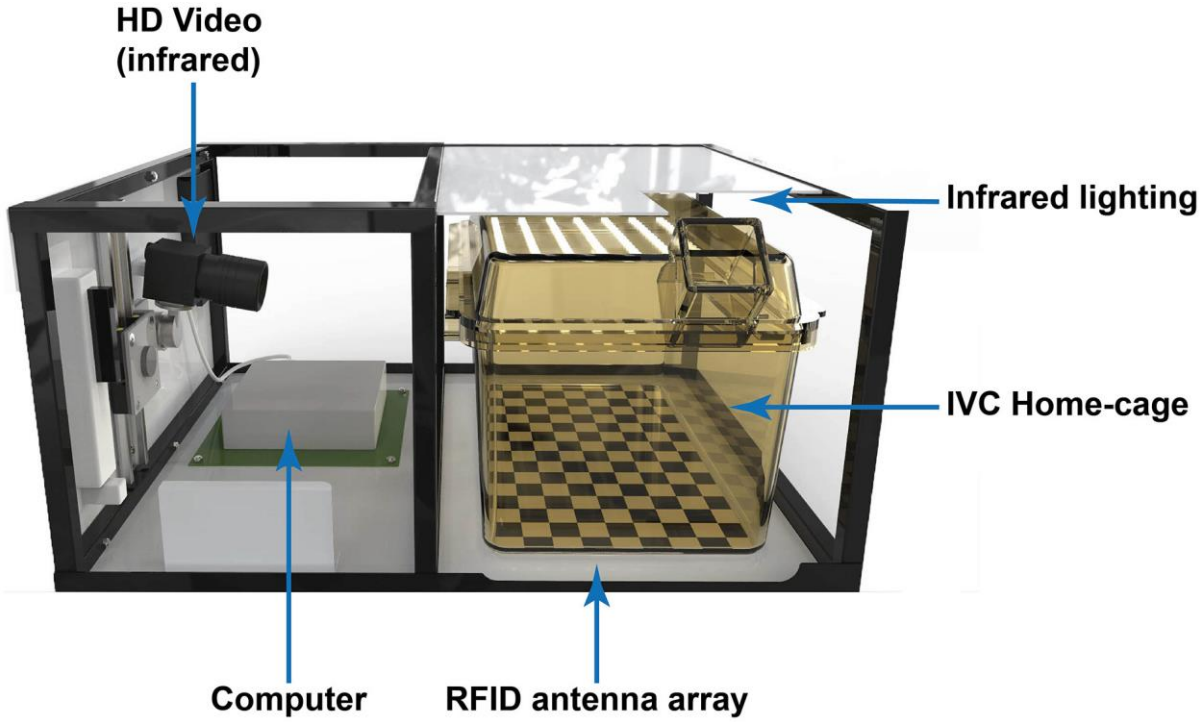


Figure 16 Illustration of Home Cage Analysis Rig setup, with main components highlighted. One half of the rig comprises an RFID reader base plate with antennae located on predetermined locations. This provides the base for placing the individually ventilated mouse home cage. The other half, fitted within the adjacent rack space, houses an infrared camera, a computer and the appropriate power supplies. The cage sits under a plate affixed to the top of the rig which is fitted with an infrared light source allowing for continuous video capture without compromising the quality of the image. (Bains, Cater et al. 2016).

2.2.6. Intraperitoneal Glucose Tolerance Test (IPGTT)

The glucose tolerance test measures the clearance of an intraperitoneally injected glucose load from the body. Mice were fasted for approximately 16 hours by transferring the mice to clean cages with no food or faeces in hopper or bottom of cage. Access to drinking water was ensured at all times. On the day of the test, the mouse was weighed, and a glucose solution prepared based on this weight measurement: 2g of glucose/kg body mass. Anaesthetic cream (EMLA Cream, 5%, AstraZeneca, UK) was applied to each mouse' tail base. The tail was gently massaged ~10 seconds to enhance the effect of the anaesthetic cream ensuring that the proposed incision site is fully covered. An appropriate amount of time must be left for the local anaesthetic to take effect (10-15 minutes). The mouse was placed in a restraining device with the tail exposed. The base of the tail was scored using a sterile scalpel blade, making a small incision in the lateral tail vein. The first small drop of blood was discarded. A small drop of blood (<5µl) was placed on the test strip of the blood glucose meter. This is the baseline glucose level (T0) and was recorded. The mouse was removed from the restraining device. The mouse was injected intraperitoneally with the appropriate amount of glucose solution, as previously determined and the time-point of injection noted. The blood glucose levels are measured at 15, 30, 60 and 120 minutes (T15, T30, T60 and T120) after glucose injection, by

placing a small drop of blood on a new test strip and recording the measurements. The same incision is used for each time point, and removing the clot from the first incision or massaging the tail can promote blood flow if it is inadequate. Results are recorded. Ensure that further blood loss from the incision is minimal by briefly applying pressure to the incision after each measurement. At the end of the experiment add food to the cage and make sure that a plentiful supply of water is available to the animals.

2.2.7. Dual-energy X-ray Absorptiometry

Dual-energy X-ray Absorptiometry (DEXA) is a method of quantifying bone mineral content and density. DEXA uses an X-ray generator of high stability to produce photons over a broad spectrum of energy levels. Its photon output is filtered to produce the two distinct peaks necessary to distinguish bone from soft tissue. Mice were anaesthetised by isoflurane gas and monitored carefully until unconsciousness was achieved. After ensuring that the mouse was adequately sedated, it was placed in the DEXA scanner with a face mask administering a low dose of isoflurane to maintain anaesthesia. A scout-scan was performed to ensure proper placement of the animal, and optimisation for the areas of interest was carried out. For the analysis of the data, regions of interest must be defined. The standard analysis comprises of a whole body analysis excluding the head area. A measure-scan was then performed. Note that the exposure dose per mouse is 300µSv. The mouse was removed from the scanner once the image had been captured, placed in a recovery cage and monitored closely until consciousness was regained.

2.2.8. Locotronic

Locotronic is used or the detailed modelling of walking and its disorders in mice and rats, with respect to motor and psychomotor skills and cognition. The Locotronic is a unique piece of apparatus consisting of a horizontal ladder (124cm in length) with sensors in each step of the ladder to assess motor coordination. As the mouse traverses the ladder, any missed steps by front or rear legs, as well as tail errors, are automatically detected by the apparatus, and are automatically exported to a data file for analysis. The Locotronic system was commercially acquired from IntelliBio Innovation.

2.2.9. Grip Strength

Grip strength test is used to measure muscle strength in all four limbs (fore and hind limbs). A grip strength meter (BioSeb, USA) was used, with a single metal grid (400x180x200 mm) attached to the sensor. The unit of measurement of the sensor was grams. The mouse was removed from its home cage, and by gripping the base of the tail between thumb and forefinger, gently lowered onto the grid so that all four paws could grip the bars. Keeping the

torso horizontal, the mouse was pulled back gently until the animal actively pulled itself upwards. The maximal grip strength was displayed on the screen, and was recorded. This procedure was repeated three times for each mouse. The mouse was then placed on a balance and it's body weight was recorded, before returning the mouse to its home cage. The grid was cleaned with ethanol (70%) and allowed to dry before testing each cage of mice.

2.2.10. Wheel running activity cages

Female mice were singly housed in cages with running wheels (TSE Systems), where they were subject to a 12 hour light/dark cycle (as in normal husbandry procedures). Each running wheel was connected to a sensor that detected each turn of the wheel and relayed the information to a computer for data collection via the TSE Phenomaster software. Output measurements included total distance travelled, number of rotations of the wheel, rotation velocity, number of wheel-running episodes and time spent running. The validation of using this system in identifying motor deficits can be found in (Mandillo, Heise et al. 2014). Each mouse had individual access to ad lib food and water at all times. After 7 days, animals were removed from the wheel running cages and placed back into their original housing groups in clean cages (without running wheels).

2.2.11. Open Field

Animals were transported to the testing room and left undisturbed for 30 minutes before the test. Lighting conditions were set to a standard level (150-200 lux). For analysis, each open field arena was divided into a peripheral zone measuring 8 cm from the edge of the arena walls, and a central zone around 40% of the total surface of the arena. Testing was conducted during the light phase, with 1 hour gap from the light/dark change. Testing was conducted during the same period of day for all mice tested. The apparatus was wiped clean with 70% ethanol and allowed to dry between mice. Each mouse was placed in the middle of a peripheral zone of the arena facing the wall and allowed to explore freely the apparatus, with the experimenter out of the animal's sight. Mice were video-tracked for 20 minutes, using Any-MAZE video-tracking software. At the end of the 20 minute run, animals were put back into their home cage. After each run, any faeces were removed and the arena was thoroughly cleaned. Males and females must be run in separate tests; males were tested first, followed by females. Analysis of the recording was done using Any-MAZE to measure the activity of each mouse in each of the zones.

2.2.12. Auditory Brainstem Response

Auditory brainstem response (ABR) test determines hearing sensitivity and other physiological parameters using evoked potential recordings in anesthetized mice. Mice were anaesthetised

via intraperitoneal injection and placed on heating blanket in the sound chamber. Subdermal needle electrodes were inserted as follows; active electrode on vertex; reference electrode overlying right bulla (as this is the ear being stimulated); ground electrode overlying left bulla. Mice were placed unrestrained in a prone position, nose forward, at the calibrated distance from the leading edge of the speaker to the mouse's interaural axis, on a thermostatically controlled blanket, inside a sound attenuating booth. Viscotears Liquid Gel was placed on the eyes of anaesthetised mice during testing. ABRs were recorded to clicks (10 µs duration, positive transient) presented from 0-85 dB SPL in 5dB steps, presented 256 times at 42.6/sec. ABRs were recorded to the following frequencies and levels; 8kHz (0-85dB SPL), 16kHz (0-85dB SPL) and 32kHz (0-85dB SPL), presented in 5dB intervals. After ABR testing, electrodes were removed and mice were placed in heated chambers and allowed to recover from anaesthesia. Thresholds were defined for each mouse and for each stimulus as the lowest intensity at which any part of the ABR waveform could be visually recognized by a trained operator. Calls were made on data from each line based on a set of rules: for each stimulus, over 60% or more of thresholds must fall outside of a 95% reference range (based on a population of wildtype data) for that result to be classed as significant. A manual call option was also used in some cases, whereby by an experienced operator was able to call whether or not to include a particular dataset, to override the rules-based call.

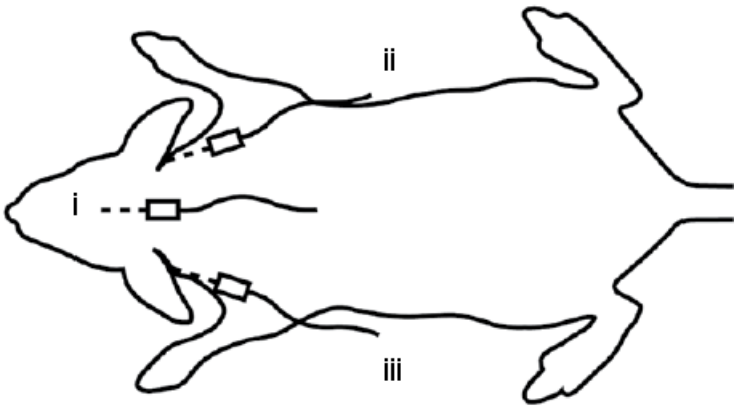


Figure 17 Schematic of subdermal electrode placement. Active electrode on vertex (i), reference electrode overlying right bulla (ii), ground electrode overlying left bulla (iii). (Adapted from (Hardisty-Hughes, Parker et al. 2010).

2.2.13. Contextual and cued fear conditioning

Fear conditioning apparatus was acquired commercially from Ugo Basille. Fear conditioning is a test of three parts; firstly the mouse is subject to a conditioned stimulus (CS) (in this case an auditory cue) and an unconditioned stimulus (US) (in this case a foot shock). This is the conditioning part of the test. Secondly, the mouse is subjected to the same environment as when it received the US (same context) but does not receive the CS or the US. Thirdly, the mouse is subjected to a new context, and receives the CS, but not the US. Freezing behaviour is measured as a way to assess fear, and therefore memory, of the US in relation to context and CS (cue).

Fear conditioning phase:

The equipment is turned on and is checked that all components are working correctly. It was ensured that the CS (auditory cue) was connected correctly and would deliver the appropriate stimulus (for the tone, 10 kHz, 80dB for 5 seconds for). It was checked that the shocker was working correctly and that the shock level was set at 0.5 mA for 1 second. The CS must co-terminate with the US. It was checked that activity/freezing detection module was working correctly.

Testing is conducted during the light phase of the cycle with 1 hour gap from the light/dark change. Animals were transported to the testing room and allowed to habituate for 30 minutes prior to testing. The mouse was then placed into the fear conditioning apparatus (first context with barred flooring to deliver shocks). Once the test had begun the mouse was allowed to acclimatise for 4 minutes, then the tone (~10 kHz, 80dB) CS is presented for 5 seconds and co-terminated by a mild (1 s, 0.5 mA) foot shock (US). This CS and US sequence is repeated three times, one minute apart. At the end of the test mice were placed back into their home cage and delivered back to their usual housing facility. The apparatus was cleaned with 70% ethanol and allowed time for it to dry in between animals. Males and females should be tested separately and were conducted on different days. The activity/immobility is recorded as index of baseline and conditioning. The mouse is considered freezing/immobile when there is a complete lack of movement for at least 2 consecutive seconds.

Contextual testing phase:

Contextual testing was performed ~24 hours following the conditioning session. Animals were transported to the testing room and allowed to habituate for 30 minutes prior to testing. It was checked that all modules were connected properly. Only the light and activity detector

should connected, the cues (auditory) and shocker were disconnected. Animals were placed back into the same chamber that was used for the conditioning and, once the test had begun, allowed to explore for 6 minutes without presentation of the auditory CS. The movement/immobility of the animal is monitored to detect freezing behaviour consequent to recognition of the chamber as the spatial context (contextual learning). The mouse is considered freezing when there is a complete lack of movement for at least 2 consecutive seconds. At the end of the test mice were placed back into their home cage and placed onto IVC racks within the test room. The apparatus was cleaned with 70% ethanol and allowed time to dry in between animals.

Cued testing phase:

Cued testing is performed ~5 hours after the contextual testing. Animals were tested in a novel test chamber of distinct appearance (wall colour, odour and floor texture were different). It was checked that the light, auditory cues and activity detector are working properly (the shocker was disconnected).T Once the test had begun, the mouse is allowed to habituate for 2 minutes then presented with three auditory cues spaced 1 minute apart. The movement of the animal is monitored to detect freezing behaviour consequent to cue presentations. The mouse is considered freezing when there is a complete lack of movement for at least 2 consecutive seconds. At the end of the test mice were placed back into their home cage and delivered back to their usual housing facility. The apparatus was cleaned with 70% ethanol and allowed time for it to dry in between animals.

2.2.14. Novel Object Test

To test learning and memory the novel object recognition test (NOR) was used. Mice were singly housed for 5 days in a light tight chamber, and subjected to a 12 hour light/dark cycle, as in normal husbandry conditions. The cages were video monitored 24 hours a day. Objects used were a choice of two: a small clip-top jar and a piece of assembled red and yellow building blocks (consisting of four pieces).

Mice were allowed to habituate for at least 24 hours prior to testing (day 1 – habituation). One day 2 of the test, a single novel object (either the jar or the building blocks) was placed into one corner of the cage of each mouse. Mice were allowed to explore the object for 2 minutes, and then the object was removed. On day 2, the same object as the previous day (familiar object) was placed in the same place in each cage. Again, mice were allowed to explore the object for 20 minutes, before the object was removed. On day 3, a different object (jar if had previously seen building blocks, and vice versa) was placed in the cage, in the

opposite corner of the cage (new object). Again, mice were allowed to explore the object for 20 minutes, before the object was removed.

Each object was cleaned with 70% ethanol when removed from the cages and dried overnight. Objects were placed in the cage at the same time each day, during the light phase. Any-MAZE video-tracking software was sued to assess time spent interacting with the object. An area was drawn in each corner of the cage for analysis. The mouse being present in this area (very close proximity to the object) corresponded to interaction time.



Figure 18 Schematic of home cage with different objects during the novel object recognition test. Day 1: a novel object is placed in one corner of the home cage. Day 2: the same object is placed in the same place of the home cage. Day 3: A new object is placed in the opposite corner of the home cage.

2.2.15. Y-Maze spontaneous alternation test

The Y-Maze is a behavioural test used to assess memory function and the willingness of rodents to explore new environments. The test apparatus used is a Y-shaped maze with three identical arms at a 120° angle from each other. The apparatus was made in house.

The mouse was removed from its home cage and placed at the far end of one of the arms of the maze (the start arm). This arm was alternated between mice to avoid this one arm becoming an invariant in the test. One of the three arms was restricted by placing a block in the entrance to the arm. This left two arms available to the mouse to explore – the start arm and the familiar arm. The mouse was allowed to explore for 5 minutes, and its time spent in each arm was recorded using Any-MAZE video-tracking software. The mouse was then removed from the Y maze apparatus, and placed back into the home cage for one minute. During this time, the apparatus was cleaned with 70% ethanol and dried. The same mouse

was placed back into the start arm, and the arm that was previously blocked off (the novel arm) was opened up for exploration. The mouse was allowed to explore for 5 minutes, and its time spent in each arm was recorded using Any-MAZE video-tracking software.

2.2.16. Acoustic Startle Response and Pre-Pulse Inhibition (PPI) test

The acoustic startle response is characterized by an exaggerated flinching response to an unexpected strong auditory stimulus. This response can be attenuated when it is preceded by a weaker stimulus (pre-pulse) and is the principle underlying pre-pulse inhibition (PPI). This test provides an operational measure of sensorimotor gating reflecting the ability of an animal to successfully integrate and inhibit sensory information.

The experimental apparatus consists of an outer attenuated chamber that serves to prevent external noise or vibrations interfering with experiment. Within this chamber a load cell platform that records the startle response is linked to the transducer and amplifier, which calibrates the load cell platform. An animal holder rests upon the load cell platform. A sound generator and the appropriate software regulate pulses from the amplifier.

The mice were transported to the testing room and left undisturbed for a minimum of 30 minutes. Care was taken not to stimulate the mouse before starting the experiment. The cage must not be changed on the day of the experiment. Each mouse was placed into the animal holder, and this chamber is loaded onto the load cell platform. The door to the sound proof chamber was then closed and the test was begun. The session was initiated with a 5 minute acclimatisation period (only background noise - NOSTIM). In addition, this time was used to acclimatise the mouse to the startle stimulus, which consisted of 110dB white noise for 40-60ms. This stimulus was presented 5 times.

The session was then continued by presentations of different trial types, each of which was presented 10 times in pseudorandom order, with an inter-trial interval (ITI) varying randomly between 20 and 30 seconds. The trials are as follows:

- Different pre-pulse trials of 20 ms duration of white noise stimuli which are presented alone (65, 75, 85dB),
- Different pre-pulse trials preceding the startle stimulus by 50-120 ms (65dB + pulse, 75dB + pulse, 85dB + pulse) to derive the pre-pulse inhibition response.

The intensities of the pre-pulse should be kept at levels above the background noise that do not elicit a significant startle response on their own, being approximately 2-20dB above background noise.

Startle response was recorded every millisecond for 65-100 ms after the onset of startle, i.e. 40-60 ms during the startle plus 25-40 ms after the startle ended; 65-100 ms from the end of the previous ITI for NOSTIM (see Figure 19).

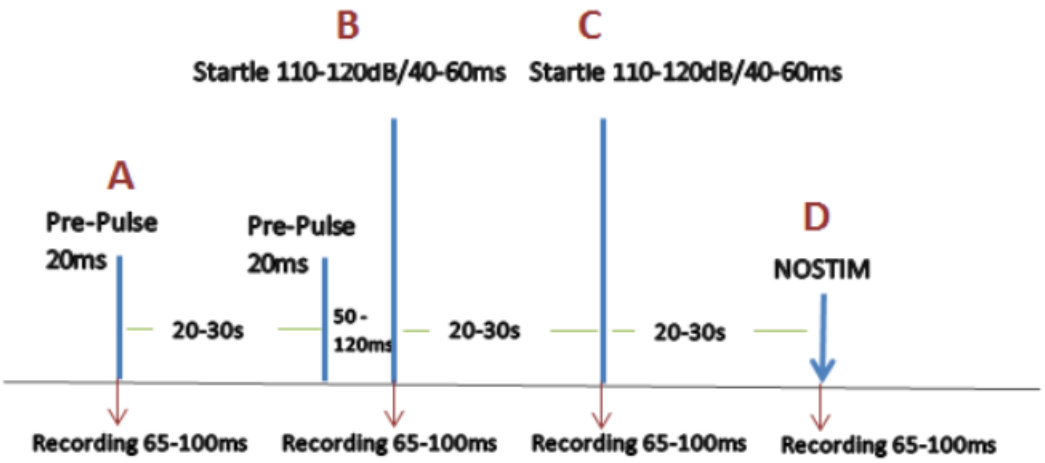


Figure 19 The different type of trials of the acoustic startle & pre-pulse inhibition test. A. Pre-pulse alone (65dB, 75dB or 85dB). B. Startle preceded by pre-pulse. C. Startle alone. D. NOSTIM.

2.2.17. Haematological analysis

Terminal blood samples for haematology were collected from mice aged 16 weeks, under terminal isofluorane inhalation anaesthesia, by retro-orbital puncture into paediatric EDTA-coated tubes. The samples were placed on a rotary mixer for 30 minutes immediately after collection and kept at room temperature until a full blood count and differential analysis was performed on board a Siemens Advia 2120 haematology analyser using settings and reagents recommended by the manufacturer.

2.3. Histological staining

2.3.1. Muscle pathology

Whole muscles were weighed upon removal from the mouse, and then snap frozen. 10 µm cross-sections of frozen gastrocnemius, soleus and EDL were examined with H&E to assess the architecture of the of the muscle fibres. Then, 10µm cross-sections of the soleus were subjected to ATPase staining (acid pre-incubation at pH 4.47) and the total number of fibres and proportion of fibre types within the soleus were assessed. Muscle morphology was analysed in wildtype and *Efl1*$^{K983R/K983R}$ littermates at 3 months of age (male, *n* = 3 per genotype).

2.3.2. p21 Immunostaining of tibiae

Tibiae were removed from 10 month old female mice, decalcified and embedded in paraffin wax. 5 µm sections were cut along the length of the bone, and were mounted in slides. VECTASTAIN Elite ABC kit (Vector Laboratories, cat# PK-6100) was used, as per manufacturer's instructions. Endogenous peroxidase were quenched by incubating with 0.3% H_2O_2 in isopropanol for 20 minutes at room temperature. p21 antibody (Santa Cruz, cat# SC-397) was used at a 1:100 dilution, incubated on sections for 20 minutes at room temperature. Sections were then counterstained using Haematoxylin solution, Gill No 1 (Sigma Aldrich, cat# GHS1128).

2.3.3. Oil Red O staining of pancreas

Pancreata were collected from 2 month old female mice and fixed in 10% formalin. Fixed tissues were frozen and cut into 3 µm thick sections, in a transverse orientation. Sections were stained with Oil Red O Sudan 5B solution in 0.5% isopropanol (Sigma Aldrich, cat# O1391) overnight at 4°C, and then counterstained with Haematoxylin solution, Gill No 1 (Sigma Aldrich, cat# GHS1128).

2.3.4. H&E staining of middle ear sections

For the analysis of middle ear histopathology, the heads of 3 month old female mice were removed and transferred to formalin and embedded in paraffin wax. Haemotoxylin and eosin (H&E) staining was performed on 5 µm thick transverse sections of the embedded heads. Measurement of the middle ear epithelial was carried out using NanoZoomer Digital Patholgy software (www.ndpserve.com). An average of five measurements along a 1000 µm section of the epithelium was taken.

2.4. Cell culture and cell-based assays

2.4.1. Mouse Embryonic Fibroblast Culture

Timed mating of Efl1$^{+/K983R}$ mice were set up and these intercross litters were harvested at E14.5. Embryos were submerged in ice-cold PBS and exsanguinated promptly to confirm death. Tails were removed and reserved for genotyping. Limbs, head and internal organs were removed, leaving the torso 'shell' of the embryo intact. The 'shell' was then placed into 2ml trypsin (0.5% EDTA) in a 3.5cm dish and chopped thoroughly with a blade. Trypsin and tissue was collected into 50ml tubes via pipetting up and down using a 5ml stripette to break up the tissue further. Trypsin and tissue were heated at 37°C for 5 minutes. Trypsin and tissue were transferred to a 10cm dish containing 10ml Dulbecco's Modified Eagle Medium (DMEM) high glucose, with sodium pyruvate (Thermo Fischer Scientific cat# 41966029) (with added foetal bovine serum (10%) and penicillin streptomycin solution (1%)) using a p1000 pipette.

2.4.2. Mouse embryonic fibroblast freezing

MEFs were grown in 10cm dishes to 70-80% confluency in DMEM high glucose, with sodium pyruvate (Thermo Fischer Scientific cat# 41966029) (with 10% foetal bovine serum (EU-approved, South American origin, Thermo Fischer Scientific cat# 10270098) and 1% penicillin streptomycin solution (Thermo Fischer Scientific cat# 15070063). Cells were detached from culture surface using 2ml trypsin (0.05% EDTA, Thermo Fischer Scientific cat# 25300054) and incubating at 37°C for 5 minutes. Cells were centrifuged at 300g for 5 minutes, and excess medium was removed from pellet. Pellet was resuspended in freezing media (foetal bovine serum and 10% Dimethyl Sulphoxide (DMSO)). 1ml aliquots were pipetted into 2ml cryotubes and placed into a cold freezing container, containing isopropanol. The freezing container was then stored at -80°C for approximately 24 hours, before transferring the cells to liquid nitrogen storage.

2.4.3. Mouse Embryonic Fibroblast Growth Assay

MEFs at passage 1 were thawed form liquid nitrogen storage and plated in DMEM high glucose, with sodium pyruvate (Thermo Fischer Scientific cat# 41966029) in 6 well plates at a density of $1x10^5$ cells/well. Enough plates were seeded for 5 measurements, and plates were incubated at 37°C, 5% CO_2 for the duration of the experiment. On days 2, 6, 9, 12 and 15, cells were washed with PBS (Dulbecco's Phosphate Buffered Saline cat# 14190094), and 500 µl trypsin (0.05% EDTA, Thermo Fischer Scientific cat# 25300054) was added per well. Cells were incubated at 37°C with trypsin for 5 minutes, before 500 µl media was added to deactivate the

enzyme. Cell counts were taken from within each well using the Millipore Sceptre Cell Counter with Sceptre sensors (60 µm). Triplicate measurements were taken for each sample. Numbers (n) = 3 per genotype.

2.4.4. Bradford Assay

7 serial dilutions of BSA were prepared as standards; 1.4mg/ml, 1mg/ml, 0.5mg/ml, 0.25mg/ml, 0.125 mg/ml, 0.06mg/ml. 1.4mg/ml was chosen as the highest standard as the Bradford assay can only detect up to this range. Samples were diluted 1:5 to allow for this upper limit of sensitivity. Bradford reagent (Sigma Aldrich, cat#, B6916) was brought up to room temperature. 5 µl of standards and diluted samples were added to a clear, flat bottomed 96 well plate (Sigma Aldrich, Greiner CELLSTAR®, cat# M3562). 250 µl of Bradford reagent was added per well. Plate was incubated at room temperature for 5 minutes. Absorbance at 480 nm was recorded, and protein concentrations were calculated using the computer program KCJunior (Bio-Tek).

2.4.5. Western Blot Analysis in Mouse Embryonic Fibroblasts

MEFs were cultured as described above. Media was removed from 10cm dishes, and cells were washed twice with PBS, and 5ml tryspin (0.05% EDTA, Thermo Fischer Scientific cat# 25300054) was added. Cells were incubated at 37°C with trypsin for 5 minutes, before 5ml media was added to deactivate the enzyme. Cells were collected in 15ml tubes and centrifuged for 5 minutes at 300g. The cell pellet was washed once with PBS, and centrifuged again for 5 minutes at 300g. PBS was removed and dry pellet was lysed with RIPA buffer (with added phosphatase inhibitors (PhosSTOP™, Sigma Aldrich, cat# 04906845001 Roche) and protease inhibitors (cOmplete™, EDTA-free Protease Inhibitor Cocktail, Sigma Aldrich, cat# 04693132001 Roche). The pellet was broken up with the lysis buffer by pipetting up and down repeatedly with vigorous vortexing. Lysates were incubated on ice for 30 minutes. Lysates were then centrifuged at max speed in a pre-cooled microfuge (4°C) for 30 minutes. Cleared lysates were transferred to a clean, pre-cooled Eppendorf.

Lysate protein concentrations were measured using the Bradford assay. Western blot samples were prepared using NuPAGE® LDS Sample Buffer (4X) (Thermo Fischer Scientific, cat# NP0008) and NuPAGE® Sample Reducing Agent (10X) (Thermo Fischer Scientific, cat# NP0004). 25 µg of protein was loaded onto NuPAGE™ Novex™ 4-12% Bis-Tris Protein Gels (Thermo Fischer Scientific, cat# NP0322BOX) in 1x sample buffer and reducing agent mix, in a total reaction volume of up to 20 µl. Western blots were run in 1x MOPS buffer (NuPAGE® MOPS SDS Running Buffer (20X), cat# NP0001) using a PowerEase® 500 Power Supply (Novex by Life

Technologies, cat# EI8600, EI8700, and EI8675), set at 150V (voltage constant) and 120mA (amplitude variable).

Transfer to nitrocellulose membranes was conducted using iBlot™ Gel Transfer Stacks (mini, nitrocellulose) (Thermo Fischer Scientific, cat# IB301002) and the iBlot™ Gel Transfer Device (Thermo Fischer Scientific, cat# IB21001). All blots were run using programme 3, for 7 minutes, apart from blots to be used for EFL1 detection, which were run with using programme 3 for 8 minutes. After transfer, membranes were blocked with 5% milk in PBS/Triton™ X-100 (Sigma Aldrich, cat# X100) for 1 hour at room temperature, whilst on a roller.

Primary antibodies were incubated at 4°C, overnight, except for α-GAPDH antibody, which was incubated at room temperature for 30 minutes. Primary antibodies used are as follows: EFL1 (1:200) (ABGENT cat# AP10373B), eEF2 (1:1000) (Abcam cat# ab33208), SBDS (1:1000) (Protein Tech, cat# 17618-1-AP), RPL28 (1:1000) (Protein Tech cat# 16649-1-AP), eIF6 (1:1000) (GenTex cat# GTX117971), RPS6 (1:1000) (Cell Signalling, cat# 2217), NMD3 (1:1000) (Protein Tech cat# 16060-1-AP), p70 S6K-total (1:1000) (Cell Signalling cat# 49D7), p70 S6K-Phospho (1:1000) (Cell Signalling cat# 108D2), eIF2α-total (1:1000) (Cell Signalling, cat# 5324), eIF2α-Phospho (S51) (1:1000) (Cell Signalling, cat# D9G8), α-puromycin, clone 12D10 (1:1000) (Sigma Aldrich, cat# MABE343), p53 (1:1000) (Santa Cruz, cat# FL-393), p21 (1:1000) (Santa Cruz, cat# SC-397).

Secondary antibodies used were goat α-rabbit, Alexa Fluor® 488 (1:20,000 +0.01% SDS) (Invitrogen) and goat α-mouse, Alexa Fluor® 647 (1:20,000 + 0.01% SDS) (Invitrogen). These secondary antibodies were incubated with the membranes at room temperature, α-rabbit for 1 hour, α-mouse for 15 minutes. A goat α-mouse IgG, Horse Radish Peroxidase (HRP)-conjugated secondary antibody (Sigma Aldrich, cat# A4416) was used for SUnSET westerns (after 12D10 primary incubation overnight), at 1:20,000 dilution, incubated with the membrane for 1 hour at room temperature.

2.4.6. Quantitative PCR in Mouse Embryonic Fibroblasts

MEFs were cultured as in 2.4.1. When at 70-80% confluency, MEFs were pelleted and lysed in 1ml QIAzol Lysis Reagent (Qiagen, cat# 79306). 200 µl chloroform was added, and samples were centrifuged at 12,000 rpm for 15 minutes at 4°C. Aqueous layer was removed and added to one volume of 70% ethanol to precipitate the RNA. RNA samples were purified using the RNeasy Plus Mini Kit (Qiagen, cat# 74134). RT-PCR was used to generate cDNA from the

extracted RNA samples, using the Superscript® III Reverse Transcriptase kit (Thermo Fisher Scientific, cat# 18080085).

qPCR was carried out for exon 2-3 of the *Efl1* gene, using Fast SYBR® Green Master Mix (Thermo Fisher Scientific, cat# 4385612), and analysed using the 7500 Fast Real-Time PCR System. Primers as follows: F - CTTCAGAAGAACACTGCCAA, R – TGCTGATTGTCTTATATCCA.

2.5. Translation Assays

2.5.1. Radioactive Methionine Assay in mouse embryonic fibroblasts

MEFs were thawed, from -80°C storage, into a 10cm dish in 10ml DMEM (Thermo Fischer Scientific cat# 41966029) and were allowed to recover overnight at 37°C, 5% CO_2. The following day, the MEFs were split 1:3. When cells reached 70-80% confluency, the media was removed, and cells washed twice with PBS (Dulbecco's Phosphate Buffered Saline cat# 14190094). Cells were seeded at 1.5x105 cells per well in a 6-well plate (Greiner, CELLSTAR® cat# 657160). The following day (or when cells reach 60-70% confluency), media was removed, cells washed with PBS, and 1ml/well of Methionine-free media was added to each well, and incubated for 30 minutes at 37°C, 5% CO_2. At this stage, cycloheximide was also added if using (concentrations used 0.1 µM, 1 µM and 50 µM for experimental control). After 30 minutes, 1.5 µl of [^{35}S]-Met label (concentration 0.37 MBq per µL) was added directly to the well, followed by gentle swirling to mix. The cells were again incubated for 30 minutes. No [^{35}S]-Met label was added to negative controls. After 30 minutes, the radioactive media was removed, and cells washed twice with PBS and 500 µl trypsin (0.05% EDTA, Thermo Fischer Scientific cat# 25300054) was added per well. Once cells were detached plates were put on ice and cells were removed from the wells and transferred to 1.5ml Eppendorfs. Cells were centrifuged at 300g in a pre-cooled microfuge, and the cells pellets were lysed in 1X Passive Lysis Buffer (Promega, cat# E1941). Lysates were incubated on ice for 1 hour. Lysates were then used for Bradford Assay (see 2.4.4) and scintillator counts (300 µl). The scintillator count lysates were transferred to a new Eppendorf and 300 µl 25% TCA solution (Sigma Aldrich, cat# T9159) was added. The TCA precipitates were incubated on ice for 30 minutes. A vacuum manifold (Millipore® XX2702550 Model 1225 Sampling Manifold Vacuum Filtration Cell Harvester for 15 ml or 50 ml Centrifuge Tubes) was used to prepare the filter papers for scintillator counting. 25 mm glass fibre Whatman filter papers (GE Healthcare Life Sciences Whatman Grade GF/A Glass Microfiber Filters, cat# 1820-025) were placed onto the manifold, with 15 ml waste tubes set up beneath. The vacuum was generated, and filter papers were wet with 200 µl 25% TCA solution. The TCA precipitated lysates were then loaded onto each

filter paper, followed by two washes of 500 µl 70% Industrial Methylated Spirit, and two washes of 500 µl Acetone (ice cold). Filter papers were allowed to dry completely on the vacuum manifold, before being placed into 20 ml scintillation vials containing 3ml scintillation cocktail (National Diagnostics Ecoscint A, cat# LS-273). Counts per minute for each vial were recorded using the 300 SL liquid scintillation counter from LabLogic Systems, according to manufacturer's instructions.

2.5.2. SUnSET western blot analysis in mouse embryonic fibroblasts

MEFs were thawed, from -80°C storage, into a 10cm dish in 10ml DMEM (Thermo Fischer Scientific cat# 41966029) and were allowed to recover overnight at 37°C, 5% CO_2. The following day, the MEFs were split 1:3. When cells reached 70-80% confluency, the media was removed, and cells washed twice with PBS (Dulbecco's Phosphate Buffered Saline cat# 14190094). 5ml of media containing puromycin (10 µg/ml stock solution) was added to make a final concentration of 1 µg/ml. Cells were incubated for 15 minutes at 37°C, 5% CO_2. After the 15 minute incubation, the puromycin media was removed, and cell were washed twice with PBS. Normal media (no puromycin) was added to the wells, and cells were incubated again for 45 minutes. After the 45 minute incubation, cells were lysed and analysed by western blot (as described in 2.4.5).

An α-puromycin primary antibody (clone 12D10, Sigma Aldrich, cat# MABE343) was incubated with the membrane overnight at 4°C on rollers. An α-mouse IgG HRP-conjugated secondary antibody (Sigma Aldrich, cat# A4416) was incubated with the membrane at room temperature for one hour. The Amersham ECL Western Blotting Detection Kit (GE Healthcare Life Sciences) was used for luminol-based detection of the HRP-conjugated secondary antibody, according to manufacturer's instructions. The ChemiDoc-It® Imager (UVP) was used to image the membrane after ECL incubation. A 2 minute exposure of UV light was used to image the membrane.

2.6. Polysome Profile Analysis

2.6.1. Polysome profiles in Mouse Embryonic Fibroblasts

MEFs were cultured as described in 2.4.1. Cells were harvested at 70% confluency for polysome profiling. Cells were incubated with cycloheximide (100 µg/ml) for 15 minutes prior to collection. After incubation, cells were washed with ice cold PBS containing cycloheximide (100 µg/ml), and 5ml trypsin, containing cycloheximide (100 µg/ml) was added and incubated for 5 minutes at 37°C. Cells were collected into 50ml tubes, and were centrifuged at 300g for 5 minutes. Cell pellets were washed in ice cold PBS containing cycloheximide (100 µg/ml), and

again centrifuged. Cell pellets were then lysed in 500 µl Lysis buffer. Cleared lysates were measured for absorbance at 260nm to assess RNA content, and were run on 5-45% sucrose gradients. Equivalent volume for 1 optical density unit was loaded for each sample.

Gradients were made in 14 ml polypropylene tubes (Beckman Coulter, cat# 331374). 5% and 45% sucrose solutions were made using 1X Gradient buffer. Gradients were spun using the Gradient Master 108 (Biocomp). Once lysates were loaded onto gradients, tubes were ultracentrifuged at 40,000rpm for 2 hours at 4°C. Gradients were passed through a spectrophotometer and 1ml fractions were collected. Absorbance traces were plotted, and areas under the curve were calculated using Microsoft™ Excel.

Gradient buffer (10X): 20 mM HEPES, 500 mM KCl, 100 mM Mg Acetate. Gradient buffer 1X: 1X gradient buffer, 10 mg/ml cycloheximide, 40 U/µl RNaseOUT™ (Thermo Fisher Scientific, cat# 10777019), 1 tablet protease inhibitor (cOmplete™, EDTA-free Protease Inhibitor Cocktail, Sigma Aldrich, cat# 04693132001 Roche). Lysis buffer (1 ml): 990 µl 1X gradient buffer, 5 µl IGEPAL® CA-630 (Sigma Aldrich, cat# I8896), 5 µl RNaseOUT, 2 µl 1M DTT.

2.6.2. Polysome profiles in liver

Livers were dissected from 6 month old male mice and snap frozen on dry ice, and stored at -80°C. 150 mg frozen tissue was weighed out, ensuring sample was kept frozen at all times. Tissue was ground to a fine powder using an ice cold pestle and mortar. The tissue was homogenised in 1 ml lysis buffer on ice. Cleared lysates were loaded onto 10-50% sucrose gradients in 12 ml tubes (5030 Open Top Polyallomer tubes, Seton Scientific, cat# 5030). Gradients were ultracentrifuged at 38,000 rpm for 2 hours at 4°C. Gradients were passed through a spectrophotometer and 1ml fractions were collected. Absorbance traces were plotted, and areas under the curve were calculated using Microsoft™ Excel.

10X Gradient buffer: 3 M NaCl, 150 mM $MgCl_2$, 150 mM Tris-HCl pH7.5, 20 mM DTT, 1 mg/ml cycloheximide. Lysis buffer: 1X gradient buffer, 1X TritonX-100, 8X RNase free water, 25 µl/ml Superase-in (Ambion, cat# AM-2696).

2.6.3. Quantitative PCR in liver polysome fractions

1ml fractions from liver polysome profiles were collected into 3 ml 7.7 M Guanidine Hydrochloride (G-HCl - for protein denaturation) and 4ml 100% ethanol, and were mixed thoroughly. Samples were stored at -20°C overnight and then centrifuged at 4000 rpm for 50 minutes to form a pellet. Pellet was resuspended in 400 µl water, vortexed, and left to stand for 2 minutes before being transferred to an Eppendorf. 40 µl of 3 M Sodium Acetate (pH 5.2)

and 1 ml 100% ethanol was added, and again samples were stored at -20°C overnight. Samples were centrifuged at maximum speed for 30 minutes, and pellet was washed with 800 µl of ice-cold 75% ethanol. Pellet and ethanol were placed into a mixer for 10 minutes. Again samples were centrifuged at maximum speed and pellets were air dried. Pellets were resuspended in RNase-free water.

RT-PCR and qPCR were carried out for the RNA samples from fraction 6-9 of the liver polysome profiles, as in 2.4.6.

Chapter 3
Genetic Characterisation of the *Efl1*-K983R mouse line

3. Genetic characterisation of the *Efl1*-K983R mouse line

The *Efl1*-K983R mutant mice described in this thesis were originally identified in the Harwell Ageing screen. The Harwell Ageing Screen is an 18 month pipeline of phenotyping tests aimed at characterising age-related phenotypes in a recessive screen of ENU-derived pedigrees. These mice were therefore discovered by their phenotypic presentation only, with no knowledge of causative mutations. This forward genetics approach is hypothesis generating, and can result in the discovery of novel gene functions.

Consequently, discovery of the mutation was the first port of call when embarking upon the characterisation of this mouse. This chapter details the genetic characterisation and identification of the causative mutation in these mice.

3.1. Positional cloning of mouse chromosome seven

The *Efl1*$^{K983R/K983R}$ mouse was originally discovered through the Harwell Ageing Screen due to the presentation of an abnormal gait. With no prior knowledge of the causative mutation, a genome wide scan was conducted to look for informative SNPs. An Illumina medium density SNP array was carried out to identify regions of homozygosity within the genomes of affected mice, compared to an unaffected mouse. Regions of C57BL/6J SNPs would indicate portions of the genomes inherited form the mutagenised founder, and therefore will give clues as to the possible locations of the ENU-derived mutation that is causing the phenotype in the affected mice.

Large regions of SNPs homozygous for C57BL/6J variations in affected mice, but not in unaffected mice, were flagged as regions of interest. The largest region of interest appeared on chromosome seven, between positions 7:70843942 and 7:95502909 (Figure 20A). Further informative SNPs were selected to further narrow down this ~25 Mb region. The SNPs selected are as follows: rs31470929 (7:71012690), rs31275887 (7:75034769), rs3686423 (7:79583258), rs3023147 (7:84249894) and rs6317573 (7:90173202). Heterozygosity for SNPs at positions 7:84249894 and 7:90173202 indicated that the critical region did not extend this far, thus narrowing the region down to ~14Mb (Figure 20B).

These data give a relatively small region in which to delve deeper into identifiying the mutation that causes the abnormal gait.

A

Sample ID	SNP ID and position					
	rs3705155 (7:68522720)	rs13479324 (7:70843942)	rs3676254 (7:72686265)	rs13479338 (7:74058986)	rs13479347 (7:76287673)	rs13479414 (7:95502909)
Affected mouse 1						
Affected mouse 2						
Affected mouse 3						
Affected mouse 4						
Affected mouse 5						
Affected mouse 6						
Affected mouse 7						
Affected mouse 8						
Unaffected mouse						

B

Sample ID	SNP ID and position										
	rs3705155 (7:68522720)	rs13479324 (7:70843942)	rs31470929 (7:71012690)	rs3676254 (7:72686265)	rs13479338 (7:74058986)	rs31275887 (7:75034769)	rs13479347 (7:76287673)	rs3686423 (7:79583258)	rs3023147 (7:84249894)	rs6317573 (7:90173202)	rs13479414 (7:95502909)
Affected mouse 1											
Affected mouse 2											
Affected mouse 3											
Affected mouse 4											
Affected mouse 5											
Affected mouse 6											
Affected mouse 7											
Affected mouse 8											
Affected mouse 9											
Affected mouse 10											
Affected mouse 11											
Affected mouse 12											
Affected mouse 13											
Affected mouse 14											
Affected mouse 15											
Unaffected mouse											

Figure 20 Schematic of SNP sequencing in critical region. A. SNP sequencing from Illumina Medium Density SNP array. 8 affected mice (left hand column in pink) and one unaffected mouse (left hand column in grey) were sent for genome wide SNP mapping using the Illumina medium density SNP array. An area of C57Bl6/J homozygosity was detected in affected mice between SNPs rs3705155 at position 7:68522720 and rs13479414 at position 7:95502909. These SNPs were homozygous for C3H variants in the unaffected mouse, indicating that this could be the region containing the causative mutation. **B. SNP sequencing with additional informative SNPs.** Five additional informative SNPs were selected within the critical region identified by the Illumina medium density SNP array. These SNPs are as follows; rs31470929 (7:71012690), rs31275887 (7:75034769), rs3686423 (7:79583258), rs3023147 (7:84249894) and rs6317573 (7:90173202) and are highlighted in the column headers in yellow. 7 additional affected mice were sequenced for these additional SNPs. This narrowed down the region of interest to between rs3705155 at position 7:68522720 and rs3023147 at position 7:84249894. Red: homozygous C57Bl6/J, Yellow: heterozygous C57Bl6/J:C3H, Green: homozygous C3H, grey: no data.

3.2. Identification of causative mutation via Next-generation sequencing

After identification of the region of interest, the specific causative mutation needed to be found. To do this, Next-generation sequencing (NGS) was carried out using DNA from the G1 founder male, focusing only on variants found in the region of interest. NGS, also known as high-throughput sequencing, is the catch-all term used to describe a number of different modern sequencing technologies. In NGS, vast numbers of short reads are sequenced in a single stroke.

Therefore, NGS is significantly cheaper, quicker, needs significantly less DNA and is more accurate and reliable than Sanger sequencing. For Sanger sequencing, a large amount of template DNA is needed for each read. Several strands of template DNA are needed for each base being sequenced, as a strand that terminates on each base is needed to construct a full sequence. In NGS however, a sequence can be obtained from a single strand, as it is broken into short segments and amplified within one sample location (slide or well). NGS is also quicker than Sanger sequencing in that multiple reads can be obtained in one read instead of just one.

NGS identified high confidence SNVs in the region of interest. Only one high confidence SNV was detected in a coding region. This SNV was a missense variant of A to G, at position 7:82763352, within the coding region of the gene *Elongation Factor-like 1* (*Efl1*) (Ensembl Gene ENSMUSG00000038563) (Table 3).

Table 3 Next generation sequencing results indicated 9 high confidence single nucleotide variations with the region of interest.

Chromosome	Position (bp)	Reference nucleotide	Variant nucleotide	Functional Class	Strand	Gene Description
chr7	**69284980**	**T**	**A**	**Intergenic variant**	**Forward**	**N/A**
chr7	**69599435**	**C**	**T**	**Intergenic variant**	**Forward**	**N/A**
chr7	**71261407**	**T**	**A**	**Intergenic variant**	**Forward**	**N/A**
chr7	**71674632**	**T**	**C**	**Intergenic variant**	**Forward**	**N/A**
chr7	**71825411**	**C**	**T**	**Intergenic variant**	**Forward**	**N/A**
chr7	**75326692**	**A**	**G**	**Intron variant**	**Forward**	**N/A**
chr7	**79213370**	**A**	**T**	**Intergenic variant**	**Forward**	**N/A**
chr7	**82763352**	**A**	**G**	**Missense variant**	**Forward**	***Elongation Factor-like 1***
chr7	**83312171**	**A**	**G**	**Intergenic variant**	**Forward**	**N/A**

3.3. Validation of Next-generation sequencing

While NGS is superior to traditional Sanger sequencing methods, it is still advisable to verify reads from NGS with ones Sanger sequencing to ensure accuracy in the read. Sanger sequencing of four of the SNVs identified in NGS was carried out to validate the next generation sequencing results, as well as the missense variant in *Efl1*. All SNVs were tested in one affected mouse (with abnormal gait) and one unaffected mouse (normal gait).

The four SNVs chosen to validate the NGS results were at the following positions: 7: 71261407 (T-A), 7: 75326692 (A-G), 7: 79213370 (A-T) and 7: 83312171 (A-G). All SNVs tested showed the nucleotide variations indicated by NGS (Figure 21).

The coding variant within *Efl1* was also validated by Sanger sequencing in two affected mice, one unaffected mouse, and also the two inbred strains used to generate the cohort; C57BL/6J and C3H.Pde (one mouse of each strain tested). Sequencing confirmed the NGS result that the affected mice carry a G residue at position 7: 82763352, and unaffected mice, including the background strains, carry an A residue (Figure 22).

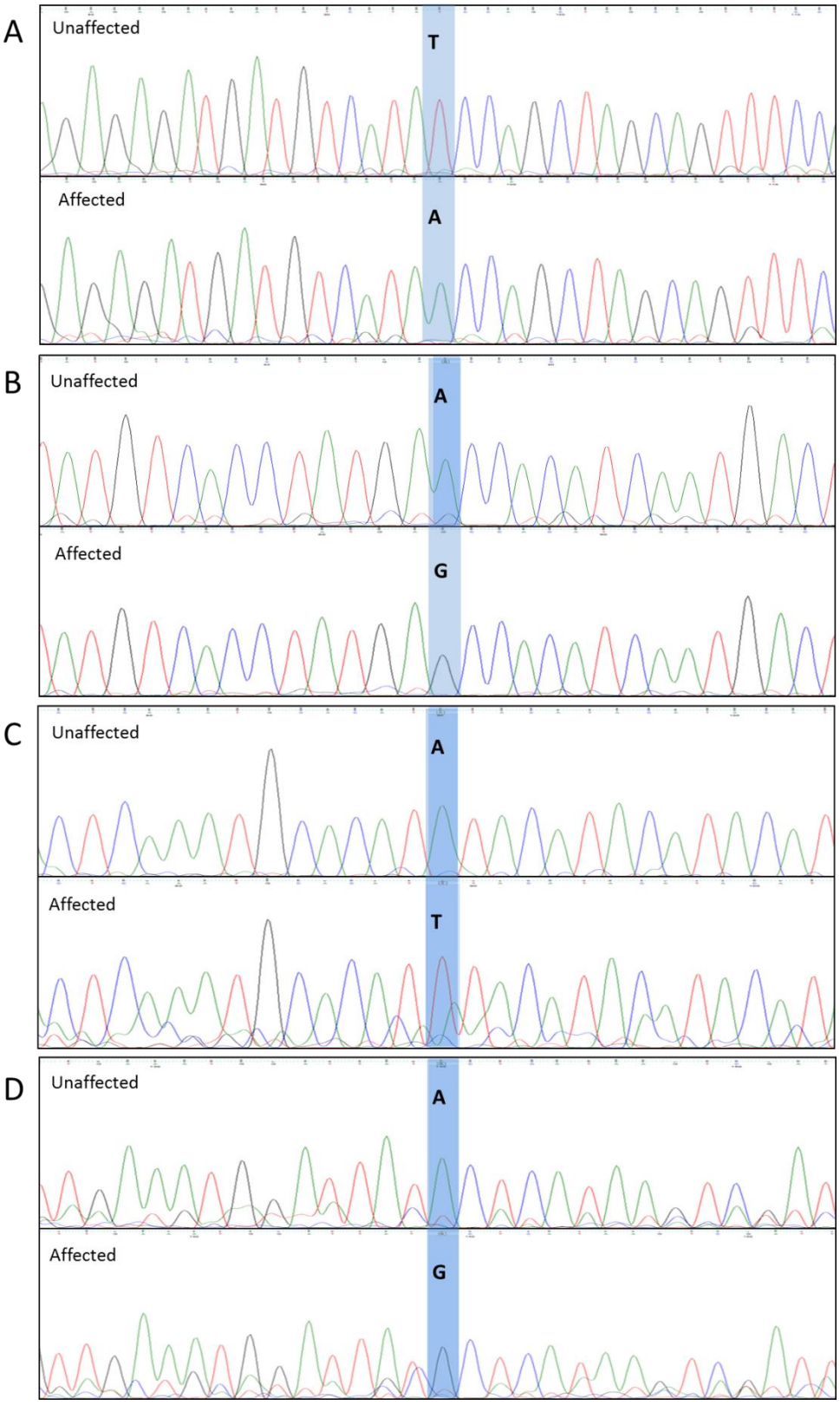


Figure 21 Sanger sequencing of four other SNVs to validate Next Generation Sequencing. A. Sanger sequencing of the SNV identified by NGS at position 7: 71261407. The SNV at position 7: 71261407 consists of a T to A variation in an intergenic region. The unaffected mouse harbours a T residue at this position, whilst the affected mouse harbours an A, confirming the NGS result. **B. Sanger sequencing of the SNV identified by NGS at position 7: 75326692.** The SNV at position 7: 75326692consists of an A to G variation in an intron. The unaffected mouse harbours an A residue at this

position, whilst the affected mouse harbours a G, confirming the NGS result. **C. Sanger sequencing of the SNV identified by NGS at position 7: 79213370.** The SNV at position 7: 79213370 consists of an A to T variation in an intergenic region. The unaffected mouse harbours an A residue at this position, whilst the affected mouse harbours a T, confirming the NGS result. **C. Sanger sequencing of the SNV identified by NGS at position 7: 83312171.** The SNV at position 7: 83312171 consists of an A to G variation in an intergenic region. The unaffected mouse harbours an A residue at this position, whilst the affected mouse harbours a G, confirming the NGS result. Numbers (N) = 1 affected, 1 unaffected.

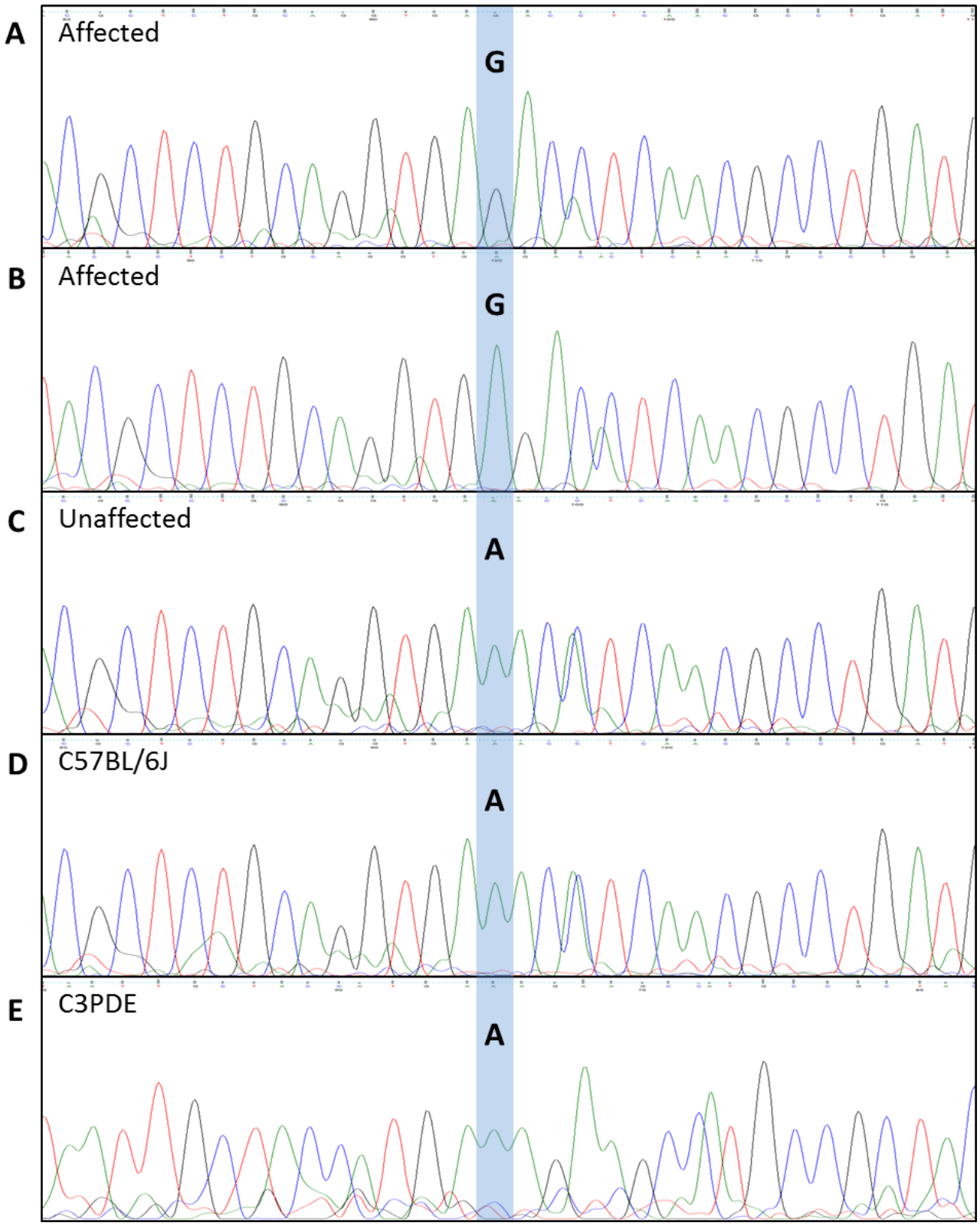


Figure 22 Sanger sequencing of the missense variant indicated by the Next Generation Sequencing results at position 7:82763352. The missense variation at position 7: 82763352 consists of an A to G variation in the gene *Elongation Factor Tu GTP binding domain containing 1* (*Eftud1*), also known as *Elongation Factor-like 1* (*Efl1*). The unaffected mouse harbours an A residue at this position, as do inbred strains C57BL/6J and C3H.Pde (both the back ground strains used to generated the affected mice cohort). The affected mice however, harbour a G residue at this position, confirming the NGS result. Numbers (N) = 2 affected, 1 unaffected, 1 C57BL/6J, 1 C3H.Pde.

3.4. Possible functional consequences of the *Efl1*-K983R mutation

The coding variant identified in the NGS was found to result in a lysine to arginine missense mutation in the protein EFL1 (Ensembl transcript ENSMUST00000039881) at position 983 (K983R) (position 3001 in the transcript). Lysine and arginine are both basic, polar, positively charged amino acids, and so this missense mutation is not likely to make a huge structural change in the protein.

However, lysine to arginine mutations are not always neutral, and can affect protein stability and/or function. Arginine is often involved in salt bridge formation where it pairs with negatively charged amino acids, such as aspartate, and forms hydrogen bonds to increase protein stability. Lysine on the other hand is adept at forming hydrogen bonds with negatively charged groups, such as phosphate groups, because it only has one amino group. Replacement of lysine with arginine might therefore affect hydrogen bonding in that specific part of the protein and affect tertiary structure.

One example of a Lys-Arg mutation that is not neutral in the mouse is the NEMO-KR mouse. This mouse line harbours a mutation in the *Nemo* (NF-κB essential modulator) gene (K392R) results in macrophages and dendritic cells with blunted response to TLR signalling (Ni, Wu et al. 2008).

Lysine and arginine also differ in their ability to be ubiquitylated. Lysine is frequently ubiquitylated in many proteins, whereas arginine does not become ubiquitylated at all. In fact, lysine to arginine mutations are often used in research to prevent ubiquitination of a protein (Ablack, Metz et al. 2015).

Computer generated ribbon models show little difference in predicted structure of mutant protein with the Arginine residue at position 983 (Figure 23). Additionally SIFT predictions state that this variant is non-harmful. These data suggest that the K983R mutation in EFL1 does not affect protein structure or function.

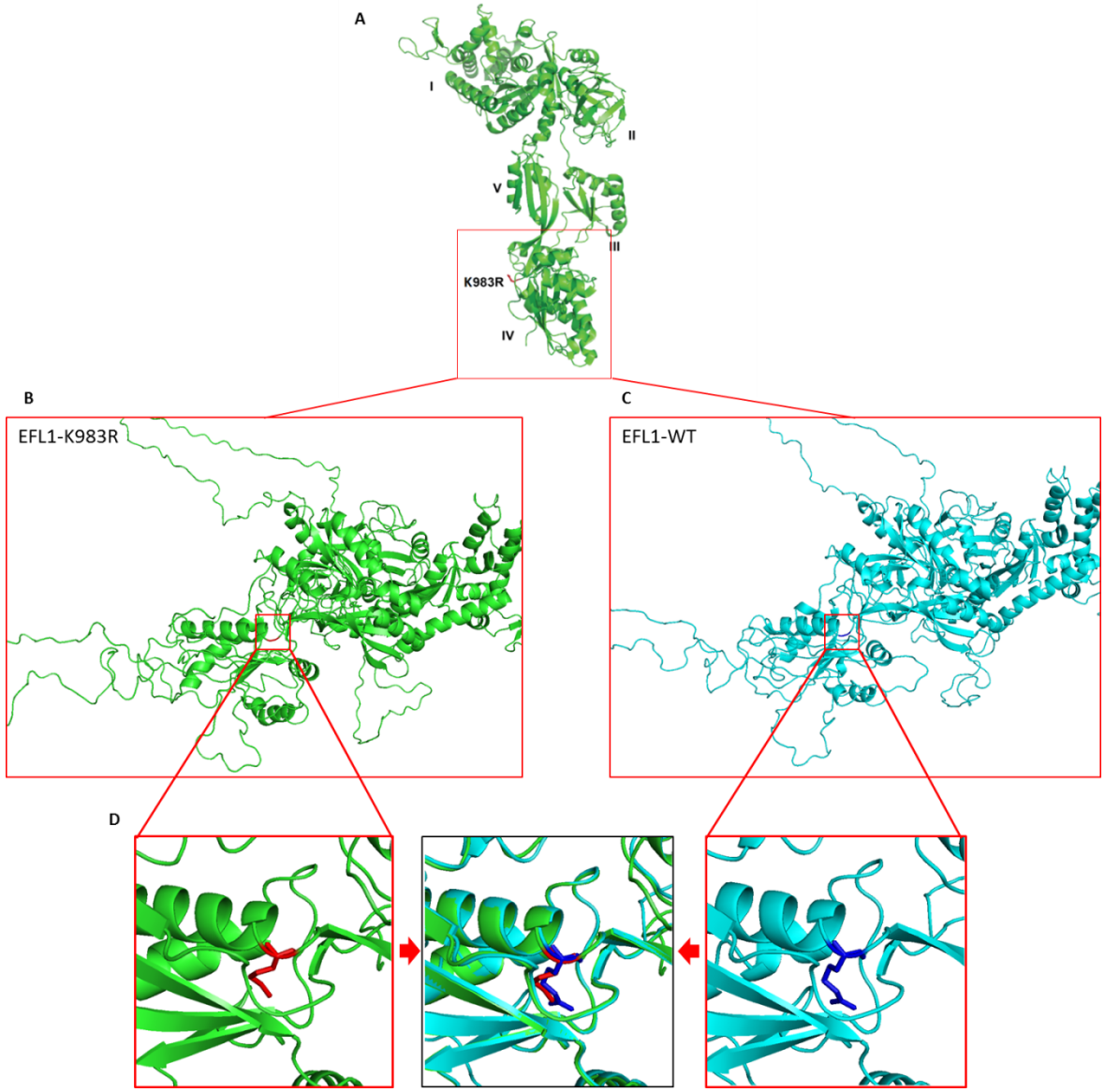


Figure 23 Computer generated ribbon models of EFL1. A. EFL1 3D structure. EFL1 is a five domain protein, with a classic GTPase composition, with the G domain in domain I of the protein and four additional domains. The K983R mutations is located in domain IV, away from the GTPase catalytic centre. **B. Domain IV of EFL1 with R983 residue.** The K983R mutation is highlighted in red. **C. Domain IV of EFL1 with wildtype K983.** The K983 residue is highlighted in dark blue. **D. Zoomed in view of residue 983 in mutant and wildtype.** Left to right: Arginine residue at position 983 (mutant variant) highlighted in red, merge of mutant arginine and wildtype lysine residues at position 983, lysine residue at position 983 (wildtype). Very little structural changes are predicted, as shown by the overlay of the two protein variants. (Created for use in this thesis by Saumya Kumar, MRC Harwell)

Chapter 4
Phenotypic Characterisation of the *Efl1*-K983R Mouse Line

4. Phenotypic characterisation of the *Efl1* K983R mouse line

A comprehensive phenotyping pipeline was designed for the *Efl1*-K983R mutants in order to study the mice in their entirety. Mutations in ribosomal protein genes are renowned for their diverse effects on the body as a whole. For example, SDS patients can present with symptoms in many different organs, including the pancreas, the haematopoietic system, the skeletal system and the brain (attention or social difficulties). For this reason, the phenotyping pipeline implemented for the *Efl1* mutants was extensive in covering multiple organs.

The *Efl1*-K983R mutation was generated by ENU mutagenesis, and after the mutation was identified by next generation sequencing, the animals were rederived with sperm from the G1 founder male through IVF. Heterozygous G3 animals were intercrossed to homozygose the mutation and produce experimental cohorts. Backcrossing the rederived *Efl1* mutants to C3 wildtype mice segregated the causative mutation from additional ENU mutations carried by the G1 animals. This ensures that other potentially functional mutations are segregated appropriately from experimental cohorts.

The phenotyping cohorts discussed below range between 2 and 4 backcrosses of segregation onto the C3H.Pde background, to ensure elimination of confounding mutations elsewhere within the genome. By selecting for the *Efl1*-K983R mutation at each backcross, the phenotypes of the mice discussed in this chapter are more than likely to be a result of the *Efl1*-K983R mutation and not other ENU-induced mutations that may have been present in the G1 founder.

4.1. Longevity and Viability

4.1.1. Life span is not affected by the *Efl1* K983R mutation

SDS patients have an average lifespan of 35 years (Brown and Buchdahl 2008). For this reason it was deemed necessary to study survival in the *Efl1*-K983R mutant mice.

Life span was not significantly different between genotypes in female mice. The median life span in females was 608, 657.5 and 655 days in $Efl1^{+/+}$, $Efl1^{K983R/+}$ and $Efl1^{K983R/K983R}$ mice respectively (Figure 24). Fighting was a common problem with the male mice in this study, and fight wounds were a common cause for welfare concerns, which often resulted in culling of the injured mice. It is possible that the male *Efl1*-K983R mutation leads to increased aggression in male mice. The frequent fighting made it very difficult to age the mice sufficiently, and therefore median life span could not be obtained for male mice. This has resulted in missing time points for male phenotyping

data in some cases. For this reason, much of the phenotyping data is limited to 6 months of age in male mice, whereas female data is available up to 14 months of age.

No obvious maladies were seen in male or female mice throughout their life span. The most common cause of death was weight loss in females (20% weight loss is cause for welfare concerns, and mice were culled if they reached this threshold) and fight wounds in males. In certain cases, head tilts were seen in females (after 6 months of age). Four mice were found dead with no obvious cause of death (one male, 3 females) (Table 4).

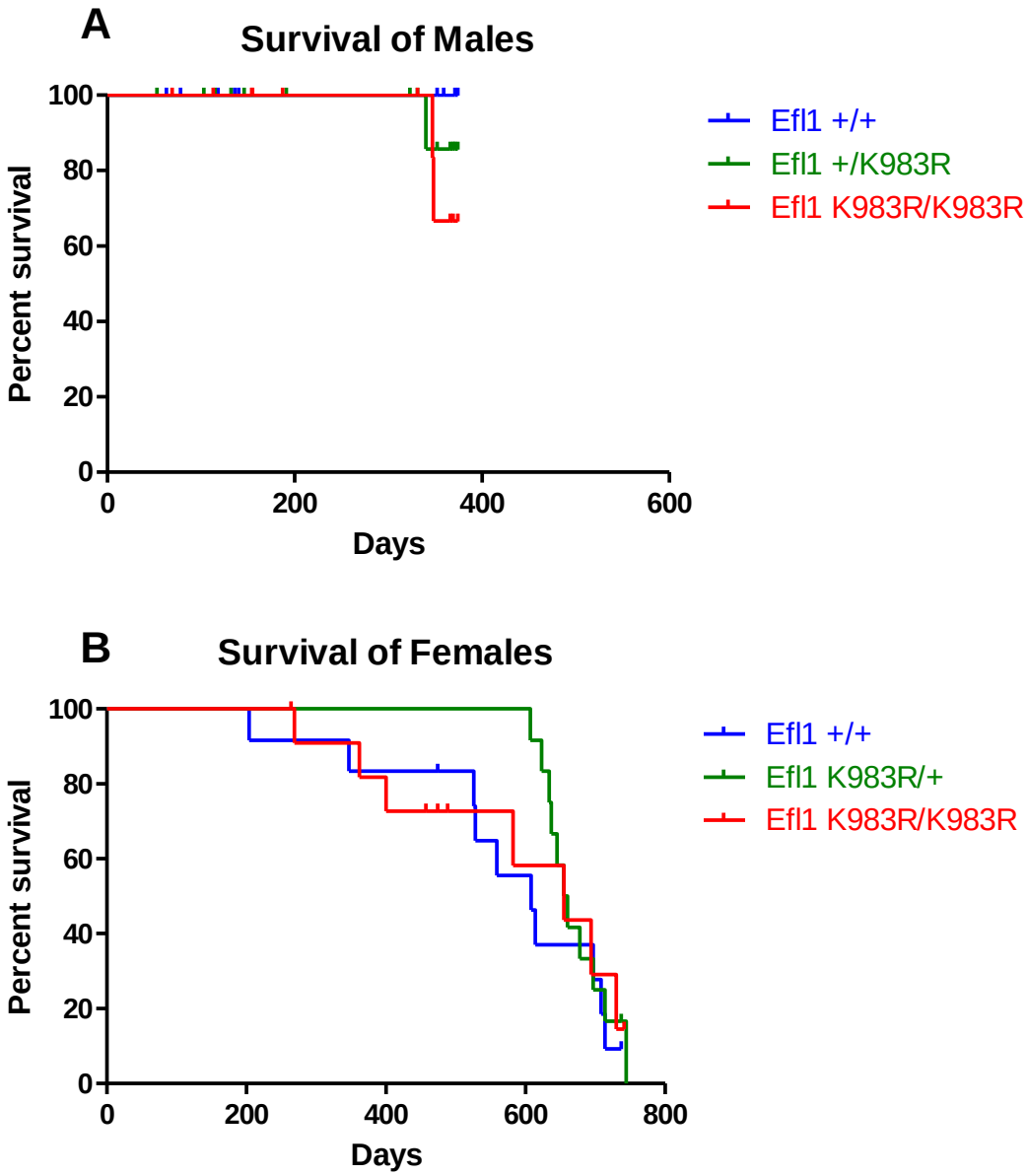


Figure 24 Survival curves of male and female mice. A. Survival curve for male mice. The median survival in male *Efl1*$^{K983R/K983R}$, *Efl1*$^{K983R/+}$ and *Efl1*$^{+/+}$ mice could not be defined due to the high number of censored subjects (culled due to fight wounds or being alone in a cage). The survival curves are not significantly different between genotypes (Log-rank p=0.0969.). **B. Survival curve for female mice.** The median survival in female *Efl1*$^{K983R/K983R}$, *Efl1*$^{K983R/+}$ and *Efl1*$^{+/+}$ mice is 655, 657.5 and 608 days, respectively. The survival curves are not significantly different between genotypes (Log-rank p=0.6537). Log-rank test for trenc used.

Table 4 Experimental cohort mice details, including age and reason for death. Animals are ordered into cages, with alternating dark and light shades. Blue = males, red = females.

A

Genotype	Fight wound	Found dead	Lone	Lump in abdomen	Tissues taken	Weight loss	Total
Efl1 +/+	5				8		13
Efl1K983R/+	7			1	8		16
Efl1K983R/K983R	3	1	3		6	1	14
Total	**15**	**1**	**3**	**1**	**22**	**1**	**43**
Percentage	**34.9**	**2.3**	**7.0**	**2.3**	**51.2**	**2.3**	**100.0**

B

Genotype	Bleeding vagina	Cateracts	Found dead	Sore underside	Lump	Swollen ankle	Tissues taken	Weight loss	Total
Phelps/Eftud1:Hom			1				5	6	12
Phelps/Eftud1:Het		1	1		7	1	1	1	12
Phelps/Eftud1:WT	1		1	1	2		2	5	12
Total	**1**	**1**	**3**	**1**	**9**	**1**	**8**	**12**	**36**
Percentage	**2.8**	**2.8**	**8.3**	**2.8**	**25.0**	**2.8**	**22.2**	**33.3**	**100.0**

4.1.2. *Efl1*$^{K983R/K983R}$ mice are smaller and weigh significantly less than littermates

Regular weighing showed that *Efl1*$^{K983R/K983R}$ mice weighed significantly less than *Efl1*$^{K983R/+}$ and wildtype mice from 3 weeks of age. This weight difference persisted throughout life, with *Efl1*$^{K983R/K983R}$ mice failing to 'catch up' to their littermates in terms of weight. *Efl1*$^{K983R/K983R}$ weight also plateaued earlier than *Efl1*$^{K983R/+}$ and wildtype weights, at around 40 weeks of age (9 months) (Figure 25). Embryos at E18.5 days post coitum (dpc) were weighed to determine if the weight difference starts *in utero*, and is developmental. There were no significant differences seen in weight at E18.5 dpc, suggesting that the weight differences begin at some point in the first 3 weeks of life. Weights could not be analysed earlier than 3 weeks of age, due to an inability to individually identify the mice before this time. Average head to anus length was measured in male mice of 3 months of age. There were no significant differences in length between genotypes at this age (**Error! R eference source not found.**C). However, *Efl1*$^{K983R/K983R}$ mice do show a shorter average length which may account for the weight differences seen. Length measurements at later time points may reveal significant size differences that could account for the weight differences seen.

Echo-MRI scans showed that at 2 months of age there were no significant differences in fat and lean mass between genotypes, thus demonstrating that weight differences are not due to fat mass differences between genotypes (the weight difference is present as early as 3 weeks of age). This suggests that it is overall size, and not fat differences that account for weight differences at this stage of life. Fat mass differences do occur however, at later time points. At 6 and 12 months of age female *Efl1*$^{K983R/K983R}$ mice have significantly less fat mass than *Efl1*$^{K983R/+}$ and wildtype littermates. Male *Efl1*$^{K983R/K983R}$ mice also have significantly less fat mass than *Efl1*$^{K983R/+}$ and wildtype littermates at 6 months of age, however no 12 month time point was available (Figure 27).

Organ weights were recorded in one year old female mice to assess if any individual organs were contributing to weight differences between genotypes. No significant differences were seen in organ weights once normalised to total body weight of the mouse, indicating that no individual organ is of abnormal size in the *Efl1*$^{K983R/K983R}$ mice. Body weight at one year of age is significantly lower in *Efl1*$^{K983R/K983R}$ mice compared to *Efl1*$^{K983R/+}$ and wildtype mice, which is to be expected given the weight data discussed above (Figure 28).

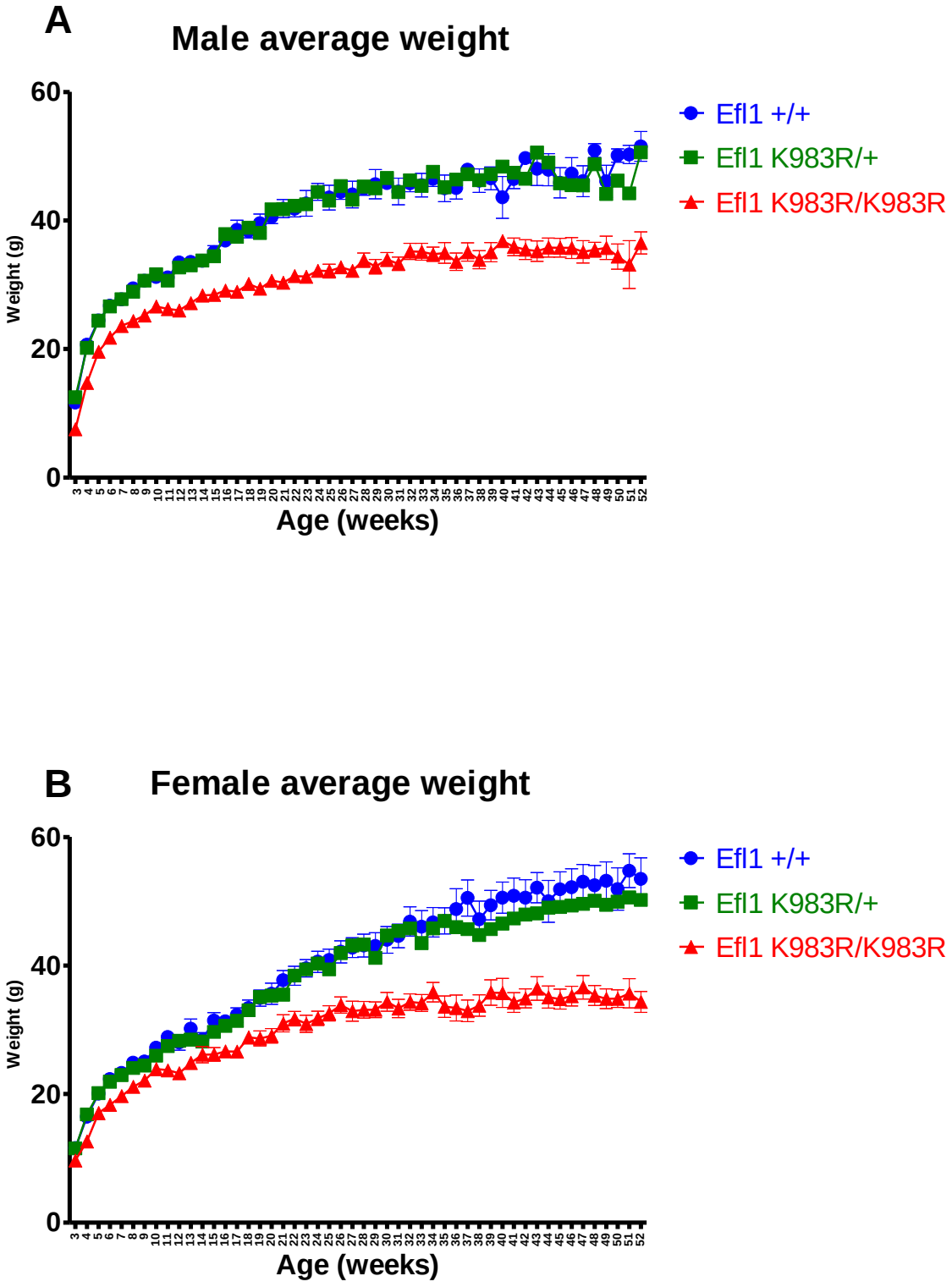


Figure 25 Average body weight of male and female mice between 3 and 52 weeks of age. A. Body weight in male mice *Efl1*$^{K983R/K983R}$ mice weighed significantly less than *Efl1*$^{K983R/+}$ and *Efl1*$^{+/+}$ mice form 3 weeks of age. This weight difference persisted throughout life (p=0.0004). Average *Efl1*$^{K983R/K983R}$ weight plateaued earlier than *Efl1*$^{K983R/+}$ and *Efl1*$^{+/+}$ weight, at approximately 40 weeks. A sharp drop was seen in *Efl1*$^{K983R/K983R}$ weight in old age (after 70 weeks of age). Numbers (n) and p values in appendix.

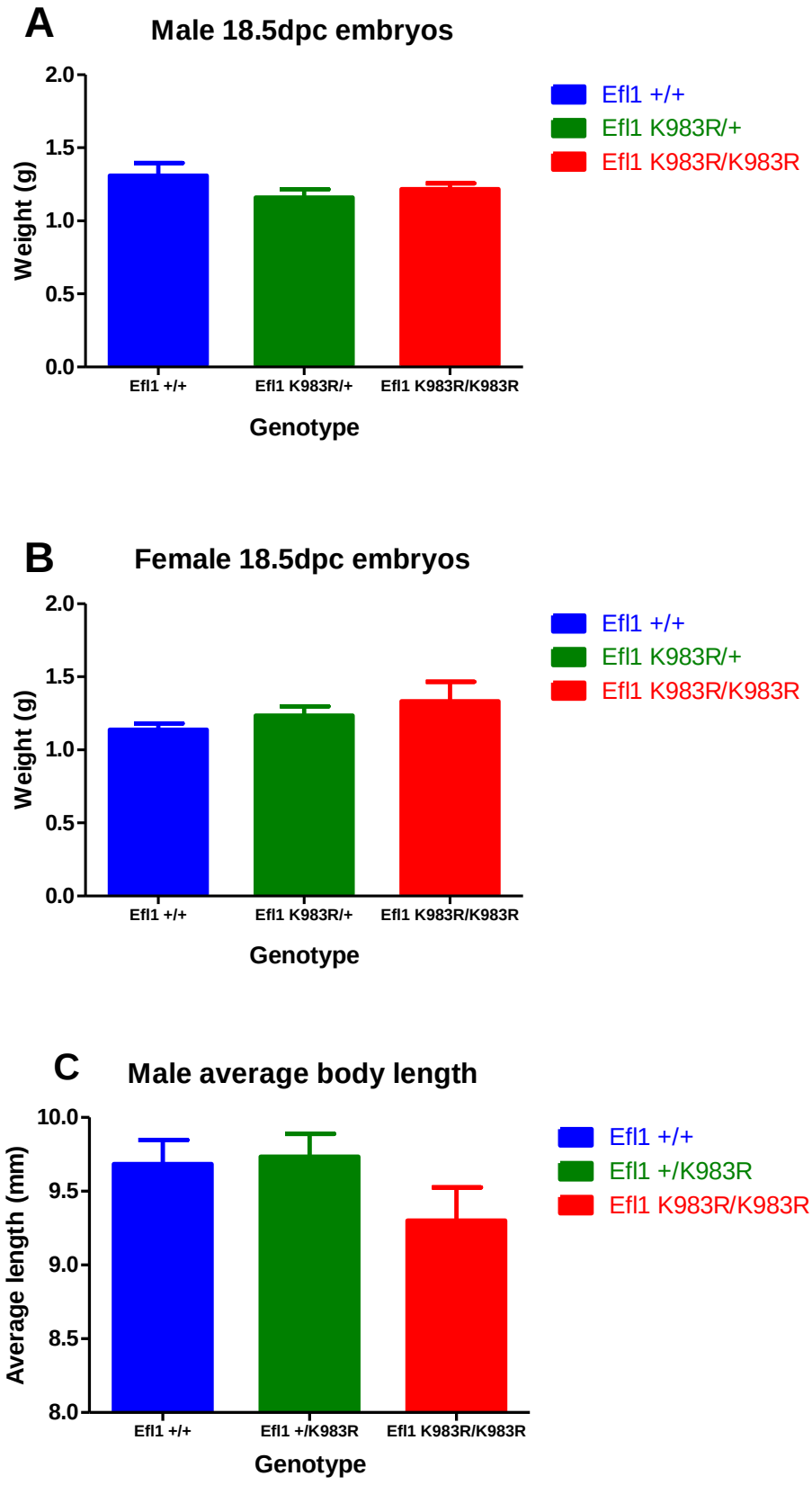


Figure 26 E18.5 day post coitum embryo weights. A, B. Male and female embryo weights at 18.5dpc. There are no significant differences in weight at 18.5dpc between genotypes, in male or female embryos. . N as follows: Male *Efl1*$^{K983R/K983R}$ n=5, *Efl1*$^{K983R/+}$ n=13, *Efl1*$^{+/+}$ n=10, female *Efl1*$^{K983R/K983R}$ n=6, *Efl1*$^{K983R/+}$ n=12, *Efl1*$^{+/+}$ n=16. **C. Average head to anus length of male mice at 3 months of age.** There are no significant differences in the average lengths of the mice between genotypes. N = 6 for all genotypes.

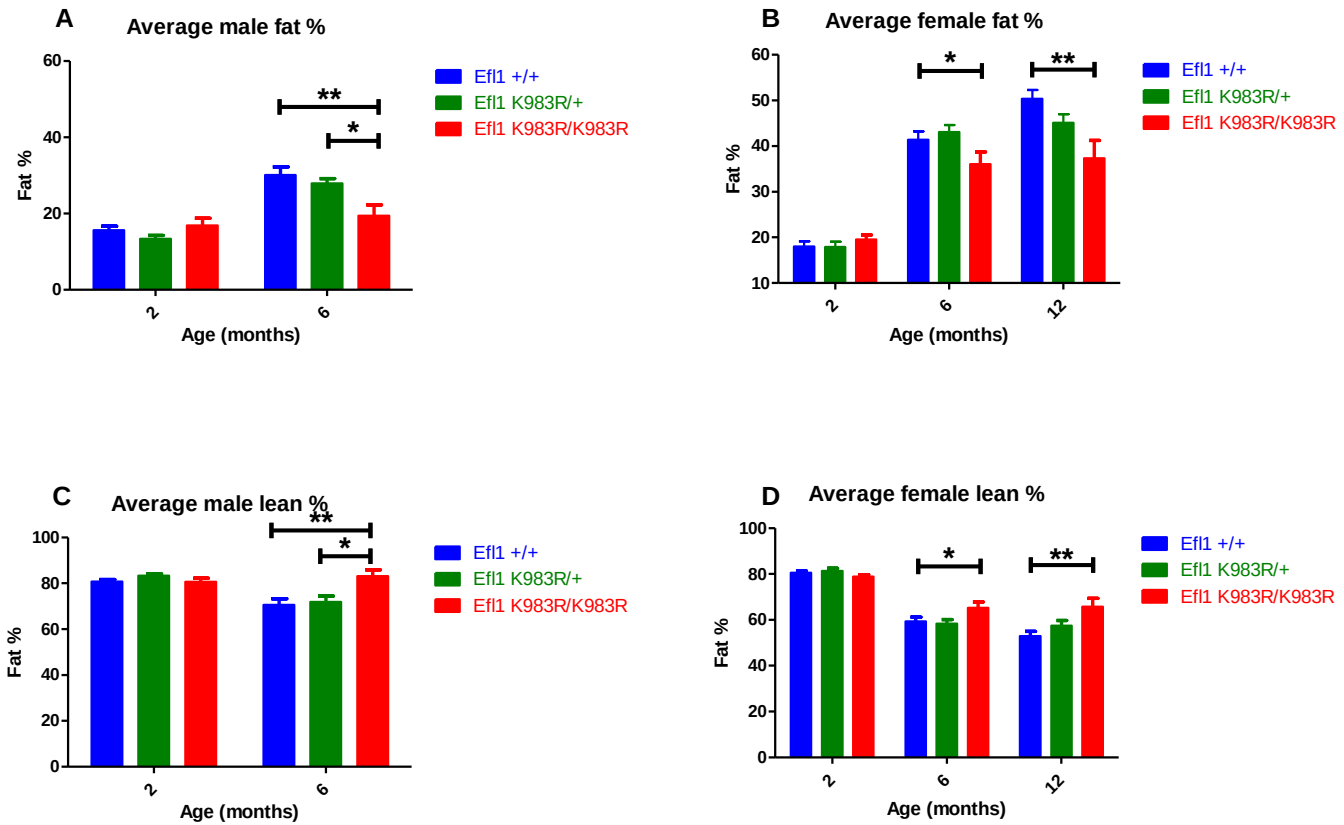


Figure 27 Fat and lean mass percentage for male and female mice. A, B. Average male and female fat percentage. No differences in body fat percentage between genotypes is seen at 2 months of age in male or female mice. Female *Efl1*$^{K983R/K983R}$ mice have significantly lower fat percentage than wildtype mice at 6 (p=0.032) and 12 (0.007) months of age. Male *Efl1*$^{K983R/K983R}$ mice have significantly lower fat percentage than *Efl1*$^{K983R/+}$ (p=0.015) and wildtype (0.009) mice at 6 months of age. There is no 12 month time point available for male mice. **C, D. Average male and female lean percentage.** No differences in lean body mass percentage between genotypes is seen at 2 months of age in male or female mice. Female *Efl1*$^{K983R/K983R}$ mice have significantly higher lean percentage than wildtype mice at 6 (p=0.038) and 12 (0.006) months of age. Male *Efl1*$^{K983R/K983R}$ mice have significantly lower fat percentage than *Efl1*$^{K983R/+}$ (p=0.012) and wildtype (0.007) mice at 6 months of age. There is no 12 month time point available for male mice. Numbers (n) as follows: n=12 for all mice at 2 months of age, female *Efl1*$^{K983R/K983R}$ n=12, 10, *Efl1*$^{K983R/+}$ n=12, 12, *Efl1*$^{+/+}$ n=10, 10 (6, 12 months, respectively), male *Efl1*$^{K983R/K983R}$ n=6, *Efl1*$^{K983R/+}$ n=7, *Efl1*$^{+/+}$ n=8 (6 months)

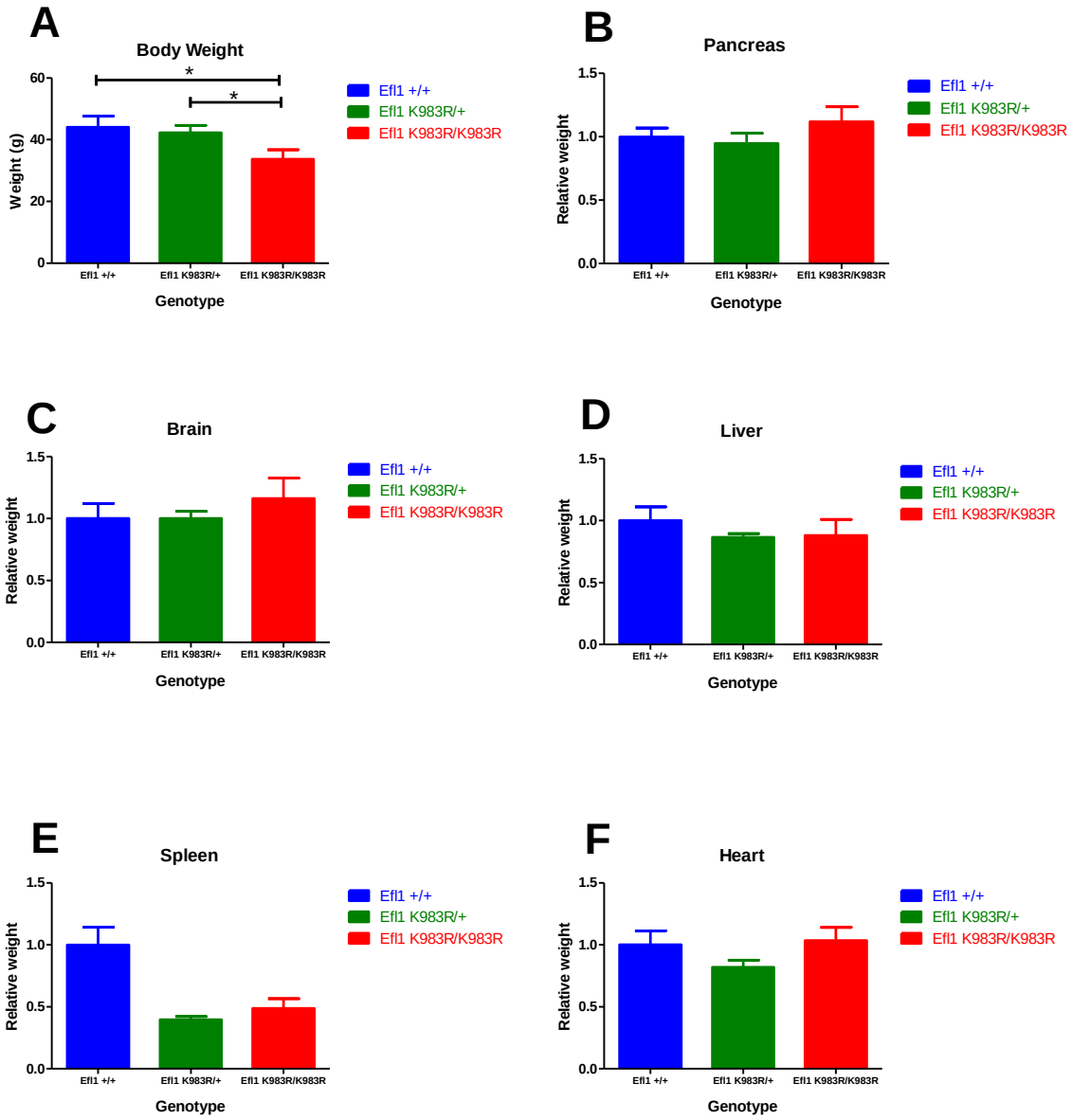


Figure 28 Body weight and individual organ weights. A. Total body weight. *Efl1*$^{K983R/K983R}$ mice weigh significantly less than wildtype and *Efl1*$^{K983R/+}$ mice at one year of age (p=0.049, p=0.045, respectively). **B-F. Relative pancreas, Brain, Liver, Spleen and Heart weight.** There are no significant differences in the relative weights of these organs in *Efl1*$^{K983R/+}$ or *Efl1*$^{K983R/K983R}$ mice compared to wildtype. Numbers (n) = *Efl1*$^{K983R/K983R}$ n=7, *Efl1*$^{K983R/+}$ n=9, *Efl1*$^{+/+}$ n=6. All females, one year of age (+/- one month).

4.1.3. Pancreatic structure is normal in *Efl1*$^{K983R/K983R}$ mice

As mentioned above, SDS patients are smaller in size due to pancreatic enzyme insufficiency. This is accompanied by lipomatosis of the pancreas, which replaces zymogen granules with fatty deposits in the liver. Therefore the pancreata of the *Efl1*-K983R mice were taken for histological analysis to determine if lipomatosis was present in these mice.

Size and weight of the pancreata in *Efl1*$^{K983R/K983R}$ mice was not significantly different to wildtype or *Efl1*$^{K983R/+}$ littermates at one year of age (Figure 28B). Oil red O staining of pancreata of 8 week old mice showed no difference in fat content of the pancreata in *Efl1*$^{K983R/K983R}$ mice compared to wildtype and *Efl1*$^{K983R/+}$ littermates (Figure 29). These data suggest that the size difference seen in *Efl1*$^{K983R/K983R}$ mice is not due to pancreatic abnormalities.

However, absence of pancreatic lipomatosis does not rule out an SDS diagnosis, as it is present in 100% of cases (Myers, Bolyard et al. 2014). Recent research is highlighting differences between genetically defined SDS and what is term 'clinical SDS', where a patient is diagnosed with SDS due to the presence of qualifying symptoms but has no mutation in the *SBDS* gene. It may be that the absence of pancreatic lipomatosis in some patients reflects the emerging variation in clinical presentation amongst SDS patients. For this reason it may be that these mice better reflect a 'clinical SDS' phenotype, rather than genetically defined disease.

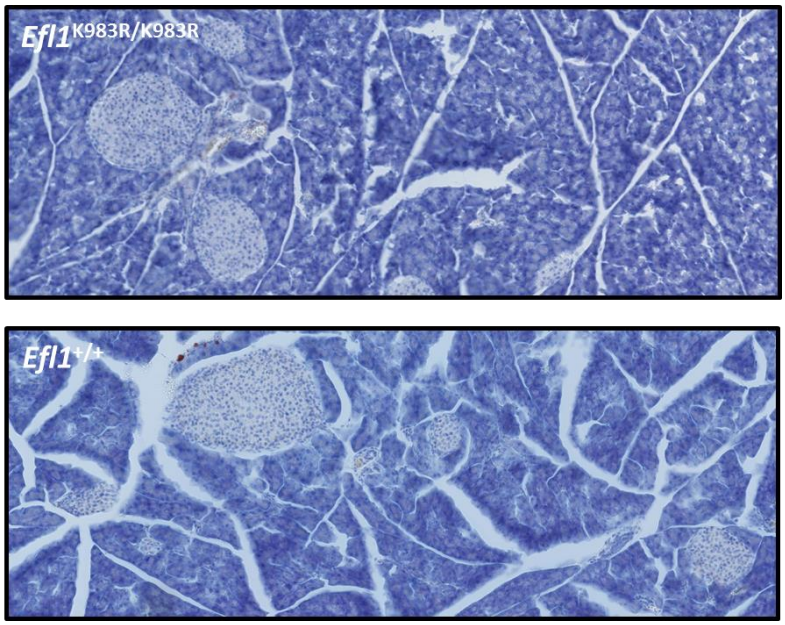


Figure 29 Oil Red O Staining of Pancreas. There are no differences in the structure or fat content of the pancreata in *Efl1*$^{K983R/K983R}$ (top image) and wildtype (bottom image) mice. Immunostaining and imageing undertaken by Marrianne Yon, MRC Harwell.

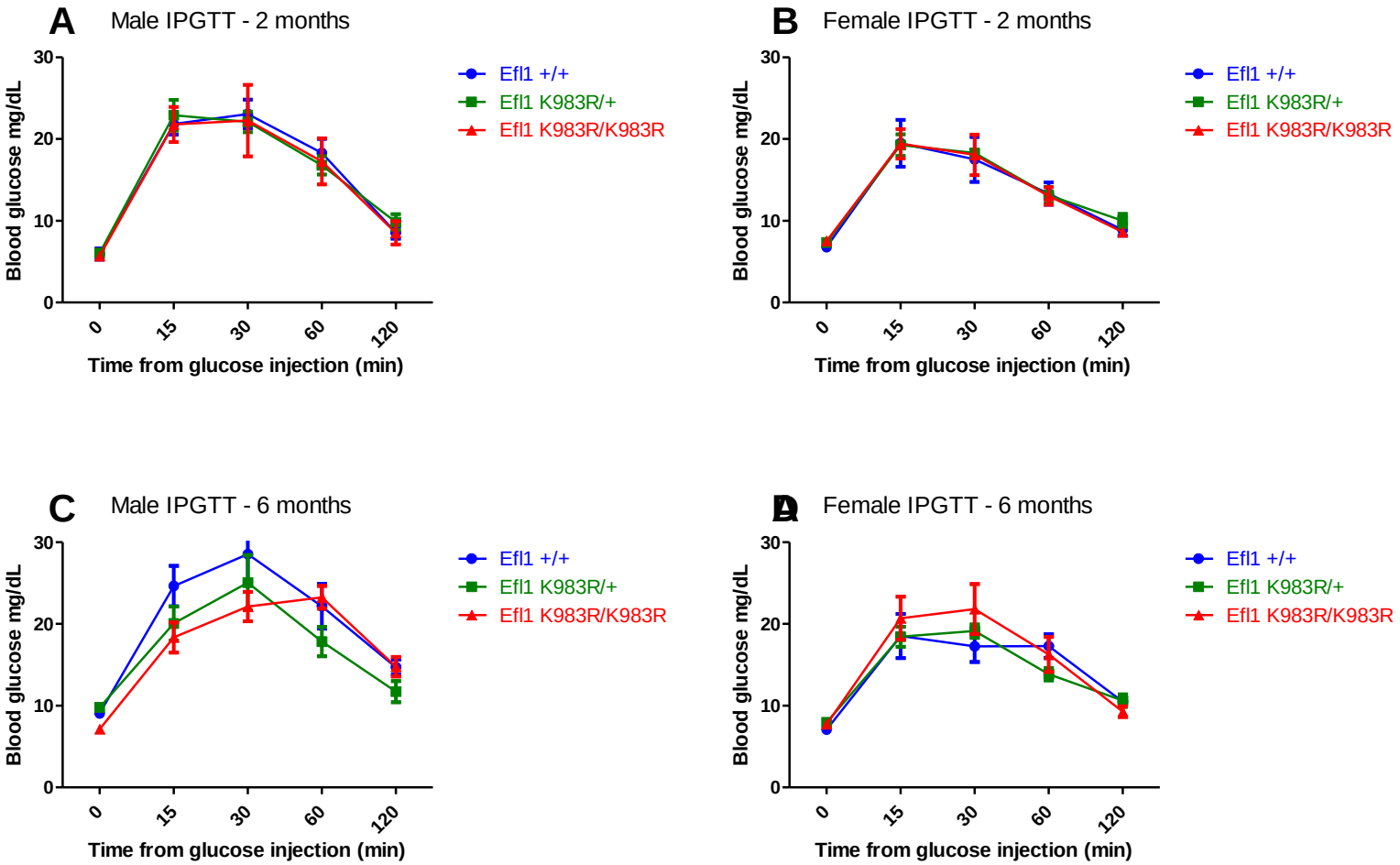


Figure 30 Intraperitoneal glucose tolerance test (IPGTT) glucose clearance for male and females. A, B. Male and female IPGTT glucose clearance at 2 months of age. There are no significant differences in the glucose clearing abilities in both male and female mice between genotypes at 2 months of age. **C, D. Male and female IPGTT glucose clearance at 6 months of age.** There are no significant differences in the glucose clearing abilities in both male and female mice between genotypes at 6 months of age. Numbers (n) = 5 for all genotypes for both males and females, at both 2 and 6 months of age.

4.1.4. Glucose tolerance is unimpaired in *Efl1*$^{K983R/K983R}$ mice

Due to the weight difference seen in *Efl1*$^{K983R/K983R}$ mice, glucose metabolism was investigated. Whilst SDS patients do show smaller size due to malabsorption in childhood due to pancreatic enzyme insufficiency, this is not the only possible cause of a size difference. For this reason, it was deemed necessary to explore other avenues relating to metabolism. The intraperitoneal glucose tolerance test (IPGTT) measures the clearance of an intraperitoneally injected glucose load from the body. Glucose tolerance can be impaired due to pancreatic phenotypes or disorders, such as diabetes.

Mice were tested at 2 and 6 months of age for their glucose tolerance clearance capacity. There were no significant differences detected between *Efl1*$^{K983R/K983R}$, *Efl1*$^{K983R/+}$ and wildtype littermates at either age (Figure 30). At 6 months of age however, the glucose clearance was not as uniform between genotypes as at the 2 month time point. This may be due to body fat difference present at this age between genotypes. . *Efl1*$^{K983R/K983R}$ mice stay leaner than littermates as they age. Body fat can affect glucose metabolism and therefore IPGTT between genotypes cannot be justly compared between genotypes when the body fat differences become significant. For this reason, no 12 month time point was carried out for IPGTT.

4.1.5. Longevity and viability conclusions

To summarise this phenotyping section, *Efl1*$^{K983R/K983R}$ mice survive as long as *Efl1*$^{K983R/+}$ and wildtype littermates. Females have an average life expectancy of 640 days (depending on genotype), and there are no significant difference between the median survival ages between genotype. Males on the other hand were very difficult to age and therefore collecting survival data was not possible. Excessive fighting in the male cages was apparent in the *Efl1*-K983R mouse line, with male mice having to be culled due to welfare concerns about the fight wounds sustained. There is no evidence to suggest that, had there been no fighting in the male mice, that males would show any difference in life span between genotype. No obvious life-threatening maladies were observed in males or females, suggesting that life span is unaffected by the *Efl1*-K983R mutation.

Efl1$^{K983R/K983R}$ mice weighed significantly less than *Efl1*$^{K983R/+}$ and wildtype littermates from three weeks of age. Earlier time points could not be obtained for weight data due to an inability to individual identify the mice before three weeks of age. Embryos at 18.5dpc were weighed as a start time point for weight data, as this is the latest stage of gestation before birth at which embryos can be harvested. No significant weight differences were seen in the embryos between genotype. This suggest that the weight differences seen in adult mice are not due to developmental differences, and that weight differences being to appear at some point in the first three weeks of life. SDS

patients are in the lower quartile for height from childhood. However, birth weights of SDS patients are normal. Weight and size differences in patients are put down to malnutrition due to pancreatic enzyme insufficiencies that cause malabsorption in the gut. Lipomatous replacement of the pancreas is present in all SDS patients, and is associated with decreased zymogen granules and enzyme production (Levin, Makitie et al. 2015, Tourlakis, Zhang et al. 2015).

Given the weight difference in the *Efl1*$^{K983R/K983R}$ mice, pancreatic structure and fat infiltration was studied in the mice. Oil red O and haematoxylin staining showed not structural abnormalities in the *Efl1*$^{K983R/K983R}$ pancreas. There was also no fat infiltration into the pancreas tissue to speak of in either *Efl1*$^{K983R/K983R}$ or wildtype pacreata. This suggests that pancreatic insufficiency is not the cause of weight difference in these mice. Glucose metabolism was also investigated in an attempt to determine the cause of the weight differences seen. However, no glucose tolerance differences were detected in any of the genotypes. The fact that pancreatic enzyme insufficiency is one of the key criteria for diagnosis of SDS suggests that the *Efl1*$^{K983R/K983R}$ mice are not true SDS models. However, there are some cases of SDS where patients do not have SBDS mutations. These patients are termed 'clinical SDS' patients and may have a slightly different form of the disease that is not officially recognised as distinct at this time. These mice may be a useful research tool to investigate the cause of disease in these 'clinical SDS' patients.

4.2. Gait abnormality and motor impairment

4.2.1. Gait abnormalities are present in *Efl1*$^{K983R/K983R}$ mice

The *Efl1*-K983R mouseline was originally discovered through the Harwell Ageing Screen because it presented with an abnormal gait that was low and 'flat'. Mice that presented with this flat gait walked with their undercarriage touching the ground, and with their legs at unusually wide angles unable to support the body weight of the mouse. This gait was assessed by monthly SHIRPA tests and a rudimentary numeric scoring system to describe the gait. Numbers 1-4 were used, with 1 being assigned to mice with ordinary gait (normal tail height, leg position and gait height) and 4 being assigned to mice with the most abnormal gait (dragging tail, wide leg position/waddling and undercarriage flat to the ground).

It was found that *Efl1*$^{K983R/K983R}$ mice showed a more 'flat' gait than wildtype and *Efl1*$^{K983R/+}$ from as young as 2 months of age (earliest age tested). This gait then progresses, and reaches higher gait scores with age (Figure 31). On average male *Efl1*$^{K983R/K983R}$ mice reached a significantly higher average gait score at 12 months then female *Efl1*$^{K983R/K983R}$ mice ($p=0.0458$), although there was no difference in the gait scores between males and females at 2 months of age. This suggests that the gait issues progress to a more severe degree in males than in females.

As discussed in 5.1.2, very few examples of sensory-motor deficits in SDS patients exist. However, there has been one case study of an 8 year old girl with severe motor difficulties in tasks like sitting up and holding her head up. The flat gait seen in the *Efl1*$^{K983R/K983R}$ may suggest a related pathogenesis to these motor defects seen in this one SDS case study. Hypotonia has also been reported, albeit rarely, in SDS. Patients can also become ataxic, and this along with hypotonia can persist throughout childhood (Aggett, Cavanagh et al. 1980).

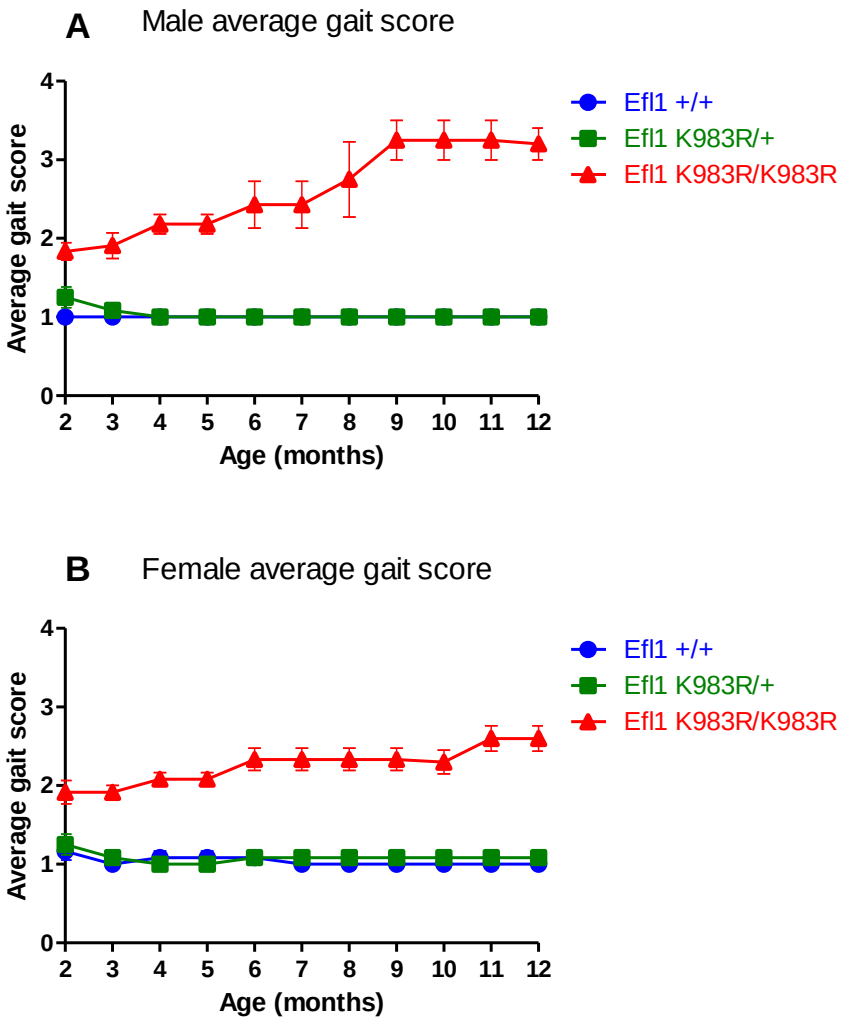


Figure 31 Average male and female gait scoring from monthly SHIRPA tests. A. Male average gait score. B. Female average gait score. Gait was assessed using a rudimentary numeric scoring system. 1 = normal (normal tail height, leg position and undercarriage height), 2 = slightly flat (slightly low undercarriage height, normal or wide leg position, normal or high tail position), 3 = flat (low undercarriage position, normal or wide leg position, normal, high or low tail position), 4 = very flat (undercarriage dragging on ground, wide led position, low tail position). On average, male and female *Efl1*$^{K983R/K983R}$ mice have a significantly higher gait score than *Efl1*$^{K983R/+}$ and wildtype mice ($p<0.0001$, in both cases). The gait score for males at 12 months of age is significantly higher than that of females at 12 months of age ($p=0.458$), indicating that ale mice have a more severe gait phenotype than females. Numbers (n) as follows: Males (age) for *Efl1*$^{+/+}$, *Efl1*$^{K983R/+}$ and *Efl1*$^{K983R/K983R}$ respectively, (2) = 12, 12, 12, (3) = 11, 12, 11, (4) = 10, 9, 11, (5) = 8,8,11, (6) = 8, 8, 7, (7) = 8, 8, 7, (8) = 8, 7, 4, (9) = 8, 7, 4, (10) = 8, 7, 4, (11) = 8, 7, 4, (12) = 8, 6, 4. Females (age) for *Efl1*$^{+/+}$, *Efl1*$^{K983R/+}$ and *Efl1*$^{K983R/K983R}$ respectively, (2-6) = 12, 12, 12, (7-9) = 11, 12, 12, (10-11) = 11, 12, 10, (12) = 10,12,10.

4.2.2. *Efl1*$^{K983R/K983R}$ mice show increased rear leg errors in locotronic tests

Locotronic is used or the detailed modelling of walking and its disorders in mice and rats, with respect to motor and psychomotor skills and cognition. The Locotronic is a unique piece of apparatus consisting of a horizontal ladder (124cm in length) with sensors in each step of the ladder to assess motor coordination. As the mouse traverses the ladder, any missed steps by front or rear legs, as well as tail errors, are automatically detected by the apparatus, and are automatically exported to a data file for analysis. The gait abnormalities seen in the *Efl1*$^{K983R/K983R}$ mice prompted further investigation into the causes of this phenotype, and therefore locotronic was selected as one of the testing methods to be used.

Locotronic tests of the *Efl1*-K983R mouse line showed that *Efl1*$^{K983R/K983R}$ mice showed, on average, no significant leg errors at 2 months of age when running the horizontal ladder. However, at 6 and 14 months of age, female *Efl1*$^{K983R/K983R}$ mice presented with significantly more rear leg errors when running the horizontal ladder than Efl1K983R/+ and wildtype mice. Male *Efl1*$^{K983R/K983R}$ mice did not show significant differences in the number of leg errors at 2 or 6 months of age. However, no male mice were available for testing at the 14 month time point.

These data suggest that leg errors are not the cause of the flat gait seen in *Efl1*$^{K983R/K983R}$ mice. It cannot be ruled out however, that the leg errors seen in female mice at 6 and 14 months of age are a by-product of the flat gait. However, male mice did not show increased leg errors at either of the ages tested their gait is significantly flatter than the females'. This suggests that the leg errors in the female mice at 6 and 14 months of age are not due to the flat gait. The leg errors may instead be a result of muscle weakness in older females. It may be that if a 14 month time point had been available in the male mice, leg errors would have occurred.

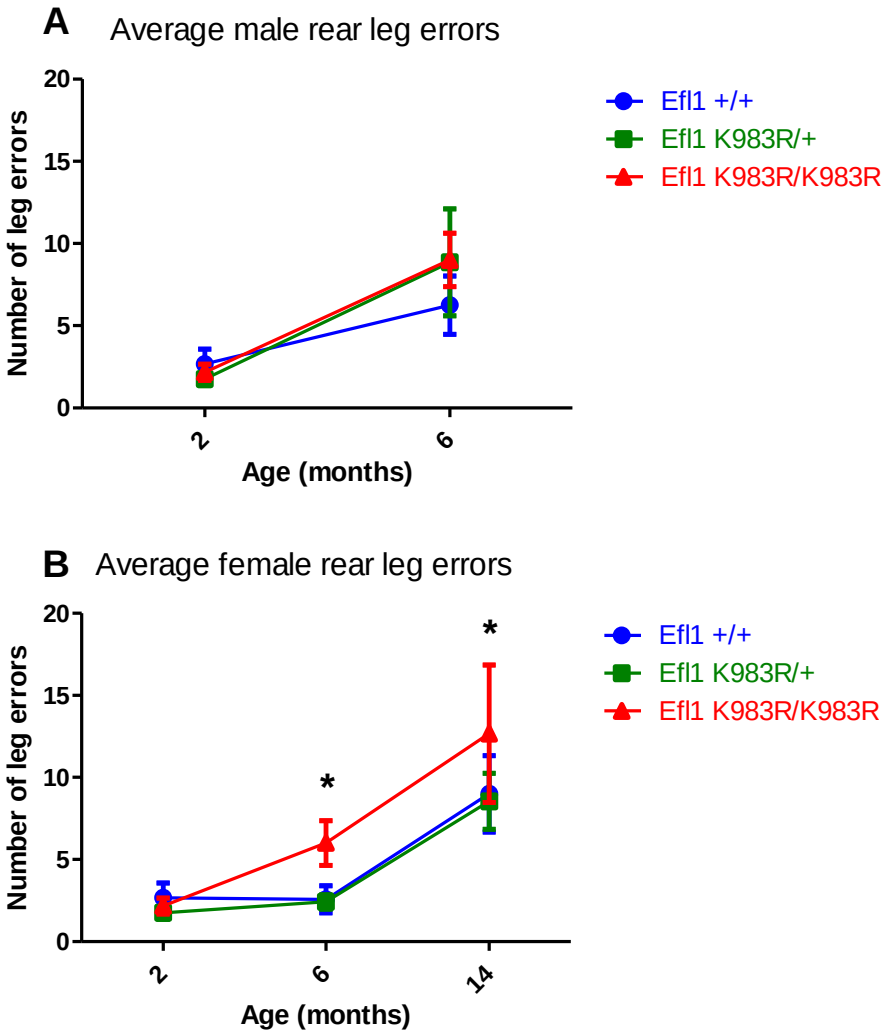


Figure 32 Average number of leg errors made on locotronic apparatus. A, B. Average male and female rear leg errors. On average, there are no differences in the number of rear leg errors between genotypes at 2 months of age, both in male and female mice. However, at 6 and 14 months of age, female *Efl1*$^{K983R/K983R}$ mice showed significantly increased number of rear leg errors compared to wildtype mice at 6 and 14 months (p=0.039, p=0.031, respectively). Male mice did not show a significantly increased number of leg errors compared to *Efl1*$^{K983R/+}$ and wildtype mice at 6 months of age, and no 14 month time point was available for male mice. Numbers (n) as follows: Females n=12 at all time points for all genotypes, male n=12 for all genotypes at 2 months of age, n=8, 7, 7 at 6 months of age for wildtype, *Efl1*$^{K983R/+}$ and *Efl1*$^{K983R/K983R}$ mice, respectively.

4.2.3. *Efl1*$^{K983R/K983R}$ mice display weaker grip strength

Muscle strength was investigated as a possible cause of the abnormal gait seen in the *Efl1*$^{K983R/K983R}$ mice, and as a possible cause of the leg errors seen in 6 and 14 month old female *Efl1*$^{K983R/K983R}$ mice. To test muscle strength and neuromuscular function in the Efl1-K983R mice, grip strength was measured in fore and hind limbs. Grip strength test is used to measure muscle strength in all four limbs (fore and hind limbs). A grip strength meter is used, with a single metal grid attached to the sensor. The mouse is placed onto the grid and the force with which the mouse pulls on it when prompted is measured.

Female *Efl1*$^{K983R/K983R}$ mice showed no differences in average grip strength at 2 months of age compared to *Efl1*$^{K983R/+}$ and wildtype mice. However, at 6 and 14 months of age, female *Efl1*$^{K983R/K983R}$ mice showed significantly lower grip strength compared to female *Efl1*$^{K983R/+}$ and wildtype mice. Male *Efl1*$^{K983R/K983R}$ mice showed significantly lower grip strength at 2 and 6 months of age compared to *Efl1*$^{K983R/+}$ and wildtype mice. Male mice were not available to conduct a 14 month time point for grip strength (

Figure 33). However, when grip strength readings were normalised against body weight, there were no significant differences between *Efl1*$^{K983R/K983R}$, *Efl1*$^{K983R/+}$ and wildtype grip strength. This suggests that, in relation to their size, *Efl1*$^{K983R/K983R}$ mice are not physically weaker than littermates. This therefore, does not explain the flat gait seen in *Efl1*$^{K983R/K983R}$ mice.

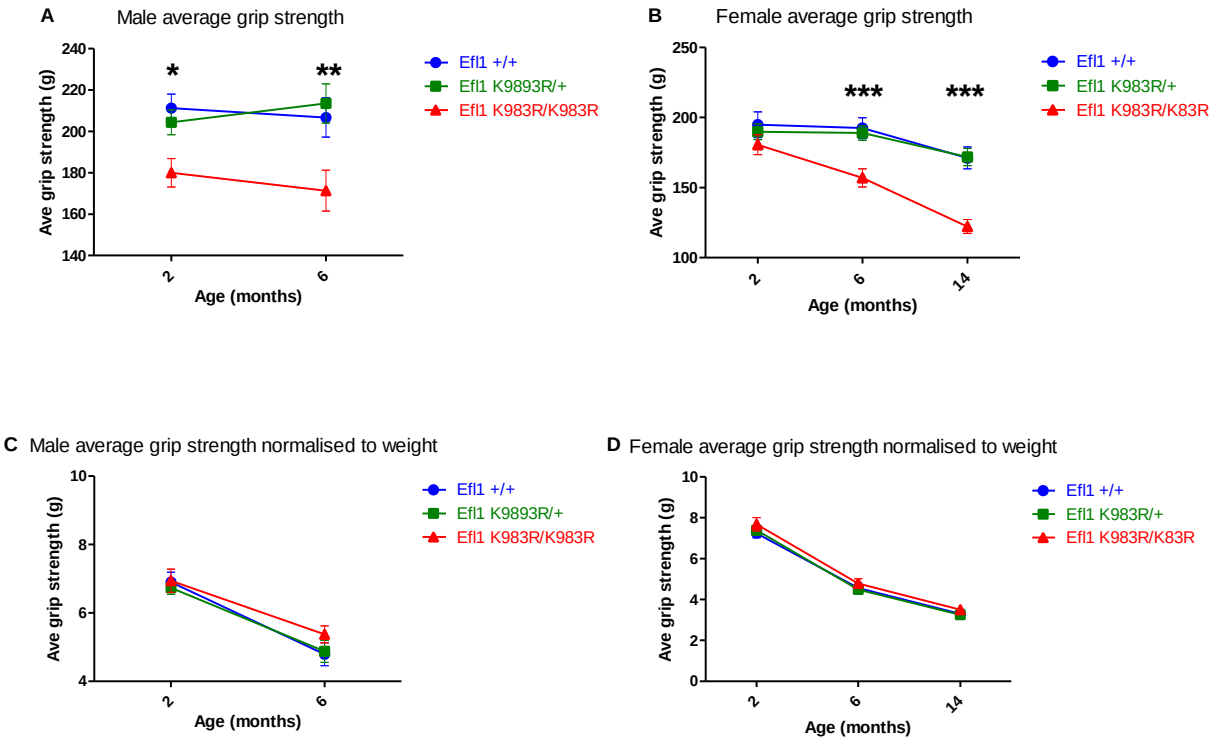


Figure 33 Average grip strength at 2, 6 and 14 months of age. A. Male average grip strength. Male *Efl1*$^{K983R/K983R}$ mice show significantly lower grip strength than Male *Efl1*$^{K983R/+}$ (p=0.014, p=0.009) and wildtype mice (p=0.0038, p=0.023) at 2 and 6 months of age. There is no 14 month time point available for male mice. **B. Female average grip strength.** There are no significant differences in grip strength between genotypes in female mic eat 2 months of age. However, at 6 and 14 months of age, female *Efl1*$^{K983R/K983R}$ mice show significantly lower grip strength than *Efl1*$^{K983R/+}$ (p=0.0008, p<0.0001) and wildtype (p=0.0015, p=0.00014) mice. **C, D. Male and female average grip strength normalised to body weight.** When normalised with total body weight, grip strength is not significantly different in male or female *Efl1*$^{K983R/K983R}$ mice compared to *Efl1*$^{K983R/+}$ and wildtype mice at any time point. Numbers (n) as follows: male n=12 for all time points and genotypes, female *Efl1*$^{K983R/K983R}$ n=12, 8, 5, *Efl1*$^{K983R/+}$ n=9, 12,10 , 12, *Efl1*$^{+/+}$ n=10, 12, 10 (2, 6, 14 months, respectively).

4.2.4. Muscle histology is normal in *Efl1*$^{K983R/K983R}$ mice

In further attempts to deduce the cause of the gait abnormalities seen in the *Efl1*$^{K983R/K983R}$ mice, histological staining and weighing of different muscle types in the leg was carried out. The hind limb muscles tibialis anterior, extensor digitorium longus, gastrocnemius and soleus muscles of 1 year old male mice were selected for weighing, with the soleus muscle being selected for additional staining of the muscle fibres. *Efl1*$^{K983R/K983R}$ hind limb muscle weights were on average 76-88% that of wildtype muscle weights. However, in relation to body weight, no differences in muscle weight were apparent between genotype. This suggests that there is no muscle wastage in the 1 year old male *Efl1*$^{K983R/K983R}$ mice (Figure 34A).

Within the soleus muscle, a myofibrillar ATPase stain was used to classify muscle fibres into type I (slow), type IIa (intermediate). No differences in fibre number were detected between *Efl1*$^{K983R/K983R}$ and wildtype solei (Figure 34B, C).

These data suggest that there are no differences in the overall structure of the hind limb muscles between *Efl1*$^{K983R/K983R}$ and wildtype mice, and that fibre types within the muscle are not different. Therefore, it is unlikely that the gait abnormalities seen in *Efl1*$^{K983R/K983R}$ mice are due to muscular dystrophy or any other muscle-related pathologies. It may be that the gait is a result of a sensorineural defect at the neuromuscular junctions in the *Efl1*$^{K983R/K983R}$ mice.

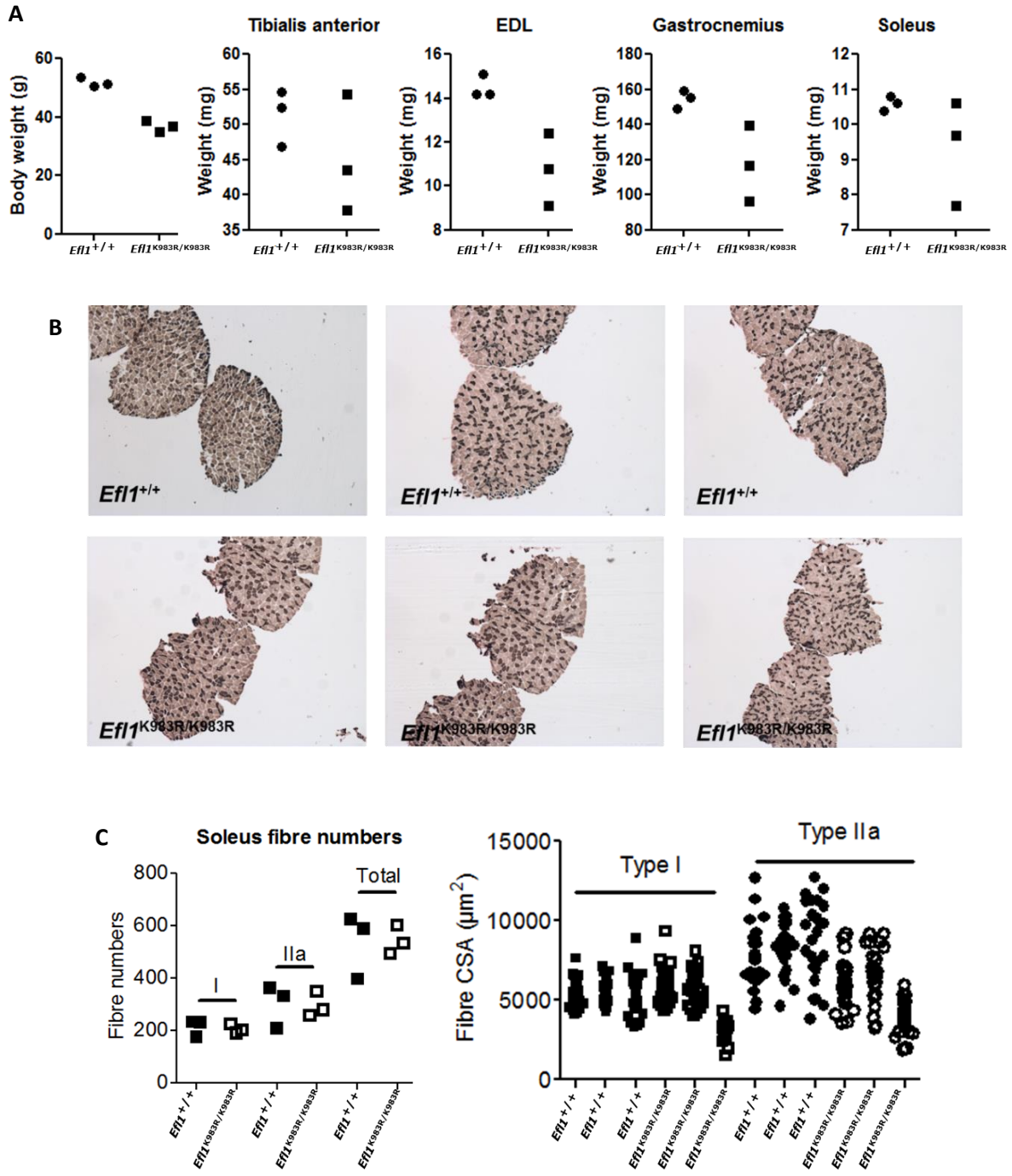


Figure 34 Skeletal muscle histology. A. Total body weight and weights of individual muscles. No difference in muscle weight was detected when normalised to body weight between *Efl1*$^{K983R/K983R}$ and wildtype mice. From left to right, Tibialis anterior, extensor digitorium longus (EDL), gastrocnemius and soleus. **B. Myofibrillar ATPase staining of soleus muscle at pH 4.47.** Type I fibre (slow) are shown in dark brown, Type IIa fibre (intermediate) are shown in pale brown. No significant differences were detected in fibre number between *Efl1*$^{K983R/K983R}$ and wildtype solei. **C. Number and size of fibres in soleus muscle.** No significant difference was seen in the number of fibres, type I or IIa, between *Efl1*$^{K983R.K983R}$ and wildtype mice. No significant difference was seen in the size (CSA=cross section area) of fibres, type I or IIa, between *Efl1*$^{K983R.K983R}$ and wildtype mice. Numbers (n) = 3 for all genotypes. Work undertaken at Henning Wackerhage's laboratory, Aberdeen University.

4.2.5. *Efl1*$^{K983R/K983R}$ mice display reduced activity on running wheels

Given that the *Efl1*$^{K983R/K983R}$ mice present with an abnormal gait, there motor activity was of interest, as it was not known if the gait actually posed any difficulties to the mice. One way of assessing motor ability is to use a running wheel. By measuring the activity of a mouse on a running wheel, it can be determined what the ability of the mouse is to move, both in terms of speed and duration, as well as how frequently a mouse has the desire to run. Wheel running is extremely appealing to mice, and a reluctance to run may indicate pain or disability.

At three months of age, female mice were placed into individual cages with unrestricted access to a running wheel for seven days. Their activity on the running wheel was recorded 24 hours a day. *Efl1*$^{K983R/K983R}$ mice performed fewer runs (individual sessions of running on the wheel from start to finish were counted), and fewer rotations within those runs compared with *Efl1*$^{K983R/+}$ and wildtype littermates (Figure 35A, B). The average maximum speed that *Efl1*$^{K983R/K983R}$ mice reached during these runs was also significantly lower than speeds reached by *Efl1*$^{K983R/+}$ and wildtype mice (Figure 35C).

These data suggest that *Efl1*$^{K983R/K983R}$ mice do not have either the desire or the ability to run on the wheel to the extent that their *Efl1*$^{K983R/+}$ and wildtype do. This may be due to difficulties associated with the abnormal gait seen in these mice.

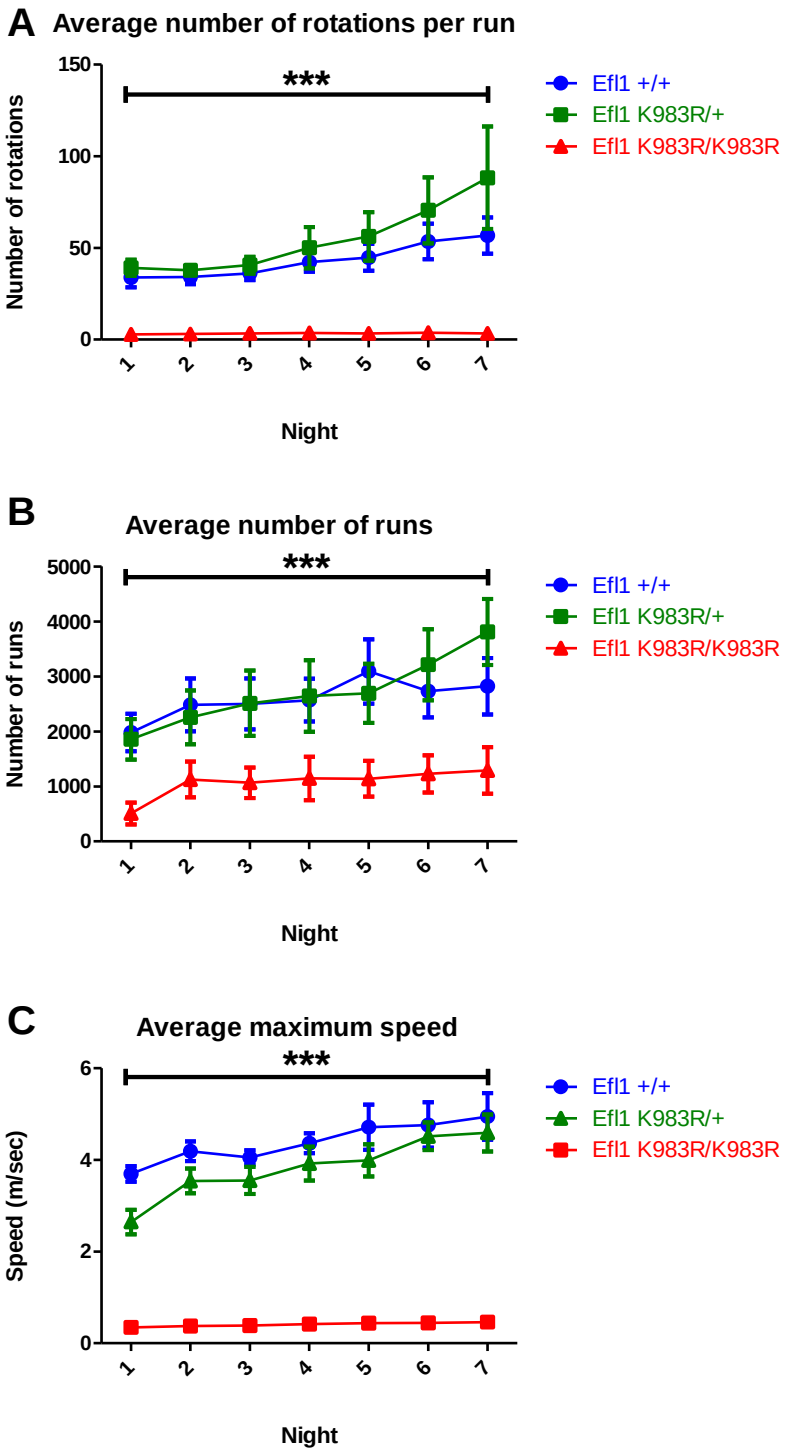


Figure 35 Free wheel running activity analysis. A. Average number of rotations per run. *Efl1*$^{K983R/K983R}$ mice performed significantly fewer rotations per run each night compared to *Efl1*$^{K983R/+}$ and wildtype littermates (p<0.0001, p<0.0001, respectively). **B. Average number of runs per night.** *Efl1*$^{K983R/K983R}$ mice performed significantly fewer runs per night compared to *Efl1*$^{K983R/+}$ and wildtype littermates (p<0.0001, p<0.0001, respectively). **C. Average maximum speed.** *Efl1*$^{K983R/K983R}$ mice reached significantly lower maximum speed during runs each night compared to *Efl1*$^{K983R/+}$ and wildtype littermates (p<0.0001, p<0.0001, respectively). Number (n) =12 for all genotypes at all time points. All mice tested were female, at 3 months of age.

4.2.6. Open field activity in *Efl1*$^{K983R/K983R}$ mice is normal

The Open Field test is used to assess anxiety and exploratory behaviours in mice. It is based on the natural tendency of an animal to explore and to protect itself using avoidance, which translates to a normal animal spending more time in the periphery of the Open Field arena than in the centre. The movement of a mouse is tracked around the Open field arena, and as such the test can be used to assess a mouse' natural desire to move around its environment.

At 2, 6 and 12 months of age, male and female mice were placed in open field arenas and their activity was recorded and analysed. Total distance travelled was measured for 30 minute (2 months of age) or 20 minute (6 and 12 months of age) sessions. No significant differences were detected in the distance travelled by *Efl1*$^{K983R/K983R}$ mice compared to *Efl1*$^{K983R/+}$ and wildtype mice (Figure 36A, B). This data shows that the *Efl1*$^{K983R/K983R}$ mice are able to walk around the Open Field arena to the same level as their littermates. This suggests that the differences seen in free wheel running (4.2.5) are not due to an inability to walk. It does not however exclude the possibility of a difficulty in running or navigating the complexity of the rungs on the wheel.

The frequency with which a mouse enters the centre area of the open field arena can be an indicator of anxiety (little time spent in the centre) or hyperactivity (extensive time spent in the centre). On the first open field test, at 2 months of age, there were no differences seen in the frequency with which mice entered the centre between genotypes, in both male and female mice. This data shows that there are no anxiety or hyperactivity differences between genotypes. Hyperactivity seen in the home cage environment in *Efl1*$^{K983R/K983R}$ mice (5.1.1) are not reflected in the Open Field data. This may be because it is a very different environment in the Open Field arena, and the movement of the mice is only tracked for 20-30 minutes at a time. Therefore, the Open Field data does not eradicate the information gained form the Crack-it video tracking system.

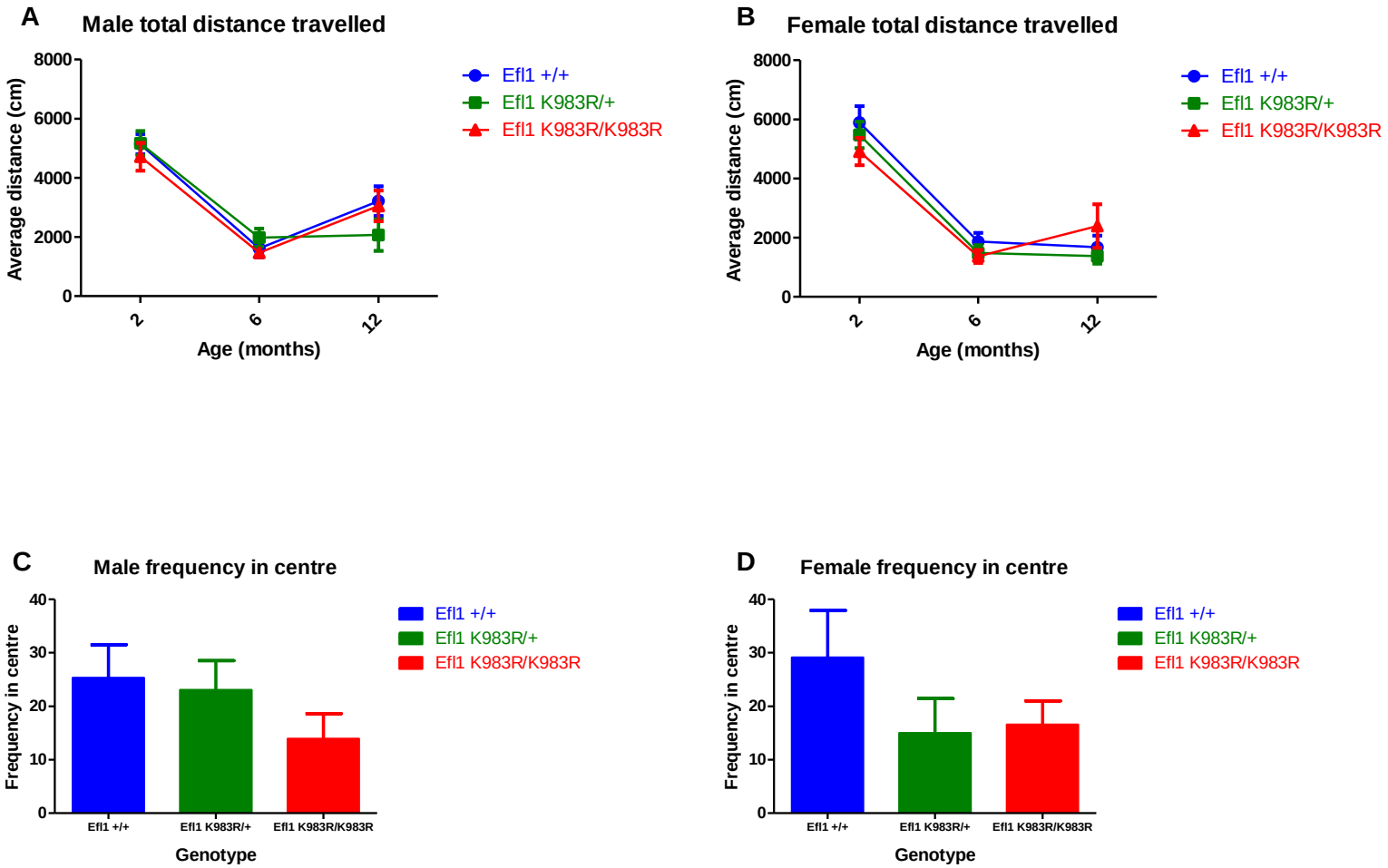


Figure 36 Open field arena analysis. A, B. Male and female total distance travelled in whole arena at 2, 6 and 12 months of age. There was no difference in the distance travelled in the whole arena between genotypes. **C, D. Male and female frequency in centre.** Male and female *Efl1*$^{K983R/K983R}$ mice entered the centre less frequently than *Efl1*$^{K983R/+}$ (p=0.2182, p=0.8412) and wildtype (p=0.1582, p=0.2148) mice, however this difference is not significant. Number (N) as follows: 2 months of age all genotypes and sexes n=12, 6 months of age *Efl1*$^{K983R/K983R}$ n=7 (male), 11 (female), *Efl1*$^{K983R/+}$ n=8 (male), 12 (female), *Efl1*$^{+/+}$ n=8 (male), 12 (female), 12 months of age *Efl1*$^{K983R/K983R}$ n=6 (male), 10 (female), *Efl1*$^{K983R/+}$ n=4 (male), 12 (female), *Efl1*$^{+/+}$ n=4 (male), 10 (female).

4.2.7. Gait and motor conclusions

The *Efl1*-K983R mouse line was originally discovered through the Harwell Ageing Screen because of the abnormal gait it presented at 6-8 months of age. After rederivation, it was observed that a flat gait could be seen as early as 2 months of age. The difference in gait onset between the original Ageing screen line and the *Efl1*-K983R line may be due simply to more detailed observations of the gait at a young age. The gait certainly progresses to a flatter stance as the mice age, and is more obvious at 6-8 months of age than at 2 months of age. Monthly SHIRPA observations and gait scoring provide a detail assessment of the gait and it progression in the *Efl1*-K983R mouse line, and show that it is a recessive trait, present only in *Efl1*$^{K983R/K983R}$ mice. The gait does not affect the mice' welfare or ability to move around the cage, eat or drink.

The cause of the gait was not identified by locotronic and grip strength tests. Locotronic data suggests that females *Efl1*$^{K983R/K983R}$ mice experience more rear leg errors than *Efl1*$^{K983R/+}$ and wildtype mice. However, this is unlikely to be causative of gait as male *Efl1*$^{K983R/K983R}$ mice did not display more leg errors than other genotypes, but were characterised as having a more severe gait phenotype than females in SHIRPA. Also the leg errors in females were only detected at 6 months of age, whereas the gait onsets from as early as 2 months of age. The leg errors are therefore more likely to be a result of the gait abnormality rather than the cause.

Grip strength was not different in *Efl1*$^{K983R/K983R}$ mice when normalised to body size, and so tis also is unlikely to be the cause of the abnormal gait. Muscle size and fibre content was also not significantly different between *Efl1*$^{K983R/K983R}$ mice and wildtype, demonstrating that muscle pathology is not the cause of the abnormal gait.

As mentioned above, the gait does not prevent the mice form moving around the home cage. Nor does it prevent them moving around the Open Field arena in the same way as *Efl1*$^{K983R/+}$ and wildtype littermates. It does however appear to inhibit their ability to run on a wheel. The speed, frequency and duration of running episodes on a running wheel were significantly reduced in *Efl1*$^{K983R/K983R}$ mice. Open Field suggests that the desire of the *Efl1*$^{K983R/K983R}$ mice to move is not different to *Efl1*$^{K983R/+}$ and wildtype mice, so it may be that the abnormal gait makes negotiating the complex structure of the running wheel more difficult for *Efl1*$^{K983R/K983R}$ mice.

As mentioned above, sensory-motor deficits in SDS patients are, and only one is known to be reported. This patient was unable to properly sit up or support her own head. The abnormal gait in this mouse line may reflect the motor difficulties experienced by this patient. It is possible more patients have these types of symptoms that have not been reported, as long term follow up in SDS

patients is a common problem in the research field. These mice may provide a model in which to model this aspect of SDS, and to determine the cause of motor deficits in relation to ribosome-related diseases. These mice also provide the first example of EFL1 function having an effect on locomotor ability.

Chapter 5
Behavioural Characterisation of the *Efl1*-K983R mouse line

5. Behavioural Phenotyping

5.1. Behavioural phenotyping

5.1.1. Social and behavioural abnormalities are present in *Efl1*$^{K983R/K983R}$ mice

As mentioned in 4.1.1 aggression in male *Efl1*$^{K983R/K983R}$ mice was a particular problem when ageing the mice. Fight wounds would often be sustained by mice (Table 5). These fight wounds often lead to culling of the mice due to welfare concerns, and this would often result in a lone *Efl1*$^{K983R/K983R}$ mouse remaining in the cage. When an *Efl1*$^{K983R/K983R}$ mouse did sustained a fight wound, another *Efl1*$^{K983R/K983R}$ mouse was present in the cage. If only one *Efl1*$^{K983R/K983R}$ mouse was present in the cage, it would not sustain fight wounds. For these reasons it was suspected that the *Efl1*$^{K983R/K983R}$ mice may be the aggressors. Social tests were carried out to investigate this further.

Table 5 Number of mice that sustained fight wounds. 38.5% of wildtype male mice, 43.8% of *Efl1*$^{K983R/+}$ male mice and 21.4% of *Efl1*$^{K983R/K983R}$ male mice sustained fight wounds severe enough to be cause for welfare concern and culling.

Genotype	Number culled for fight wounds	Total number of mice	% culled for fight wounds
Efl1$^{+/+}$	5	13	38.5
Efl1$^{K983R/+}$	7	16	43.8
Efl1$^{K983R/K983R}$	3	14	21.4

Social dominance tests were carried out to determine if *Efl1*$^{K983R/K983R}$ mice were socially dominant over *Efl1*$^{K983R/+}$ and wildtype littermates. Social dominance testing involves two mice (opponents) being placed into each end of an open-ended tube. The natural inclination of the mouse will be to head to the other end of the tube, and in order to exit the tube one mouse must push their opponent back and out. Male *Efl1*$^{K983R/K983R}$ mice succeeded in pushing their opponent out of the tube in 100% of trials, indicating that they are socially dominant. Female *Efl1*$^{K983R/K983R}$ mice did not dominate 100% of trials, showing that social dominance traits are found only in the male *Efl1*$^{K983R/K983R}$ mice. This correlates to the observations of fighting within the male cages, as no fighting or aggressive behaviours were observed in the female cages.

Table 6 Social dominance in male and female mice. A. Male social dominance trials. Male *Efl1*$^{K983R/K983R}$ mice dominated 100% of the trials they entered. Male *Efl1*$^{K983R/+}$ mice dominated 33.3% of the trials they entered. Male wildtype mice dominated 16.7% of the trial they entered. This shows that male *Efl1*$^{K983R/K983R}$ mice are socially dominant compared to *Efl1*$^{K983R/+}$ and wildtype mice. **B. Female social dominance trials.** Female *Efl1*$^{K983R/K983R}$ mice dominated 58.3% of the trials they entered. Female *Efl1*$^{K983R/+}$ mice dominated 41.7% of the trials they entered. Female wildtype mice dominated 75% of the trial they entered. This shows that female *Efl1*$^{K983R/K983R}$ mice are not socially dominant compared to *Efl1*$^{K983R/+}$ and wildtype mice. Numbers (n) = 6 for male mice for all genotypes, 7 for female mice of all genotypes. Trials were conducted in duplicate. Mice were 6 months of age.

Males	Trials dominated	Percentage trials dominated
Efl1$^{+/+}$	2/12	16.7
Efl1$^{K983R/+}$	4/12	33.3
Efl1$^{K983R/K983R}$	12/12	100

Females	Trials dominated	Percentage trials dominated
Efl1$^{+/+}$	9/14	64.3
Efl1$^{K983R/+}$	7/14	50
Efl1$^{K983R/K983R}$	5/14	35.7

Next, a pilot resident intruder test was carried out. The resident intruder paradigm involves the resident mouse, in its home cage environment, and an 'intruder' mouse (unfamiliar to the resident mouse) being placed into the cage. The behaviour of the resident mouse is observed and recorded, and behaviours such as offensive, violent or defensive actions are monitored. In the pilot resident intruder test three mice of each genotype were tested against an unrelated C57BL/6N strain male mouse. Only three mice were tested due to welfare concerns presented by the Animal Welfare and Ethics Review Board (AWERB). One *Efl1*$^{K983R/K983R}$ mouse and one *Efl1*$^{K983R/+}$ mouse, out of three, attacked the intruder and very little aggressive behaviours were observed prior to the attacks, indicating that, at least in this paradigm, *Efl1*$^{K983R/+}$ and *Efl1*$^{K983R/K983R}$ mice are not overtly aggressive.

Table 7 Resident intruder test results. No wildtype mice displayed attack behaviour in the ten minute trials. One *Efl1*$^{K983R/+}$ and one *Efl1*$^{K983R/K983R}$ did display attack behaviour during the tem minute trial.

Genotype	Number of trials with attacks	Attack latency (10:00 min trial)
Efl1$^{+/+}$	0/3	NA
Efl1$^{K983R/+}$	1/3	04:30
Efl1$^{K983R/K983R}$	1/3	09:30

However, the resident intruder test has limitations. For example, the resident mouse was only placed into its 'home cage' for 24 hours before testing, due to welfare concerns from the AWERB. This may not be enough time to establish territory for the resident mouse. Conversely, because the test involved the resident mouse being housed solo for a period of 24 hours, it is not representative of the actual home cage environment in which fighting had originally occurred.

To gain a more accurate view of the behaviour of the *Efl1*$^{K983R/K983R}$ mice in the home cage, Crack-it video tracking was performed on three cages of mice, each containing one *Efl1*$^{K983R/K983R}$ mouse out of three mice in the cage. The mice had microchips implanted prior to video tracking, allowing each mouse to be individually identified whilst moving in the home cage. Several abnormal behaviours were observed in the *Efl1*$^{K983R/K983R}$ mice during Crack-it video tracking. *Efl1*$^{K983R/K983R}$ mice showed hyperactivity and abnormal social behaviours, such as jumping on fellow cage mates during bouts of hyperactivity or isolating itself from other mice in the cage. Extremely repetitive patterns of movement were also observed in *Efl1*$^{K983R/K983R}$ mice, as well as head rearing, and in one extreme case, back flipping during a repetitive head rearing episode.

To conclude, various behavioural abnormalities are present in *Efl1*$^{K983R/K983R}$ mice. These behaviours include increased social dominance over wildtype and *Efl1*$^{K983R/+}$ cage mates and abnormal socialisation in the home cage environment. Although mice were not seen to overtly aggressive in resident intruder tests, a high level of fight wounds were sustained in male cages within the *Efl1*-K983R cohorts, suggesting there is abnormal social and aggressive behaviours within the male mice. Behavioural and social difficulties are sometimes experienced by SDS patients, including aggressive behaviour in some children (Perobelli, Nicolis et al. 2012). These results, therefore, may reflect a resemblance of some of the behavioural aspects of SDS.

5.1.2. Balance issues were present in *Efl1*$^{K983R/K983R}$ mice

While life span in the *Efl1*$^{K983R/K983R}$ mice is unaffected, various abnormal traits afflicted them. These included head tilts and balance issues, ranging from mild to severe. In one extreme case, a male mouse was found to be back flipping. The earliest head tilts were detected at 3 months of age. Head tilts were more prominent in female mice, but this may be because female mice were aged more than males due to the fighting issues previously discussed in 4.1.1.

Balance issues were further investigated by swim testing in female mice at 1 year of age. In a pilot study of 3 mice of each genotype, *Efl1*$^{K983R/K983R}$ mice showed an inability to swim, and tumbled immediately when placed into the water. Due to the severe tumbling phenotype, no more mice were tested due to welfare concerns. The tumbling may be indicative of a vestibular defect in these mice. *Efl1*$^{K983R/+}$ and *Efl1*$^{+/+}$ mice were able to swim well, with tail and feet moving in normal rhythmic motions and travelling around the bath.

Table 8 Swim test results. Wildtype, *Efl1*$^{K983R/+}$ and *Efl1*$^{K983R/K983R}$ mice were tested and their swimming abilities recorded. All wildtype and *Efl1*$^{K983R/+}$ swam normally, whereas all *Efl1*$^{K983R/K983R}$ mice tumbled in the water and did not swim at all. Numbers (n) = 3 for all genotypes. All females at 1 year of age.

Mouse ID	Genotype	Swim phenotype
16.7b	*Efl1*$^{+/+}$	Normal
17.3d	*Efl1*$^{+/+}$	Normal
18.7b	*Efl1*$^{+/+}$	Normal
16.6a	*Efl1*$^{K983R/+}$	Normal
16.6b	*Efl1*$^{K983R/+}$	Normal
16.7c	*Efl1*$^{K983R/+}$	Normal
16.6c	*Efl1*$^{K983R/K983R}$	Tumbling
16.6d	*Efl1*$^{K983R/K983R}$	Severe tumbling
16.7d	*Efl1*$^{K983R/K983R}$	Tumbling

While balance issues are not widely reported as symptoms of SDS, at least one case study has been reported of an 8 year old girl with severe sensory-motor functioning defects. This patient was unable to sit up right or control her bodily movements appropriately. This patient also had severe learning difficulties and behavioural problems (Kerr, Ellis et al. 2010). The muscular and balance phenotypes seen in the *Efl1*$^{K983R/K983R}$ mice may therefore reflect a resemblance to these sensory-motor functioning deficits in this SDS patient.

5.1.3. Startle reflex and pre-pulse inhibition is unimpaired in *Efl1*$^{K983R/K983R}$ mice

The startle response is characterized by a flinching response to an unexpected strong auditory stimulus (pulse). This response can be attenuated when it is preceded by a weaker stimulus (pre-pulse) and this is the principle underlying pre-pulse inhibition (PPI). While the startle reflex is a good indicator of hearing in the mouse, PPI has been used in numerous species, including mice and humans as an operational measure of sensorimotor gating. Sensory motor gaiting is the mechanism by which an animal receives and responds to sensory input appropriately. Testing PPI responses in mice can determine the ability of an animal to successfully integrate and inhibit sensory information.

Although no psychotic disorders have been reported in SDS patients, the mice do display abnormal behaviours. The sensory motor gaiting reflex is an example of a complex neuronal circuit within the mammalian brain, and optimal neuronal function is critical to this. With regards to the *Efl1* mutant mice, startle and PPI testing was carried out to assess higher level neuronal function.

Mice were tested at 2 and 6 months of age. No significant differences between genotypes were detected in response levels to a startle stimulus (pulse) (Figure 37A, C, E&G). This indicates that in both male and females hearing is not impaired, even at 6 months of age. It also shows that *Efl1*$^{K983R/K983R}$ mice have a normal startle response, and that this reflex is not defective as a result of the *Efl1*-K983R mutation.

Responses of the mice to a pulse after pre-pulses at 65, 75 or 85dB were also not significantly different between genotypes, in either males or females, at any age tested (Figure 37B, D, F&H). These data suggest that sensory motor gaiting mechanism is intact in *Efl1*$^{K983R/K983R}$ mice. With regards to behaviour, this data can also be taken to mean that the *Efl1*$^{K983R/K983R}$ mice do not have any psychotic traits, or other disorders of defective neuronal circuitry.

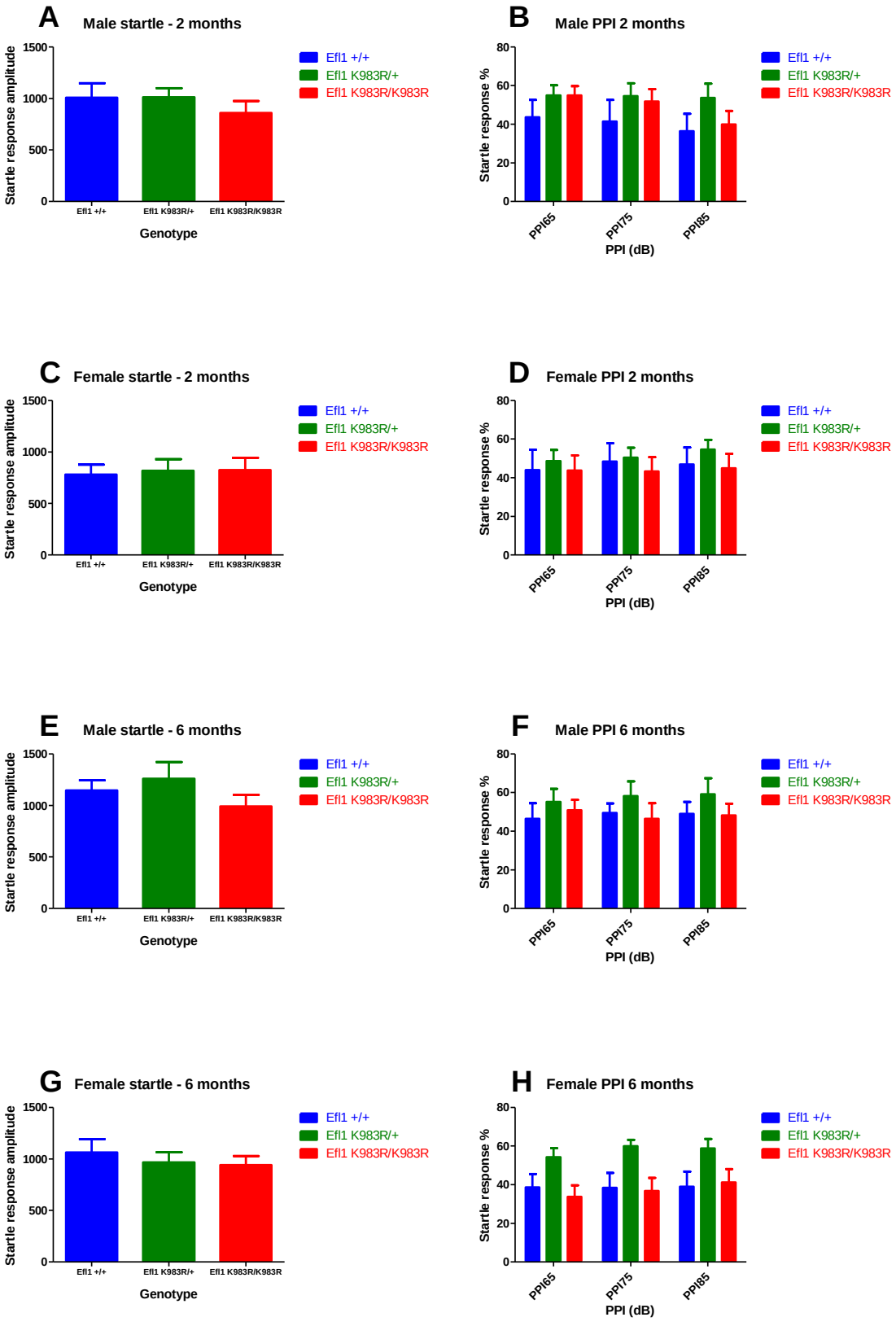


Figure 37 Startle and pre-pulse inhibition sensorimotor gating test in males and females. A, B. Male startle response and pre-pulse inhibition response at 2 months of age. There are no significant differences in startle response amplitude, or the percentage response to pre-pulses of varying decibel level (65, 75 and 85 dB) (percentage response compared to

startle response) between genotypes in male mice of 2 months of age. **C, D. Female startle response and pre-pulse inhibition response at 2 months of age.** There are no significant differences in startle response amplitude, or the percentage response to pre-pulses of varying decibel level (65, 75 and 85 dB)(percentage response compared to startle response) between genotypes in female mice of 2 months of age. **E, F. Male startle response and pre-pulse inhibition response at 6 months of age.** There are no significant differences in startle response amplitude, or the percentage response to pre-pulses of varying decibel level (65, 75 and 85 dB)(percentage response compared to startle response) between genotypes in male mice of 6 months of age. **G, H. Female startle response and pre-pulse inhibition response at 6 months of age.** There are no significant differences in startle response amplitude, or the percentage response to pre-pulses of varying decibel level (65, 75 and 85 dB)(percentage response compared to startle response) between genotypes in female mice of 6 months of age. Numbers (n) as follows: 2 months n=12 for all genotypes for both male and female mice, 6 months n=12 for females of all genotypes, n=7 for males of all genotypes.

5.1.4. Behavioural conclusions

To conclude the behavioural phenotyping section, Efl1K983R/K983R mice display many abnormal traits, both social and behavioural. Male Efl1K983R/K983R mice show increased social dominance, and increased aggression has been noted in the male cages (although the aggressors could not be unequivocally determined). Crack-it video tracking in the home cage environment showed unusual behaviours in the Efl1K983R/K983R mice, including repetitive racing from one end of the cage to another, excessive use of the enrichment in the cage such as the cardboard tube, complete ignorance of other cage mates and periods of social isolation (sleeping alone) and in one extreme case back flipping. The back flipping may be a consequence of the balance issues detected in the Efl1K983R/K983R mice. Head tilts were particularly prominent in female mice, but male mice were also seen with head tilts, and this apparent sex difference may be due to the fact that female mice reached older ages than males. Swim testing revealed a complete inability of the Efl1K983R/K983R mice to swim in the water, and severe tumbling was displayed. This, along with the head tilts suggests an issue in the Efl1K983R/K983R mice with balance and/or coordination. These issues may arise form a vestibular defect, however this was not tested further.

The hyperactivity seen in the home cage environment in Efl1K983R/K983R mice is not reflected in the open field data, where no differences in the time spent in the centre were detected. This may be because the open field arena is a very different environment to the home cage. Also, the mouse' movements are only tracked for 20-30 minutes at a time in the open field tests. Therefore, the open field data does not eradicate the information gained form the Crack-it video tracking system.

As mentioned above, many SDS patients suffer from various behavioural and social difficulties. These symptoms are actually rated as one of the highest complaints amongst patients and their families, above their physical symptoms such as skeletal abnormalities and cytopenias (Kerr, Ellis et al. 2010). Many SDS patients cannot live independently, and some cannot work as a result of these issues. Higher education is not common in SDS patients, children with SDS score lower in intellectual tests in various areas, and remedial teachers are commonly assigned to SDS patients in school. These data suggest learning and memory deficits, and attention deficits have also been reported. In terms of behaviour, some SDS patients display aggressive or 'rule-breaking' behaviour, and also show attention deficits and learning difficulties (Perobelli, Nicolis et al. 2012). The behavioural abnormalities seen in the Efl1K983R/K983R mice may reflect many of the difficulties faced by SDS patients, and thus may provide a model in which to study the mechanisms and processes behind these disorders.

5.2. Learning and memory

Many SDS patients have cognitive and social disorders, including attention deficit disorders, aggressive and rule-breaking behaviour, anti-social behaviour and learning difficulties. The majority of SDS patients will have had difficulties in school, with most achieving lower grades than that of siblings or the general population. Children with SDS display weaker overall intellectual reasoning, higher-order language skills, perceptual reasoning, visual-motor processing speed, visual motor-integration, visual executive problem-solving, attention, and aspects of academic achievement, as well as lower functional level of independence relative to the general population (Kerr, Ellis et al. 2010). For these reasons, learning and memory tests were conducted in the *Efl1*-K983R mouse line to determine if any cognitive processing differences were present in the mutant mice.

5.2.1. *Efl1*$^{K983R/K983R}$ mice show contextual fear conditioning defect

Fear conditioning is a phenotyping method used to test two types of memory in mice; contextual and cued. Fear conditioning to either a cue or a context represents a form of associative learning that has been well studied in many species. The measurement used in contextual and cued fear conditioning is a freezing response that takes place following pairing of an unconditioned stimulus (foot shock), with a conditioned stimulus (a particular context and/or cue). Increased freezing behaviour indicates an association between the unconditioned stimulus and the context/cue, and that a memory has been formed. In contrast, reduced freezing in response to the conditioned stimulus indicates that less of an association has been made, i.e. that memory formation was not fully successful.

Fear conditioning consists of three phases: conditioning, context and cue. The conditioning phase, on day 1, entails the mouse being placed into an arena (the context) and having time to habituate, in which time freezing behaviour is measured (baseline freezing). The mouse is then played a tone (the cue) after which it receives a foot shock (unconditioned stimulus). This is repeated three times. The context and cue phases are carried out 24 hours later. Firstly, the context phase is conducted. This phase entails the mouse being placed into the same arena (context) as when it received the shocks. Freezing behaviour is measured throughout the trial, and no tones are played. At least 4 hours after the context phase, the cue phase is carried out. This entail the mouse being placed into a novel arena (new context), and hearing the tones (cues). Freezing behaviour is measured before the tomes are played (pre-cue) and after. The two phases on day 2 aim to determine if an association between the unconditioned stimulus (foot shock) and either the context or the cue has been made.

Fear conditioning in the *Efl1*-K983R mice was carried out at 3 months of age. *Efl1*$^{K983R/K983R}$ and *Efl1*$^{K983R/+}$ male mice showed reduced freezing behaviour compared to wildtype littermates when

placed in the same context as when they received the unconditioned stimulus (foot shock). This indicates that there is an issue with contextual learning in *Efl1*$^{K983R/K983R}$ and *Efl1*$^{K983R/+}$ mice compared to wildtype mice. Cued fear conditioning showed no freezing behaviour differences between genotypes in male mice, indicating that cued memory formation is unaffected by the *Efl1*-K983R mutation. Female *Efl1*$^{K983R/K983R}$ and *Efl1*$^{K983R/+}$ mice showed no differences in freezing behaviour in either the context or cued conditions. These data suggest that only male mice have contextual fear conditioning deficits. These data also suggests that learning and memory defects, at least in a fear conditioning context, are an autosomal dominant trait of the Efl1-K893R mutation, as heterozygous mice are affected as well as homozygous mice.

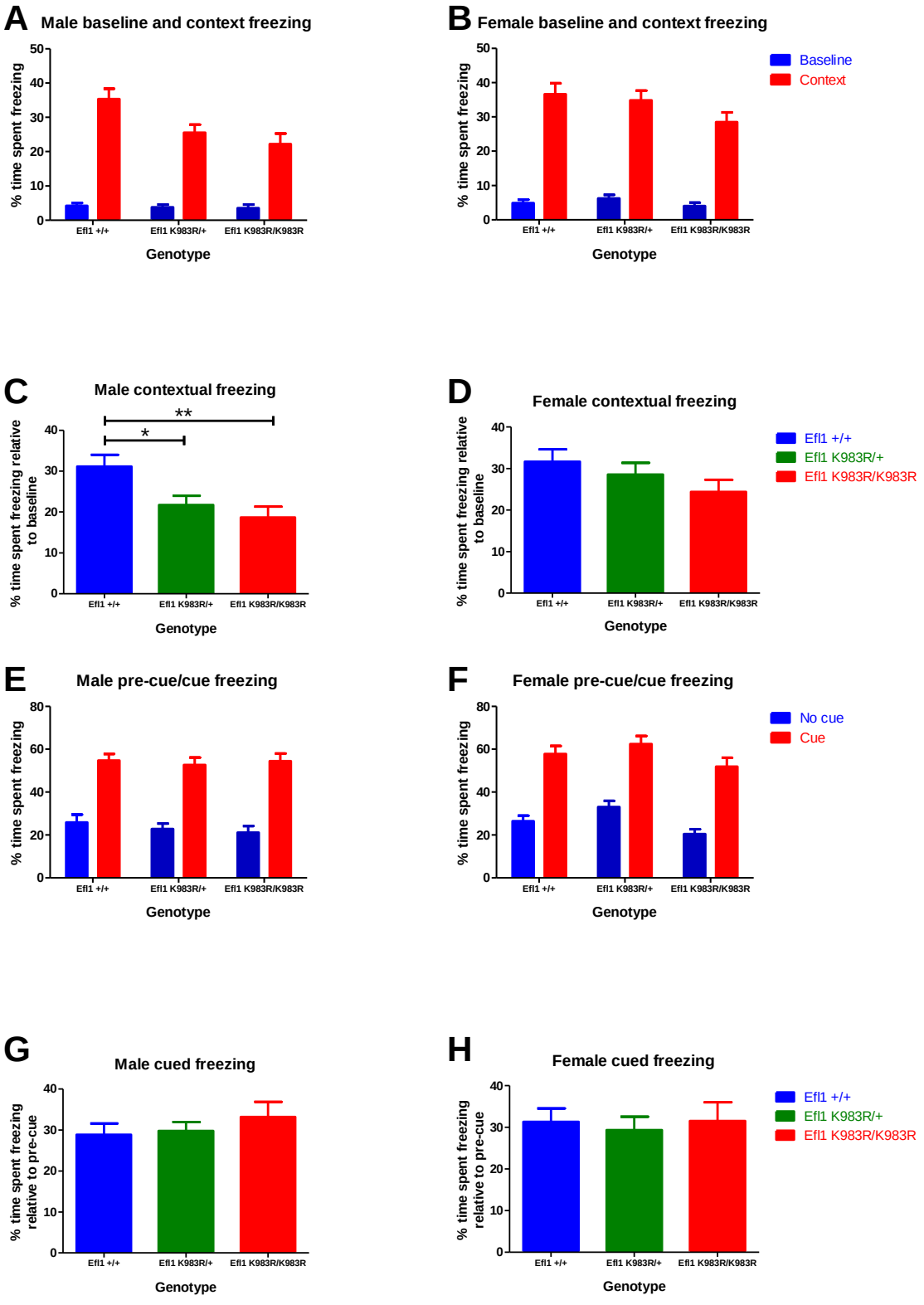


Figure 38 Fear conditioning freezing behaviour in male and females. A-B. Baseline and contextual freezing behaviour in males and females. One the first day of the fear conditioning protocol, mice are placed into an arena (the context), and hear three tones (the cue) followed by a foot shock (the unconditioned stimulus). Their freezing behaviour is measured before any tones are heard or shocks received. This is known as the baseline level of freezing, and is the natural tendency of the mouse to freeze in this environment. The freezing behaviour measured in the contextual phase of the fear conditioning protocol (day 2, when the mouse is placed back into the same arena (context) but hears no tones and receives no shocks) can then be compared to baseline freezing. **C. Male freezing behaviour in contextual fear conditioning,**

relative to baseline freezing. *Efl1*$^{K983R/K983R}$ and *Efl1*$^{K983R/+}$ mice show significantly less freezing behaviour in the contextual fear conditioning setting, compared to wildtype littermates (p=0.003, p=0.013, respectively). Percentages shown are the difference between baseline and contextual freezing, not total freezing time in the contextual phase. **D. Female freezing behaviour in contextual fear conditioning.** No differences in freezing behaviour in the contextual fear conditioning setting were observed between *Efl1*$^{K983R/K983R}$ mice and *Efl1*$^{K983R/+}$ (p=0.3073) or wildtype (p=0.0869). Percentages shown are the difference between baseline and contextual freezing, not total freezing time in the contextual phase. **E-F. Pre-cue and cue freezing behaviour in male and female mice.** The cue phase of the fear conditioning protocol is carried out. Mice are placed into a novel arena (new context) and hear three tones (the cue) and freezing behaviour is measured. The time the mice spend freezing in the novel arena before they hear a tone is called the pre-cue phase. This freezing behaviour reflects the natural freezing behaviour of the mouse in this context, without the cue. Freezing behaviour throughout the cue phase is then recorded. The freezing behaviour measured in the cue phase of the fear conditioning protocol can then be compared to pre-cue freezing. **G. Male freezing behaviour in cued fear conditioning.** No differences in freezing behaviour in the cued fear conditioning setting were observed between *Efl1*$^{K983R/K983R}$ mice and *Efl1*$^{K983R/+}$ (p=0.4418) or wildtype (p=0.3550). Percentages shown are the difference between pre-cue and cue freezing, not total freezing time in the cue phase. **H. Female freezing behaviour in cued fear conditioning.** No differences in freezing behaviour in the cued fear conditioning setting were observed between *Efl1*$^{K983R/K983R}$ mice and *Efl1*$^{K983R/+}$ (p=0.6991) or wildtype (p=0.9743). Percentages shown are the difference between pre-cue and cue freezing, not total freezing time in the pre-cue/cue phase. Numbers (n) as follows: male *Efl1*$^{K983R/K983R}$ n=24, *Efl1*$^{K983R/+}$ n=21 and wildtype n=21, female *Efl1*$^{K983R/K983R}$ n=22, *Efl1*$^{K983R/+}$ n=21 and wildtype n=25. All 3 months of age.

5.2.2. *Efl1*$^{K983R/K983R}$ mice show an attention deficit in novel object recognition

In a further attempt to investigate learning and memory in the female *Efl1*-K983R mice, recognition memory was tested using the novel object recognition test. Novel object recognition is used to evaluate cognition, particularly recognition memory, in mice. The test is based on the spontaneous tendency of rodents to spend more time exploring a novel object than a familiar one. The choice to explore the novel object reflects the use of learning and recognition memory.

The test consists of one object (novel) being placed into the mouse' home cage, and exploratory behaviour being measured, before the object is removed. After a period of 24 hours, the same object is placed in the cage (familiar), and again exploratory behaviour is measured before the object is removed. After a second period of 24 hours, a new object, that looks and feels different (new), is placed in the cage, and again exploratory behaviour is measured. Reduced interaction with a novel or new object, or equal interaction with a familiar object would indicate defective recognition memory.

Female mice were put through the novel object recognition test at 6 months of age. *Efl1*$^{K983R/K983R}$ and *Efl1*$^{K983R/+}$ mice showed significantly less interaction with the novel object than wildtype mice, which may indicate an attention deficit or general lack of exploratory behaviour in these mice. Given that *Efl1*$^{K983R/K983R}$ mice show abnormal behaviours in the home cage (see 5.1.1), it may be that the reduced interaction seen is a by-product of behaviour, and that hyperactivity prevents long stints of object recognition. *Efl1*$^{K983R/K983R}$ mice also show significantly less interaction with the familiar object and the new object compared to wildtype mice. However, the time spent with the familiar and the new object by the *Efl1*$^{K983R/+}$ mice is not significantly different to that of wildtype. These data suggest that *Efl1*$^{K983R/K983R}$ mice, and to some extent *Efl1*$^{K983R/+}$ mice, have issues with recognition memory.

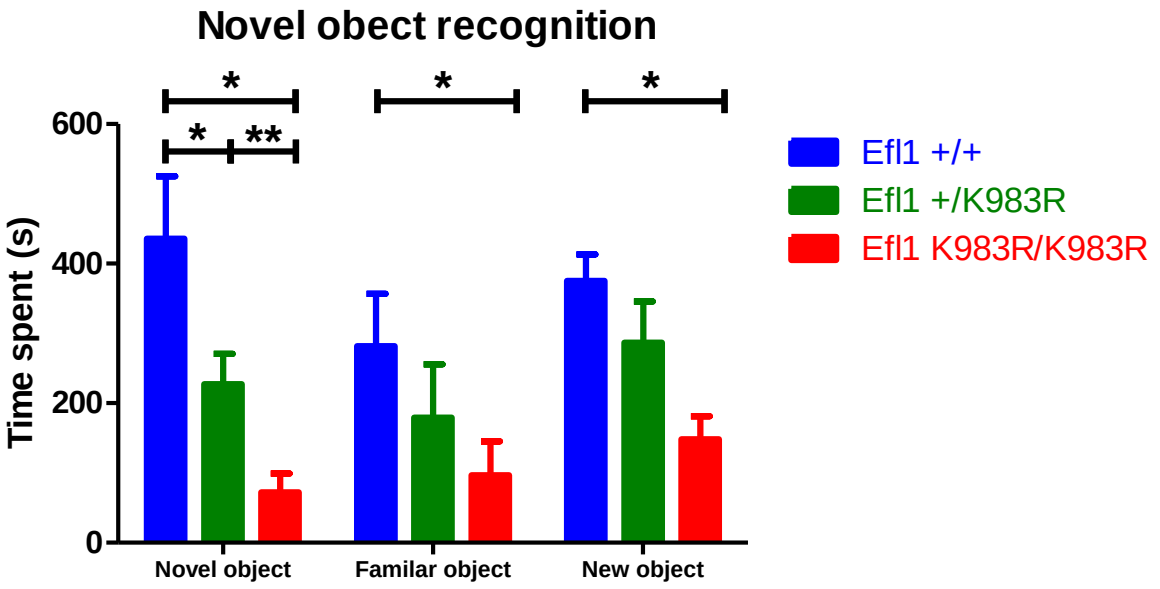


Figure 39 Novel object recognition test. A. Time spent interacting with objects in novel object recognition test. *Efl1*$^{K983R/K983R}$ and *Efl1*$^{K983R/+}$ mice spend significantly less time interacting with the novel object on day 1 compared to wildtype mice (p=0.002, p=0.039, respectively). *Efl1*$^{K983R/K983R}$ also spend significantly less time interacting with the novel object on day 1 compared to *Efl1*$^{K983R/+}$ mice (p=0.008). *Efl1*$^{K983R/K983R}$ mice interact significantly less with objects on each day compared to wildtype mice, regardless of novelty or familiarity with the object (novel object p=0.002, familiar object p=0.043, new object p=0.029). All mice were female, 6 months of age.

5.2.3. *Efl1*$^{K983R/K983R}$ mice display abnormal Y maze behaviour

Another investigation into learning and memory in the *Efl1*-K983R mice was carried out in the form of spontaneous alternation in the Y maze. Y maze is a working memory test based on spontaneous exploration and alternation between arms of a y-shaped maze. Three identical arms on an equilateral triangular centre form the apparatus. One arm is the start arm (where the mouse is placed at the beginning of the test). In the first test, only one additional arm is open to the mouse – the familiar arm. Video tracking is used to measure the amount of time the mouse spends in each arm. In a subsequent test, all three arms are available to the mouse, including the previously unavailable arm – the novel arm. Again, video tracking is used to measure the amount of time the mouse spends in each arm. Based on spontaneous alternation, it is expected that the mouse will spend more time in the novel arm than the familiar arm in the second part of the test.

3 month old female mice were tested in the Y maze. In the first phase of the test (habituation) there were no significant differences in the time spent in the start arm or the familiar arm in any of the genotypes. This is indicative of normal exploratory behaviour (Figure 40A). In the second phase of the test however, when the novel arm is available in addition to the start and familiar arms, both

Efl1$^{K983R/+}$ and wildtype mice spend significantly more time in the novel arm than in the start arm. Wildtype mice spend significantly more time in the novel arm than in the start arm or the familiar arm, indicating normal exploratory behaviour of the new area, in preference to previously explored areas. *Efl1*$^{K983R/+}$ mice however do not spend significantly different amounts of time in the familiar arm and the novel arm, suggesting that the memory of the familiar arm may not be as strong as in these mice as in wildtype. *Efl1*$^{K983R/K983R}$ mice on the other hand do not show any significant differences in time spent in any of the arms during the second phase of the test (Figure 40B).

These data suggest that the *Efl1*$^{K983R/K983R}$ mice have issues with working memory, and have of little or no memory of any of the arms from the habituation phase of the test. Alternatively, it may be that the hyperactivity sometimes seen in the *Efl1*$^{K983R/K983R}$ mice hinders this type of spatial testing in these mice.

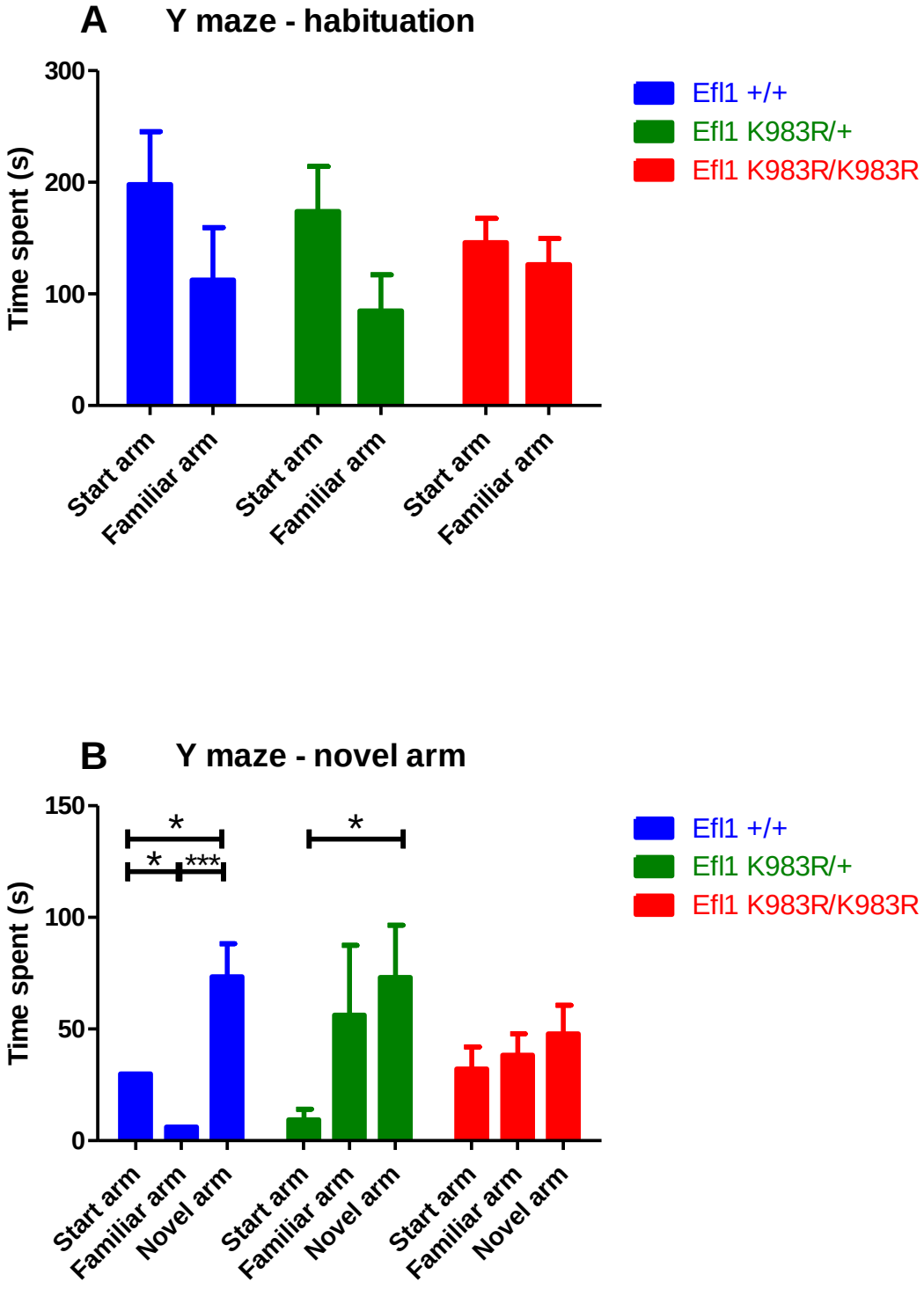


Figure 40 Y maze working memory test. A. Habituation phase of Y maze. In the habituation phase of the Y maze, only the start and familiar arms are available to the mouse. Time spent in each arm is recorded. All genotypes spend a similar amount of time in each arm, with no significant differences between genotypes. **B. Novel phase of Y maze.** In the novel phase of Y maze, the novel (third) arm is available to the mouse in addition to the start and familiar arms. Time spent in each arm is recorded. Both wildtype mice and *Efl1*$^{K983R/+}$ mice spend significantly more time in the novel arm than in the start arm (p=0.043, p=0.025, respectively). Wildtype mice also spend significantly more time in the novel arm and the start arm than in the familiar arm (p=0.0002, p=0.011, respectively). *Efl1*$^{K983R/K983R}$ mice do not show significantly different amounts of time spent in any of the arms during the novel phase of the test. Numbers (n) as follows: *Efl1*$^{K983R/K983R}$ n=8, *Efl1*$^{K983R/+}$ n=7, *Efl1*$^{+/+}$ n=6. All females, 6 months of age.

5.2.4. Learning and memory conclusions

To conclude the learning and memory section, *Efl1*$^{K983R/K983R}$ mice display various deficits when it comes to different cognitive tasks. *Efl1*$^{K983R/+}$ mice display learning and memory deficits in certain situations. Both *Efl1*$^{K983R/K983R}$ and *Efl1*$^{K983R/K983R}$ mice show contextual fear conditioning deficits, suggesting that associative learning in these mice is affected by the *Efl1*-K983R mutation in an autosomal dominant manner. However, sexual differences in fear conditioning have been reported in mice (Archer 1975, Gupta, Sen et al. 2001, Maren 2001, Wiltgen, Sanders et al. 2001).

Efl1$^{K983R/K983R}$ mice display a possible attention deficit phenotype in the context of the novel object recognition test. *Efl1*$^{K983R/+}$ mice also display an intermediate phenotype in object recognition, in that they do not interact with the novel object as much as wildtype littermates. However when faced with the object again, and a new object, the interaction times were not significantly different to wildtype. *Efl1*$^{K983R/K983R}$ mice on the other hand spent significantly less time interacting with all of the objects compared to wildtype mice. This may suggest a either deficit in recognition memory formation in *Efl1*$^{K983R/K983R}$ mice, and perhaps to a certain extent in *Efl1*$^{K983R/+}$ mice, or an attention deficit that prevents the mice from interacting with any object, novel or not, for any extensive period of time. The latter is more likely, as if the problem was with recognition memory, the interaction with the first object would not be impaired, but upon seeing the object again, the interaction time would not be reduced.

Working memory was tested in the Y maze, where *Efl1*$^{K983R/K983R}$ mice showed no preference for any area when exploring the apparatus, regardless of its novelty to the mouse. This suggest that the *Efl1*$^{K983R/K983R}$ mice have issues with forming spatial memories and explore all areas equally as a result. *Efl1*$^{K983R/+}$ mice show no preference over a familiar arm and a novel arm, but do spend more time in the novel arm than the start arm. This may reflect an intermediate phenotype in the *Efl1*$^{K983R/+}$ mice in terms of working memory.

In summary, learning and memory appears to be detrimentally affected by the *Efl1*-K983R mutation, possibly in a dose-dependent manner. A confounding factor in all of these learning and memory tests however is that they require movement. *Efl1*$^{K983R/K983R}$ mice have been shown to have a gait abnormality, and have also been observed displaying periods of hyperactivity. Both of these phenotypes may affect the learning and memory tests performed. *Efl1*$^{K983R/+}$ mice however, have not been shown to experience any of these confounding factors, and yet still display an intermediate phenotype in the learning and memory discipline.

5.3. Deafness and Otitis Media

5.3.1. *Efl1*$^{K983R/K983R}$ mice display elevated hearing thresholds

It was observed that *Efl1*$^{K983R/K983R}$ mice would present with a head tilt between 3 and 6 months of age, and so it was decided to investigate ear phenotypes in these mice. Auditory brainstem response (ABR) testing was carried out to determine if any hearing loss was present in the mice. ABR testing involves subcutaneous electrodes detecting an auditory brainstem response from sound stimuli of various frequencies, in increasing decibels (dB). A click stimulus is presented to the mouse, which is a sound made up of various frequencies in one tone, and then individual frequencies (8kHz, 16kHz and 32kHz) are tested. The higher the decibel level required to elicit a response, the higher the hearing threshold of the mouse.

Mice from the *Efl1*-K983R line were tested at 3 (females only) and 6 months of age. Both male and female *Efl1*$^{K983R/K983R}$ mice show significantly elevated hearing thresholds in response to a click stimulus compared to both *Efl1*$^{K983R/+}$ and wildtype mice at the ages tested (Figure 41A, B). Both male and female *Efl1*$^{K983R/K983R}$ mice show significantly elevated hearing thresholds in response to 8kHz, 16kHz and 32kHz stimuli compared to *Efl1*$^{K983R/+}$ and wildtype mice at the ages tested (Figure 41C, D). This indicates that *Efl1*$^{K983R/K983R}$ mice have impaired hearing at various frequencies.

Different frequencies are used to test different sections of the cochlea. High frequencies, such as 32kHz are detected by hair cells at the base of the cochlea, mid-frequencies, such as 16 kHz, are detected in the middle section of the cochlea, and low frequencies, such as 8kHz are detected at the apex of the cochlea. The increased threshold in *Efl1*$^{K983R/K983R}$ mice at all frequencies, including click, suggests that hearing impairment is not localised to a specific area of the cochlea, but is a wide spread effect. No hair cell loss was seen in electron microscopy of the cochlear at basal or apical regions (Figure 42), therefore hearing loss is unlikely to be sensorineural.

5.3.2. *Efl1*$^{K983R/K983R}$ mice have otitis media

SDS patients have been known to develop secondary deafness as a result of recurrent otitis media infections (Grinspan and Pikora 2005, Rezaei, Farhoudi et al. 2005). Otitis media is a disease, common in children, that causes inflammation of the epithelial lining of the middle ear.

For this reason, H&E staining of the middle ear in *Efl1*$^{K983R/K983R}$ and wildtype mice at 4-6 weeks of age was carried out. The staining showed inflammation of the epithelial lining of the middle ear in *Efl1*$^{K983R/K983R}$ mice, at least unilaterally, with varying degrees of severity. The inflammation causes

the epithelial lining to become thickened, and infiltration of inflammatory cells can be seen in response to the infection in *Efl1*$^{K983R/K983R}$ middle ear canals (Figure 43). Otitis media was detected in 4-6 week old mice, and deafness is thought to onset at around 3 months of age, although testing was not done at earlier time points. Nevertheless, the hearing loss seen in the *Efl1*$^{K983R/K983R}$ mice is likely to be secondary to otitis media, as in SDS patients.

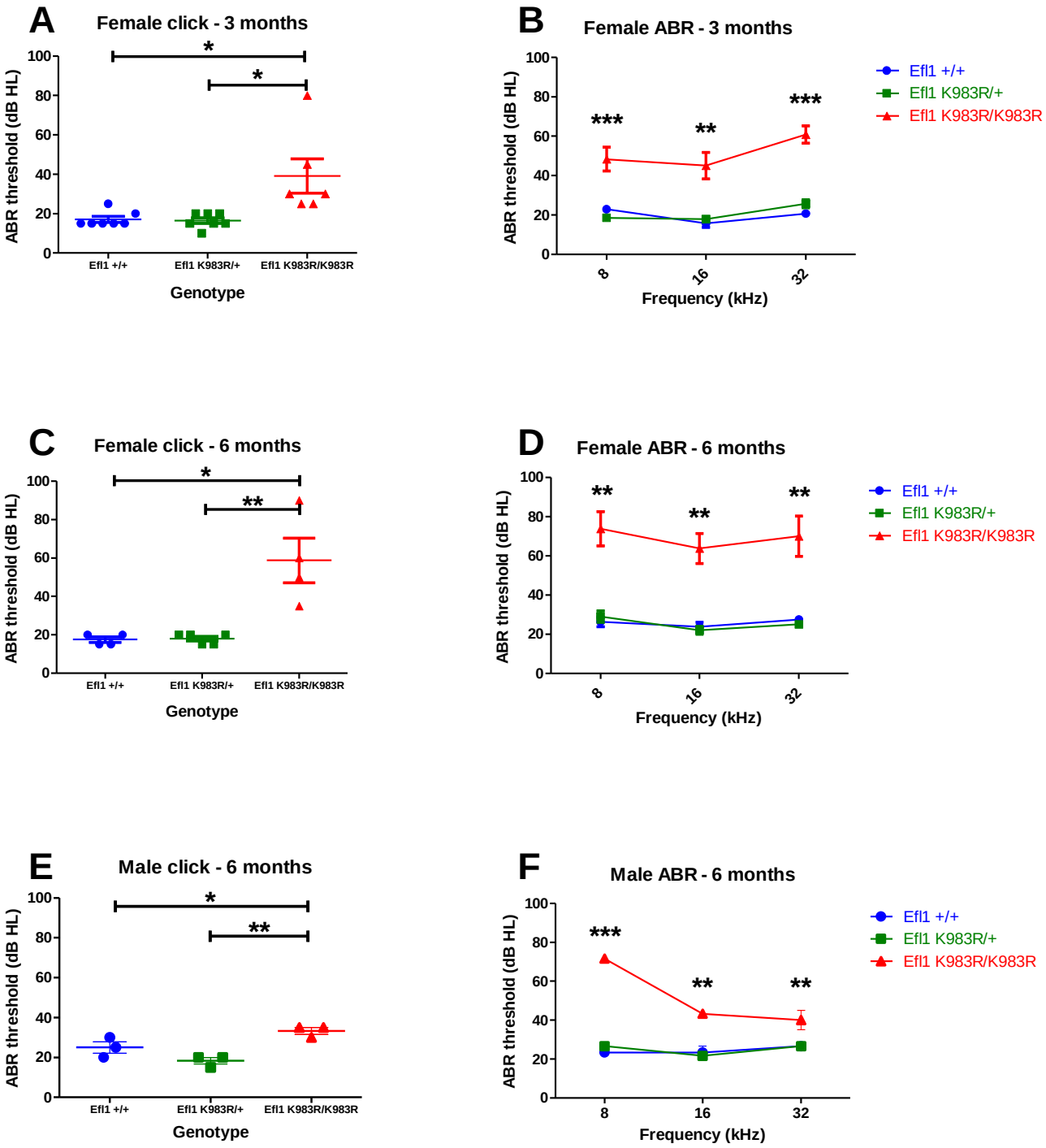


Figure 41 ABR thresholds for male and female mice at varying frequencies. A. Female hearing threshold for click stimulus at 3 months old. *Efl1*$^{K983R/K983R}$ mice show significantly elevated hearing thresholds in response to a click stimulus compared to both *Efl1*$^{K983R/+}$ and wildtype mice (p=0.018, 0.021, respectively). Both *Efl1*$^{K983R/K983R}$ and wildtype mice hearing thresholds are not significantly different. **B. Female hearing threshold at varying frequencies at 3 months old.** *Efl1*$^{K983R/K983R}$ mice show significantly elevated hearing thresholds at 8kHz compared to both *Efl1*$^{K983R/+}$ and wildtype mice (p<0.0001, p<0.0001, respectively) and *Efl1*$^{K983R/+}$ mice show significantly lower hearing thresholds than wildtype mice (p=0.031). *Efl1*$^{K983R/K983R}$ mice show significantly elevated hearing thresholds at 16kHz (p=0.001, p<0.0001, respectively) and 32kHz (p<0.0001, p<0.0001, respectively) frequencies compared to both *Efl1*$^{K983R/+}$ and wildtype mice. Both *Efl1*$^{K983R/+}$ and wildtype mice hearing thresholds are not significantly different at 16kHz and 32kHz frequencies. **C. Female hearing threshold for click stimulus at 6 months old.** *Efl1*$^{K983R/K983R}$ mice show significantly elevated hearing thresholds in response to a click stimulus compared to both *Efl1*$^{K983R/+}$ and wildtype mice (p=0.005, 0.012, respectively). Both *Efl1*$^{K983R/+}$ and wildtype mice hearing thresholds are not significantly different. **D. Female hearing threshold at varying frequencies at 6**

months old. *Efl1*$^{K983R/K983R}$ mice show significantly elevated hearing thresholds compared to both *Efl1*$^{K983R/+}$ and wildtype mice, at 8kHz (p=0.001, p=0.002), 16kHz (p=0.0006, p=0.003) and 32kHz (p=0.008, p=0.007). Both *Efl1*$^{K983R/+}$ and wildtype mice hearing thresholds are not significantly different at any frequency. **E. Male hearing threshold for click stimulus at 6 months old.** *Efl1*$^{K983R/K983R}$ mice show significantly elevated hearing thresholds in response to a click stimulus compared to both *Efl1*$^{K983R/+}$ and wildtype mice (p=0.003, 0.013, respectively). Both *Efl1*$^{K983R/+}$ and wildtype mice hearing thresholds are not significantly different. **F. Male hearing threshold at varying frequencies at 6 months old.** *Efl1*$^{K983R/K983R}$ mice show significantly elevated hearing thresholds compared to both *Efl1*$^{K983R/+}$ and wildtype mice at 8kHz (p<0.0001, p<0.0001, respectively) 16kHz (p<0.0001, p=0.006, respectively) and 32kHz (p=0.002, p=0.002, respectively) frequencies. Both *Efl1*$^{K983R/+}$ and wildtype mice hearing thresholds are not significantly different at any frequency. Numbers (n) as follows: male n=3 for *Efl1*$^{K983R/K983R}$, *Efl1*$^{K983R/+}$ and wildtype, females (3 months) n=6 for *Efl1*$^{K983R/K983R}$, n=7 for *Efl1*$^{K983R/+}$ and wildtype, females (6 months) n=4 for *Efl1*$^{K983R/K983R}$, n=5 for *Efl1*$^{K983R/+}$ and n=4 for wildtype.

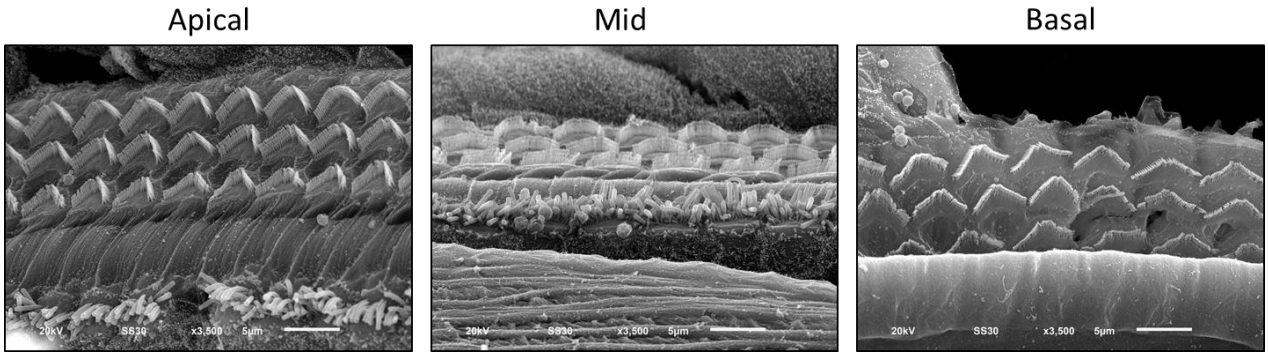


Figure 42 Electron Microscopy images of apical, mid and basal regions of the cochlea, showing inner hair cells. Representative images from one *Efl1*$^{K983R/K983R}$ are shown. No hair cells loss is seen in any of the regions of the cochlea imaged, indicating that hearing loss is not due to sensorineural pathology. Work undertaken by Andrew Parker, MRC Harwell, for use in this thesis.

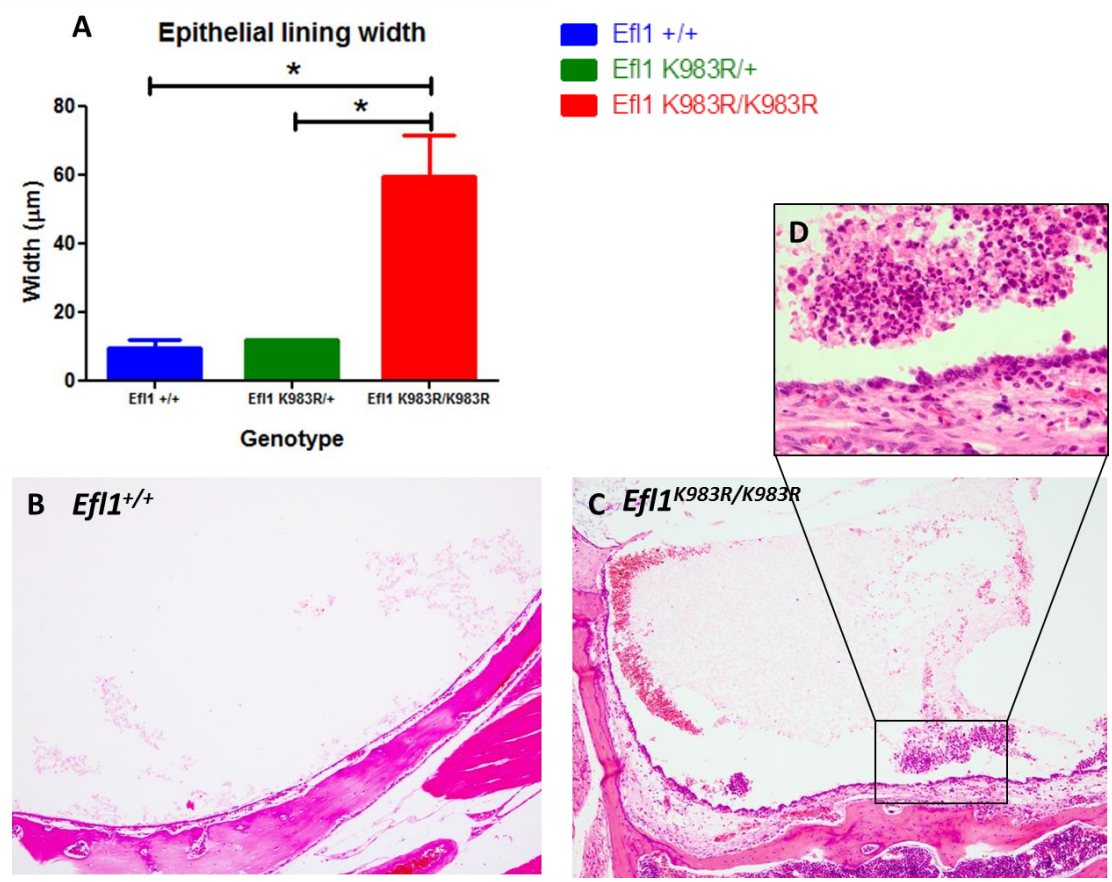


Figure 43 H&E staining and width measurements of middle ear epithelial lining. A. Width measurements of epithelial lining. *Efl1*$^{K983R/K983R}$ mice show significantly increased width of the middle ear epithelial lining due to inflammation, compared with *Efl1*$^{K983R/+}$ and wildtype mice (p=0.049, p=0.016, respectively). **B. H&E staining of middle ear epithelial lining in *Efl1*$^{+/+}$ mouse.** The middle ear epithelial lining in the wildtype ear is thin and uniform. No infiltration of inflammatory cells is seen. **C. H&E staining of middle ear epithelial lining in *Efl1*$^{K983R/K983R}$ mouse.** The middle ear epithelial lining in the *Efl1*$^{K983R/K983R}$ ear shows severe inflammation, with a thickening of the epithelial lining and infiltration of inflammatory cells into the middle ear. **D. Zoomed in view of inflammatory cells in middle ear.** Inflammation is seen in the middle ear epithelial lining in the *Efl1*$^{K983R/K983R}$ mouse, and granulated white blood cells are seen. (Images representative of n=5 for both *Efl1*$^{K983R/K983R}$ and wildtype, all females 4-6 weeks of age. *Efl1*$^{K983R/+}$ not tested.) (Immunostaining and imageing undertaken by Hilda Tateossian, for use in this thesis)

Chapter 6
Bone and Haematological Characterisation of the *Efl1*-K983R mouse line

6. Bone and Haematological Characterisation

6.1. Bone and Haematological Abnormalities

A common feature of SDS is various haematological abnormalities, namely cytopenias. Most common of these cytopenias is neutropenia, but other forms have been reported, such as thrombocytopenia and macrocytic anaemia (Burroughs, Woolfrey et al. 2009). For this reason, comprehensive haematological testing was carried out to evaluate the levels of different blood cell types in the *Efl1*-K983R mouse line. Mice were tested at 4-6 weeks of age, as it was desirable to test young mice. This is because spontaneous remission has been known to occur in SDS patients even in the most severe cases of cytopenia (Audrey Anna Bolyard 2002). General amelioration of the cytopenias is common in SDS, even if it is not eradicated completely by adulthood. Decreased cellularity in the bone marrow has also been reported in SDS patients, with elevated levels of p53, providing a possible causative link for the cytopenias of haematological cell types (Burroughs, Woolfrey et al. 2009).

6.1.1. *Efl1*$^{K983R/K983R}$ mice show features of macrocytic anaemia

Red blood cell counts, size and haemoglobin concentration were measured to assess the erythrocyte phenotype in 4-6 week old male and female mice. Male *Efl1*$^{K983R/K983R}$ and *Efl1*$^{K983R/+}$ mice have significantly lower red blood cell counts compared to wildtype littermates. However, female *Efl1*$^{K983R/K983R}$ and *Efl1*$^{K983R/+}$ red blood cell counts are not significantly different to wildtype counts (Figure 44A, B). While the red cell count in males is down, both male and female *Efl1*$^{K983R/K983R}$ mice have significantly larger red cell volumes compared to *Efl1*$^{K983R/+}$ and wildtype littermates.

Both male and female *Efl1*$^{K983R/K983R}$ mice have significantly lower haemoglobin concentrations than wildtype littermates. Female *Efl1*$^{K983R/K983R}$ mice also have significantly lower haemoglobin concentrations than female *Efl1*$^{K983R/+}$ littermates. Males *Efl1*$^{K983R/+}$ mice on the other hand, have significantly lower haemoglobin concentrations than male wildtype littermates, showing that male mice have a dominant phenotype when it comes to haemoglobin concentration (Figure 44C-F).

Large red cell size and decreased haemoglobin concentrations are both features of macrocytic anaemia. Macrocytic anaemia usually also involves an insufficient number of red blood cells, however in this case only the male mice have a decreased red blood cell count. This may show a sexual dimorphic effect of the *Efl1*-K983R mutation. The male mice therefore fulfil all of the criteria for macrocytic anaemia. The females however do not as they only have the increased size and decreased haemoglobin, and not a decrease in red cell count. It may be that the female mutant mice have an intermediate phenotype in terms of macrocytic anaemia.

Macrocytic anaemia has been reported in some SDS patients (42-82% of patients), although neutropenia is more commonly associated with the disease (88-100% of patients) (Burroughs, Woolfrey et al. 2009). Macrocytic anaemia has been linked to other ribosomopathies, including DBA and 5q-syndrome. Also, p53 induction has been shown to be critical for macrocytic anaemia caused by ribosomal dysfunction (Sakamoto, Shimamura et al. 2010, Shenoy, Kessel et al. 2012), adding another link between p53 signalling and ribosome dysfunction.

6.1.2. *Efl1*$^{K983R/K983R}$ mice show features of thrombocytopenia

The platelet counts and platelet size were also measured in 4-6 week old male and female mice to investigate any thrombocytic phenotypes. *Efl1*$^{K983R/K983R}$ mice also display significantly reduced platelet counts and platelet size (plateletcrit) compared to *Efl1*$^{K983R/+}$ and wildtype mice. This is indicative of thrombocytopenia, which is sometimes seen in SDS patients (24-88% of patients) (Figure 45).

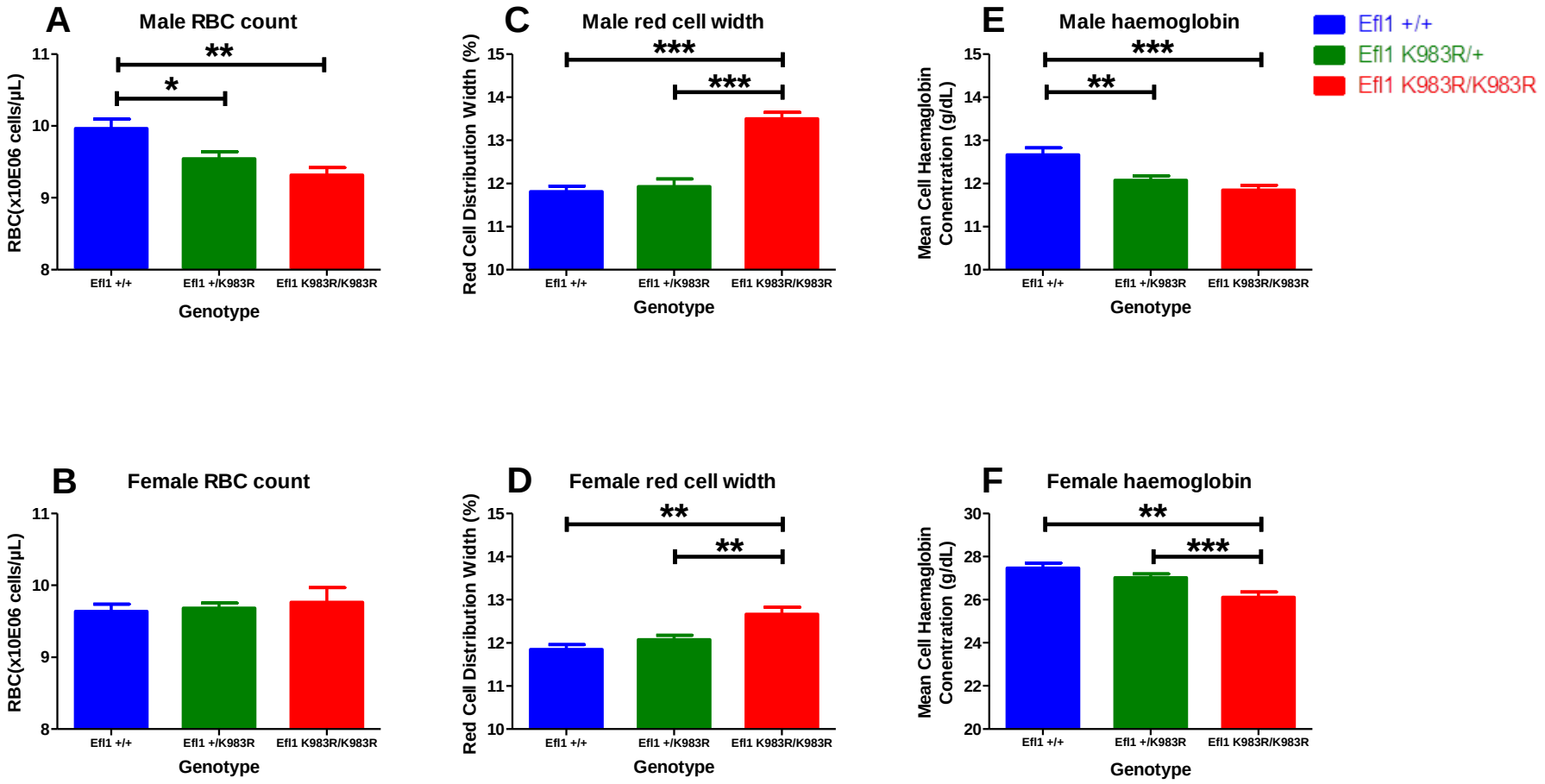


Figure 44 Red blood cell phenotypes in male and female mice. **A. Male red blood cell counts.** Male *Efl1*$^{K983R/K983R}$ and *Efl1*$^{K983R/+}$ mice have significantly lower red blood cell counts than wildtype (p=0.001, p=0.018, respectively). **B. Female red blood cell counts.** Female *Efl1*$^{K983R/K983R}$ and *Efl1*$^{K983R/+}$ mice do not have significantly different red blood cell counts compared to wildtype mice. **C, D. Male and female red cell distribution width.** Both male and female *Efl1*$^{K983R/K983R}$ mice have significantly larger red cell width compared to *Efl1*$^{K983R/+}$ and wildtype mice (male p<0.0001, p<0.0001, respectively, female p=0.0003, p=0.003, respectively). **E. Male haemoglobin concentration.** Male *Efl1*$^{K983R/K983R}$ and *Efl1*$^{K983R/+}$ mice have significantly lower haemoglobin concentrations compared to wildtype mice (p=0.0004, p=0.003, respectively). **F. Female haemoglobin concentration.** Female *Efl1*$^{K983R/K983R}$ mice have significantly lower haemoglobin concentrations compared to and *Efl1*$^{K983R/+}$ and wildtype mice (p=0.0064, p=0.0007, respectively). Numbers (n) as follows: male *Efl1*$^{K983R/K983R}$ n=11, *Efl1*$^{K983R/+}$ n=10, *Efl1*$^{+/+}$ n=8, female *Efl1*$^{K983R/K983R}$ n=9, *Efl1*$^{K983R/+}$ n=17, *Efl1*$^{+/+}$ n=13. All 6 weeks of age +/- 2 weeks.

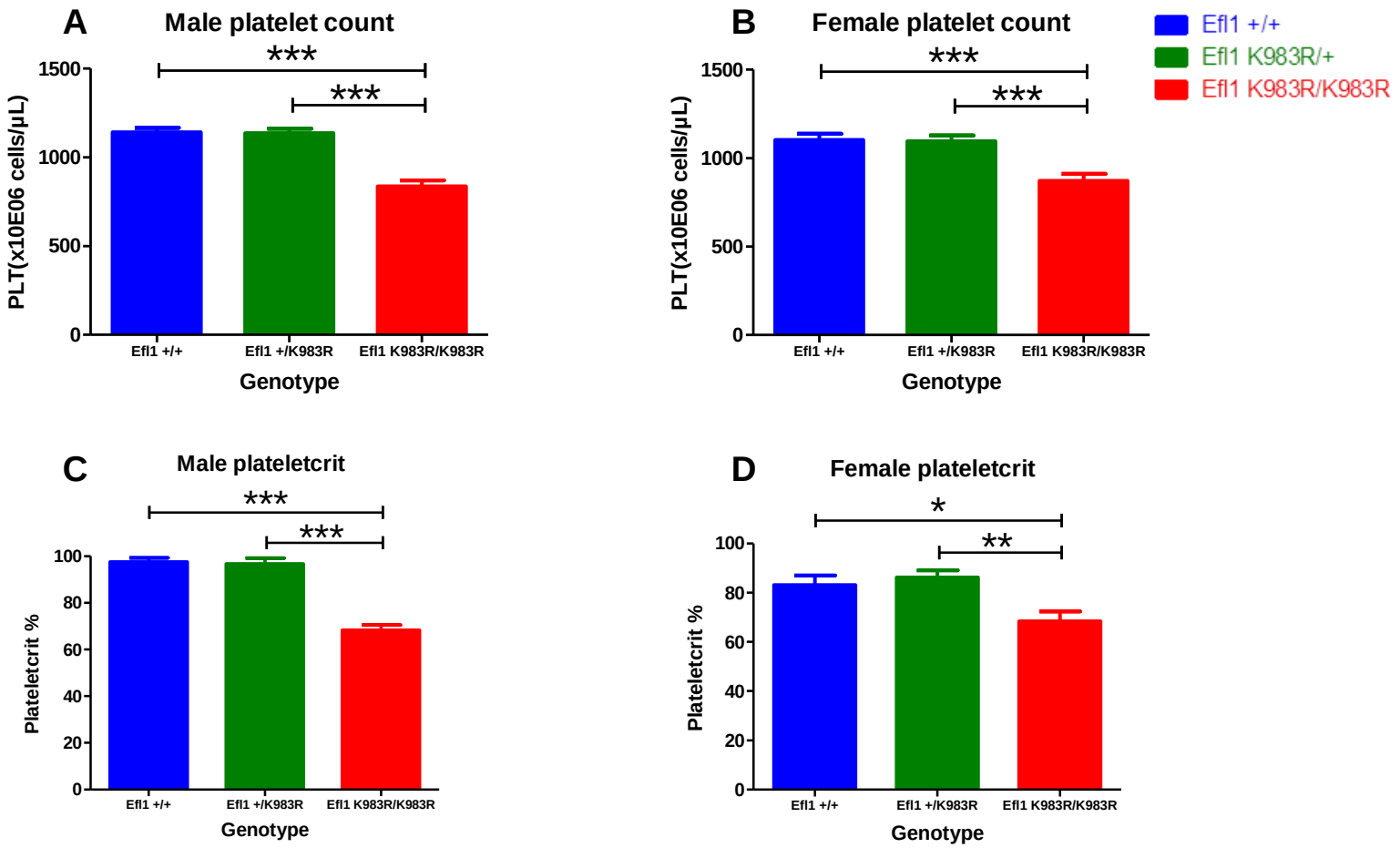


Figure 45 Platelet counts and plateletcrit for males and females. A, B. Male and female platelet count. Both male and female *Efl1*$^{K983R/K983R}$ mice have significantly lower platelet counts compared to *Efl1*$^{K983R/+}$ and wildtype mice (male p<0.0001, p<0.0001, respectively, female p=0.0004, p=0.0004, respectively). **C, D. Male and female plateletcrit percentage.** Both male and female *Efl1*$^{K983R/K983R}$ mice have significantly lower platelet counts compared to *Efl1*$^{K983R/+}$ and wildtype mice (male p<0.0001, p<0.0001, respectively, female p=0.017, p=0.001, respectively). Numbers (n) as follows: male *Efl1*$^{K983R/K983R}$ n=11, *Efl1*$^{K983R/+}$ n=10, *Efl1*$^{+/+}$ n=8, female *Efl1*$^{K983R/K983R}$ n=9, *Efl1*$^{K983R/+}$ n=17, *Efl1*$^{+/+}$ n=13. All 6 weeks of age +/- 2 weeks.

6.1.3. *Efl1*$^{K983R/K983R}$ mice have white blood cell variations

White blood cell counts were measured to investigate the white cell phenotype in 4-6 week old male and female mice. Both male and female *Efl1*$^{K983R/K983R}$ mice have significantly lower white blood cell counts as a whole compared to wildtype mice (Figure 46). This measurement includes all subpopulations of white blood cells pooled into one group.

The most common haematological deficiency in SDS patients, however, is of the neutrophils, so an in depth analysis of white blood cell subpopulations was also carried out. Both male and female *Efl1*$^{K983R/K983R}$ mice display significant differences in eosinophil count, however the heterozygous phenotypes differ between sexes. Male *Efl1*$^{K983R/K983R}$ mice have significantly lower eosinophil counts compared male to *Efl1*$^{K983R/+}$ and wildtype mice, and female *Efl1*$^{K983R/K983R}$ and *Efl1*$^{K983R/+}$ mice have significantly lower eosinophil counts compared to wildtype mice (Figure 47A, B). These data show that the female mice have an autosomal dominant effect of the mutation on eosinophil counts.

Male *Efl1*$^{K983R/K983R}$ and *Efl1*$^{K983R/+}$ mice have significantly lower monocyte counts compared to male wildtype mice, however female mice do not display significant genotype differences in monocyte counts (Figure 47C, D). In contrast, female *Efl1*$^{K983R/K983R}$ and *Efl1*$^{K983R/+}$ mice have significantly higher leucocyte and basophil counts compared to wildtype mice, whereas male mice do not display significant genotype differences in these fields. The higher counts for leucocytes and basophils in female *Efl1*$^{K983R/K983R}$ and *Efl1*$^{K983R/+}$ mice is surprising, considering that cytopenias are mostly associated with SDS, not increased cell counts (Figure 47E-H).

The neutropenia counts in both male and female mice are not significantly different between genotypes. This is somewhat surprising considering that neutropenia is the most common form of cytopenia observed in SDS (Figure 47I, J). While neutropenia is the most common form of cytopenia in SDS patients, a recent study has subcategorised SDS and 'clinical SDS' and compiled symptoms in each. This study found that 'clinical SDS' patients were more likely to suffer from one of the non-canonical anaemias such as macrocytic anaemia and thrombocytopenia than neutropenia. This posits the possibility that these mice are in fact more of a model for 'clinical SDS' than genetically defined SDS.

It is possible that the white blood cell counts in these mice are affected by otitis media infection. It is likely that if an otitis media infection is present that certain subpopulations of white blood cells would increase. Although these specific mice were not tested for otitis media, other mice at this age were found to have otitis media infections, at least unilaterally (see 5.3). It is possible that this is the cause of the increased basophil and leucocyte counts in female *Efl1*$^{K983R/K983R}$ and *Efl1*$^{K983R/+}$ mice. *Efl1*$^{K983R/+}$ mice were not tested for otitis media.

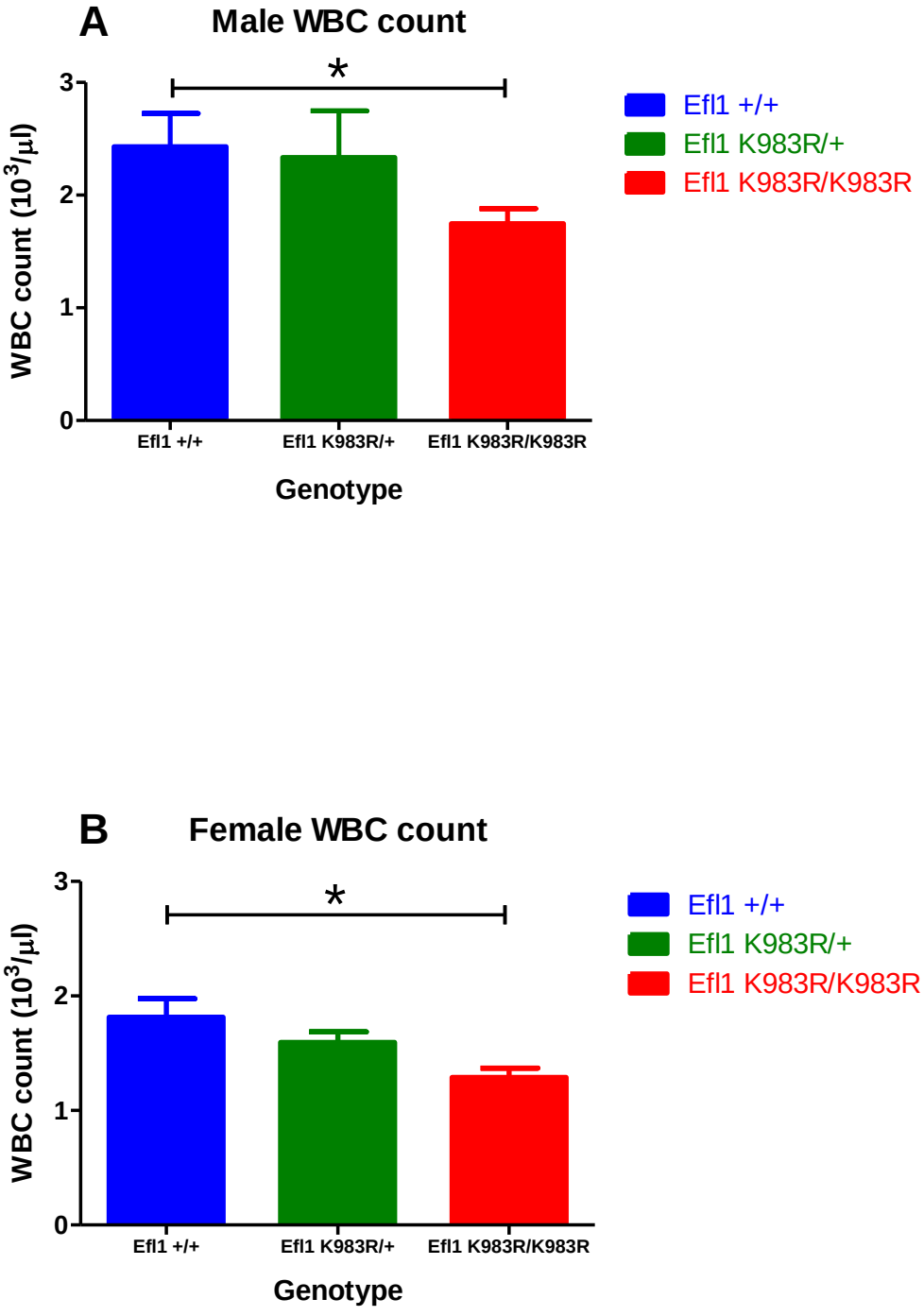


Figure 46 White blood cell counts for males and females. A, B. Male and female white blood cell count. Both male and female *Efl1*$^{K983R/K983R}$ mice have significantly lower platelet counts compared to wildtype mice (p=0.033, p<0.049, respectively). Numbers (n) as follows: male *Efl1*$^{K983R/K983R}$ n=11, *Efl1*$^{K983R/+}$ n=10, *Efl1*$^{+/+}$ n=8, female *Efl1*$^{K983R/K983R}$ n=9, *Efl1*$^{K983R/+}$ n=17, *Efl1*$^{+/+}$ n=13. All 6 weeks of age +/- 2 weeks.

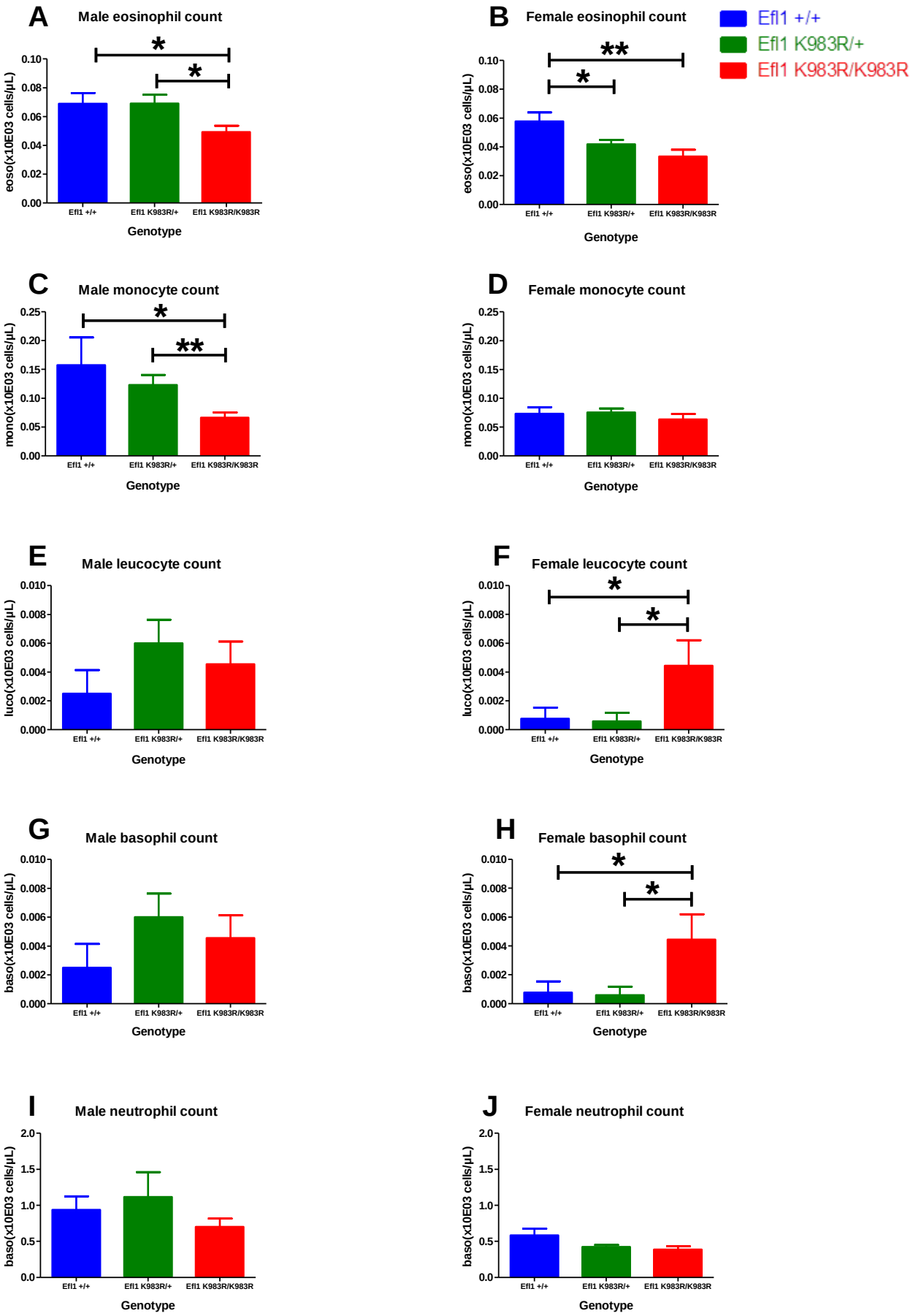

A
Male eosinophil count
eoso(x10E03 cells/µL)
0.10
0.08
0.06
0.04
0.02
0.00
*
*
Efl1 +/+
Efl1 K983R/+
Efl1 K983R/K983R
Genotype
B
Female eosinophil count
**
*
Efl1 +/+
Efl1 K983R/+
Efl1 K983R/K983R
C
Male monocyte count
mono(x10E03 cells/µL)
0.25
0.20
0.15
0.10
0.05
0.00
*
**
D
Female monocyte count
E
Male leucocyte count
luco(x10E03 cells/µL)
0.010
0.008
0.006
0.004
0.002
0.000
F
Female leucocyte count
*
*
G
Male basophil count
baso(x10E03 cells/µL)
H
Female basophil count
I
Male neutrophil count
2.0
1.5
1.0
0.5
0.0
J
Female neutrophil count

Figure 47 White blood subpopulation counts for male and females. A. Male eosinophil counts. Male *Efl1*$^{K983R/K983R}$ mice have significantly lower eosinophil counts compared to *Efl1*$^{K983R/+}$ and wildtype mice (p=0.015, p=0.029, respectively). **B. Female eosinophil counts.** Female *Efl1*$^{K983R/K983R}$ and *Efl1*$^{K983R/+}$ mice have significantly lower eosinophil counts compared wildtype mice (p=0.009, p=0.018, respectively). **C. Male monocyte counts.** Male *Efl1*$^{K983R/K983R}$ mice have significantly lower monocyte counts compared to *Efl1*$^{K983R/+}$ and wildtype mice (p=0.043, p=0.008, respectively). **D. Female monocyte counts.** Monocyte counts in females are not significantly different between any of the genotypes. **E. Male leucocyte counts.** Leucocyte counts in males are not significantly different between any of the genotypes. **F. Female leucocyte counts.** Female *Efl1*$^{K983R/K983R}$ mice have significantly lower leucocyte counts compared to *Efl1*$^{K983R/+}$ and wildtype mice (p=0.045, p=0.017, respectively). **G. Male basophil counts.** Basophil counts in males are not significantly different between any of the genotypes. **F. Female basophil counts.** Female *Efl1*$^{K983R/K983R}$ mice have significantly lower basophil counts compared to *Efl1*$^{K983R/+}$ and wildtype mice (p=0.045, p=0.017, respectively). **I, J. Male and female neutrophil counts.** Neutrophil counts in both male and female mice are not significantly different between any of the genotypes. Numbers (n) as follows: male *Efl1*$^{K983R/K983R}$ n=11, *Efl1*$^{K983R/+}$ n=10, *Efl1*$^{+/+}$ n=8, female *Efl1*$^{K983R/K983R}$ n=9, *Efl1*$^{K983R/+}$ n=17, *Efl1*$^{+/+}$ n=13. All 6 weeks of age +/- 2 weeks.

6.2. Bone Abnormalities

Skeletal abnormalities are one of the defining features of SDS. The primary skeletal defects are related to abnormal development of the growth plates, in particular, the metaphyses. Metaphyseal dysostosis has been reported in roughly 50% of the patients, is usually asymptomatic, and most commonly involves the femoral head. Other sites that may be affected include the knees, humeral heads, wrists, ankles and vertebrae. Ribcage abnormalities are found in 30%–50% of patients, including narrow ribcage, shortened ribs with flared anterior ends, and costochondral thickening. Case reports have described respiratory failure in the newborn period as a result of these rib cage abnormalities. Other skeletal abnormalities described in patients with SDS include slipped femoral epiphysis, digit abnormalities (clinodactyly, syndactyly, and supernumerary thumbs), and progressive spinal deformities (kyphosis, scoliosis, and vertebral collapse). Low turnover osteopenia and osteoporosis has also been reported (Burroughs, Woolfrey et al. 2009).

6.2.1. *Efl1*$^{K983R/K983R}$ mice have lower bone mass density

Bone mass density is used clinically to as an indirect indicator of osteoporosis and fracture risk. Bone mass density is a factor of both bone mineral content (calcium and other minerals in bone tissue) and size/area of the bone, and is an indicator of bone strength. Low bone mass density can indicate osteoporosis or osteopenia, conditions which are both known to be associated with SDS (Conway, Morton et al. 2000).

Dual-Energy X-ray Absorption (DEXA) scanning was carried out in mice of 2, 6 and 12 (females only) months of age to investigate bone density phenotypes in the *Efl1*-K983R mice. DEXA scans revealed that female *Efl1*$^{K983R/K983R}$ mice have significantly lower BMD compared to wildtype mice at all ages tested ($p=0.0044$, $p=0.036$, $p=0.016$, at 3, 6 and 12 months respectively). Female *Efl1*$^{K983R/K983R}$ mice were also shown to have significantly lower BMD compared to *Efl1*$^{K983R/+}$ mice at 3 months of age ($p=0.0072$), however, this difference disappeared by 6 months of age (Figure 48A). This may be because BMD is affected by both bone mineral content (BMC) and size of the bone. While *Efl1*$^{K983R/+}$ mice grow at a rate similar to wildtype mice, *Efl1*$^{K983R/K983R}$ mice show reduced size compared to both wildtype and *Efl1*$^{K983R/+}$ mice. This size difference may be the reason for BMD normalising in *Efl1*$^{K983R/+}$ mice by 6 months of age. BMC on the other hand is significantly lower in female *Efl1*$^{K983R/K983R}$ mice compared to both wildtype and *Efl1*$^{K983R/+}$ mice at all ages tested (3 months $p<0.0001$, $p=0.0001$, 6 months $p=0.0019$, $p=0.0025$, 12 months $p=0.003$, $p=0.0289$, respectively), as this is not affected by size (Figure 48D). This data suggests that the bones in *Efl1*$^{K983R/K983R}$ and *Efl1*$^{K983R/+}$ mice are less dense and possibly weaker compared to wildtype mice, and may also indicate osteoporosis or osteopenia.

Male mice did not show such a clear pattern of BMD differences between genotypes. At 3 months of age, male *Efl1*$^{K983R/K983R}$ mice showed significantly lower BMD compared to *Efl1*$^{K983R/+}$ mice (p=0.0188), but no significant difference compared to wildtype mice. At 6 months of age, male *Efl1*$^{K983R/+}$ mice showed significantly higher BMD compared to wildtype mice (p=0.0336), but no significant differences compared to *Efl1*$^{K983R/K983R}$ mice (Figure 48A). BMC in male mice was also not as clearly related to genotype as in the female mice. Again, *Efl1*$^{K983R/+}$ mice at 3 months of age had significantly higher BMC compared to *Efl1*$^{K983R/K983R}$ mice, but were not significantly different to wildtype. At 6 months of age, male *Efl1*$^{K983R/+}$ mice have significantly higher BMC compared to both wildtype and *Efl1*$^{K983R/K983R}$ mice (Figure 48B). These data suggest it is male *Efl1*$^{K983R/+}$ mice that have abnormal bone density phenotypes, and that they actually have higher bone densities than wildtype or homozygous littermates.

The apparent sexual dimorphism in the bone phenotypes in these mice are unexplained, as both male and female SDS patients can suffer from generalised skeletal disorders that include low bone mass density, low bone mineral concentration and increased risk of fractures. Further study would be required to determine if this sexual dimorphism is in fact true, and if so why it is only male *Efl1*$^{K983R/+}$ mice that show a phenotype.

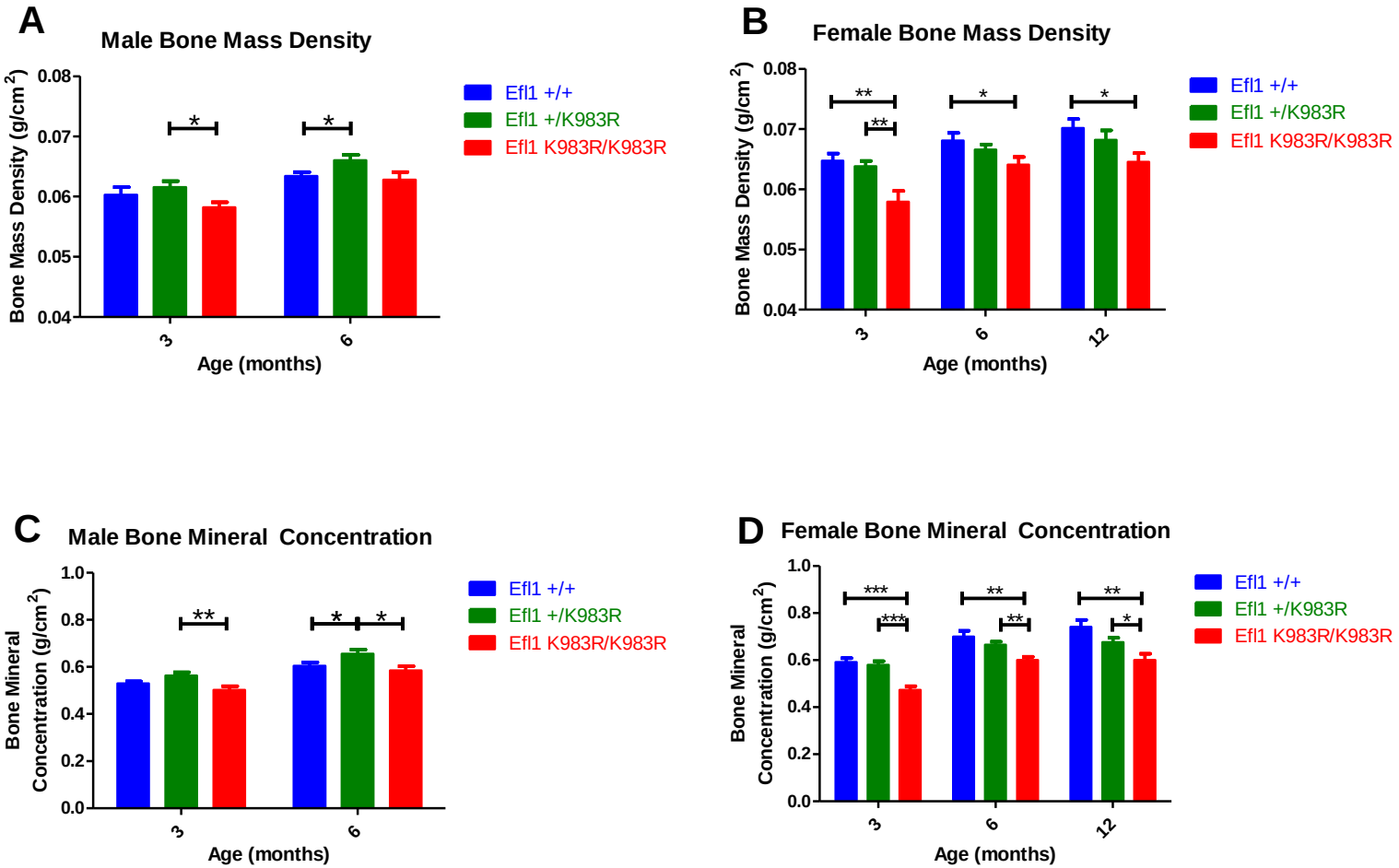


Figure 48 Bone Mass Density and Bone Mineral Concentration. A. Male Bone Mass Density. Male *Efl1*$^{K983R/+}$ mice have significantly higher bone mass density compared to *Efl1*$^{K983R/K983R}$ mice at 3 months of age (p=0.0188). Wildtype and *Efl1*$^{K983R/K983R}$ bone mass density are not significantly different at this age. At 6 months of age, male *Efl1*$^{K983R/+}$ mice have significantly higher bone mass density compared to wildtype mice (p=0.0336). **B. Female Bone Mass density.** Female *Efl1*$^{K983R/K983R}$ mice have significantly lower bone mass density compared to wildtype mice at 3 (p=0.0044), 6 (p=0.036) and 12 (p=0.0164) months of age. Female *Efl1*$^{K983R/K983R}$ mice also have significantly lower bone mass density compared to *Efl1*$^{K983R/+}$ mice at 3 months of age (p=0.0072), but not at any other ages tested. **C. Male Bone mineral Concentration.** Male *Efl1*$^{K983R/+}$ mice have significantly higher bone mineral concentration compared to *Efl1*$^{K983R/K983R}$ mice at 3 months of age (p=0.0084). Wildtype and *Efl1*$^{K983R/K983R}$ bone mineral concentration are not significantly different at this age. At 6 months of age, male *Efl1*$^{K983R/+}$ mice have

significantly higher bone mineral concentration compared to both wildtype and *Efl1*$^{K983R/K983R}$ mice (p=0.0445, p=0.017). **D. Female Bone Mineral Concentration.** Female *Efl1*$^{K983R/K983R}$ mice have significantly lower bone mineral concentration compared to wildtype mice at 3 (p<0.0001), 6 (p=0.0019) and 12 (p=0.003) months of age. Female *Efl1*$^{K983R/K983R}$ mice also have significantly lower bone mineral concentration compared to *Efl1*$^{K983R/+}$ mice at 3 (p=0.0001), 6 (p=0.0025) and 12 (p=0.0289) months of age. Numbers (n) as follows: male *Efl1*$^{K983R/K983R}$ n=12, 12, 7, *Efl1*$^{K983R/+}$ n=12, 8, *Efl1*$^{+/+}$ n=10, 9 (3, 6 months respectively), female *Efl1*$^{K983R/K983R}$ n=12, 12, 7, *Efl1*$^{K983R/+}$ n=9, 12, 12, 12, *Efl1*$^{+/+}$ n=12, 10, 9 (3, 6, 12 months, respectively).

6.2.2. Bone cellularity appears normal in *Efl1*$^{K983R/K983R}$ mice

Patients with SDS have generalised osteopenia and have several risk factors for osteoporosis. These include malabsorption and compromised nutrition due to pancreatic insufficiency, vitamin D and vitamin K deficiency, delayed puberty and infections. Osteoporosis in SDS patients has been shown to be due to low turn-over and therefore low numbers of osteoclasts and osteoblasts, and a reduced amount of osteoid (Toiviainen-Salo, Mäyränpää et al. 2007). This together with osteopenia results in bone marrow that is hypocellular, thus explaining the low BMC and BMC values that patients have (Myers, Bolyard et al. 2014).

Staining of the tibiae of 3 month old female *Efl1*$^{K983R/K983R}$ and wildtype mice was carried out to investigate the cellularity of the bone marrow, and to further study the decreased BMD phenotypes seen in 6.2.1. The staining revealed no obvious differences in cellularity in the bone marrow. This suggests that osteopenia is not present in these mice. p21 staining was also carried out to determine whether the p53 signalling pathway is upregulated in the bone marrow. No differences were seen in the levels of p21 protein between of *Efl1*$^{K983R/K983R}$ and wildtype tibiae.

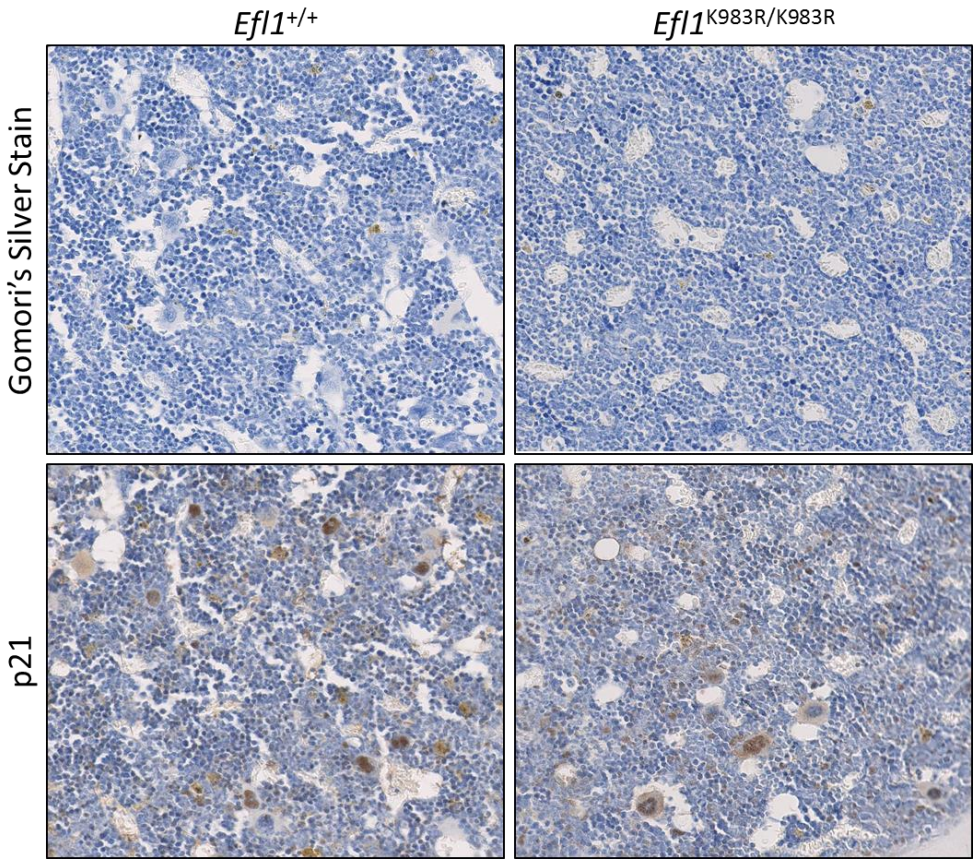


Figure 49 p21 immunostaining of tibiae sections. Tibiae from wildtype and *Efl1*$^{K983R/K983R}$ mice were stained using the VECTASTAIN Elite ABC kit and a p21 antibody (Santa Cruz, cat# SC-397). Cellularity is not significantly different between wildtype and *Efl1*$^{K983R/K983R}$ bones, as indicated by counterstaining with haematoxylin. P21 levels are not significantly different between wildtype and *Efl1*$^{K983R/K983R}$ bones, as indicated by the immunostaining. Numbers (n) = 1 for both genotypes. Mice were females, 3 months of age.

6.2.3. Bone and Haematological conclusions

The *Efl1*-K983R mutation has been shown to affect many of the haematological lineages in both *Efl1*$^{K983R/K983R}$ and *Efl1*$^{K983R/+}$ mice at a young age (406 weeks). Red blood cells are both smaller and contain less haemoglobin in both male and female *Efl1*$^{K983R/K983R}$ mice, and red blood cell counts are significantly lower in *Efl1*$^{K983R/K983R}$ and *Efl1*$^{K983R/+}$ male mice. These data suggest a form of macrocytic anaemia in these mice. In addition, thrombocytic traits were observed in both male and female mice in the form of a reduced platelet count and average size. The white blood cell population was also affected by the *Efl1*-K983R mutation, with both male and female *Efl1*$^{K983R/K983R}$ displaying significantly reduced whole white blood cell counts compared to wildtype mice.

Upon investigation into the white blood cell subpopulations, it was observed that there are sexual dimorphic changes in certain classes of white blood cell in *Efl1*$^{K983R/K983R}$ mice. For instance, both male and female *Efl1*$^{K983R/K983R}$ mice have significantly reduced eosinophil counts compared to wildtype, but monocyte counts are only significantly reduced in male *Efl1*$^{K983R/K983R}$ mice, not females. Conversely, basophil and leucocyte counts are only significantly reduced in female *Efl1*$^{K983R/K983R}$ mice, not males. To add another layer of complexity, *Efl1*$^{K983R/+}$ mice also show some difference in white blood cell populations, even though their overall white blood cell counts are not significantly different to wildtype levels. Female *Efl1*$^{K983R/+}$ mice show a significantly reduced count for eosinophils compared to wildtype in addition to the *Efl1*$^{K983R/K983R}$ mice having a deficiency of this cell type. Male *Efl1*$^{K983R/+}$ mice do not display a significant difference in eosinophil count compared to wildtype mice.

The white blood cell phenotype in these mice is extremely complex, and may be affected other factors. For example, infections of any kind will affect the level of white blood cells in the mice. Whilst every effort is taken to ensure sterility in the mouse's environment, some infections can spontaneously occur. For example otitis media has been found in male and female *Efl1*$^{K983R/K983R}$ mice. SDS patients are known to suffer from immunodeficiency due to neutropenia and/or chemotaxic impairment of the neutrophils (Burroughs, Woolfrey et al. 2009). This may have contributed to the contraction of the otitis media infection in the *Efl1*$^{K983R/K983R}$ mice prior to blood testing, and as a result may have disturbed the balance of white blood cells in these mice. Blood for these tests was taken terminally at 4-6 weeks of age, the same age at which otitis media has been detected.

In terms of bone phenotypes, it is clear that the bone mass density and bone mineral concentration are affected by the *Efl1*-K983R mutation. Females show a clear genotype-related phenotype in that bone mineral concentration is significantly lower in *Efl1*$^{K983R/K983R}$ mice compared to both *Efl1*$^{K983R/+}$

and wildtype mice. Bone mass density was also significantly lower at 3 months of age in *Efl1*$^{K983R/+}$ mice, however, when size differences between *Efl1*$^{K983R/+}$ and *Efl1*$^{K983R/K983R}$ mice increase this difference in bone mass density disappears, indicating that only *Efl1*$^{K983R/K983R}$ mice have a long-term defect in bone density. While staining of the tibiae of 3 month old mice did show obvious hypocellularity, it is possible that mice at later time points may have displayed a more striking difference.

Chapter 7
In vitro Characterisation of the *Efl1*-K983R mouse line

7. In vitro characterisation of the *Efl1*-K983R mutation

In addition to phenotypic characterisation, we sought to investigate the *in vitro* pathways affected by the *Efl1*-K983R mutation. This was carried out using predominantly primary cells from the mutant mice in the form of mouse embryonic fibroblasts (MEFs). Investigation of the ribosomal maturation pathway was also undertaken in the form of polysome profiling. In this chapter we give details of the findings in these areas.

7.1. Molecular pathways in the *Efl1*-K983R mouse line

7.1.1. EFL1 protein levels are dramatically reduced in *Efl1*$^{K983R/K983R}$ mice

Firstly, we wanted to look at any possible differences in the EFL1 protein in cells and tissues harbouring the Efl1-K983R mutation. Western blot analysis in multiple tissues from K983R mutant mice, including MEFs, revealed that EFL1 protein levels are significantly reduced in *Efl1*$^{K983R/K983R}$ and *Efl1*$^{K983R/+}$ mice. This was shown to be true in both embryonic tissues (MEFs) (Figure 52B) and adult tissues (brain, liver and pancreas) (Figure 52). *Efl1*$^{K983R/K983R}$ EFL1 protein levels range between 3% and 17% of that of wildtype, and *Efl1*$^{K983R/+}$ EFL1 protein levels range between 24% and 57% of that of wildtype.

Western blot analysis in MEFs was carried out for various other proteins associated with EFL1. SBDS levels were tested because SBDS and EFL1 work cooperatively to remove eIF6 from the 60S subunit during ribosomal maturation. Also, SDS patient-derived cells have been shown to have a deficiency of SBDS protein (Burwick, Coats et al. 2012, In, Zaini et al. 2016). eEF2 levels were tested, as this is a structural homologue of EFL1, and the two proteins share a binding site on the 60S subunit. For this reason, it is feasible that in the absence of EFL1, eEF2 may act in a compensatory mechanism. eIF6 levels were tested to see if the deficiency of EFL1, which may affect the release of eIF6 from the 60S subunit, would in turn alter the levels of the anti-association factor in an attempt to compensate for any defect in ribosomal subunit joining. There were no differences in protein levels of SBDS, eEF2 and eIF6 seen, therefore suggesting that proteins associated with EFL1 are unaffected by its deficiency (Figure 50C-E). These data suggest that EFL1 is independently reduced in the *Efl1*$^{K983R/K983R}$ mice.

Another EFL1 antibody was also used to detect EFL1 in MEF lysates, however this gave very faint bands. However, a similar pattern of expression was seen between genotypes, which suggests that the antibody described above is indeed detecting EFL1, and its binding is not hindered to the protein by the K983R mutation. The two antibodies used detected epitopes at the N terminal end of the protein. The first antibody described here (Figure 50), and the one used throughout this thesis

detected residues 1062-1090, whilst the second antibody discussed here (Figure 51**Error! Reference source not found.**) detected residues 1106-1120. Due to the faintness of the bands of this second antibody, the prior was chosen as the antibody of choice for this thesis.

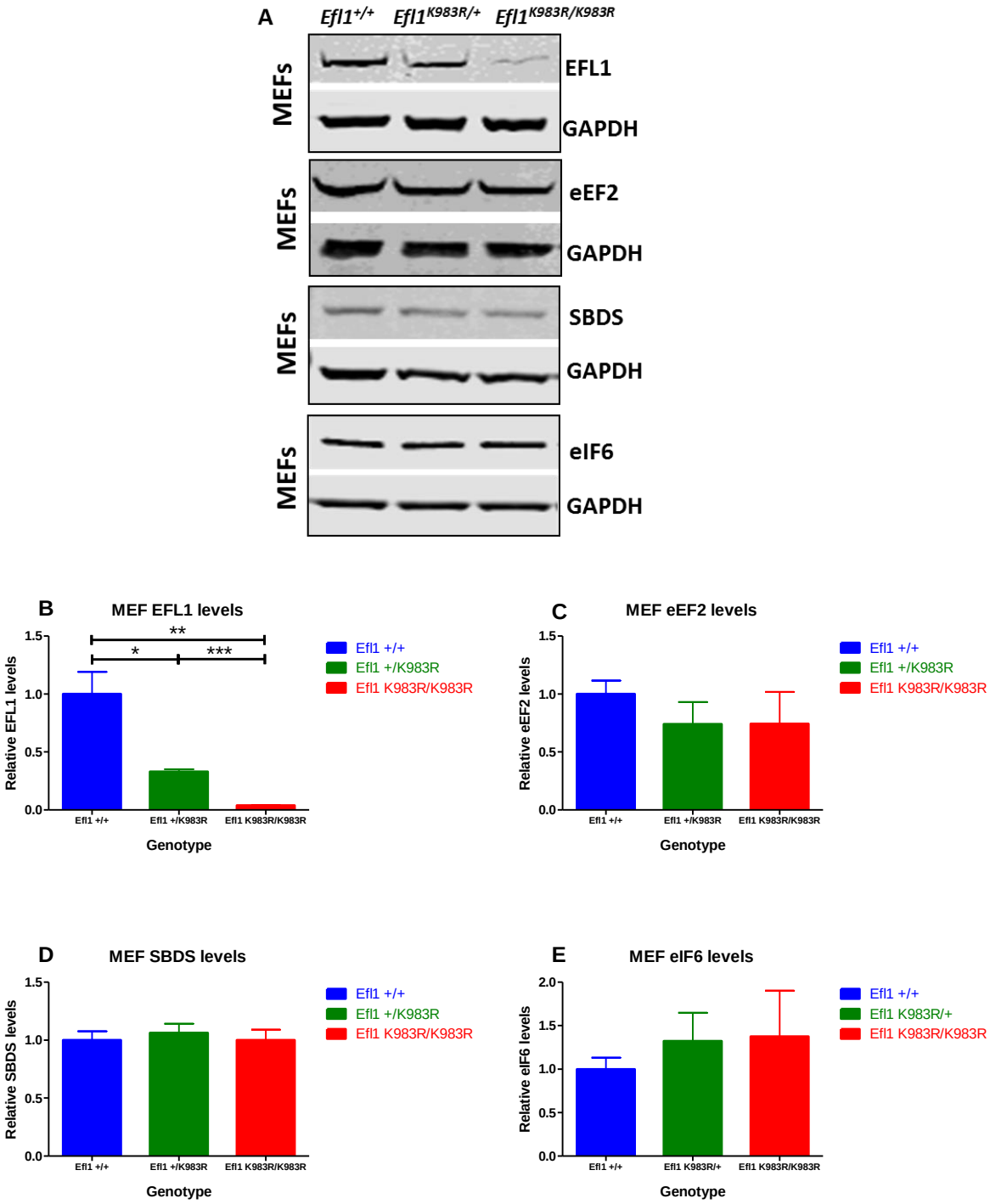


Figure 50 Mouse embryonic fibroblast (MEF) protein levels. A. Representative blots for EFL1, eEF2, SBDS and eIF6 in MEF lysates, with GAPDH for normalisation. B. MEF EFL1 protein levels. Efl1K983R/K983R MEFs have significantly lower EFL1 protein levels compared to Efl1K983R/+ and wildtype MEFs (p=0.0002, p=0.0073, respectively. Efl1K983R/+ MEFs also have significantly lower EFL1 protein levels compared to wildtype MEFs (p=0.0253). N=3 for all genotypes. **C-E. MEF eEF2, SBDS and eIF6 protein levels.** There are no significant differences in eEF2, SBDS or eIF6 protein levels in MEFs between genotypes. Numbers (n) =3 for all genotypes.

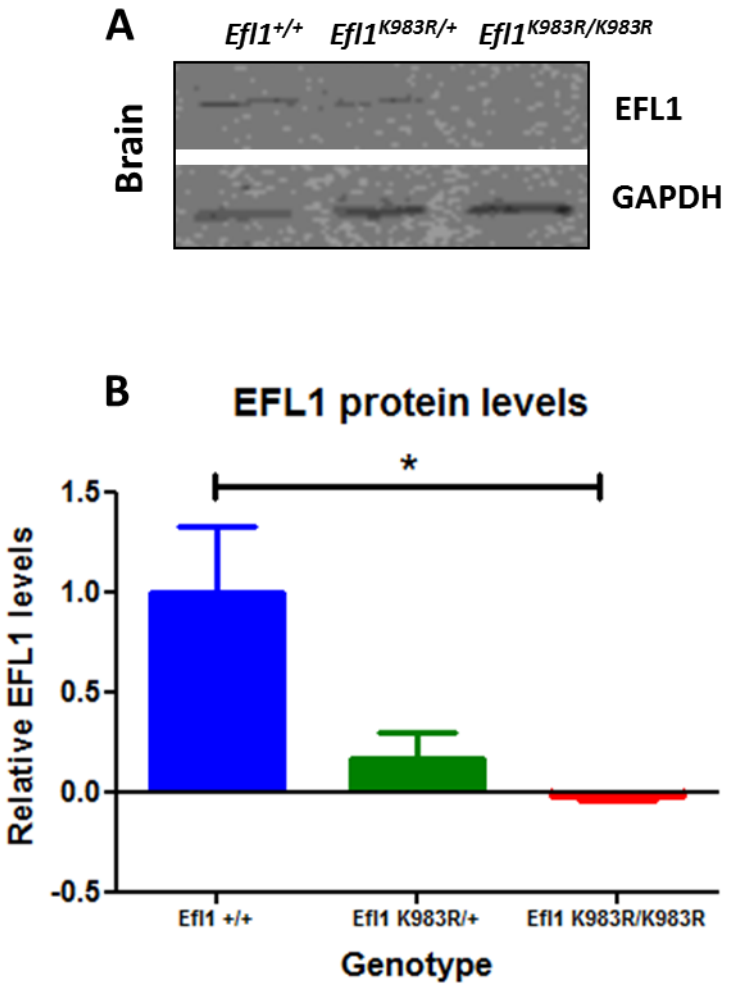


Figure 51 Mouse embryonic fibroblast (MEF) protein levels, using alternative antibody. A. Representative blots for EFL1, with GAPDH for normalisation. B. MEF eFL1 protein levels, relative to GAPDH. *Efl1*$^{K983R/K983R}$ MEFs have significantly lower EFL1 protein levels compared to wildtype MEFs (p=0.0365). Numbers (n) = 3 per genotype.

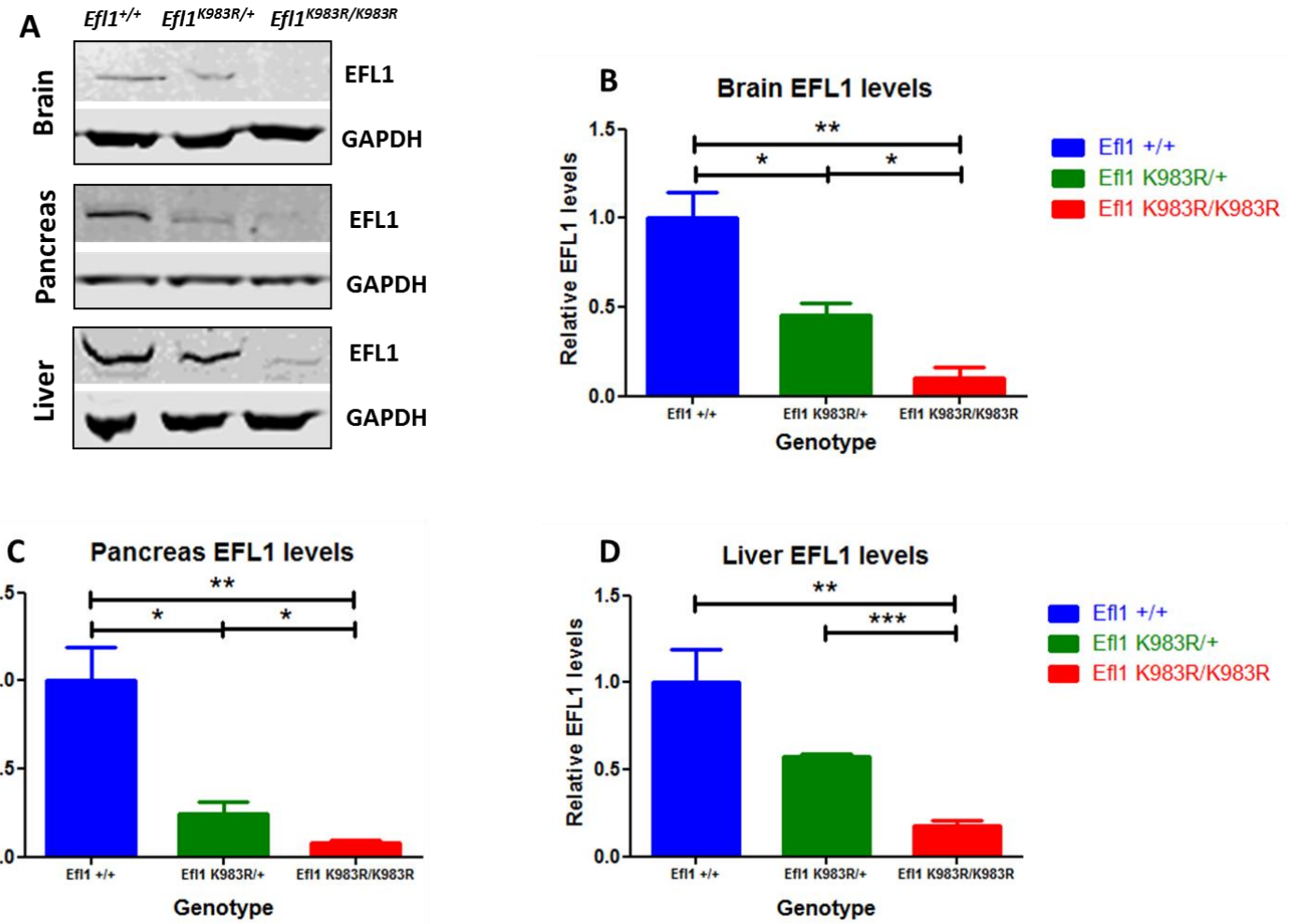


Figure 52 Adult tissue EFL1 protein levels. A. Brain EFL1 protein levels. *Efl1*$^{K983R/K983R}$ brain tissue has significantly lower EFL1 protein levels compared to *Efl1*$^{K983R/+}$ and wildtype MEFs (p=0.0198, p=0.0046, respectively. *Efl1*$^{K983R/+}$ MEFs also have significantly lower EFL1 protein levels compared to wildtype MEFs (p=0.0276). N=3 for all genotypes. **B. Liver EFL1 protein levels.** *Efl1*$^{K983R/K983R}$ liver tissue has significantly lower EFL1 protein levels compared to *Efl1*$^{K983R/+}$ and wildtype MEFs (p<0.0001, p=0.0052, respectively. N=4 for all genotypes. **C. Pancreas EFL1 protein levels.** *Efl1*$^{K983R/K983R}$ pancreas tissue has significantly lower EFL1 protein levels compared to *Efl1*$^{K983R/+}$ and wildtype MEFs (p=0.0085, p=0.049, respectively. *Efl1*$^{K983R/+}$ MEFs also have significantly lower EFL1 protein levels compared to wildtype MEFs (p=0.0202). N=3 for all genotypes.

7.1.2. EFL1 transcript levels are unaffected by the *Efl1*-K983R mutation

As discussed in 7.1, EFL1 protein levels are significantly lower in *Efl1*$^{K983R/K983R}$ mice in multiple tissues. There are various possibilities for this, one of which being that EFL1 is downregulated in *Efl1*$^{K983R/K983R}$ mice. qPCR analysis of MEF RNA was carried out to assess whether the changes in protein level were due to a deficiency of *Efl1* transcript being present in the cells.

Relative quantification by qPCR of *Efl1* transcripts showed that there are no significant differences between wildtype, *Efl1*$^{K983R/+}$ or *Efl1*$^{K983R/K983R}$ transcript levels (Figure 53). This suggests that the *Efl1* gene is being transcribed normally in the mutants, and that the level of transcription of the gene is not the cause for protein deficiency.

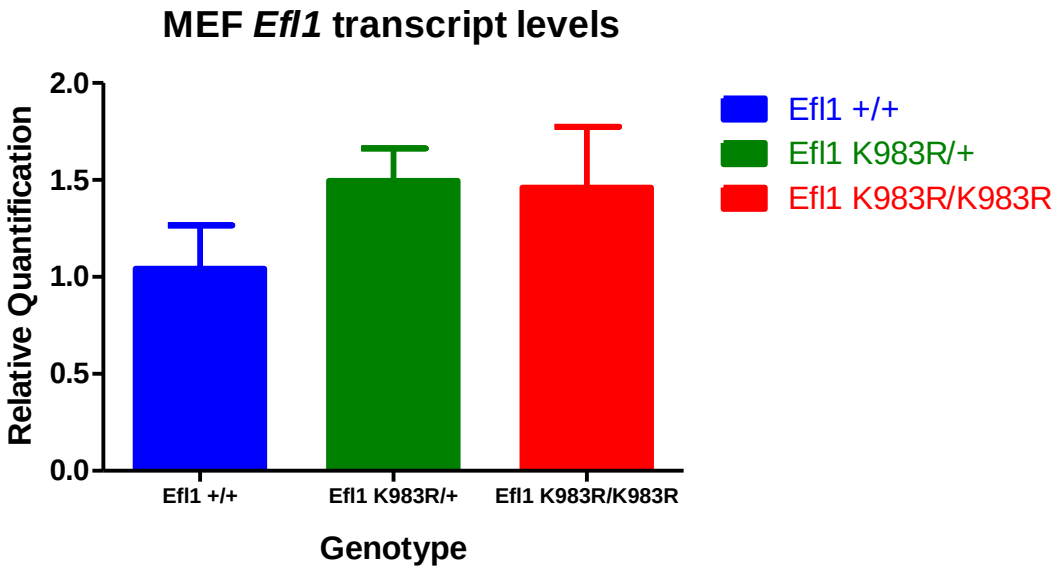


Figure 53 Relative quantification of MEF *Efl1* transcript levels. Relative quantification was calculated by comparing qPCR results to one representative wildtype sample. It was found that there are no significant differences in *Efl1* transcript levels in *Efl1*$^{K983R/+}$ or *Efl1*$^{K983R/K983R}$ MEFs, relative to wildtype levels. Numbers (n) =5 for all genotypes.

Alternatively, it is feasible that the protein deficiency is a result of faulty loading of the mRNA transcript into the ribosome, and therefore less of the transcript being translated into protein. To test this theory, we conducted qPCR analysis of *Efl1* transcripts in polysomal fractions from liver polysome profiles (referred to later in 7.2.4). During the process of polysome profiling, tissue or cell lysate is separated on a sucrose density gradient. Polysomes (mRNA transcripts with ribosome(s) attached) can be seen at the end of the profiles, due to their high density. These fractions were collected and RNA extraction was carried out in order to determine *Efl1* transcript levels that are being actively translated.

Four fractions of the liver polysome profiles contained polysomes; fractions 6, 7, 8 and 9. Each fraction represents an increase of the number of ribosomes attached to the mRNA transcripts (Gandin, Sikström et al. 2014). We pooled the results from each fraction, to gain a view of all polysomes present in the liver. The aim was to determine if there are differences in the amount of *Efl1* transcript engaged with ribosomes in tissues harbouring the *Efl1*-K983R mutation. No significant differences were seen in the levels of *Efl1* transcript in the polysomal fractions of wildtype liver profiles compared to that of $Efl1^{K983R/+}$ or $Efl1^{K983R/K983R}$ polysomes (Figure 54). This suggests that the *Efl1* transcript is being loaded into the ribosome efficiently. This does not unequivocally prove that these transcripts are then being translated, however it does suggest that decreased translation initiation is not the cause of EFL1 protein deficiency.

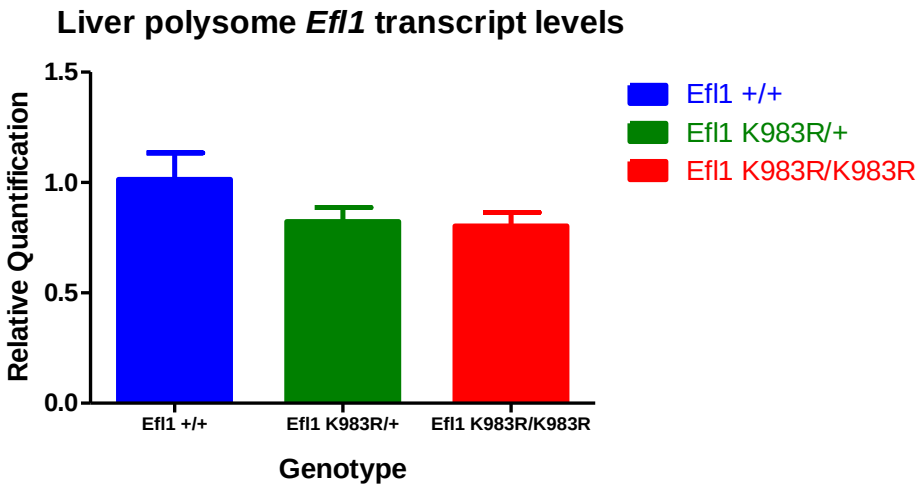


Figure 54 Relative quantification of liver polysome *Efl1* transcript levels. Relative quantification (RQ) (to one wildtype sample) was collected for each fraction individually. Total *Efl1* transcript levels for all four fractions (6, 7, 8 and 9) were calculated by averaging RQ values from qPCR analysis of all fractions. No significant differences were seen in *Efl1* transcript levels in the polysomes between genotypes. Numbers (n) = 3 for all genotypes, and all fractions.

7.1.3. p53 signalling is unaffected by the *Efl1*-K983R mutation

The p53 pathway responds to various cellular stressors, both intrinsic an extrinsic. These stressors include DNA damage, hypoxic conditions, heat- or cold-shock, inflammation (via nitric oxide signalling) and ribosomal imbalances. Abnormalities in the ribosomes functionality indicate that the cell is ill-equipped to progress through the cell cycle, and thus programmed cell death is activated. For most of these stress signals, the p53 protein is modified by phosphorylation and acetylation, which leads to the activation of the p53 protein as a transcription factor that initiates a program of cell cycle arrest, cellular senescence or apoptosis. p53 does this by activating transcription of the p21 gene. P21 then goes on to inhibit cyclin E-CDK2. This cyclin-dependent kinase acts upon the Retinoblastoma (Rb) protein to derepress the E2F1 activity that promotes the transcription of genes involved in preparing a cell to progress from G-1 to S phase in the cell cycle.

It has been shown that SDS patients have increased levels of p53 protein in their bone marrow, which may indicate a cause for the hypocellularity associated with the disease. For this reason, p53 was of interest in the case of the *Efl1*-K983R mutant mouse line. p53 levels in MEFs were investigated by western blot. It was found that p53 levels are not significantly different in *Efl1*$^{K983R/K983R}$ MEFs compared to wildtype. *Efl1*$^{K983R/+}$ and wildtype p53 levels were also not significantly different. p21 levels are also investigated, as this is the downstream effector of p53 activation. However, p21 levels are not significantly different between genotypes (Figure 55).

MEFs may not be the ideal testing context for p53 signalling, considering that SDS patient p53 levels were found to be increased in the bone marrow. For this reason, p21 levels in the bones of the *Efl1*-K983R mouse line was investigated. Immunostaining of the tibiae showed that p21 protein levels in the bone marrow of *Efl1*$^{K983R/K983R}$ mice were not significantly different than wildtype (see Figure 49). These data suggest that p53 signalling is not upregulated in the *Efl1*$^{K983R/K983R}$ mice as it is in SDS patient bone marrow. However, the *Efl1*$^{K983R/K983R}$ mice do show similar haematological abnormalities to SDS patients. This may indicate that either the haematological abnormalities in these mice are distinct in from those seen in SDS, or that the anaemias seen in SDS are not caused by p53 signalling in the bone. No definitive causative link between p53 signalling and hypocellularity in the bone marrow of patients has been made to the anaemias seen in these patients.

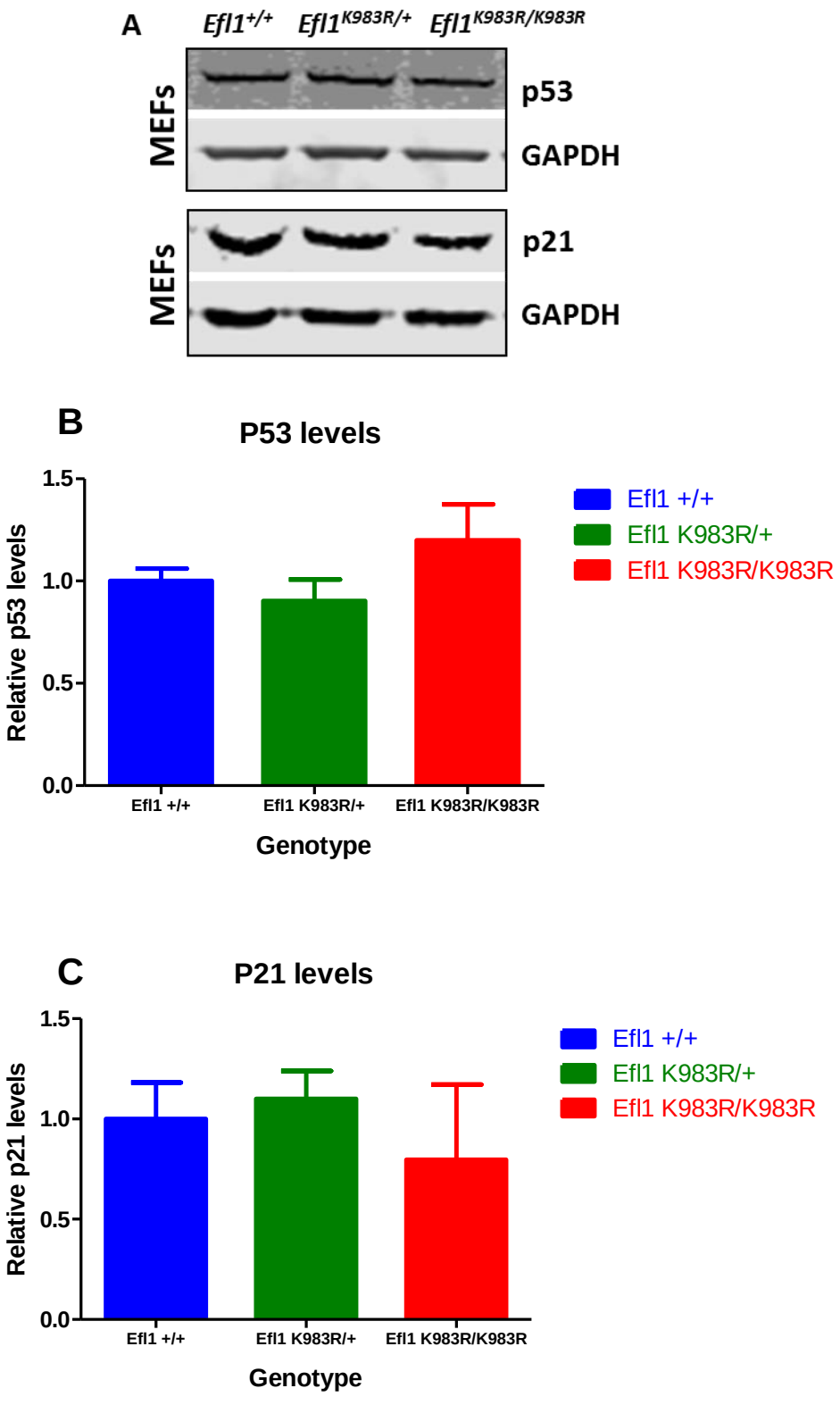


Figure 55 p53 and p21 protein levels in mouse embryonic fibroblasts. A. Representative blots of p53 and p21 in MEFs, with GAPDH for normalisation. B. Relative levels of p53 protein in MEFs. The level of p53 protein in MEFs is not significantly different between genotypes. **C. p21 protein levels in MEFs, relative to GAPDH.** The level of p21 protein in MEFs is not significantly different between genotypes. Numbers (n) = 3 for all genotypes.

7.1.4. mTOR signalling is unaffected by the *Efl1*-K983R mutation

Mammalian Target Of Rapamycin (mTOR) is a master growth regulator that senses and integrates diverse nutritional and environmental cues, including growth factors, energy levels, cellular stress, and amino acids (Jewell, Russell et al. 2013). Regulation of protein synthesis is crucial for cell viability, therefore ribosome biogenesis has to meet the demand of protein synthesis. In eukaryotic cells, ribosome biogenesis is tightly controlled by the availability of nutrients and growth factors. For this reason, mTOR signalling is often affected by ribosomopathy-associated pathways within the cell (Boultwood, Yip et al. 2013). Upregulation of mTOR complex 1 (mTORC1) activity leads to activation of the S6 kinase (S6K) pathway, which in turn upregulates ribosome biosynthesis by promoting the selective recruitment of ribosomal protein mRNAs to actively translating polysomes (Thomas 2000).

Activation of the mTORC1 pathway has been shown to be beneficial in one ribosomopathy in particular: DBA. Patients with DBA suffer with macrocytic anaemia, and erythroblasts obtained from these patients show impaired mRNA translation. Therefore, mTORC1 was investigated a sa potential therapeutic target for its role in activating translation. Leucine is known to be the one of the major amino acid activators of mTORC1, via the leucine tRNA synthetase protein (LRS) (Han, Jeong et al. 2012). For this reason, leucine supplementation was trialled in DBA patients for its translation enhancing effects. Increased translation was seen in DBA lymphocytes, and one patient has been shown to become transfusion dependent as a result of leucine treatment (Cmejlova, Dolezalova et al. 2006), demonstrating the importance of mTORC1 activity in translation and in ameliorating translation-deficient diseases. While translation defects have been proposed to play a role in anaemia in DBA patients, through a reduction in translation of GATA1 (Ludwig, Gazda et al. 2014), there is also substantial evidence that p53 has a role in the anaemia seen in DBA mouse models (McGowan and Mason 2011). Furthermore, it has been shown that steroid treatment, which is commonly used to treat anaemia in DBA patients, reduces p53 levels in the mouse DBA model. Therefore, the transaltion defects seen are likely to stem from perturbations in p53 signalling (Narla and Ebert 2010).

Considering the implications of the mTORC1 pathway in DBA, and that SDS patient derived cells show deficient translation (Burwick, Coats et al. 2012), mTORC1 activity was investigated in *Efl1*-K983R mutant MEFs. mTORC1 phosphorylates and activates S6K1 and S6K2, whose substrate is ribosomal protein S6 (RPS6), a component of the 40S subunit that mediates translation initiation at the 5'm^7G cap of mRNA. RPS6 undergoes phosphorylation by S6K which potentiates its cap binding activity, thereby promoting translation initiation, particularly of ribosomal protein genes (Thomas 2000).

Western blot analysis of both total and phosphorylated forms of S6K in MEFs was performed. No significant differences were detected in the levels of phosphorylated S6K, relative to the total amount of S6K, between any of the genotypes (Figure 56B). This indicates that mTOR signalling in MEFs is unaffected by the *Efl1*-K983R mutation. In DBA the reduced translation seen is thought to underlie the anaemias found in patients. These data suggest that DBA-related mechanisms are not causative of the macrocytic anaemia or any of the other haematological abnormalities seen in the *Efl1*-K983R mice. Of course this data does not irrefutably show that mTORC1 activity is not affected by the *Efl1*-K983R mutation, only that the S6K pathway is unaltered. Therefore, another pathway related to mTORC1 was analysed.

eIF2α is phosphorylated during cellular stress in pathways such as the PERK pathway. When eIF2α becomes phosphorylated, recycling of the ternary complex (TC) is inhibited, and translation of cap-dependent mRNAs is repressed. In these circumstances, cells favour cap-independent translation and translate mRNAs containing uORFs, which tend to encode stress related proteins such as ATF4 or CHOP (Boultwood, Yip et al. 2013). Although not directly activated by mTORC1 itself, eIF2α is linked to mTORC1 activity in an inverted relationship. Increased mTORC1 activity correlates to reduced eIF2α phosphorylation and vice versa (Gandin, Masvidal et al. 2016). eIF2 is an essential component of the TC, which is required for translation initiation. Phosphorylation of eIF2α at serine 51 inhibits protein synthesis at the initiation stage by preventing dissociation of eIF2 from eIF2B, thereby hindering its participation in the ternary complex (Ma and Blenis 2009). Thus translation is downregulated when eIF2α is phosphorylated.

Western blot analysis of both total and phosphorylated forms of eIF2α in MEFs was performed. No significant differences were detected in the levels of phosphorylated eIF2α relative to the total amount of these proteins between any of the genotypes (Figure 56C). This data suggests that the cells are not undergoing stress pathways that lead to eIF2α phosphorylation, and inhibition of translation.

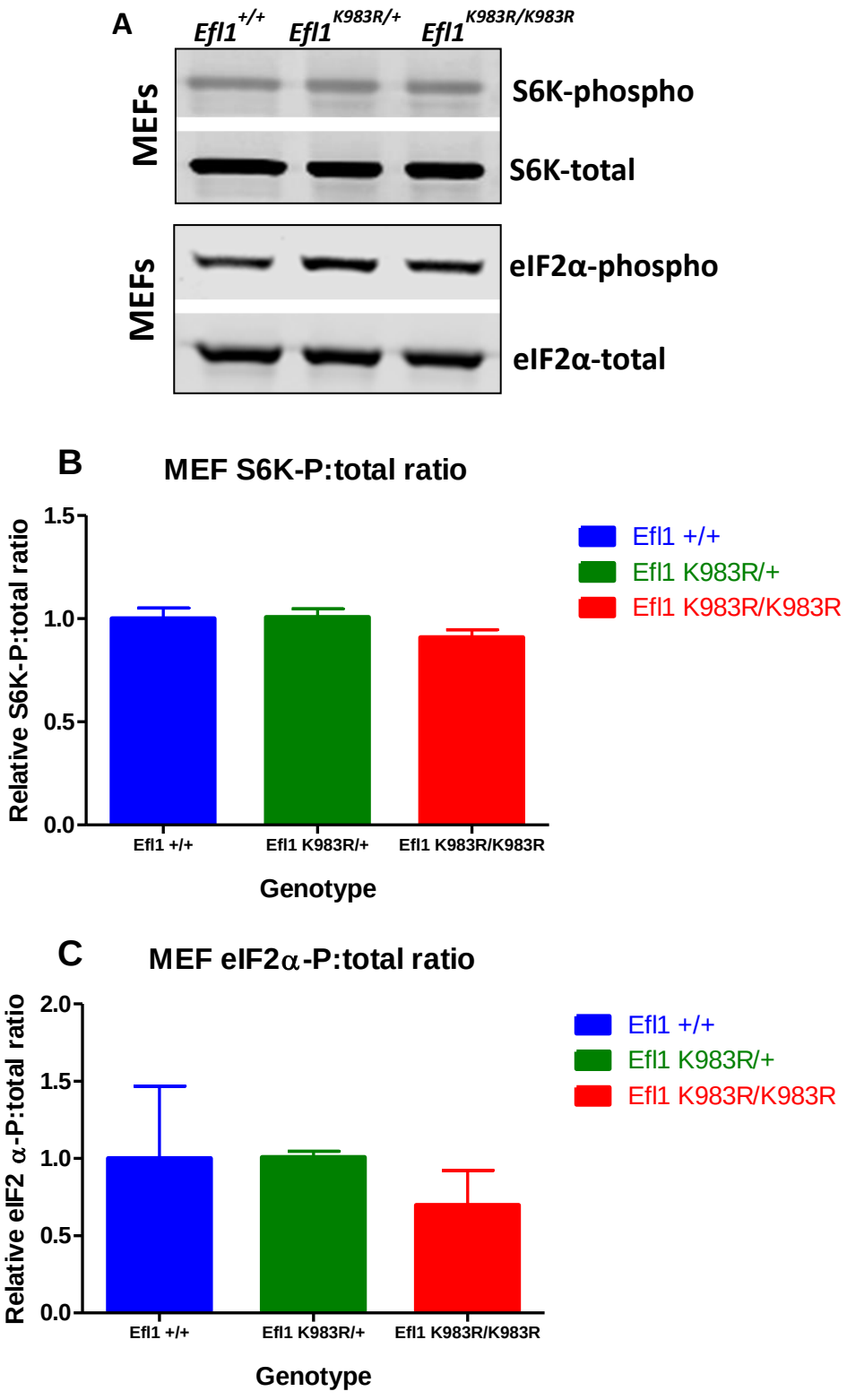


Figure 56 mTOR signalling markers; eIF2α and S6K protein levels. A. Representative blots for S6K and eIF2α, phosphorylated, and total for normalisation. B. eIF2α-phosphorylation ratio. Levels of eIF2α-P were normalised to levels of total eIF2α, to give a ratio of how much of the total eIF2α is phosphorylated in MEFs. There are no significant differences in the phosphorylated levels of eIF2α between genotypes. **C. SK6-phosphorylation ratio.** Levels of S6K-P were normalised to levels of total S6K, to give a ratio of how much of the total RPS6 is phosphorylated in MEFs. There are no significant differences in the phosphorylated levels of S6K between genotypes. Numbers (n) = 3 for all genotypes.

7.1.5. *In vitro* characterisation conclusions

To conclude this section we deduce that there is a dramatic reduction in the amount of EFL1 protein present in the cells and tissues of Efl1K983R/K983R and Efl1K983R/+ mice compared to wildtype. The level of protein reduction seems to be dose-dependent, as Efl1K983R/+ mice have significantly more protein than Efl1K983R/K983R mice, but less than wildtype. The cause of the EFL1 protein deficiency is not clear, however it has been shown in this section that the Efl1 gene is being transcribed normally, and that the transcript is being loaded into the ribosome for translation at the same level as wildtype. This indicates that the mutated transcript is not dissimilar in its translational efficiency, however, the translation of the transcript specifically has not been determined. These data suggest that the deficiency in EFL1 may likely be down to protein stability. It may be that the mutant protein is degraded due to being recognised as faulty by the cells internal degradation pathways, such as the ubiquitin proteasome pathway. At least in silico, the lysine residue at position 983 is not predicted to be ubiquitylated, which would suggest that the mutant protein would not be differentially ubiquitylated compared to the wildtype protein. However, further investigation is required to confirm this.

Two key signalling pathways were investigated in this section: p53 signalling and the mTOR pathway. p53 signalling was investigated because it has been found that SDS patients show overexpression of p53 in the bone marrow (Elghetany and Alter 2002). However, MEFs from *Efl1*-K983R mutants showed no differences in p53 or p21 protein levels. In addition, p21 levels were not different in the bone marrow of *Efl1*$^{K983R/K983R}$ mice compared to wildtype. No significant differences were seen in mTORC1 activity in *Efl1*$^{K983R/K983R}$ MEFs. This was measured indirectly by determining the levels of phosphorylated S6K, and by measuring phosphorylation of eIF2α, a cellular stress indicator that has an inverted relationship with mTORC1 signalling.

There are no differences in the phosphorylated levels of S6K in the *Efl1*$^{K983R/K983R}$ MEFs, nor is the phosphorylation of the cellular stress indicator eIF2α different between genotypes. These data suggest that the mutant cells are not undergoing stress pathways that phosphorylate eIF2α in order to supress translation. This is somewhat surprising considering the almost non-existent EFL1 levels in the *Efl1*$^{K983R/K983R}$ mice, and the crucial role EFL1 plays in ribosomal biogenesis. Also, ribosomal mutants, with excess free ribosomal proteins, have been reported to have increased phosphorylation of eIF2α (Jiménez-Díaz, Remacha et al. 2014). One might assume that translation would be under pressure in these ribosomally challenging conditions, however two pathways related to translation are not affected in the *Efl1*-K983R mutant cells. This may be because translation is already under pressure, and so additional pathways that might reduce translation are not activated by the cell. However, this is unlikely, as eIF2α phosphorylation promotes cap-independent

translation, which in turn results in the upregulation of stress-adaption proteins that may be crucial in rescuing the cell. A more detailed analysis of the ribosomal maturation pathway is required to elucidate the effects of this protein deficiency in the mutant cells, and its effect on translation. In addition, analysis of protein ubiquitination and degradation is required to determine the cause of EFL1 protein deficiency in *Efl1*-K983R mutants.

7.2. Ribosome biogenesis and translation in *Efl1*-K983R mutants

7.2.1. Growth is reduced in *Efl1*$^{K983R/K983R}$ in mouse embryonic fibroblast

Growth assays using MEFs showed that Efl1K983R/K983R cells grew poorly compared to *Efl1*$^{K983R/+}$ and wildtype cells. This difference was significant from day 2, and persisted through to day 15. *Efl1*$^{K983R/K983R}$ MEFs grew to approximately 50% of that of *Efl1*$^{K983R/+}$ and wildtype MEFs (Figure 57). However, we should emphasise here the distinction between growth (an increase in cell mass) and proliferation (an increase in cell number). This assay measured cell number on consecutive days of allowing the cells to grow in optimal conditions. Therefore it is a measure of cell proliferation rate. Slow growth is epitomised by the Minutes Drosophila models, which are a collective of ribosomal protein deficient mutants that are characterised by small size (Thomas 2000). *Minutes* have slow overall growth rates, presumably as a result of a decreased rate of ribosome biogenesis, which may concur with the slow growth rates seen in the *Efl1*$^{K983R/K983R}$ MEFs shown here. The reduced growth phenotype could be expanded to explain many of the growth-deficient phenotypes seen in the *Efl1*-K983R mutant mouse line. For example, the weight differences seen in the mice (Figure 25) suggest a parallel to the small size of SDS patients. SDS patients' small size is put down to failure to thrive due to malabsorption, secondary to a pancreatic enzyme insufficiency. No evidence of a pancreatic phenotype has been found in these mice. It may therefore be a growth problem that causes the weight differences seen in the *Efl1*$^{K983R/K983R}$ mice, as seen in *Minutes*.

In addition, body fat differences are seen from 6 months of age in the *Efl1*$^{K983R/K983R}$ mice (see Figure 27). The *Efl1*$^{K983R/K983R}$ mice stay lean, and have significantly less fat mass than *Efl1*$^{K983R/+}$ and wildtype counterparts. The growth deficits seen in the MEFs may suggest a link to this fat-deficient phenotype, as MEFs are of the mesoderm lineage; the same lineage that generates adipocytes. It is feasible that the deficient growth of *Efl1*$^{K983R/K983R}$ MEFs could reflect poor growth of mesoderm lineages in general, and this may translate to a deficit in fat cell growth. MEFs also share a progenitor lineage with chondrocytes and osteocytes. Therefore, in a similar way to the adipocyte growth, decreased bone mass density in the *Efl1*$^{K983R/K983R}$ mice (see Figure 48) may also be linked to the deficient growth of mesoderm lineages. However, just because one mesoderm lineage show

slow growth, and in vitro at that, it does not mean that all these lineages will be effected. More work is required to determine the cause of the phenotype discussed here.

The cause of the growth deficiency is not clear at this stage. mTORC1 is the major regulator of growth in the cell, but mTORC1 activity does not appear to be effected by the *Efl1*-K983R mutation (see 7.1.4). Alternatively, translation could be hindered in the mutant cells and this could be the cause of the growth defect in MEFs.

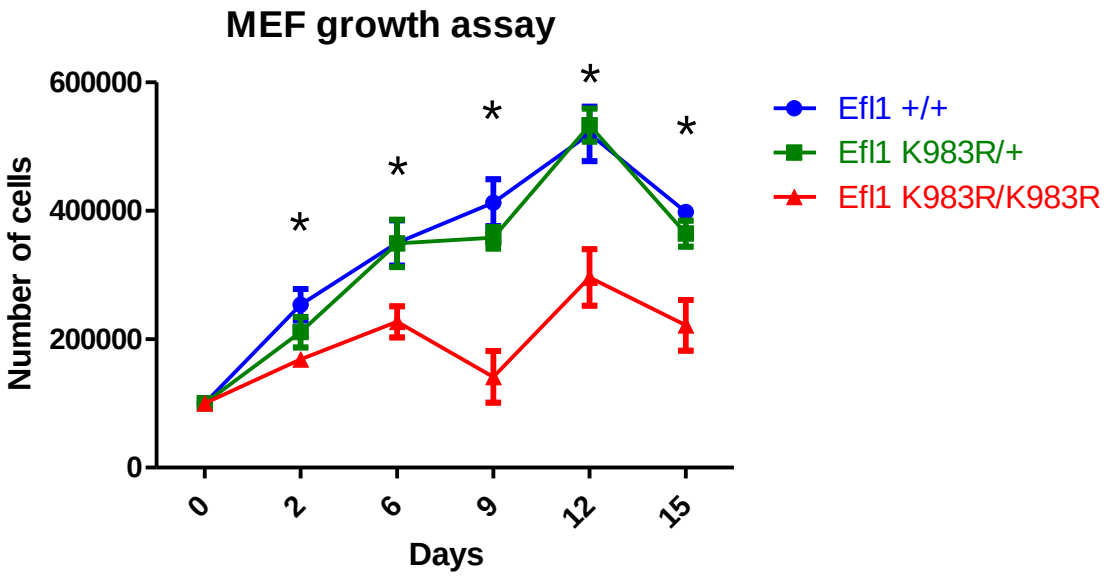


Figure 57 Mouse embryonic fibroblast growth assay. All cells were seeded equally on day 0, at 1x10^5/well. *Efl1*$^{K983R/K983R}$ cells grew significantly less than to *Efl1*$^{K983R/+}$ and wildtype cells on all days tested. P values for *Efl1*$^{K983R/K983R}$ versus wildtype as follows: day 2 p=0.0312, day 6 p= 0.0450, day 9 p=0.007, day 12 p=0.0215, day 15 p= 0.0128. Numbers (n) = 3 for all genotypes.

7.2.2. Mouse embryonic fibroblast polysome profiles indicate defective eIF6 release and subunit joining defect

Polysome profiling is a technique used to visualise the ribosomal subunit content of a cell or tissue lysate. This is carried out by running the lysate on a sucrose density gradient by ultracentrifugation, to separate molecules in the lysate by size. The gradient is then passed through a spectrophotometer, and light absorbance at 254 nm (absorbance of RNA) is measured. This gives a series of peaks, each representing the 40S, 60S, 80S and polysomes sequentially (in order of increasing size). By doing this, it is possible to determine subunit levels, as well as 80S ribosome levels, peak ratios, i.e. 60S:80S ratio and and polysome levels, all fo which are indicators of state of ribosome biogenesis and functionality in the cell. Polysome profiling is a common technique in the field of ribosomopathy research, and has been used to study SDS disease mechanisms. Yeast carrying SDS-associated mutations in *Sdo1* (yeast orthologue of *SBDS*) show an increased 60S:80S

ratio, indicating that there is more 60S subunit present in these cells. These yeast also show impaired eIF6 release, and its retention on the 60S subunit is evident form polysome profiles. Taken together these findings suggest a subunit joining defect in these yeast models, resultant of eIF6 retention on the 60S subunit (Finch, Hilcenko et al. 2011). This has also been shown in SDS patient-derived cells, although the 60S:80S ratio is not always obviously different in the patient-derived cell polysome profiles (Wong, Traynor et al. 2011).

Polysome profiling using MEFs was carried out for the *Efl1*-K983R mouse line. MEFs that were growing at an exponential rate (approximate confluency 70%) were lysed and run on 5-45% sucrose gradients by ultracentrifugation. 40S, 60S, 80S and polysomal peaks were detected by spectrophotometry and sequential 1ml fractions were collected for western blot analysis.

It was found that the 60S:80S peak ratio in *Efl1*$^{K983R/K983R}$ MEF profiles was significantly larger than wildtype. Also, western blot analysis of the fractions for eIF6 showed that more eIF6 is present in the 60S fraction of the *Efl1*$^{K983R/K983R}$ profiles compared to wildtype profiles. *Efl1*$^{K983R/+}$ profiles also showed more eIF6 present in the 60S fractions compared to wildtype, however not as much as in *Efl1*$^{K983R/K983R}$ profiles, suggesting a dose-dependent effect of the *Efl1*-K983R mutation on ribosomal maturation pathway (Figure 58).

These data suggest that there is a subunit joining defect in the *Efl1*$^{K983R/K983R}$ MEFs, where the 60S subunit is not able to join with the 40S subunit to form the 80S ribosome. This is also seen in other models of SDS, such as yeast, *Dictyostelium* and murine *Sbds* conditional knockouts (Finch, Hilcenko et al. 2011, Wong, Traynor et al. 2011, Tourlakis, Zhang et al. 2015). These data also suggest that the joining defect is a result of hindered release of eIF6 from the 60S subunit, demonstrated by the presence of eIF6 in the 60S fraction in the *Efl1*$^{K983R/K983R}$ and *Efl1*$^{K983R/+}$ profiles. This has been previously shown in the liver of conditionally deleted *Sbds* deficient mice and patient-derived cells (Finch, Hilcenko et al. 2011, Wong, Traynor et al. 2011). However, it can not be discounted that eIF6 is accumulating in the 60S fraction for some other reason, and more work is needed to fully determine if eIF6 is not being released from the 60S subunit in the *Efl1*$^{K983R/K983R}$ and *Efl1*$^{K983R/+}$ MEFs, such as an eIF6 release assay.

The profiles were also used to assess other marker proteins in order to analyse the subunit joining pathway. EFL1 was detected in wildtype profiles in the free fractions (1-3), but not in *Efl1*$^{K983R/K983R}$ profiles, while *Efl1*$^{K983R/+}$ profiles showed less EFL1 than wildtype but more than *Efl1*$^{K983R/K983R}$. These findings concur with the MEF western blot results for EFL1 (see 7.1.1). SBDS was also detected in the free fractions, and to a similar degree between genotypes. This concurs with MEF western blot

results showing no significant differences in SBDS levels between genotypes. RPL28 was used as a marker for the 60S subunit, and this protein is present from the 60S fraction onwards in all genotypes, as expected. NMD3, a protein that is released from the 60S subunit after eIF6, was detected in free fractions, as wells as in 60S and 80S fractions in all genotypes. GAPDH was used as a loading control, and was detected in free fractions in all genotypes.

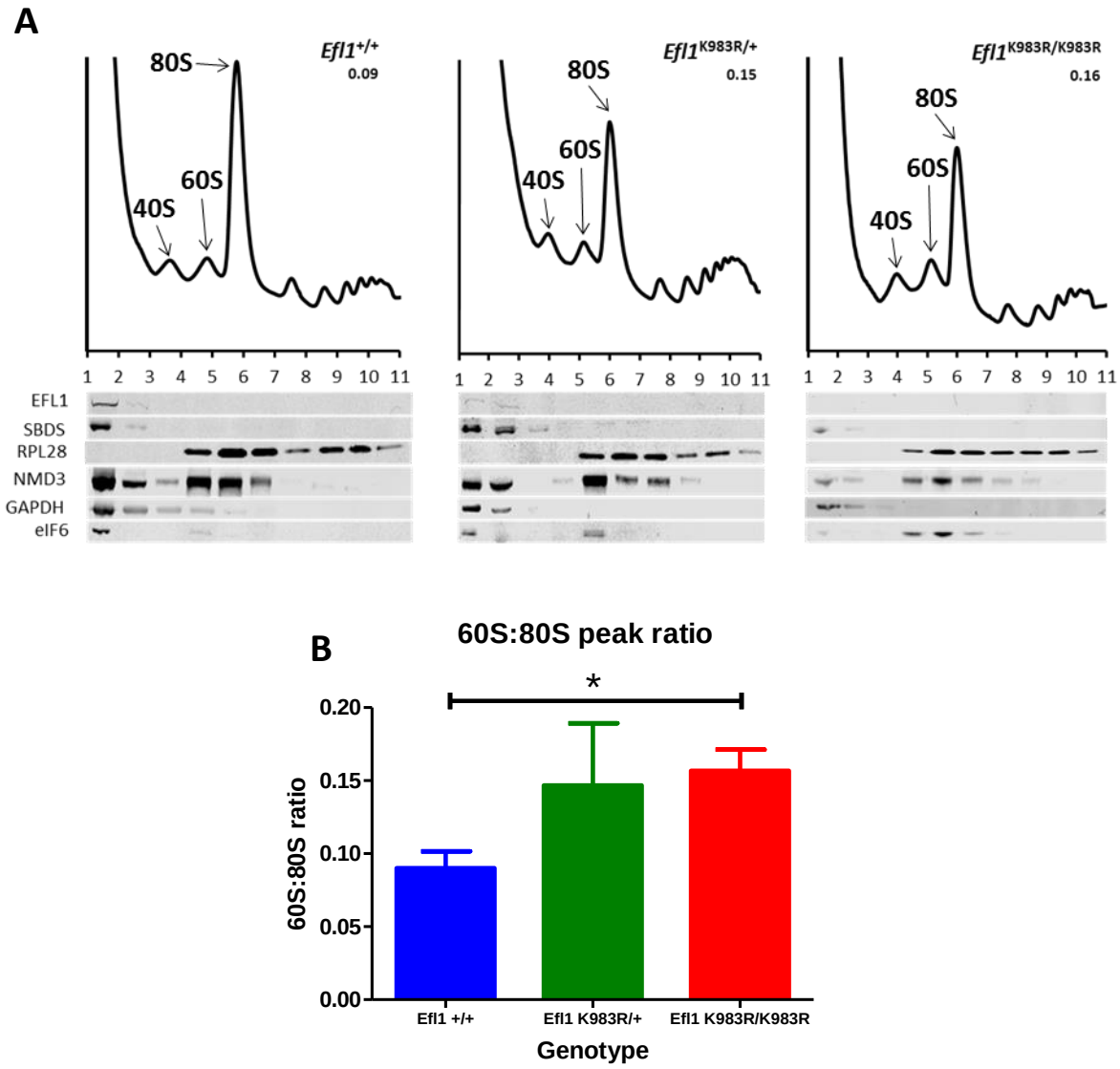


Figure 58 Mouse embryonic fibroblast polysome profiles and western blot analysis. A. Polysome profiles for *Efl1*$^{+/+}$, *Efl1*$^{K983R/+}$ and *Efl1*$^{K983R/K983R}$ MEFs with corresponding blots for EFL1, SBDS, RPL28, NMD3, GAPDH and eIF6. *Efl1*$^{+/+}$ polysome profiles show an average 60S:80S ratio of 0.09, indicating that on average free 60S subunits in wildtype MEFs are 9% that of 80S levels. *Efl1*$^{K983R/+}$ and *Efl1*$^{K983R/K983R}$ polysome profiles show an average 60S:80S ratio of 0.15 and 0.16, respectively, indicating that on average free 60S subunits in *Efl1*$^{K983R/+}$ and *Efl1*$^{K983R/K983R}$ MEFs are 15% and 16% that of 80S levels. There are no differences in protein levels of SBDS, RPL28, NMD3 or GAPDH between genotypes. EFL1 is virtually undetectable in the *Efl1*$^{K983R/K983R}$ polysome profile, and *Efl1*$^{K983R/+}$ profiles show less EFL1 than wildtype. The localisation of EFL1 in wildtype and *Efl1*$^{K983R/+}$ profiles is unchanged. eIF6 is present in all the 60S fractions, however wildtype profiles show only slight presence of eIF6 in the 60S fraction, whereas *Efl1*$^{K983R/+}$ and *Efl1*$^{K983R/K983R}$ profiles show more retention of eIF6 in the 60S fractions. **B. Average 60S:80S ratios in *Efl1*$^{+/+}$, *Efl1*$^{K983R/+}$ and *Efl1*$^{K983R/K983R}$ MEFs.** *Efl1*$^{K983R/K983R}$ MEFs have a significantly higher 60S:80S ratio than wildtype MEFs (p=0.023). Numbers (n) = 3 for all genotypes. Polysome profiles shown are representative of three.

7.2.3. eIF6 accumulates in the cytoplasm in *Efl1*$^{K983R/K983R}$ mouse embryonic fibroblasts

eIF6 shuttles between the nucleus and the cytoplasm, via the 60S subunit. eIF6 is required for export of the 60S subunit into the cytoplasm, where it is released by the actions of EFL1 and SBDS, and is recycled back for another round of export. In yeast models of SDS, eIF6 accumulates in the cytoplasm due to being retained on the 60S subunit. This in turn prevents eIF6 from being recycled to the nucleus, and this leads to a deficiency in 60S subunits. This however is not the case in the mouse. *Sbds*-deleted mouse liver cells do show accumulation of eIF6 in the cytoplasm, and this is due to its retention on the 60S subunit. However, this does not lead to a deficiency in 60S subunit. This suggests that eIF6 is not limiting in the nucleolus in mammals as it is in yeast, and the lack of eIF6 being recycled does not affect export of new 60S subunits into the cytoplasm (Finch, Hilcenko et al. 2011).

Polysome profiling in MEFs indicated that *Efl1*$^{K983R/K983R}$ MEFs have an accumulation of eIF6 on the 60S subunit. We therefore wanted to investigate if there was a cytoplasmic accumulation of eIF6 relative to that in the nucleus, to determine if the *Efl1*-K983R mutation has a similar effect on this pathway as *Sbds* deletion in mice. Cytoplasmic and nuclear extraction from MEFs, followed by western blot analysis revealed that while eIF6 in wildtype MEFs is on average 80% nuclear and 20% cytoplasmic, *Efl1*$^{K983R/K983R}$ eIF6 is more evenly distributed, with an average of 54% nuclear and 45% cytoplasmic (

Figure 59). If the wildtype data represents the norm, and the expected distribution of eIF6 between the nucleus and the cytoplasm, the eIF6 distribution in *Efl1*$^{K983R/K983R}$ MEFs is significantly different to this ($p<0.0001$). This may reflect the retention of eIF6 on the 60S subunit seen in the polysome profiles for *Efl1*$^{K983R/K983R}$ MEFs.

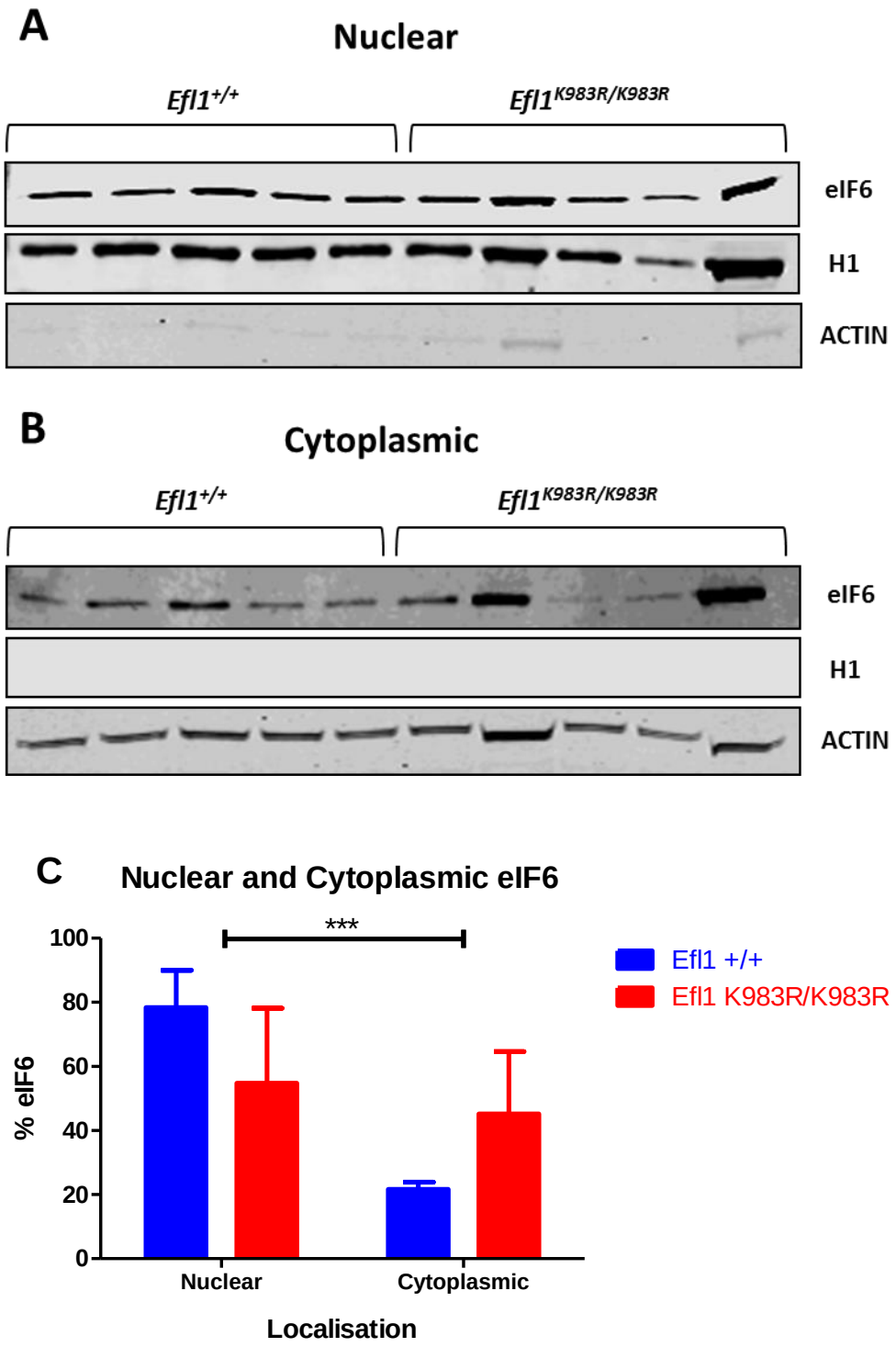


Figure 59 Nuclear and cytoplasmic eIF6 levels in MEFs. A, B. Nuclear and cytoplasmic fraction blots of wildtype and *Efl1*$^{K983R/K983R}$ MEFs. Nuclear and cytoplasmic extraction was performed on wildtype and *Efl1*$^{K983R/K983R}$ MEFs using NE-PER™ Nuclear and Cytoplasmic Extraction Reagents (Thermo Fisher Scientific) and nuclear and cytoplasmic fractions were immunoblotted for eIF6, Histone 1 (H1) (nuclear control) and ACTIN (cytoplasmic control). **C. Percentage representation of the relative levels of eIF6 (normalised to relevant controls).** The relative levels of eIF6 in the nucleus and cytoplasm differ between wildtype and *Efl1*$^{K983R/K983R}$ MEFs, with wildtype eIF6 being 78% nuclear and 22% cytoplasmic, and *Efl1*$^{K983R/K983R}$ eIF6 being 55% nuclear and 45% cytoplasmic. There are no significant differences in the nuclear or cytoplasmic levels of eIF6 between genotypes, however, the difference in eIF6 localisation in *Efl1*$^{K983R/K983R}$ MEFs is significantly different from the expected values (wildtype levels) (Chi^2-test, $p<0.0001$). Numbers (n) = 5 for all genotypes.

7.2.4. Liver polysome profiles show mislocalisation of eIF6 in the cytoplasm

To investigate whether the subunit joining defect seen in MEF polysome profiles was also present in adult tissues, polysome profiling using liver tissue was carried out for the *Efl1*-K983R mouse line. Tissue lysates were run on 10-50% sucrose gradients by ultracentrifugation. 40S, 60S, 80S and polysomal peaks were detected by spectrophotometry and sequential 1ml fractions were collected for western blot and qPCR analysis. It was not possible to calculate the 60S:80S peak ratio for liver polysome profiles, as the peaks were merged together. This may have occurred due to an overload of ribosomal content in the liver samples, as liver is known to have high levels ribosomes compared to other tissues.

Western blot analysis of the fractions showed that eIF6 is more densely accumulated in the 60S subunit fraction of the *Efl1*$^{K983R/K983R}$ profile compared to *Efl1*$^{K983R/+}$ and wildtype profiles. Wildtype profiles show a more spread-out distribution of the eIF6 bands around the 60S subunit fraction compared to *Efl1*$^{K983R/K983R}$ profiles, with *Efl1*$^{K983R/+}$ profiles showing an intermediate degree of eIF6 spread. This may indicate a general accumulation of eIF6 in the cytoplasm in *Efl1*$^{K983R/+}$ and wildtype livers, but also may indicate that eIF6 is being released from the 60S subunit as the bands are not solely detected in one fraction in these genotypes. The denser band in the 60S fraction of the *Efl1*$^{K983R/K983R}$ profile may suggest retention of eIF6 on the 60S subunit in these livers. Further investigation into the distribution of eIF6 in the liver would be beneficial in determining a clearer representation of eIF6 release in this tissue.

Other marker proteins were used to analyse the subunit joining pathway. There are no differences in protein levels of SBDS, RPS6 or GAPDH between genotypes. The localisation of RPL28 is unchanged between genotypes, however there is more RPL28 protein present in *Efl1*$^{K983R/K983R}$ profiles compared to *Efl1*$^{K983R/+}$ and wildtype profiles. This may indicate an increased presence of 60S subunits in *Efl1*$^{K983R/K983R}$ livers compared to *Efl1*$^{K983R/+}$ and wildtype. However, it was not possible to determine 60S:80S ratio in the liver profiles. Liver tissue is renowned for having a high ribosome content, and it may be that this tissue is not ideal for polysome profiling due to an overloaded sample causing the peaks to merge. It would therefore be useful to conduct polysome profiling other tissues to determine if there is a global subunit joining defect in these mice. However, trials of polysome profiling with pancreas and brain were unsuccessful, and more work is required to refine the methods involved for these particular tissues.

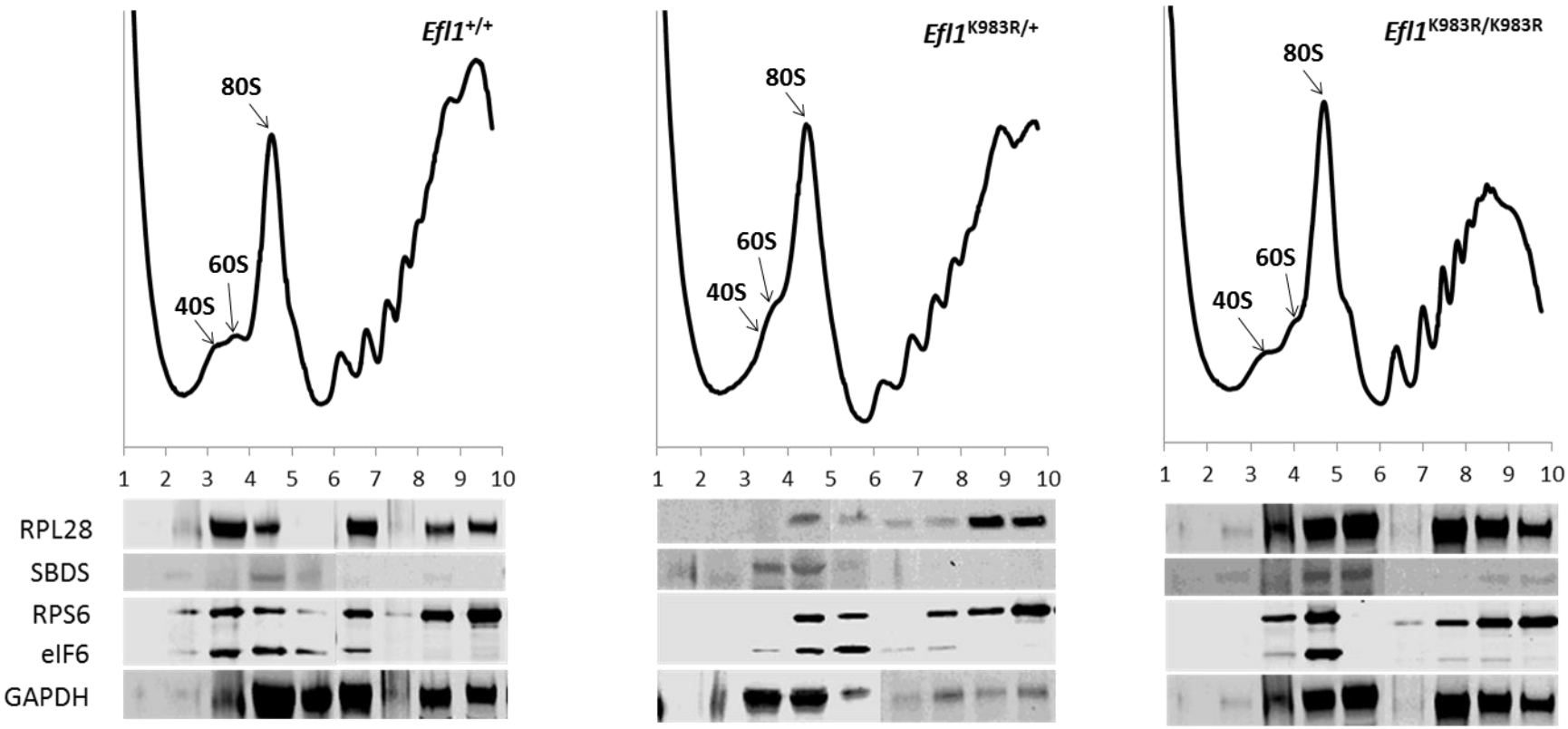


Figure 60 Liver Polysome Profiles and Western Blot Analysis. *Efl1*$^{+/+}$ polysome profiles show a merged 40S and 60S peak (3-4) followed by a large 80S peak (4-5) and high polysomal peaks (6-9). *Efl1*$^{K983R/+}$ and *Efl1*$^{K983R/K983R}$ polysome profiles show a similar pattern of peaks. The main difference in the polysome profiles between genotypes is the size of the polysomal peaks. *Efl1*$^{+/+}$ polysome profiles show polysomal peaks greater than the 80S peaks, indicating a high level of translation occurring in the wildtype liver. *Efl1*$^{K983R/+}$ polysome profiles show polysomal peaks equal to the height of the 80S peak, again indicating a high level of translation, although perhaps not as much as in wildtype livers. *Efl1*$^{K983R/K983R}$ polysome profiles show polysomal peaks less than the height of the 80S peak, indicating that the level of translation is lower in *Efl1*$^{K983R/K983R}$ livers than in wildtype, and possible heterozygote, livers. There are no differences in protein levels of SBDS, RPS6 or GAPDH between genotypes. The localisation of RPL28 is unchanged between genotypes, however there is much more present in wildtype profiles compared to *Efl1*$^{K983R/+}$ and *Efl1*$^{K983R/K983R}$ profiles. eIF6 is present in all the 60S fractions, however wildtype profiles show a more densely accumulated band at the 60S subunit compared to *Efl1*$^{K983R/+}$ and *Efl1*$^{K983R/K983R}$ profiles. Livers form 6 month old male mice (n=3). Profiles shown are representative of three per genotype.

7.2.5. Translation is unaffected by the *Efl1*-K983R mutation in MEFs

Translation can only occur when the 40S and 60S subunits join to form the 80S ribosome. Therefore, if there is a defect in the release of eIF6 from the 60S subunit, this is likely to affect 80S formation. In addition to this, cellular models have shown that deficiency of SBDS results in reduced glibal translation (Ball, Zhang et al. 2009). As is indicated in the western blot analysis of polysome profile fractions, *Efl1*$^{K983R/K983R}$ MEFs have more eIF6 bound to the 60S subunits than wildtype MEFs. This along with the difference in 60S:80S ratio between *Efl1*$^{K983R/K983R}$ and wildtype MEFs suggests that a joining defect is present. Therefore, we investigated translation in *Efl1*$^{K983R/K983R}$ MEFs compared to wildtype.

Two methods of measuring translation were employed. Firstly, radioactive S^{35}-methionine assays were carried out in MEFs, to measure the level of methionine incorporation in these cells. Methionine is the first amino acid in any mammalian protein, as the Met-tRNA recognises the AUG start codon, and therefore methionine incorporation is a direct measure of protein synthesis. No significant differences were detected in the levels of methionine incorporation between *Efl1*$^{K983R/K983R}$ and wildtype MEFs. To add a challenge to the assay, MEFs were treated with a range of concentrations of cycloheximide. Cycloheximide is a compound that inhibits translation elongation by blocking translocation of the amino-acyl tRNAs (AA-tRNAs) from the A-P sites to the E-P sites. By exerting this challenge on the translational apparatus, we aimed to tease out any defects in the *Efl1*-K983R mutant MEFs that may have been undetectable under basal conditions. However, no significant differences in translation were detected, at any of the tested cycloheximide concentrations, between *Efl1*$^{K983R/K983R}$ and wildtype MEFs (Figure 61).

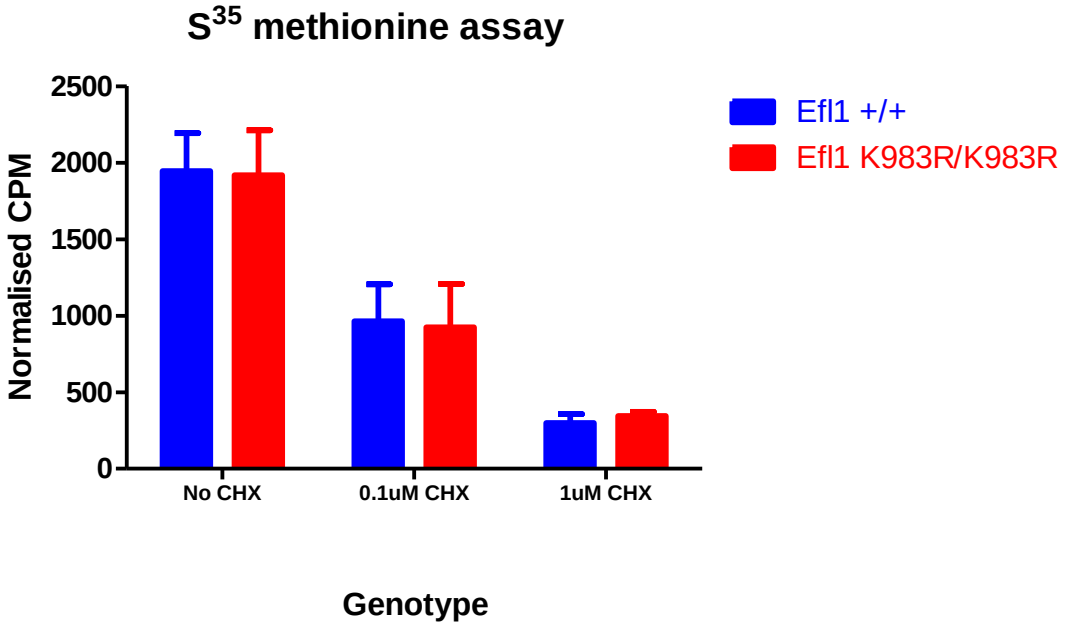


Figure 61 S^{35}-Methionine incorporation assay in MEFs. S^{35}-Methionine incorporation was measured in *Efl1*$^{K983R/K983R}$ and wildtype MEFs with varying concentrations of cycloheximide (CHX). Counts per minute (CPM) were normalised to background CPM, which were obtained by a maximal CHX dose (50 µM) that reduced translation to a minimum without killing the cells. No significant differences were detected in CPM between *Efl1*$^{K983R/K983R}$ and wildtype MEFs under basal conditions, with no CHX. No significant differences were detected in CPM between *Efl1*$^{K983R/K983R}$ and wildtype MEFs at either 0.1 µM or 1 µM CHX treatments. Numbers (n) = 3 for all genotypes.

Secondly, we carried out a non-radioactive translation assay – SUrface SEnsing of Translation (SUnSET). SUnSET uses the antibiotic and structural analogue of amino-acyl-tRNAs (AA-tRNA), puromycin. Because of its structural similarities to AA-tRNAs (specifically, Tyrl-tRNA), puromycin can be incorporated into peptide chains during translation. However, whereas aminoacyl-tRNAs contain a hydrolysable ester bond between their tRNA ribose moiety and the attached amino acid molecule, puromycin has a non-hydrolysable amide bond in the equivalent position. This prevents a new peptide bond being formed with the next AA-tRNA, and therefore stalls translation elongation. Truncated proteins tagged with puromycin are thus released from the stalled ribosome, and these can be detected using an antibody that binds to puromycin. Western blot analysis of cell lysates using an anti-puromycin antibody can, in this way, give an indirect measure of protein synthesis. No significant differences in puromycin incorporation were detected between *Efl1*$^{K983R/K983R}$, *Efl1*$^{k983R/+}$ and wildtype MEFs (Figure 62).

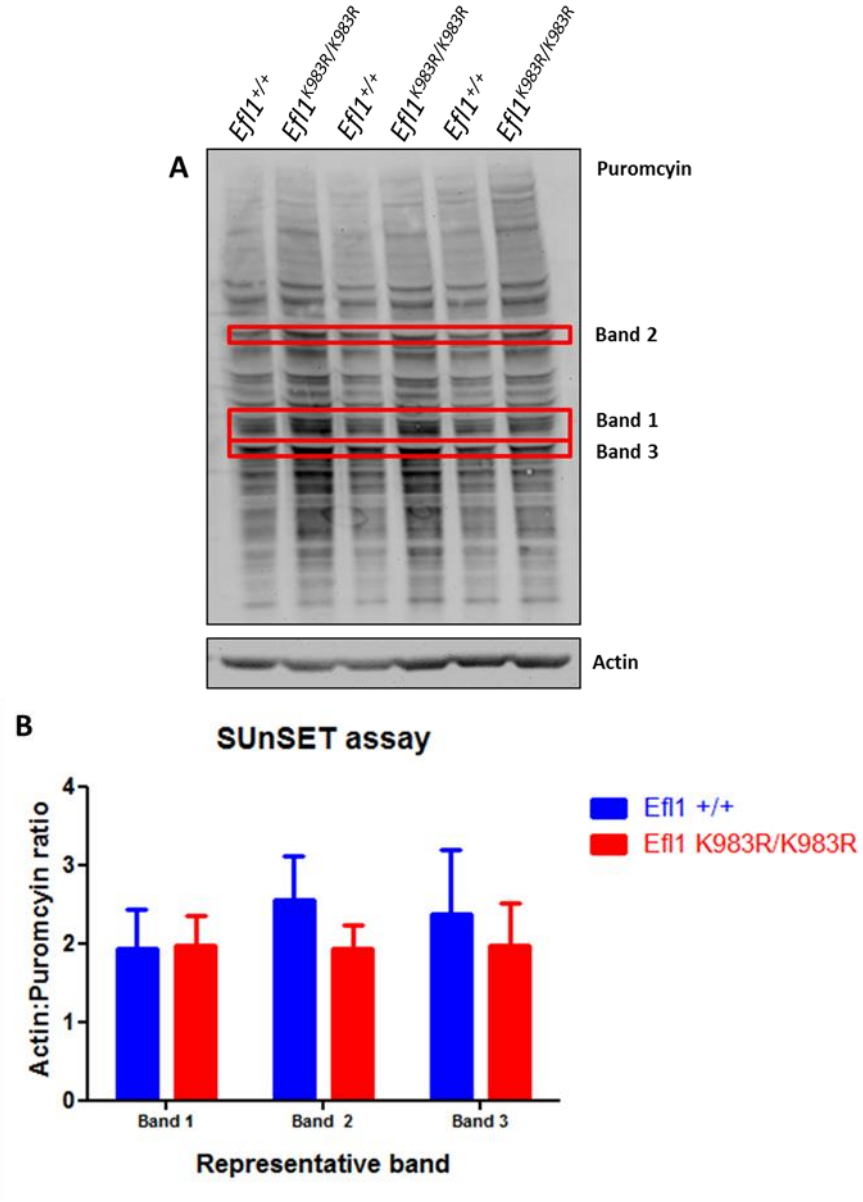


Figure 62 SUnSET translation assay with MEFs. A. Example western blot analysis of puromycin tagged proteins in MEFs using 12D10 antibody, and chosen representative bands. SUnSET is a non-radioactive translation assay that utilises the antibiotic puromycin, and an antibody specific to puromycin, 12D10. Western blot analysis detects multiple bands, all of which represent proteins that are tagged with puromycin. Three bands were selected to be representative of translation as a whole. **B. Puromycin levels in representative bands normalised to actin.** Puromycin levels were normalised to actin levels for each sample and the ratios were compared. There are no significant differences between *Efl1*$^{K983R/K983R}$ MEF puromycin incorporation compared to wildtype, in any of the chosen representative bands. Number (n) = 3 for each genotype.

7.2.6. Ribosome biogenesis conclusions

In this section we show that *Efl1*$^{K983R/K983R}$ mice, and to a lesser extent *Efl1*$^{K983R/+}$ mice, display disturbances in their ribosomal maturation pathways. MEFs show a significantly altered 60S:80S ratio in polysome profiles, indicating that more 60S subunit is present in the *Efl1*$^{K983R/K983R}$ cells than in wildtype. A possible explanation for this is that the 60S subunits are not joining with the 40S subunits to form the 80S ribosome, and so are accumulating in the cytoplasm. Increased retention of eIF6 on the 60S subunit was detected by immunblot, suggesting that the reason for the joining defect is that eIF6 is not being released. eIF6 was also shown to accumulate in the cytoplasm to a greater extent in *Efl1*$^{K983R/K983R}$ MEFs than in wildtype, again giving weight to the theory that eIF6 is being retained on the 60S subunit. This mechanism has previously been described in yeast models of SDS that have disease-associated *Sdo1* mutations, and the *Efl1*-K983R MEFs show a similar phenotype here, linking the *Efl1* mutation with an SDS-like phenotype. However, as mentioned above, an eIF6 release assay is needed in these MEFs to unequivocally determine if eIF6 is being retained on the 60S subunit.

However, although there is a joining defect apparent in the MEFs, general translation seems unaffected. Global translation has been shown to be reduced in *SBDS*-deficient cells, in which ribosomal subunit joining defects are also seen (Ball, Zhang et al. 2009, Zhang 2009). For this reason it might be expected that cells harbouring *Efl1*-K983R mutations would also display translational deficits. At least in the context tested here, it seems that this is not the case for the *Efl1*-K983R mutants. It may be that fibroblasts are not the best model for investigating translation, and that other tissues or cell types may exhibit a detectable difference in translational capacity. However, *Sbds*-deficient MEFs have been used previously to show decreased translation (Zhang 2009). It is of course possible however that these mice do not have general translational deficits of any kind, and that *Efl1* mutations result in a unique phenotype that is unrelated to *SBDS* deficiency in terms of translation.

Lastly, we investigated the ribosomal maturation pathway in liver. Polysome profiles of liver tissue were unable to resolve the individual peaks for 40S, 60S and 80S ribosomes, and so the ratio of peaks was not attainable. Immunoblots were carried out however which did show a difference in eIF6 distribution between genotypes. eIF6 was more densely accumulated in the 60S fraction of the *Efl1*$^{K983R/K983R}$ profile than in the wildtype, with the *Efl1*$^{K983R/+}$ profile being an intermediate between the two. The more spread out appearance of the eIF6 immunoblot bands could be an indicator of eIF6 release in the wildtype and *Efl1*$^{K983R/+}$ profiles. Increased RPL28 was also detected in the *Efl1*$^{K983R/K983R}$ liver profiles, which may suggest an increase in 60S subunits. This may suggest an attempt by the cells of the liver to overcome the 60S-related obstacle of eIF6 retention by producing

more subunit. Therefore, whilst not as clear-cut as the MEF profiles, these liver profiles do show differences in the ribosomal maturation pathway in the *Efl1*$^{K983R/K983R}$ profiles. One of the differences between the liver profiles was the levels of polysome peaks between genotypes. *Efl1*$^{K983R/K983R}$ profiles showed lower levels of heavy polysome peaks (on the right of the profiles) than wildtype profiles, which may indicate a reduction in multiple ribosomes on a single mRNA. This may in turn reflect differences in translation in the *Efl1*$^{K983R/K983R}$ liver compared to wildtype. This does not concur with the translation assays carried out in MEFs, nor is this effect seen in the MEF profiles, thus showing that further investigation of translation in different tissues is required.

Overall, the MEFs and adult tissue tested in the polysome profiles show a similar phenotype to that of *Sbds*-depleted cells and tissues, in that eIF6 distribution is differentially effected by the *Efl1*-K983R mutation and that subunit levels may be affected. These findings indicate that the disease pathway underlying the phenotypes seen in these mice may be the same as in SDS. However, no translation defects were detected in the *Efl1*$^{K983R/K983R}$ MEFs, which is unexpected considering that *Sbds*-deficient cells do show reduced translation. These results indicate that further investigation into *in vivo* translation in different tissues is required.

Chapter 8
Discussion

8. Discussion

8.1. The relevance of *Efl1*$^{K983R/K983R}$ for EFL1 function

The only Mouse Genome Informatics registered phenotype associated with *Efl1* is Glioma (Saito, Iizuka et al. 2014), and thus all the phenotypes presented here in this thesis are novel and previously not described in the literature. It should be duly noted here that there are no known *EFL1* mutations in humans, nor are there any *Efl1* deficient mouse models in the literature. Thus the *Efl1*-K983R mouse line represents an opportunity to study the function of EFL1 in a mammalian system. While EFL1's role in ribosomal maturation has become more and more clear over the past decade, phenotypes associated with its loss have not been studied in great detail. Here we establish a mammalian model of *Efl1* deficiency-induced cytopenia, small stature, bone mass reduction, and behavioural abnormalities, revealing a novel role for EFL1 in these areas.

The *Efl1*$^{K983R/K983R}$ mice were originally discovered due to an abnormal gait that resembled a flat, 'swimming'-like motion. This motor abnormality is a unique addition to phenotypes associated with *Efl1* and defective subunit joining. No SDS models have before been reported to have motor defects, or any other neurological abnormality. However, there are reports of neurological issues in SDS patients. It has been reported that children with SDS are delayed in various developmental milestones, including motor and speech development. Examples include not sitting by 9 months, not walking by 18 months, and not saying a single word before 18 months (Kerr, Ellis et al. 2010, Perobelli, Nicolis et al. 2012). Persistent hypotonia and ataxia has been reported in children with SDS, including ataxic diplegia and truncal ataxia (Aggett, Cavanagh et al. 1980). Both of these types of ataxia could explain the flat gait seen in the *Efl1*$^{K983R/K983R}$ mice, as it is unclear from gait analysis in SHIRPA whether it is the limbs or trunk that cause the low body position. No trunk curls were detected in SHIRPA assessments however, nor were any differences seen in body tone or limb tone. Alternatively, this motor abnormality may be unique to *Efl1* mutation, and is not representative of SDS in any way. Although rare, ataxic conditions in SDS patients have not been extensively addressed in SDS research. This mouse model may be a first to represent these conditions, and provide an opportunity in which to study them, alongside other SDS traits such as the subunit joining defect.

Balance issues were also observed in *Efl1*$^{K983R/K983R}$ mice, with head tilts presenting from ~3 months of age. This may have been caused by unilateral OM in these mice. However, swim tests were conducted in order to identify any balance issues or vestibular defects. Swim tests revealed extreme balance issues, as *Efl1*$^{K983R/K983R}$ mice tumbled immediately upon contact with water. This suggests a vestibular defect in these mice, and may in fact contribute to the abnormal gait. No vestibular

defects have been reported in SDS patients, nor have any vestibular phenotypes been associated with *Efl1* previously. This is therefore a novel function that may be attributed to *Efl1* deficiency.

Western blot analysis revealed a dramatic reduction in EFL1 protein levels in both *Efl1*$^{K983R/K983R}$ and *Efl1*$^{K983R/+}$ mice. *Efl1*$^{K983R/K983R}$ mice show 3-17% of the EFL1 protein levels of wildtype, depending on the tissue (MEFs 3.8%, pancreas 7.6%, brain 10% and liver 17%), and *Efl1*$^{K983R/+}$ mice show 24-57% (pancreas 24%, MEFs 33%, brain 45% and liver 57%). It is unclear why different tissue types would harbour different levels of EFL1, however differences in metabolism or the activity of protein clearing pathways could account for the variation. With such dramatic reductions in protein levels, it might be expected that ribosomal maturation would be under extreme pressure. In SDS, SBDS deficiency results in a ribosomal subunit joining defect and reduced translation (Ball, Zhang et al. 2009, Wong, Traynor et al. 2011), the former of which is also seen in the *Efl1*$^{K983R/K983R}$ mice. In SDS, this was thought to be a consequence of no functional protein being present in patient tissues as a result of the truncating and frameshift mutations common to the disease. However, it is now thought there is a small amount of functional protein present in SDS patient cells due to alternative splicing, namely in patients with the 258+2T>C mutation. This suggests that complete loss of SBDS is not necessary for the manifestation of SDS symptoms, and residual amount of protein may allow cells to 'get by' (Minelli, Maserati et al. 2009). This concurs with the findings in this thesis, where the *Efl1*$^{K983R/K983R}$ mice display various phenotypes akin to SDS, but can carry up to 17% of the EFL1 protein levels of wildtype. It is possible that more protein could be present in other tissues.

While residual levels of EFL1 protein are present in various tissues in the *Efl1*$^{K983R/K983R}$ and *Efl1*$^{K983R/+}$ mice, the functionality of the protein is not known. It may be that the levels of protein present are non-functional, and therefore do represent a complete loss of EFL1 in the homozygous mice. qPCR showed that *Efl1* transcription is not affected by the mutation, and therefore the difference in protein levels are likely to be due to either translational defects or instability of the protein. While general translation is unaffected, it may be that certain transcripts are differentially translated in *Efl1*$^{K983R/K983R}$ mice. Cellular stressors of various types are known to inhibit translation of the majority of mRNAs, allowing preferential translation of stress adaption mRNAs. Inhibition of the translation of ribosomal protein genes is often used as a mechanism of preventing unnecessary translation in times of stress (Flick and Kaiser 2012). Therefore, it is plausible that *Efl1* translation would be suppressed due to the ribosomal stress that the cells harbouring the *Efl1*-K983R mutation are experiencing. Alternatively, the mutation could construe instability upon the protein, leading to its degradation. Proteolysis by the proteasome plays an important role in stress response pathways. One important function is the removal of damaged proteins to avoid accumulation as potentially

harmful aggregates and to eliminate proteins with compromised activity. If the *Efl1*-K983R mutation does affect the degradation of the protein, this may explain the differences in levels of protein in different tissues. Cellular stressors are diverse, as are the responses they elicit. This is particularly true for higher eukaryotes where various tissues and cell types are differentially affected by the same insult. The type and extent of the stress response can therefore differ greatly among cell types, and may result in differential levels of degradation of the same protein (Kim, Jang et al. 2006). In order to fully elucidate the pathogenic mechanisms of the *Efl1*-K983R mutation, the stability of the protein should be investigated further, using degradation and ubiquitination assays. Autophagy could also play a role in the degradation of the EFL1 protein, although mTORC1 activity does not appear to be changed in *Efl1*$^{K983R/K983R}$ MEFs. This however does not rule out autophagic degradation of this specific protein, and this should also be investigated in the future.

The molecular mechanism resulting from the *Efl1*-K983R mutation was elucidated through polysome profiling. Polysome profiles of homozygous and heterozygous MEFs showed retention of the anti-association factor eIF6 on the 60S subunit, indicating that its release was impaired in these cells. MEF profiles also showed an increase in the amount of 60S subunit present in the cells in relation to the amount of 80S ribosomes. This suggests that a joining defect is taking place, in which the 60S subunit cannot join with the 40S subunit to form the 80S ribosome. These data confirm the role of EFL1 in the ribosomal maturation pathway and more specifically in the release of eIF6 as a prerequisite for subunit joining (Finch, Hilcenko et al. 2011).

Polysome profiling was also conducted in liver, and increased presence of eIF6 was detected in the 60S fractions. However, it was not possible to determine a 60S:80S ratio due to a merging of the peaks in the profile. Other tissues were also attempted for polysome profiling, including pancreas and brain. However, polysome profiling is an extremely intricate procedure, and it can differ greatly for each individual tissue. While cells are reasonably straight forward to profile, tissues are very difficult. This is due to increased complexity of an organ, and the presence of many different cell types, as well as other factors such as fat and blood within the tissues. Different buffers are required for different tissues, as different lysing agents and ionic concentrations may be required for individual organs. For this reason, only liver and MEFs were successfully profiled, and the liver profiles could be improved in the future. It would be beneficial to achieve polysome profiling of more tissues from the *Efl1*$^{K983R/K983R}$ mice in future, as this would enable the detection of the subunit joining defect in different systems. The multi-organ nature of the *Efl1*$^{K983R/K983R}$ mice is one of the major benefits of this model for research into SDS (discussed in further detail below).

8.2. The relevance of *Efl1*$^{K983R/K983R}$ for SDS

SDS is caused by biallelic loss of function of *SBDS* in 90% of patients. It should be noted that no SDS patients have been found to have *EFL1* mutations, nor have any *EFL1* mutations been detected in any human condition. SDS is a rare disease that is difficult to study in human patients due to small sample size and wide heterogeneity in genetic aetiology and clinical manifestations. It is therefore essential to generate accurate and clinically relevant animal models in order to study the disease processes involved in SDS. Current models focus on conditional knockouts, to circumvent the embryonic lethality of *Sbds* knockout (Finch, Hilcenko et al. 2011, Tourlakis, Zhang et al. 2015, Zambetti, Bindels et al. 2015). These models do not reflect the multi-system nature of SDS, in which multiple organs are affected by the SBDS deficiency that is consequent of biallelic loss of function. Embryonic models have also been established, and provide a global representation of the effects of SBDS deficiency during development (Zhang, Shi et al. 2006). However, SDS is a disease in which many symptoms onset after birth, and which has many temporal aspects associated. For example, the exocrine pancreatic insufficiency seen in children with SDS ameliorates with age, and many patients are independent of pancreatic enzyme supplementation by adulthood. Cytopenias can also abate, with spontaneous remission of cytopenia seen in some patients (Audrey Anna Bolyard 2002). These embryonic models therefore do not reflect the adult aspects of SDS, nor the progression of the disease.

As mentioned in 1.3.4, EFL1 is critical for the release of eIF6 from the 60S subunit during ribosomal maturation. Its function is inextricably linked with that of SBDS, and so it may not be surprising that EFL1 deficiency results in similar outcomes, phenotypically, to that of SBDS loss. Several findings in this study point towards *Efl1*$^{K983R/K983R}$ mice being a model for SDS. Firstly, small stature from a young age, but not from birth, suggests a parallel with SDS patients, who are below the lower third percentile for height but have normal birth weights (Burroughs, Woolfrey et al. 2009). In SDS, this short stature is due to a failure to thrive in infancy, which in turn is down to a pancreatic enzyme insufficiency and consequent malabsorption of nutrients. Low serum levels of α-amylase and trypsinogen are commonly used as diagnostic markers for pancreatic enzyme insufficiency in SDS patients, however normal serum levels of these enzymes does not rule out an SDS diagnosis (Tourlakis, Zhang et al. 2015). While pancreatic enzyme levels have not been determined for the *Efl1*$^{K983R/K983R}$ mice, this may be the cause of the small size and also the lean phenotype seen, as fat malabsorption is a consequence of digestive enzyme insufficiency.

Secondly, significantly lower bone mass density (BMD) was seen in *Efl1*$^{K983R/K983R}$ mice from 3 months of age, and persisted throughout life (up to 12 months of age in females). SDS patients often display

decreased BMD and an increased risk of fragility fractures. They are also prone to developing low - turn over bone disorders such as osteoporosis and/or osteopenia (Toiviainen-Salo, Mäyränpää et al. 2007). While *Efl1*$^{K983R/K983R}$ mice showed low BMD at all ages tested, *Efl1*$^{K983R/+}$ mice also showed a BMD reduction at 3 months of age. However this normalised at 6 and 12 months of age, suggesting that at early stages heterozygous mice may have low bone mass density. However, as the mice grow in size their BMD normalises. This may be because BMD is a factor of both bone area and bone mineral concentration (BMC), with low bone area artificially lowering BMD. This could also be a confounding factor in the *Efl1*$^{K983R/K983R}$ mice, as they are small in size, and this persists throughout life. However, BMC is also significantly lower in *Efl1*$^{K983R/K983R}$ mice throughout life, which is not affected by the bone area. *Efl1*$^{K983R/+}$ mice do not have significantly different BMC. This suggests that *Efl1*$^{K983R/K983R}$ mice do suffer from true low BMD and BMC, which may be reflective of the low BMD seen in SDS patients, as well as bone-related symptoms such as osteopenia.

Neutropenia is reported to be the principle haematological manifestation of SDS. However, other haematological cytopenias are also reported, including macrocytic anaemia and thrombocytopenia (Burroughs, Woolfrey et al. 2009). A third parallel of the *Efl1*$^{K983R/K983R}$ mice and SDS arises in this area, with homozygous, and in some cases heterozygous, mice showing abnormalities in red blood cell, platelet and white blood cell populations. *Efl1*$^{K983R/K983R}$ and *Efl1*$^{K983R/+}$ mice display reduced red blood cell counts (males only), and greater cell width is seen in the *Efl1*$^{K983R/K983R}$ mice. Decreased haemoglobin concentration in the red cells is also detected in *Efl1*$^{K983R/K983R}$ mice. These are features of macrocytic anaemia, in which red cells are reduced in number, become enlarged and are unable to efficiently load haemoglobin. Although macrocytic anaemia is more common in DBA, it has been reported in SDS. The reason for the sexual dimorphism seen in this phenotype (only males have lower red blood cell count) is unclear. However intermittent anaemia in SDS is not uncommon. For example, ~one third of patients have chronic neutropenia, while the other two thirds have intermittent episodes (Burroughs, Woolfrey et al. 2009). This may contribute to variation within data sets when analysing haematology in cohorts of mice at set time points. *Efl1*$^{K983R/K983R}$ mice also display reduced platelet counts and platelet size, both males and females, which may reflect the rare reports of thrombocytopenia in SDS patients (Burroughs, Woolfrey et al. 2009).

While neutropenia is not present in *Efl1*$^{K983R/K983R}$ mice specifically, the white blood cell count as a whole is significantly lower in these mice than wildtype and heterozygous counterparts. While individual subpopulations do show differences between genotypes, neutrophils are not significantly different in either males or females. One cell population that is affected, in both males and females, is eosinophils, with homozygous mice having significantly fewer eosinophils than wildtype

littermates. Heterozygotes in this category show sexual dimorphism however, with female *Efl1*$^{K983R/+}$ mice displaying significantly lower cell counts compared to wildtype, but male *Efl1*$^{K983R/+}$ mice showing comparable levels to wildtype. Further differences in white blood cell sub populations include significantly reduced monocyte levels in male *Efl1*$^{K983R/K983R}$ mice, and significantly elevated lymphocyte and basophil levels in female *Efl1*$^{K983R/K983R}$ mice, compared to wildtype.

While this white blood cell phenotype is not specifically indicative of SDS, these data confirm haematological abnormalities within the white blood cells in mice harbouring the *Efl1*-K983R mutation, either in heterozygous or homozygous form. Mice were tested at a young age (4-6 weeks) for haematological variations because it is known that some SDS patients achieve a durable remission of neutropenia within 3 years of their initial diagnosis (Audrey Anna Bolyard 2002). Although testing was conducted at a young age, it is possible that some of the mice used in this data analysis were either in remission, or in an intermittent phase of cytopenia. It is therefore difficult to unquestionably state the presence or absence of cytopenia in individuals from this study.

Cytopenia is one of the key focuses of SDS research, however studies have been limited to *in vitro* cell work due to the lack of a mammalian model. A *Sbds* null zebrafish has been generated using CRISPR/Cas9 technology that survives up to 6 weeks, unlike *Sbds* null mice which die embryonically. This zebrafish model does display neutropenia, as well as growth retardation and liver atrophy. While this may represent a model in which to study neutropenia, mammalian models would likely be more translational to the human condition. While neutropenia is not present in the *Efl1*$^{K983R/K983R}$ mice, the white blood cells are affected, as are the red blood cells and the platelets. It is important to remember that while neutropenia is the most common form of cytopenia in SDS patients, it is not the only one, with macrocytic anaemia and thrombocytopenia also occurring in a great number of patients. For this reason it may be beneficial to study a mouse model with multi-lineage cytopenias such as the *Efl1*$^{K983R/K983R}$ mice.

A possible consequence of the white blood cell cytopenia seen in *Efl1*$^{K983R/K983R}$ mice, and another parallel between the mice and human patients, was the discovery of otitis media (OM) in the homozygous mice. SDS patients can suffer from recurrent infections of various types. One such infection that is common amongst SDS patients is OM. OM is an infection of the middle ear that causes inflammation and a build-up of fluid behind the eardrum. Chronic infections can cause conductive hearing loss due to a thick fluid being present in the middle ear (Grinspan and Pikora 2005). OM was detected, at least unilaterally, in *Efl1*$^{K983R/K983R}$ mice at 4-6 weeks of age. Hearing loss was also observed in female *Efl1*$^{K983R/K983R}$ mice at three months of age, with the hearing threshold increasing further with age (males and females also tested at 6 months of age). These data suggest

that the *Efl1*$^{K983R/K983R}$ mice suffer from deafness secondary to otitis, as is seen in SDS. The C57BL/6 inbred strains do suffer from hearing loss and cochlear degeneration, beginning in mid-life, due to the presence of the *age-related hearing loss* (*ahl*) locus on chromosome 10. The *Efl1*-K983R mice were generated on a mixed background of C57BL/6J and C3H.Pde. However, the hearing loss shown in these mutants far precedes mid-life (elevated hearing thresholds detected at 3 months of age in female *Efl1*$^{K983R/K983R}$ mice), suggesting that the hearing phenotype seen is not due to the *ahl* locus. The strain may still affect the onset of hearing loss in these mice however, and further study using alternative strains, which do not have the *ahl* locus, may be of use in determining the full extent of the *Efl1*-K983R mutation in hearing loss (Keithley, Canto et al. 2004).

While neutropenia appears to be a convenient explanation for the susceptibility of SDS patients to infections, neutropenia severity does not correlate to the rate of infections in patients. It has been found however that neutrophil mobility is impaired in SDS patients with neutropenia, and that this may contribute to their predisposition to succumb to infections (Stepanovic, Wessels et al. 2004, Burroughs, Woolfrey et al. 2009). As such, these mice could provide a model basis for testing mobility of various cell types, including white blood cells in an effort to elucidate the mechanisms behind infection susceptibility in SDS patients. No other infections were observed in the *Efl1*-K983R mice over the course of this study. However, the mice were housed in Individually-Ventilated Cages (IVC) conditions and so infections are unlikely in any cohort of mice at the facility.

Lastly, polysome profiling with MEF and liver tissue show that retention of eIF6 on the 60S subunit occurs in homozygous tissues, both embryonic and adult. This is similar to the effect seen in *Sbds*-deleted livers and patient-derived B cell polysome profiles (Senger, Lafontaine et al. 2001, Menne, Goyenechea et al. 2007, Finch, Hilcenko et al. 2011, Wong, Traynor et al. 2011). In MEFs harbouring the *Efl1*-K983R mutation, a significant increase in 60S:80S ratio was observed, indicating an increase in the amount of 60S subunits in these cells. eIF6 retention and increased 60S subunits suggests a joining defect in the ribosome maturation pathway akin to that seen in SDS. Given EFL1's reputed role in cooperatively working with SBDS to release eIF6 from the 60S subunit, it is perhaps unsurprising that a dramatic reduction in EFL1 protein levels would result in a subunit joining defect, in a way that is similar to SBDS deficiency. These data suggest that the *Efl1*$^{K983R/K983R}$ mice are indeed models of SDS, at least on a molecular level, in terms of subunit joining.

Interestingly, heterozygous tissues appear to show an intermediate phenotype in the ribosomal maturation pathway, with less eIF6 retention than homozygous tissues, and in the case of MEFs, a smaller increase in average 60S:80S peak ratio. These data suggest that while heterozygotes are seemingly unaffected by the mutation in some areas, e.g. size, bone mass density and deafness,

areas that are affected may be due to this more subtle ribosomal maturation defect. For example, in the cognitive phenotyping tests (fear conditioning, novel object recognition and Y maze) heterozygous mice appear to display an intermediate phenotype. Heterozygous mice show significantly impaired contextual fear conditioning, similar to their homozygous littermates. Additionally, heterozygous mice show significantly less interaction time with a novel object than wildtype mice, indicating an attention deficit phenotype similar to that seen in their homozygous counterparts, although not as severe. Lastly, heterozygous mice do not show completely normal behaviour in the Y maze. While they spend more time exploring the novel arm than the start arm, there is no significant difference between the time spent in the novel arm and the familiar arm, suggesting that the memories formed in the maze in these mice is not as effectual as in the wildtypes. Cognition is an extremely vast and complex subject, and as such it might be expected that higher functioning of the brain may be more susceptible to perturbations in ribosomal maturation than perhaps less demanding systems such as growth, and this may be why heterozygous mutation of *Efl1* has an effect in these areas. As discussed above, some haematological abnormalities were also observed in heterozygous mice.

In contrast to the *Efl1*$^{K983R/+}$ mice, heterozygosity of *Sbds* mutations results in no phenotypes in mice, hence the difficulty in generating *Sbds* null mutants. Therefore, humans with monoallelic *SBDS* mutations do not have SDS, but are carriers of SDS-associated alleles. However, it may be possible that *Sbds* heterozygous mutants have very minor symptoms that do not warrant medical attention and go unnoticed in everyday life. Indeed some SDS patients with biallelic loss of *SBDS* go through a great portion of their life before being diagnosed (usually after the diagnosis of their offspring) because their symptoms were not severe enough to seek medical attention. Alternatively, this does-dependent affect may be unique to *Efl1* deficiency. With no *Efl1* mutations having been reported in humans this remains to be explored.

While exocrine pancreatic insufficiency was not investigated in the *Efl1*-K983R mouse line, it may be that the *Efl1*$^{K983R/K983R}$ mice, which are significantly smaller and leaner than littermates, show similar pancreatic enzyme profiles to SDS patients. This requires further investigation, and is important to establish this mouse as a model for SDS, as the pancreatic symptoms of the disease are the most common amongst patients. In fact SDS was originally described as a syndrome of pancreatic insufficiency and bone marrow dysfunction, indicating these two features as the key manifestations of the disease (Shwachman, Diamond et al. 1964).

8.3. The relevance of *Efl1*$^{K983R/K983R}$ for studying cognitive symptoms in SDS patients

SDS patients can display a plethora of behavioural and social difficulties, and self-evaluation of emotional and mental health often results in low scores amongst patients (Perobelli, Nicolis et al. 2012). There are significant differences observed in school performance, the highest grade attained, the incidence of school problems, and special services for learning support in the SDS and control groups. Children (3-17 years old) with SDS often show a high prevalence of learning problems, and remedial teachers are often assigned to these students. Speech therapy and psychomotricity are also commonly provided to SDS patients. These additional assistance methods are more frequent in males with SDS than females. Children with SDS also display a high frequency of ''social problems'', ''rule-breaking behaviour'', ''attention deficit disorders'' and ''somatic complaints''. Some patients are classified as having developmental retardation, and many have reduced IQ assessment scores (Aggett, Cavanagh et al. 1980). Adults living with SDS also encounter frequent social and behavioural difficulties. Many adults cannot live independently, do not have an occupation or a source of independent income, and many do not attain a driver's license. The living situations amongst adults with SDS are thought to be a result of a culmination of learning and behavioural difficulties (Kerr, Ellis et al. 2010, Perobelli, Nicolis et al. 2012).

As mentioned above, no *Efl1* mouse models are currently available, making the *Efl1*$^{K983R/K983R}$ mice a unique insight into the effects of EFL1 loss. One of the major findings of this study was the behavioural and cognitive differences seen in mice harbouring the *Efl1*-K983R mutation. Homozygous and heterozygous mice showed learning and memory defects in multiple scenarios, attention deficits and social abnormalities. This link between EFL1 and cognitive impairment is a novel association that has not been previously described. Firstly, homozygous and heterozygous mice showed contextual fear conditioning defects. This means that the mice were less able to form associative memories of an unconditioned stimulus (foot shock) and the context in which they received that stimulus (the arena). Homozygous, and to a lesser extent heterozygous, mice also showed impaired learning in a maze, whereby the time spent in novel areas was measured. Homozygous mice displayed no preference for novel, unexplored areas compared to areas that were previously explored. This suggests that spatial and working memory in these mice is impaired. Another finding in this area was that homozygous, and to a lesser extent heterozygous, mice show little interaction with novel objects. This suggests an attention deficit in these mice, as the natural behaviour of a mouse is to explore novel spaces or objects. SDS patients often experience learning difficulties, as discussed above. This may reflect the learning and memory deficits seen in the mice harbouring *Efl1*-K983R mutations. These mice therefore represent an opportunity in which to study

memory formation in relation to the subunit joining defect seen in both these mice and in SDS patients.

In addition to these learning and memory phenotypes, increased social dominance was seen in male *Efl1*$^{K983R/K983R}$ mice. Abnormal social behaviours in the home cage were also observed using a home-cage monitoring system called Crack-it (Bains, Cater et al. 2016). This system uses video tracking to individually monitor mice in group housing conditions. Videos obtained from this system showed *Efl1*$^{K983R/K983R}$ mice running around the cage in repetitive patterns, showing manic episodes, and excluding themselves from cage mates in activities such as grooming or sleeping. This hyperactivity was so severe in one case, that the *Efl1*$^{K983R/K983R}$ mouse back-flipped during one of the manic episodes. SDS patients can suffer from behavioural difficulties, including increased anti-social behaviour and 'rule-breaking' behaviours in school. The social abnormalities observed in the *Efl1*$^{K983R/K983R}$ mice may reflect these social aspects of SDS that are experienced by some patients, and therefore represent an opportunity to study the processes that cause these kinds of behavioural difficulties.

There are obviously limitations in comparing rodent and human behaviour, but the data presented in this thesis indicate uncharacteristic behaviours and impaired learning in these mice, which may result from abnormal cognitive processing. The cognitive processes behind behavioural irregularities may share a common basis between mice and humans, and the *Efl1*-K983R mouse line may therefore provide a model in which to investigate this further. It is worth noting that the cognitive side of symptoms of SDS remain the largest complaint amongst patients, and therefore addressing these problems is critical for patient wellbeing and care.

8.4. The effects of the *Efl1*-K983R mutation on translation

One potential limitation in the *Efl1*-K983R story is that, while the molecular process and many of the consequent phenotypes of the mutant mice are in line with SDS, no translation defects have been detected in MEFs from the *Efl1*$^{K983R/K983R}$ mice. Translation was tested via two different methods; 1) an S^{35}-Met labelling assay and 2) a non-radioactive puromycin assay. Both were conducted using MEFs, and both techniques showed no significant differences in the level of translation in these cells. This is somewhat surprising considering that polysome profiling with MEFs showed a subunit joining defect. Cycloheximide was used in an attempt to stress the cells. The logic behind this was to potentially recapitulate the stress that may be affecting the cells *in vivo*, due to the ribosomal maturation pathway being defective. Ribosomal stress result in suppression of translation and cell death, and therefore it is unlikely that cells with a subunit joining defect, like in the *Efl1*$^{K983R/K983R}$ mice and in SDS patient cells (Wong, Traynor et al. 2011), are devoid of cellular stress pathways. However,

even with cycloheximide, at multiple concentrations, there were no significant differences in translation detected in the MEFs. However, defects in translation have been detected in *SBDS*-depleted HEK293 cells and in MEFs carrying disease-associated mutations (Ball, Zhang et al. 2009, Zhang 2009). In future, it may be beneficial to study translation in other primary cells *in vitro*, as well as *in vivo*, in adult tissues to elucidate any potential translation defects in the *Efl1*$^{K983R/K983R}$ mice.

Given the cooperative role of SBDS and EFL1, and the consequent subunit joining defects that occur in deficiency of either of these proteins, it might be assumed that translation would also be impaired in the *Efl1*$^{K983R/K983R}$ mice. The lack of any translation defects in the *Efl1*$^{K983R/K983R}$ MEFs indicates that this may be an effect unique to SBDS depletion. However, it may suggest that EFL1 is redundant and that there is a compensatory mechanism occurring in these mutants to preserve general translation.

To elaborate on this theme, EFL1 is a homologue of, and shares a binding site with, eEF2. This may indicate a possibility of redundancy between EFL1 and eEF2. It is thought that one of EFL1's roles in ribosomal maturation is to prevent eEF2 binding to the 60S subunit prematurely (Panse and Johnson 2010). The major difference between the two proteins is the insertion of approximately 160 amino acids in domain II of EFL1 that is not present in eEF2. The role of this insertion domain is not clear, and there is debate over whether it is needed for eIF6 release. Direct interaction between EFL1 and SBDS via this insertion domain has been reported, detailing that it is intrinsically disordered and flexible until SBDS binds EFL1. This finding of two states of the EFL1 insertion domain –disordered in the absence of SBDS and rigid upon SBDS binding – suggested a dual-functionality: prevention of premature eEF2 binding in the disordered state, and eIF6 release in the rigid state (Asano, Atsuumi et al. 2014). However, this direct contact between EFL1 and SBDS was found out of context of the 60S subunit. It is unlikely that proteins will behave in the exact same manner when free in solution compared to a biologically relevant environment; in this case bound to the 60S subunit. Therefore, the binding behaviour of EFL1 is more accurately detailed in structural studies of the protein in complex with the 60S subunit. These studies show that the insertion domain is dispensable for *in vivo* function (Weis, Giudice et al. 2015). This suggests that this distinguishing feature of EFL1 is redundant for ribosome biogenesis functionality, and therefore it may be possible for eEF2 to carry out the same functions. eEF2 levels were shown to be comparable to wildtype levels in *Efl1*$^{K983R/K983R}$ MEFs. eEF2 is a GTPase, and shares a binding site with EFL1 with its G domain occupying the canonical GTPase centre, in close proximity to eIF6's binding site on the 60S subunit. It is plausible therefore, that translation in the *Efl1*$^{K983R/K983R}$ tissues may be spared in the absence of EFL1 due to a compensatory mechanism by eEF2.

However, the plethora of phenotypes seen in these mice suggests that the mutation is not harmless, and translation is therefore unlikely to be spared completely. It is possible therefore that translation, although not globally reduced, is limited to essential or stress-related proteins only. Various stressors, such as reduced nutrient availability, oxidative stress, viral infection or misfolded proteins trigger inhibition of general protein synthesis, but stimulate translation of specific mRNAs. Ribosomal stress has also been shown to induce stress-related pathways (Jones, Lynn et al. 2008, Gazda, Preti et al. 2012). Most eukaryotic mRNAs are translated via this cap-dependent mechanism, but it is approximated that around half of cellular mRNAs can utilise cap-independent mechanisms of translational initiation that do not require the 43S PIC. In times of cellular stress, elements of the 43S PIC are downregulated, and thus translation initiation of the many mRNAs is supressed. This makes way for mRNAs containing cap-independent regulatory elements to be translated (Xue and Barna 2012).

Gene-specific translational control in times of cellular stress depends on regulatory elements in the mRNA, such as upstream open reading frames (uORFs) or RNA secondary structures such as Internal Ribosome Entry Site (IRES). One example of a regulatory mechanism is the phosphorylation of eIF2. Phosphorylation of eIF2α (eIF2α-P) reduces protein synthesis to conserve resources and facilitate preferential translation of transcripts that promote stress adaptation (Young, Willy et al. 2015). However, western blot analysis of phosphorylated forms of eIF2α relative to total levels showed no differences between wildtype and *Efl1*-K983R carrying MEFs. However, it is possible that another form of stress-related translation is occurring in these mice.

IRES-mediated translation is another mechanism by which stress-adaption genes can be translated. The IRES is an RNA structured element positioned at the 5' UTR of specific mRNAs that can recruit the ribosome directly to the initiation region of mRNAs with a reduced requirement for canonical initiation factors. Emerging evidence suggests that ribosomal proteins themselves may function to recognize specific IRES elements. Consistent with this idea, RPS19 and RPL11, two ribosomal proteins that are mutated in patients with Diamond-Blackfan anaemia (DBA), regulate IRES-dependent translation of at least two mRNAs that are important for erythroid differentiation, namely *BCL-2-associated athanogene* (*BAG1*) and *cold shock domain containing protein E1* (*CSDE1*) (Xue and Barna 2012). This shows that perturbations in ribosomal proteins can affect translation, not only on a global scale but at specific mRNA levels. It is possible that this is occurring in *Efl1*$^{K983R/K983R}$ mice. However, p53, a gene that is translated in an IRES-dependent manner, is not differentially expressed between *Efl1*$^{K983R/K983R}$ and wildtype MEFs. However, this is just one IRES-containing gene, and others may be affected in *Efl1*$^{K983R/K983R}$ mice.

8.5. *Efl1* could be candidate for genetically undefined SDS

It is important to bear in mind that only 90% of SDS patients have a genetic diagnosis, with 10% harbouring no known *SBDS* mutations. These patients are referred to as 'genetically undefined', and fulfil the clinical diagnostic criteria for SDS but lacked biallelic mutations in the *SBDS* gene. Mutations causing disease in these patients remain undiscovered. Given the similarities of the *Efl1*$^{K983R/K983R}$ mice and SDS discussed in this thesis, we propose that *EFL1* could be a candidate gene for investigation into 'genetically undefined' SDS. While no human *EFL1* mutations have been reported, no studies have yet sequenced this gene in SDS patients.

When SDS symptoms have been discussed in this thesis, care has been taken to stress that there is great heterogeneity in the symptoms, and that not all patients will present with all manifestations to the same degree. Comparison of the clinical presentations of SDS and 'genetically undefined' SDS is therefore important to assess whether there is divergence based on the genetic differences between these two branches of the disease. This type of analysis is difficult due to small patient registry sizes, but one such study has been carried out. This comparison found that cytopenias were present for both *SBDS* mutation positive and negative cohorts, with neutropenia the most common event in 94% and 81% respectively. Bone marrow hypocellularity was reported in 91% of those with *SBDS* mutations and 69% of those without. Marrow dysplasia was reported in 65% of those with SBDS mutations and none of those without (Myers, Bolyard et al. 2015). These data suggest that there are differences in the symptoms associated with the stem and progenitor cell compartment.

The lack of a hypocellular bone marrow phenotype in the *Efl1*$^{K983R/K983R}$ mice may reflect the fact the 'genetically undefined' cohort of SDS patients in this study showed less frequency of bone marrow hypocellularity than those with biallelic *SBDS* mutations. In the same way, neutropenia was less frequent in the 'genetically undefined' cohort than in *SBDS* mutation patients, suggesting that the *Efl1*-K983R mice may reflect a category of SDS that does not present with neutropenia. Additionally, no marrow dysplasia was seen in the 'genetically undefined' cohort, indicating that these patients do not develop myelodysplastic syndrome (MDS). MDS refers to bone marrow disorders characterised by abnormal stem cells, which may precede the development of acute myeloid leukaemia (AML), a cancer in which stem cells that would normally develop into granulocytes become malignant and abnormally proliferate. While clonal abnormalities were present in both cohorts, they were less frequent and intermittent in the 'genetically undefined' cohort (Myers, Bolyard et al. 2015). These data taken together suggest that 'genetically undefined' SDS patients are less likely to develop malignancies such as AML compared to *SBDS* mutation-carrying patients. Indeed, in the cohort

study discussed above, one *SBDS* mutation positive patient developed AML, while none of the negative cohort patients did. No cancers of any kind were detected in the *Efl1*$^{K983R/K983R}$ mice, supporting the hypothesis that these mice represent a model of 'genetically undefined' SDS. However, it should be noted that the risk of developing MDS and or AML in SDS patients (genetically defined) is approximately 30%, and is therefore not an inevitability of the condition (Myers, Bolyard et al. 2014).

8.6. EFL1 and ribosome biogenesis in cancer

EFL1 has been shown to be overexpressed in glioma cell lines, and human glioma tissue. Glioma is a malignant tumour of the glial tissue of the nervous system that is characterised by deregulated cell cycle due to overexpression of Cyclin-dependent kinases (Ouyang, Xu et al. 2016). Downregulation of *EFL1* by siRNA in glioma cell lines leads to cell-cycle arrest and apoptosis, and subsequently reduced glioma cell proliferation. *In vitro* knockdown of *Efl1* in mouse xenograft models results in significant growth suppression of the tumour (Saito, Iizuka et al. 2014). The mechanism behind this inhibitory effect on tumour growth is impairment of ribosome biogenesis. G1 cell-cycle arrest is triggered by downregulation of *EFL1*, and apoptosis via caspase 3/7 is induced after 6 days of siRNA transfection in glioma cell lines. Additionally, p53 and p21 protein activation was supressed in *EFL1* knockdown glioma cell lines. Autophagy was also increased in *EFL1* knockdown glioma cell lines. Given that cells respond to reduced protein synthesis by digesting their own cytoplasmic materials into amino acids and fatty acids to maintain cellular energy this is not surprising. In addition, various cancers, including glioma, have been shown to induce autophagy in response to nutrient deprivation, low protein synthesis, hypoxia and anti-cancer treatments (Saito, Iizuka et al. 2014).

The link between EFL1 and glioma highlights the tight link between disruptions in ribosome biogenesis and cancer. For some time now, ribosome biogenesis has been linked to cancer. Cancer cells produce excessive ribosomes, which subsequently are responsible for the excessive protein synthesis associated with aberrant cancer cell growth (Saito, Iizuka et al. 2014). Another hallmark of transformation in a cell is a change in nucleolar structure. There are also reports of overexpression of *eIF6* in head and neck carcinomas and colorectal cancer (Sanvito, Vivoli et al. 2000, Rosso, Cortesina et al. 2004) suggesting a specific link between ribosome biogenesisand cancer. It has also been reported that inactivation of *eIF6* suppressed transformation and delayed tumour growth in mice (Gandin, Miluzio et al. 2008, Miluzio, Beugnet et al. 2011). One of the most striking links between ribosome biogenesis and cancer is with nucleolar protein nucleophosmin (NPM1), which is mutated in approximately 30% of leukaemias. Many r-proteins have been found to harbour mutations in various types of cancer. Mutations in r-protein genes have for example been found in

endometrial cancer (RPL22), T-cell acute lymphoblastic leukemia (RPL10, RPL5 and RPL11), chronic lymphocytic leukemia (RPS15), colorectal cancer (RPS20), and glioma (RPL5). This taken in addition to the fact that ribosomopathy patients have a higher risk of developing cancers, strongly suggests that ribosome biogenesis, or rather defects in ribosome biogenesis, are inextricably linked to cancer (Pelava, Schneider et al. 2016).

Given its role in ribosome biogenesis, it is plausible that overexpression of *EFL1* might cause increased translation, an override of quality control check points and lead to malignant transformation as seen in glioma. Indeed, a deficiency of SBDS in cells leads to a decrease in global translation (Ball, Zhang et al. 2009), so perhaps in the opposite situation (overexpression of a subunit joining factor) an increase in translation may be consequent. However, the *Efl1*$^{K983R/K983R}$ mice, that are deficient in EFL1, did not show any translation differences compared to wildtype, and no cancers were detected of any kind throughout the life span of the mice.

It has long been a phenomenon of the ribosomopathy field that a disease that produces a growth-deficient environment also causes a disease of aberrant growth – cancer. In SDS, this is thought to be related to the clonal chromosome abnormalities often seen in the bone marrow of SDS patients, indicating that the mutation of *SBDS* may be a first event in a multi-step tumour-formation process. Two clonal chromosome abnormalities are frequently detected in SDS patients; iso(7)q and del(20)q. Other clonal chromosome abnormalities have been reported, each with a different associated risk of developing AML (Minelli, Maserati et al. 2009). The del(20)q chromosomal abnormalities seen in the bone marrow of SDS patients is thought to include the deletion of the *eIF6* gene, thus providing a mechanism to circumvent to defect in ribosome biogenesis presented by the SBDS deficiency, and allow inappropriate protein synthesis and subsequent growth. The *SBDS* gene is located on 7q11, and thus bone marrow cells with the iso(7)q abnormality have three copies of the mutated gene. The reason for the development of these clonal chromosome abnormalities is debateable. They are not restricted to SDS patients, and occur in many different bone marrow failure disorders (Minelli, Maserati et al. 2009). There may however be a strong selective pressure in cells with loss of SBDS for mutations that can allow cells to escape growth arrest or apoptosis, predisposing them to genomic instability. In addition, SBDS has been shown to support the mitotic spindle, and so depletion of this protein (or functional loss through mutation) may make cells prone to genomic instability (Ball, Zhang et al. 2009). This role for SBDS in genomic stability may explain the predisposition of SDS patients to accumulate these clonal chromosome abnormalities. This may also suggest why chromosome abnormalities in 'genetically undefined' SDS patients, who have normal

SBDS protein levels, are only intermittent if present at all (Austin, Gupta et al. 2008). These types of intermittent abnormalities are present in non-ribosomopathy cases too. Likewise, this may explain why no cancerous symptoms were detected in the *Efl1*$^{K983R/K983R}$ mice, as their SBDS protein levels are normal, again giving weight to the possibility of these mice representing a model of 'genetically undefined' SDS.

8.7. p53 signalling in ribosomopathies and the *Efl1*$^{K983R/K983R}$ mice

There is increasing evidence from animal models and human studies that defective ribosome biogenesis causes p53-dependent pathologies that are mediated by the HDM2/MDM2 stress signalling pathway. As mentioned above, p53 protein overexpression has been seen in the bone marrow of SDS patients, more specifically p53 is overexpressed in immature cells of the bone marrow (Wong, Traynor et al. 2011, Zambetti, Bindels et al. 2015). It has also been reported that SDS patient B cells have increased levels of p53 (Ball, Zhang et al. 2009).

Activation of p53 has been proposed as a common mechanism in the pathogenesis of various different ribosomopathies, including SDS, DBA, TCS and 5q-syndrome (Fumagalli and Thomas 2011). It is known that certain ribosomal proteins regulate p53 activity. These include, RPL5, RPL11, RPL26 and RPS7, which are found to be mutated in DBA patients. DBA is a ribosomopathy that results in refractory anaemia as a result of impaired erythropoiesis. The pathophysiological mechanisms of DBA are not clear, however increased apoptosis of erythroid progenitor cells has been demonstrated which may contribute to the anaemia seen in patients. The sensitivity of this particular cell lineage in DBA is thought to be due to an increase of free r-proteins. R-proteins affect p53 activity by sequestering HDM2, the E3 ubiquitin ligase that targets p53 to the proteasome for degradation, or by favouring p53 translation (Gazda, Preti et al. 2012). p53 is therefore upregulated as a result of rRNA processing defects.

Haploinsufficiency of *TCOF1*, the gene mutated in TCS, has also been found to increase levels of p53 protein, and apoptosis, further supporting the link between ribosomal stress and p53 activation. Interestingly, a study by Jones et al showed that chemical and genetic inhibition of p53 activity in *Tcof1* haploinsufficient mice can prevent the craniofacial abnormalities normally seen in these TCS mouse models, showing that p53 is also implicated in other ribosomopathy pathogenesis pathways (Narla and Ebert 2010).

Elevated protein levels of p53 have been detected in the bone marrow of SDS patients, supporting a potential role for p53 in the bone marrow-related symptoms of the disease (Elghetany and Alter 2002). It could be postulated that increased levels of p53 due to the ribosomal stress caused by the

SBDS mutations could cause cell death in the bone marrow population. This could explain such symptoms as the hypocellularity seen in the bone marrow. *Sbds* loss in the murine pancreas results in severe atrophy that is p53 dependent. This p53 dependence was not specific to the pancreas, as loss of p53 impacted many phenotypes of an embryonic SDS mouse model, in that it had a restorative effect on haematological progenitor levels in the *Sbds* null embryo, and reduced apoptosis was seen in the foetal brain. Loss of p53 also lessened disturbances seen in polysome profiles of foetal livers of *Sbds* null embryos, with 80S levels increasing slightly, but still remaining below wildtype levels (Tourlakis, Zhang et al. 2015).

As mentioned in **Error! Reference source not found.**, p53 and p21 protein activation is supressed in *E FL1* knockdown glioma cell lines. This may suggest that the p53-p21 axis is not activated in *EFL1* deficient cells as it is in *SBDS*-depleted cells. In concurrence with this, the *Efl1*$^{K983R/K983R}$ mice did not show significantly different levels of p53 or p21 protein in MEFs or in the bone marrow (p21 only). This may suggest that the symptoms of SDS, which are caused by *SBDS* deficiency, are not all mediated by p53 signalling. Therefore, different aspects of the disease could be caused by distinct pathogenic pathways. The *Efl1*$^{K983R/K983R}$ mice may provide an insight into the p53-independent aspects of SDS, thus allowing for better understanding of the many systems affected in the disease. p53 expression levels in 'genetically undefined' SDS patients has not been investigated, and so this may be another level of differentiation between the two branches of SDS. The reason for the difference in p53 expression in *EFL1* and *SBDS* deficient models is not clear, and is seemingly counter-intuitive. One might assume that if the ribosomal stress caused by subunit joining defects in SDS is sufficient to elevate p53 levels, then the *Efl1*$^{K983R/K983R}$ mice would also elicit this response. However, there are differences between SDS and the *Efl1*$^{K983R/K983R}$ mouse model, such as the lack of a translation deficit in the *Efl1*$^{K983R/K983R}$ MEFs. The translation and p53 data taken together may suggest that the syndrome seen in the *Efl1*$^{K983R/K983R}$ mice is not as predictive of SDS as *SBDS* loss models.

8.8. <u>The ribosomopathy phenomenon: tissue-specific disease from a universal process</u>

Ribosomes are essential in all cell types, yet mutations in ribosomal proteins or assembly factors result in tissue-specific disease. All ribosomopathies show cell-specific symptoms, whereby only a select group of organs are affected by a ubiquitous mutation. Furthermore, different subsets of organs are affected in different ribosomopathies. One of the fundamental gaps in our understanding of ribosomopathies stems from this phenomenon: why does a defect in protein synthesis machinery, which is essential to all cells, only affect certain cell types? Selective susceptibility may be due to differential expression levels of certain components of the ribosome

biogenesis pathway, proliferative capacity of some cell types, or threshold requirements for translation (Tourlakis, Zhang et al. 2015). However the definitive cause of this selective organ defects has not yet been determined. It has been shown that highly proliferative tissues have higher expression of the protein SBDS in mice, which may hint to a correlation between proliferation and susceptibility to ribosome deficiency (Zhang, Shi et al. 2006).

Differential mRNA translation may account for tissue specific disease. Ribosomal proteins are usually produced in excess, and the superfluous proteins then degraded in the nucleolus. This is presumably a mechanism to allow protein synthesis to occur at very short notice, to meet the cells demands, and to compensate for problems in the ribosomal maturation pathway should they occur. Many ribosomopathy models show a reduction in ribosomal subunits (40S, 60S and/or 80S) and reduced translation, however this is not always accompanied by diminished polysomes, suggesting that even though the subunit abundancy is changed, the amount of actively translating ribosomes is not greatly reduced (Finch, Hilcenko et al. 2011, Wong, Traynor et al. 2011). This might be explained by the excessive production of ribosomal proteins described above. It may also be explained by normal initiation of translation, but impaired elongation, resulting in decreased protein synthesis. Gismondi et al. showed that protein synthesis in RPS19 deficient cell lines was inhibited at the elongation level, but that initiation of translation was not impaired. It is known that inhibition of elongation leads to increased recruitment of mRNAs that have low intrinsic initiation efficiency ('weak' mRNAs). Gismondi et al. also showed that treatment of cells deficient in RPS19 with cycloheximide, an elongation inhibitor, resulted in increased recruitment of 'weak' mRNAs to the polysomes, but did not have a substantial effect on 'strong' mRNAs (mRNAs with high initiation efficiency). This may be due to the partial inhibition, or slowing, of elongation removing the competition of mRNAs at the initiation stage disadvantaging the 'strong' mRNAs. This could be a mechanism to favour translation of mRNAs of ribosomal proteins that could compensate for their inadequate availability, in an attempt to maintain ribosome production. This kind of compensatory mechanism has also been shown in *Xenopus laevis* cells treated with transcriptional inhibitors (Gismondi, Caldarola et al. 2014).

Differential gene expression in tissue may also account for tissue specificity seen in ribosomopathies. In the case of SDS for example, it has been demonstrated that *SBDS* expression is high in marrow stromal cells and early hematopoietic precursors, and murine models demonstrate altered marrow stromal function after targeted *Sbds* depletion, suggesting that the bone marrow may have a special status as a vulnerable tissue to SBDS deficits (Burwick, Coats et al. 2012). EFL1 is expressed in all tissues, with no apparent escalations in any specific tissues, so this theory does not support the

tissue specific phenotypes seen in the *Efl1*$^{K983R/K983R}$ mice. It has also been reported that translation of the *C/EBPα* and *-β* mRNAs, pancreas-specific genes that are indispensable regulators of granulocytic differentiation, are altered by *SBDS* mutations or knockdown. Myeloid progenitors derived from the bone marrow of SDS patients have a reduced proliferation capacity with low frequency of CD34+ cells and reduced colony forming ability. These data suggest that the haematopoietic progenitor compartment in SDS patients is compromised due to the lack of these critical differentiation factors. This supports the notion of differential mRNA translation, rather than global reduction in protein synthesis, is the cause of tissue-specific symptoms in SDS.

More research is required into this field to fully elucidate tissue-specific disease mechanisms. To do this it is critical to develop mammalian models of disease that show multi-organ phenotypes that can be studied in adulthood, to better mimic the disease processes associated with subunit joining defects. The *Efl1*$^{K983R/K983R}$ mice represent an opportunity to study these lesser known areas of SDS, and perhaps further knowledge of the tissue-specificity phenomenon of ribosomopathies.

8.9. Concluding remarks

Here we have presented a prime example of how forward genetics can produce novel and unexpected mouse models of disease. From a mouse with an abnormal gait, a phenotype previously unrelated to SDS, careful characterisation has led to the elucidation of SDS-like phenotypes and potential model of disease. Gait abnormalities and SDS have not been linked in mouse models previously, and so a novel genotype-phenotype distinction has been made.

Parallels between the *Efl1*$^{K983R/K983R}$ mice and SDS are as follows: small size, leanness (maybe due to fat malabsorption), reduced BMD, haematological abnormalities, learning impairment and behavioural irregularities and a subunit joining defect due to retention of eIF6. All of the phenotypes identified in this thesis are novel, as no *Efl1* mouse models are currently available.

There are of course differences between the *Efl1*$^{K983R/K983R}$ mice and SDS in patients. Some of the stark differences include the lack of translation impairment in MEFs from *Efl1*$^{K983R/K983R}$ mice, the absence of a confirmed pancreatic phenotype and a lack of cancerous phenotypes. Further study is required in these areas in the future. Translational assays should be carried out in different cell types that may be more clinically relevant to SDS. It may also be advantageous to carry out translation assays in adult tissues, through use of *in vivo* techniques. SuNSET can be used *in vivo*, by injecting the mice with puromycin, and collecting tissues for FACS or western blot (Goodman and Hornberger 2013). To investigate the pancreatic phenotype in the *Efl1*$^{K983R/K983R}$ mice, serum levels of α-amylase and trypsinogen should be measured, perhaps via ELISA techniques. In terms of cancer, it

would be interesting to identify any clonal chromosome abnormalities in the *Efl1*$^{K983R/K983R}$ mice, and also whether these abnormalities correlate to those found within SDS patient bone marrow (most commonly chromosome 7 abnormalities). It seems apparent form the *Efl1*$^{K983R/K983R}$ mice that the phenotypes seen are p53-independent. However, further study in this area could elucidate any underlying p53-dependent disease processes that may be occurring due to ribosomal stress. *p53* null mice are often used as a modifier for diseases relating to p53 signalling. It would be interesting to cross the *Efl1*$^{K983R/K983R}$ mice with a *p53* null line to determine if any of the phenotypes were ameliorated or accentuated by the absence of p53.

An alternative hypothesis was recently presented at the 8th International Congress on SDS by Dr Joanna Rommens (University of Toronto), which may explain the lack of a translation phenotype in the *Efl1*$^{K983R/K983R}$ mice. The concept of different types of ribosomes has become increasingly attractive in the field of translational machinery research. Heterogeneity in ribosome composition resulting from differential expression and post-translational modifications of ribosomal proteins, rRNA diversity and the activity of ribosome-associated factors may generate 'specialized ribosomes' that have a substantial impact on how the genomic template is translated into functional proteins. A similar concept was put forward by Dr Rommens that 60S subunits with eIF6 still retained can form 80S ribosomes, albeit not in a canonical form. She hypothesised that these ribosomes cannot take part in normal translation but are able to bind mRNA, perhaps only 'weak' mRNAs that have little secondary structure and low GC content. This would explain why polysome profiles from SDS patients' B cells do not always show an obvious difference in peak ratios or polysomes, despite showing eIF6 retention. It might also explain why translation is not affected in the *Efl1* $^{K983R/K983R}$ mice. This rather radical notion is supported by the spread of eIF6 immunoblotting from fractions of polysome profiles from SDS patient B cells in which eIF6 is not simply restricted to one fraction (the 60S fraction) but is spread throughout the 80S fractions as well (Wong, Traynor et al. 2011). This is also a trait seen in the liver polysome profiles from *Efl1*$^{K983R/K983R}$ mice presented in this thesis. However, this is not limited to the mutant profiles in this thesis, and is also present in the wildtype profiles, suggesting that this is not an effect of the mutation but rather an artefact of the methodology. No published data has been presented to support this theory, but the emerging field of specialised ribosomes certainly shows that the complexity of the ribosome and its functions *in vivo* are far from fully elucidated. This should remind us that only though further investigation of the ribosome, both functional and dysfunctional, can we hope to understand it's biology.

We postulate in this thesis that the *Efl1*$^{K983R/K983R}$ mice are a model of 'genetically undefined' SDS, rather than true SBDS-deficient SDS. 'Genetically undefined' SDS does not lead to AML or persistent

clonal chromosomal abnormalities, as seen in SDS, and so the *Efl1*$^{K983R/K983R}$ mice, which seem to have no cancerous phenotype, may be reflective of this difference. The other differences described above may also be a reflection of the *Efl1*$^{K983R/K983R}$ mice being a subtle deviation from SDS. Considering there are no leads for a candidate gene for 'genetically undefined' SDS, the *Efl1*$^{K983R/K983R}$ mice represent a system in which to study this further. We propose here that *Efl1* may be a candidate for 'genetically undefined' SDS, and that human screens for *Efl1* mutations should be carried out in SDS patients with no genetic diagnosis.

Table 9 Summary of parallels and differences of the *Efl1*$^{K983R/K983R}$ mice and Shwachman-Diamond Syndrome.

SDS symptom	Paralleled in the *Efl1*$^{K983R/K983R}$ mice?	Details of phenotype
Small stature	Yes	Weigh less, small size
Fat malabsorption	Yes	Stay lean
Pancreatic enzyme insufficiency	Not tested	
Skeletal abnormalities	No	X-rays are normal
Decreased BMD, osteoporosis, osteopenia	Yes	Decreased BMD and BMC
Hypocellular bone marrow	No	Bone marrow cellularity normal
Neutropenia	Yes	Reduced WBC count
Macrocytic anaemia	Yes	Reduced RBC count, increased size, decreased Hb
Thrombocytopenia	Yes	Reduced platelet count and size
Otitis media and deafness	Yes	Otitis media and deafness
AML/clonal abnormalities	No	No cancer detected
Increased p53 expression	No	p53 expression levels normal
Impaired eIF6 release and subunit joining	Yes	Retention of eIF6 in 60S fraction, and increased 60S:80S ratio
Learning difficulties, attention deficits	Yes	Learning and memory impaired, attention deficit
Behavioural difficulties	Yes	Social dominance, abnormal social interactions
Hypotonia/ataxia	Yes	Abnormal gait

8.10. Future work

There are still some aspects of this project that would benefit from further investigation. Firstly, the protein levels of EFL1 were found to be diminished in both homozygous and heterozygous mice. The cause of this protein deficiency however was not elucidated. In order to address this, assays could be undertaken to investigate whether the mutant form of EFL1 is being aberrantly degraded. For example, a proteasome degradation assay could be carried out, whereby the proteasomal inhibitor MG132 is used to block degradation via this pathway and monitoring EFL1 protein levels over time. Alternaitvly, the mutant form of EFL1 could be being ubiquitylated in a way that the wildtype protein is not. Ubiquitylation assays could be carried out to determine if this is the case. Another anomaly that could be addressed in this area is the fact that heterozygous cells and tissues do not have exactly 50% of the EFL1 of wildtype tissues, as would be expected for carrying one mutant and one wildtype allele. This could be because EFL1 is capable of forming homodimers within the cell. If this were the case, mutant EFL1 could form a dimer with wildtype EFL1 in heterozygous tissues, and thereby direct both the mutant and wildtype forms for degradation. One way to test this hypothesis would be to run cell and tissue lysates in a native gel, and see if a dimer band is present for EFL1.

One way to be certain that th effects we are seeing in the mice are due to an EFL1 deificency, would be to artificially knock down EFL1 in cells, and see if this recapitulates the MEF phenotypes seen. siRNA experiments could be used to knock down EFL1, and these cells could then be used for growth assays and polysome profiles to compare the data with primary MEFs. Another use for these types of experiment woud be to generate siRNAs that reduce protein amounts by a certain amount, and not eliminate it completely. This would allow the identification of threshold levels at which different cell types can cope with EFL1 deficiency. This is an interesting concept as tissue specificity is one of the phenomena of the ribosomopathy field. In this way it could be estabilished if some tissues are more vulnerable than others to EFL1 reduction.

Further work in the mice would be beneficial to establish themice as a model of SDS, or 'genetically undefined' SDS. One area that could be addressed is the pancreatic insuffieicney that is seen in SDS patients and SDS mouse models (pancreatic *Sbds* knockout). This could be tested in the *Efl1*-K983R mice using ELISA techniques that detect α-amylase in serum. Alternative, vitamin K or prothrombin levels could be determined in the serum of the mice as an indirect indicator of pancreatic function. Steatorrhoea tests could also be undertaken with the mice. Steatorrhoea is a symptom of the pancreatic insufficiency in pateints, as fat is not absorbed efficiently in the gut.

In conclusion, although more work needs to be done, the mice presented in this thesis provide a new mammalian model system in which to study the *in vivo* functions of EFL1 and the effect that EFL1 deficiency has on ribosomal maturation. Furthermore, the mice also provide the first long-lived mouse model of a ribosomal joining defect, which is likely to occur in multiple tissues. Such a model would be useful in the field of SDS research, as well as ribosome biogenesis research in general.

Bibliography

Ablack, J. N. G., P. J. Metz, J. T. Chang, J. M. Cantor and M. H. Ginsberg (2015). "Ubiquitylation of CD98 limits cell proliferation and clonal expansion." Journal of Cell Science **128**(23): 4273-4278.

Acevedo-Arozena, A., S. Wells, P. Potter, M. Kelly, R. D. Cox and S. D. Brown (2008). "ENU mutagenesis, a way forward to understand gene function." Annu Rev Genomics Hum Genet **9**: 49-69.

Aggett, P. J., N. P. Cavanagh, D. J. Matthew, J. R. Pincott, J. Sutcliffe and J. T. Harries (1980). "Shwachman's syndrome. A review of 21 cases." Arch Dis Child **55**(5): 331-347.

Alberts, B., Johnson, A., Lewis, J., Raff, M., Roberts, K., Walter, P. (2007). Molecular Biology of the Cell. United States fo America, Garland Science, Taylor & Francis Group, LLC.

Archer, J. (1975). "Rodent sex differences in emotional and related behavior." Behav Biol **14**(4): 451-479.

Armache, J. P., A. Jarasch, A. M. Anger, E. Villa, T. Becker, S. Bhushan, F. Jossinet, M. Habeck, G. Dindar, S. Franckenberg, V. Marquez, T. Mielke, M. Thomm, O. Berninghausen, B. Beatrix, J. Soding, E. Westhof, D. N. Wilson and R. Beckmann (2010). "Localization of eukaryote-specific ribosomal proteins in a 5.5-A cryo-EM map of the 80S eukaryotic ribosome." Proc Natl Acad Sci U S A **107**(46): 19754-19759.

Armistead, J. and B. Triggs-Raine (2014). "Diverse diseases from a ubiquitous process: The ribosomopathy paradox." FEBS Letters **588**(9): 1491-1500.

Asano, N., H. Atsuumi, A. Nakamura, Y. Tanaka, I. Tanaka and M. Yao (2014). "Direct interaction between EFL1 and SBDS is mediated by an intrinsically disordered insertion domain." Biochem Biophys Res Commun **443**(4): 1251-1256.

Asif T. Chinwalla, L. L. C., Kimberly D. Delehaunty, Ginger A. Fewell, Lucinda A. Fulton Members of the Mouse Genome Analysis Group for Mouse Genome Sequencing Consortium (2002). "Initial sequencing and comparative analysis of the mouse genome." Nature **420**(6915): 520-562.

Audrey Anna Bolyard, R. N., B.S., Tammy Cottle, Carole Edards, R.G.N./R.S.C.N. Bsc., Sally Kinsey, M.D., Beate Schwinzer, Ph.D., Cornelia Zeidler, M.D. (2002) "Types of Severe Chronic Neutropenia."

Austin, K. M., M. L. Gupta, Jr., S. A. Coats, A. Tulpule, G. Mostoslavsky, A. B. Balazs, R. C. Mulligan, G. Daley, D. Pellman and A. Shimamura (2008). "Mitotic spindle destabilization and genomic instability in Shwachman-Diamond syndrome." J Clin Invest **118**(4): 1511-1518.

Bains, R. S., H. L. Cater, R. R. Sillito, A. Chartsias, D. Sneddon, D. Concas, P. Keskivali-Bond, T. C. Lukins, S. Wells, A. Acevedo Arozena, P. M. Nolan and J. D. Armstrong (2016). "Analysis of Individual Mouse Activity in Group Housed Animals of Different Inbred Strains using a Novel Automated Home Cage Analysis System." Frontiers in Behavioral Neuroscience **10**: 106.

Ball, H. L., B. Zhang, J. J. Riches, R. Gandhi, J. Li, J. M. Rommens and J. S. Myers (2009). "Shwachman-Bodian Diamond syndrome is a multi-functional protein implicated in cellular stress responses." Hum Mol Genet **18**(19): 3684-3695.

Ban, N., P. Nissen, J. Hansen, P. B. Moore and T. A. Steitz (2000). "The complete atomic structure of the large ribosomal subunit at 2.4 A resolution." Science **289**(5481): 905-920.

Banks, G., I. Heise, B. Starbuck, T. Osborne, L. Wisby, P. Potter, I. J. Jackson, R. G. Foster, S. N. Peirson and P. M. Nolan (2015). "Genetic background influences age-related decline in visual and nonvisual retinal responses, circadian rhythms, and sleep()." Neurobiology of Aging **36**(1): 380-393.

Bashan, A. and A. Yonath (2008). "Correlating ribosome function with high-resolution structures." Trends Microbiol **16**(7): 326-335.

Ben-Shem, A., N. Garreau de Loubresse, S. Melnikov, L. Jenner, G. Yusupova and M. Yusupov (2011). "The Structure of the Eukaryotic Ribosome at 3.0 Å Resolution." Science **334**(6062): 1524-1529.

Boocock, G. R., J. A. Morrison, M. Popovic, N. Richards, L. Ellis, P. R. Durie and J. M. Rommens (2003). "Mutations in SBDS are associated with Shwachman-Diamond syndrome." Nat Genet **33**(1): 97-101.

Boultwood, J., B. H. Yip, C. Vuppusetty, A. Pellagatti and J. S. Wainscoat (2013). "Activation of the mTOR pathway by the amino acid (L)-leucine in the 5q- syndrome and other ribosomopathies." Adv Biol Regul **53**(1): 8-17.

Bradatsch, B., J. Katahira, E. Kowalinski, G. Bange, W. Yao, T. Sekimoto, V. Baumgartel, G. Boese, J. Bassler, K. Wild, R. Peters, Y. Yoneda, I. Sinning and E. Hurt (2007). "Arx1 functions as an unorthodox nuclear export receptor for the 60S preribosomal subunit." Mol Cell **27**(5): 767-779.

Brown, S. M. N. and R. Buchdahl (2008). "Shwachman-Diamond syndrome in a child presenting with cystic fibrosis-type symptoms and a false-positive sweat test." Journal of the Royal Society of Medicine **101**(Suppl 1): 39-43.

Burroughs, L., A. Woolfrey and A. Shimamura (2009). "Shwachman Diamond Syndrome – a review of the clinical presentation, molecular pathogenesis, diagnosis, and treatment." Hematology/oncology clinics of North America **23**(2): 233-248.
Burwick, N., S. A. Coats, T. Nakamura and A. Shimamura (2012). "Impaired ribosomal subunit association in Shwachman-Diamond syndrome." Blood **120**(26): 5143-5152.
Bussiere, C., Y. Hashem, S. Arora, J. Frank and A. W. Johnson (2012). "Integrity of the P-site is probed during maturation of the 60S ribosomal subunit." J Cell Biol **197**(6): 747-759.
Cmejlova, J., L. Dolezalova, D. Pospisilova, K. Petrtylova, J. Petrak and R. Cmejla (2006). "Translational efficiency in patients with Diamond-Blackfan anemia." Haematologica **91**(11): 1456-1464.
Conway, S., A. Morton, B. Oldroyd, J. Truscott, H. White, A. Smith and I. Haigh (2000). "Osteoporosis and osteopenia in adults and adolescents with cystic fibrosis: prevalence and associated factors." Thorax **55**(9): 798-804.
Danilova, N. and H. T. Gazda (2015). "Ribosomopathies: how a common root can cause a tree of pathologies." Disease Models & Mechanisms **8**(9): 1013-1026.
de Oliveira, J. F., M. L. Sforca, T. M. Blumenschein, M. B. Goldfeder, B. G. Guimaraes, C. C. Oliveira, N. I. Zanchin and A. C. Zeri (2010). "Structure, dynamics, and RNA interaction analysis of the human SBDS protein." J Mol Biol **396**(4): 1053-1069.
Dever, T. E. and R. Green (2012). "The elongation, termination, and recycling phases of translation in eukaryotes." Cold Spring Harb Perspect Biol **4**(7): a013706.
Diaconu, M., U. Kothe, F. Schlunzen, N. Fischer, J. M. Harms, A. G. Tonevitsky, H. Stark, M. V. Rodnina and M. C. Wahl (2005). "Structural basis for the function of the ribosomal L7/12 stalk in factor binding and GTPase activation." Cell **121**(7): 991-1004.
Doudna, J. A. and E. Charpentier (2014). "Genome editing. The new frontier of genome engineering with CRISPR-Cas9." Science **346**(6213): 1258096.
Draptchinskaia, N., P. Gustavsson, B. Andersson, M. Pettersson, T.-N. Willig, I. Dianzani, S. Ball, G. Tchernia, J. Klar, H. Matsson, D. Tentler, N. Mohandas, B. Carlsson and N. Dahl (1999). "The gene encoding ribosomal protein S19 is mutated in Diamond-Blackfan anaemia." Nat Genet **21**(2): 169-175.
Elghetany, M. T. and B. P. Alter (2002). "p53 protein overexpression in bone marrow biopsies of patients with Shwachman-Diamond syndrome has a prevalence similar to that of patients with refractory anemia." Arch Pathol Lab Med **126**(4): 452-455.
Finch, A. J., C. Hilcenko, N. Basse, L. F. Drynan, B. Goyenechea, T. F. Menne, A. Gonzalez Fernandez, P. Simpson, C. S. D'Santos, M. J. Arends, J. Donadieu, C. Bellanne-Chantelot, M. Costanzo, C. Boone, A. N. McKenzie, S. M. Freund and A. J. Warren (2011). "Uncoupling of GTP hydrolysis from eIF6 release on the ribosome causes Shwachman-Diamond syndrome." Genes Dev **25**(9): 917-929.
Flick, K. and P. Kaiser (2012). "Protein Degradation and the Stress Response." Seminars in cell & developmental biology **23**(5): 515-522.
Fumagalli, S. and G. Thomas (2011). "The role of p53 in ribosomopathies." Semin Hematol **48**(2): 97-105.
Gandin, V., L. Masvidal, M. Cargnello, L. Gyenis, S. McLaughlan, Y. Cai, C. Tenkerian, M. Morita, P. Balanathan, O. Jean-Jean, V. Stambolic, M. Trost, L. Furic, L. Larose, A. E. Koromilas, K. Asano, D. Litchfield, O. Larsson and I. Topisirovic (2016). "mTORC1 and CK2 coordinate ternary and eIF4F complex assembly." Nat Commun **7**.
Gandin, V., A. Miluzio, A. M. Barbieri, A. Beugnet, H. Kiyokawa, P. C. Marchisio and S. Biffo (2008). "Eukaryotic initiation factor 6 is rate-limiting in translation, growth and transformation." Nature **455**(7213): 684-688.
Gandin, V., K. Sikström, T. Alain, M. Morita, S. McLaughlan, O. Larsson and I. Topisirovic (2014). "Polysome Fractionation and Analysis of Mammalian Translatomes on a Genome-wide Scale." Journal of Visualized Experiments : JoVE(87): 51455.
Gao, H., J. Sengupta, M. Valle, A. Korostelev, N. Eswar, S. M. Stagg, P. Van Roey, R. K. Agrawal, S. C. Harvey, A. Sali, M. S. Chapman and J. Frank (2003). "Study of the structural dynamics of the E coli 70S ribosome using real-space refinement." Cell **113**(6): 789-801.
Gazda, H. T., M. Preti, M. R. Sheen, M. F. O'Donohue, A. Vlachos, S. M. Davies, A. Kattamis, L. Doherty, M. Landowski, C. Buros, R. Ghazvinian, C. A. Sieff, P. E. Newburger, E. Niewiadomska, M. Matysiak, B. Glader, E. Atsidaftos, J. M. Lipton, P. E. Gleizes and A. H. Beggs (2012). "Frameshift mutation in p53 regulator RPL26 is associated with multiple physical abnormalities and a specific pre-ribosomal RNA processing defect in diamond-blackfan anemia." Hum Mutat **33**(7): 1037-1044.
Gijsbers, A., A. Garcia-Marquez, A. Luviano and N. Sanchez-Puig (2013). "Guanine nucleotide exchange in the ribosomal GTPase EFL1 is modulated by the protein mutated in the Shwachman-Diamond Syndrome." Biochem Biophys Res Commun **437**(3): 349-354.

Gonzales, B., D. Henning, R. B. So, J. Dixon, M. J. Dixon and B. C. Valdez (2005). "The Treacher Collins syndrome (TCOF1) gene product is involved in pre-rRNA methylation." Human Molecular Genetics **14**(14): 2035-2043.
Goodman, C. A. and T. A. Hornberger (2013). "Measuring protein synthesis with SUnSET: a valid alternative to traditional techniques?" Exercise and sport sciences reviews **41**(2): 107-115.
Greber, B. J. (2016). "Mechanistic insight into eukaryotic 60S ribosomal subunit biogenesis by cryo-electron microscopy." RNA **22**(11): 1643-1662.
Greer, J. P., Arber, D.A., Glader, B., List, A.F., Means, R.T., Paraskevas, F., Rodgers, G.M. (2013). Wintrobe's Clinical Hematology, Lippincott Williams & Wilkins.
Grinspan, Z. M. and C. A. Pikora (2005). "Infections in patients with Shwachman-Diamond syndrome." Pediatr Infect Dis J **24**(2): 179-181.
Gupta, R. R., S. Sen, L. L. Diepenhorst, C. N. Rudick and S. Maren (2001). "Estrogen modulates sexually dimorphic contextual fear conditioning and hippocampal long-term potentiation (LTP) in rats(1)." Brain Res **888**(2): 356-365.
Han, J. M., S. J. Jeong, M. C. Park, G. Kim, N. H. Kwon, H. K. Kim, S. H. Ha, S. H. Ryu and S. Kim (2012). "Leucyl-tRNA synthetase is an intracellular leucine sensor for the mTORC1-signaling pathway." Cell **149**(2): 410-424.
Handin, R. I., Lux, S.E., Stossel, T.P. (2003). Blood: Principles and Practice of Hematology, Lippincott Williams & Wilkins.
Hardisty-Hughes, R. E., A. Parker and S. D. Brown (2010). "A hearing and vestibular phenotyping pipeline to identify mouse mutants with hearing impairment." Nat Protoc **5**(1): 177-190.
Harms, J., F. Schluenzen, R. Zarivach, A. Bashan, S. Gat, I. Agmon, H. Bartels, F. Franceschi and A. Yonath (2001). "High resolution structure of the large ribosomal subunit from a mesophilic eubacterium." Cell **107**(5): 679-688.
Henras, A. K., C. Plisson-Chastang, M.-F. O'Donohue, A. Chakraborty and P.-E. Gleizes (2015). "An overview of pre-ribosomal RNA processing in eukaryotes." Wiley Interdisciplinary Reviews: RNA **6**(2): 225-242.
Hinnebusch, A. G. (2014). "The scanning mechanism of eukaryotic translation initiation." Annu Rev Biochem **83**: 779-812.
Hofer, A., C. Bussiere and A. W. Johnson (2007). "Mutational analysis of the ribosomal protein Rpl10 from yeast." J Biol Chem **282**(45): 32630-32639.
In, K., M. A. Zaini, C. Müller, A. J. Warren, M. von Lindern and C. F. Calkhoven (2016). "Shwachman–Bodian–Diamond syndrome (SBDS) protein deficiency impairs translation re-initiation from C/EBPα and C/EBPβ mRNAs." Nucleic Acids Research.
Jewell, J. L., R. C. Russell and K.-L. Guan (2013). "Amino acid signalling upstream of mTOR." Nat Rev Mol Cell Biol **14**(3): 133-139.
Jiménez-Díaz, A., M. Remacha, J. P. G. Ballesta and J. J. Berlanga (2014). "Phosphorylation of Initiation Factor eIF2 in Response to Stress Conditions Is Mediated by Acidic Ribosomal P1/P2 Proteins in <italic>Saccharomyces cerevisiae</italic>." PLoS ONE **8**(12): e84219.
Jones, N. C., M. L. Lynn, K. Gaudenz, D. Sakai, K. Aoto, J.-P. Rey, E. F. Glynn, L. Ellington, C. Du and J. Dixon (2008). "Prevention of the neurocristopathy Treacher Collins syndrome through inhibition of p53 function." Nature medicine **14**(2): 125-133.
Jones, N. C., M. L. Lynn, K. Gaudenz, D. Sakai, K. Aoto, J. P. Rey, E. F. Glynn, L. Ellington, C. Du, J. Dixon, M. J. Dixon and P. A. Trainor (2008). "Prevention of the neurocristopathy Treacher Collins syndrome through inhibition of p53 function." Nat Med **14**(2): 125-133.
Justice, M. J., D. A. Carpenter, J. Favor, A. Neuhauser-Klaus, M. Hrabe de Angelis, D. Soewarto, A. Moser, S. Cordes, D. Miller, V. Chapman, J. S. Weber, E. M. Rinchik, P. R. Hunsicker, W. L. Russell and V. C. Bode (2000). "Effects of ENU dosage on mouse strains." Mamm Genome **11**(7): 484-488.
Justice, M. J., J. K. Noveroske, J. S. Weber, B. Zheng and A. Bradley (1999). "Mouse ENU mutagenesis." Hum Mol Genet **8**(10): 1955-1963.
Keays, D. A., T. G. Clark and J. Flint (2006). "Estimating the number of coding mutations in genotypic- and phenotypic-driven N-ethyl-N-nitrosourea (ENU) screens." Mammalian Genome **17**(3): 230-238.
Keithley, E. M., C. Canto, Q. Y. Zheng, N. Fischel-Ghodsian and K. R. Johnson (2004). "Age-related hearing loss and the ahl locus in mice." Hearing research **188**(1-2): 21-28.
Kerr, E. N., L. Ellis, A. Dupuis, J. M. Rommens and P. R. Durie (2010). "The behavioral phenotype of school-age children with shwachman diamond syndrome indicates neurocognitive dysfunction with loss of Shwachman-Bodian-Diamond syndrome gene function." J Pediatr **156**(3): 433-438.
Khatter, H., A. G. Myasnikov, S. K. Natchiar and B. P. Klaholz (2015). "Structure of the human 80S ribosome." Nature **520**(7549): 640-645.

Kim, T.-S., C.-Y. Jang, H. D. Kim, J. Y. Lee, B.-Y. Ahn and J. Kim (2006). "Interaction of Hsp90 with Ribosomal Proteins Protects from Ubiquitination and Proteasome-dependent Degradation." Molecular Biology of the Cell **17**(2): 824-833.
Klann, E. and T. E. Dever (2004). "Biochemical mechanisms for translational regulation in synaptic plasticity." Nat Rev Neurosci **5**(12): 931-942.
Koolhaas, J. M., C. M. Coppens, S. F. de Boer, B. Buwalda, P. Meerlo and P. J. A. Timmermans (2013). "The Resident-intruder Paradigm: A Standardized Test for Aggression, Violence and Social Stress." (77): e4367.
Kressler, D., E. Hurt and J. Bassler (2010). "Driving ribosome assembly." Biochim Biophys Acta **1803**(6): 673-683.
Levin, T. L., O. Makitie, W. E. Berdon and R. S. Lachman (2015). "Shwachman-Bodian-Diamond syndrome: metaphyseal chondrodysplasia in children with pancreatic insufficiency and neutropenia." Pediatr Radiol **45**(7): 1066-1071.
Lewis, M. A., E. Quint, A. M. Glazier, H. Fuchs, M. H. De Angelis, C. Langford, S. van Dongen, C. Abreu-Goodger, M. Piipari, N. Redshaw, T. Dalmay, M. A. Moreno-Pelayo, A. J. Enright and K. P. Steel (2009). "An ENU-induced mutation of miR-96 associated with progressive hearing loss in mice." Nat Genet **41**(5): 614-618.
Limaye, A., B. Hall and A. B. Kulkarni (2009). "Manipulation of Mouse Embryonic Stem Cells for Knockout Mouse Production." Curr Protoc Cell Biol **CHAPTER**: Unit-19 1324.
Ludwig, L. S., H. T. Gazda, J. C. Eng, S. W. Eichhorn, P. Thiru, R. Ghazvinian, T. I. George, J. R. Gotlib, A. H. Beggs, C. A. Sieff, H. F. Lodish, E. S. Lander and V. G. Sankaran (2014). "Altered translation of GATA1 in Diamond-Blackfan anemia." Nat Med **20**(7): 748-753.
Luft, F. (2010). "The rise of a ribosomopathy and increased cancer risk." J Mol Med (Berl) **88**(1): 1-3.
Ma, X. M. and J. Blenis (2009). "Molecular mechanisms of mTOR-mediated translational control." Nat Rev Mol Cell Biol **10**(5): 307-318.
Mandillo, S., I. Heise, L. Garbugino, G. P. Tocchini-Valentini, A. Giuliani, S. Wells and P. M. Nolan (2014). "Early motor deficits in mouse disease models are reliably uncovered using an automated home-cage wheel-running system: a cross-laboratory validation." Disease Models & Mechanisms **7**(3): 397-407.
Maren, S. (2001). "Neurobiology of Pavlovian fear conditioning." Annu Rev Neurosci **24**: 897-931.
Marygold, S. J., J. Roote, G. Reuter, A. Lambertsson, M. Ashburner, G. H. Millburn, P. M. Harrison, Z. Yu, N. Kenmochi, T. C. Kaufman, S. J. Leevers and K. R. Cook (2007). "The ribosomal protein genes and Minute loci of Drosophila melanogaster." Genome Biol **8**(10): R216.
McGowan, K. A. and P. J. Mason (2011). "Animal models of Diamond Blackfan Anemia." Seminars in hematology **48**(2): 106-116.
Menne, T. F., B. Goyenechea, N. Sanchez-Puig, C. C. Wong, L. M. Tonkin, P. J. Ancliff, R. L. Brost, M. Costanzo, C. Boone and A. J. Warren (2007). "The Shwachman-Bodian-Diamond syndrome protein mediates translational activation of ribosomes in yeast." Nat Genet **39**(4): 486-495.
Miluzio, A., A. Beugnet, S. Grosso, D. Brina, M. Mancino, S. Campaner, B. Amati, A. de Marco and S. Biffo (2011). "Impairment of cytoplasmic eIF6 activity restricts lymphomagenesis and tumor progression without affecting normal growth." Cancer Cell **19**(6): 765-775.
Minelli, A., E. Maserati, E. Nicolis, M. Zecca, L. Sainati, D. Longoni, F. Lo Curto, G. Menna, F. Poli, E. De Paoli, M. Cipolli, F. Locatelli, F. Pasquali and C. Danesino (2009). "The isochromosome i(7)(q10) carrying c.258+2t>c mutation of the SBDS gene does not promote development of myeloid malignancies in patients with Shwachman syndrome." Leukemia **23**(4): 708-711.
Myers, K. C., A. A. Bolyard, J. Leung, J. Moore, S. Loveless, L. Mount, R. E. Harris, S. M. Davies, S. Keel, D. C. Dale and A. Shimamura (2015). "The North American Shwachman-Diamond Syndrome Registry: Genetically Undefined Shwachman-Diamond Syndrome." Blood **126**(23): 3614-3614.
Myers, K. C., A. A. Bolyard, B. Otto, T. E. Wong, A. T. Jones, R. E. Harris, S. M. Davies, D. C. Dale and A. Shimamura (2014). "Variable clinical presentation of Shwachman-Diamond syndrome: update from the North American Shwachman-Diamond Syndrome Registry." J Pediatr **164**(4): 866-870.
Nakhoul, H., J. Ke, X. Zhou, W. Liao, S. X. Zeng and H. Lu (2014). "Ribosomopathies: Mechanisms of Disease." Clin Med Insights Blood Disord **7**: 7-16.
Narla, A. and B. L. Ebert (2010). "Ribosomopathies: human disorders of ribosome dysfunction." Blood **115**(16): 3196-3205.
Ni, C.-Y., Z.-H. Wu, W. C. Florence, V. V. Parekh, M. P. Arrate, S. Pierce, B. Schweitzer, L. Van Kaer, S. Joyce, S. Miyamoto, D. W. Ballard and E. M. Oltz (2008). "Cutting Edge: K63-Linked Polyubiquitination of NEMO Modulates TLR Signaling and Inflammation In Vivo." Journal of immunology (Baltimore, Md. : 1950) **180**(11): 7107-7111.

Nikulin, A., I. Eliseikina, S. Tishchenko, N. Nevskaya, N. Davydova, O. Platonova, W. Piendl, M. Selmer, A. Liljas, D. Drygin, R. Zimmermann, M. Garber and S. Nikonov (2003). "Structure of the L1 protuberance in the ribosome." Nat Struct Biol **10**(2): 104-108.
Ouyang, Q., L. Xu, H. Cui, M. Xu and L. Yi (2016). "MicroRNAs and cell cycle of malignant glioma." International Journal of Neuroscience **126**(1): 1-9.
Palade, G. E. (1955). "A small particulate component of the cytoplasm." J Biophys Biochem Cytol **1**(1): 59-68.
Panse, V. G. and A. W. Johnson (2010). "Maturation of eukaryotic ribosomes: acquisition of functionality." Trends Biochem Sci **35**(5): 260-266.
Pelava, A., C. Schneider and Nicholas J. Watkins (2016). "The importance of ribosome production, and the 5S RNP–MDM2 pathway, in health and disease." Biochemical Society Transactions **44**(4): 1086-1090.
Perobelli, S., F. Alessandrini, G. Zoccatelli, E. Nicolis, A. Beltramello, B. M. Assael and M. Cipolli (2015). "Diffuse alterations in grey and white matter associated with cognitive impairment in Shwachman-Diamond syndrome: evidence from a multimodal approach." Neuroimage Clin **7**: 721-731.
Perobelli, S., E. Nicolis, B. M. Assael and M. Cipolli (2012). "Further characterization of Shwachman-Diamond syndrome: psychological functioning and quality of life in adult and young patients." Am J Med Genet A **158A**(3): 567-573.
Potter, P. K., M. R. Bowl, P. Jeyarajan, L. Wisby, A. Blease, M. E. Goldsworthy, M. M. Simon, S. Greenaway, V. Michel, A. Barnard, C. Aguilar, T. Agnew, G. Banks, A. Blake, L. Chessum, J. Dorning, S. Falcone, L. Goosey, S. Harris, A. Haynes, I. Heise, R. Hillier, T. Hough, A. Hoslin, M. Hutchison, R. King, S. Kumar, H. V. Lad, G. Law, R. E. MacLaren, S. Morse, T. Nicol, A. Parker, K. Pickford, S. Sethi, B. Starbuck, F. Stelma, M. Cheeseman, S. H. Cross, R. G. Foster, I. J. Jackson, S. N. Peirson, R. V. Thakker, T. Vincent, C. Scudamore, S. Wells, A. El-Amraoui, C. Petit, A. Acevedo-Arozena, P. M. Nolan, R. Cox, A. M. Mallon and S. D. Brown (2016). "Novel gene function revealed by mouse mutagenesis screens for models of age-related disease." Nat Commun **7**: 12444.
Quwailid, M. M., A. Hugill, N. Dear, L. Vizor, S. Wells, E. Horner, S. Fuller, J. Weedon, H. McMath, P. Woodman, D. Edwards, D. Campbell, S. Rodger, J. Carey, A. Roberts, P. Glenister, Z. Lalanne, N. Parkinson, E. L. Coghill, R. McKeone, S. Cox, J. Willan, A. Greenfield, D. Keays, S. Brady, N. Spurr, I. Gray, J. Hunter, S. D. Brown and R. D. Cox (2004). "A gene-driven ENU-based approach to generating an allelic series in any gene." Mamm Genome **15**(8): 585-591.
Reis, A. (2014). CRISPR/Cas9 and Targeted Genome Editing: A New Era in Molecular Biology NEB expressions, New England Biolabs, Inc.
Rezaei, N., A. Farhoudi, A. Ramyar, Z. Pourpak, A. Aghamohammadi, B. Mohammadpour, M. Moin, M. Gharagozlou, M. Movahedi, B. M. Ghazi, M. Izadyar and M. Mahmoudi (2005). "Congenital neutropenia and primary immunodeficiency disorders: a survey of 26 Iranian patients." J Pediatr Hematol Oncol **27**(7): 351-356.
Ribbeck, K. and D. Gorlich (2002). "The permeability barrier of nuclear pore complexes appears to operate via hydrophobic exclusion." EMBO J **21**(11): 2664-2671.
Robledo, S., R. A. Idol, D. L. Crimmins, J. H. Ladenson, P. J. Mason and M. Bessler (2008). "The role of human ribosomal proteins in the maturation of rRNA and ribosome production." RNA **14**(9): 1918-1929.
Rosso, P., G. Cortesina, F. Sanvito, A. Donadini, B. Di Benedetto, S. Biffo and P. C. Marchisio (2004). "Overexpression of p27BBP in head and neck carcinomas and their lymph node metastases." Head Neck **26**(5): 408-417.
Ruggero, D. and P. P. Pandolfi (2003). "Does the ribosome translate cancer?" Nat Rev Cancer **3**(3): 179-192.
Russell, W. L., E. M. Kelly, P. R. Hunsicker, J. W. Bangham, S. C. Maddux and E. L. Phipps (1979). "Specific-locus test shows ethylnitrosourea to be the most potent mutagen in the mouse." Proc Natl Acad Sci U S A **76**(11): 5818-5819.
Saito, K., Y. Iizuka, S. Ohta, S. Takahashi, K. Nakamura, H. Saya, K. Yoshida, Y. Kawakami and M. Toda (2014). "Functional analysis of a novel glioma antigen, EFTUD1." Neuro Oncol **16**(12): 1618-1629.
Sakamoto, K. M., A. Shimamura and S. M. Davies (2010). "Congenital Disorders of Ribosome Biogenesis and Bone Marrow Failure." Biology of Blood and Marrow Transplantation **16**(1, Supplement): S12-S17.
Sanvito, F., F. Vivoli, S. Gambini, G. Santambrogio, M. Catena, E. Viale, F. Veglia, A. Donadini, S. Biffo and P. C. Marchisio (2000). "Expression of a highly conserved protein, p27BBP, during the progression of human colorectal cancer." Cancer Res **60**(3): 510-516.
Seiser, R. M., A. E. Sundberg, B. J. Wollam, P. Zobel-Thropp, K. Baldwin, M. D. Spector and D. E. Lycan (2006). "Ltv1 is required for efficient nuclear export of the ribosomal small subunit in Saccharomyces cerevisiae." Genetics **174**(2): 679-691.
Selmer, M., C. M. Dunham, F. V. t. Murphy, A. Weixlbaumer, S. Petry, A. C. Kelley, J. R. Weir and V. Ramakrishnan (2006). "Structure of the 70S ribosome complexed with mRNA and tRNA." Science **313**(5795): 1935-1942.

Senger, B., D. L. Lafontaine, J. S. Graindorge, O. Gadal, A. Camasses, A. Sanni, J. M. Garnier, M. Breitenbach, E. Hurt and F. Fasiolo (2001). "The nucle(ol)ar Tif6p and Efl1p are required for a late cytoplasmic step of ribosome synthesis." Mol Cell **8**(6): 1363-1373.
Shammas, C., T. F. Menne, C. Hilcenko, S. R. Michell, B. Goyenechea, G. R. Boocock, P. R. Durie, J. M. Rommens and A. J. Warren (2005). "Structural and mutational analysis of the SBDS protein family. Insight into the leukemia-associated Shwachman-Diamond Syndrome." J Biol Chem **280**(19): 19221-19229.
Shenoy, N., R. Kessel, T. D. Bhagat, S. Bhattacharyya, Y. Yu, C. McMahon and A. Verma (2012). "Alterations in the ribosomal machinery in cancer and hematologic disorders." Journal of Hematology & Oncology **5**: 32-32.
Shwachman, H., L. K. Diamond, F. A. Oski and K.-T. Khaw (1964). "The syndrome of pancreatic insufficiency and bone marrow dysfunction." The Journal of Pediatrics **65**(5): 645-663.
Silver, L. M. (1995). Mouse Genetics: Concepts and Applications, Oxford University Press.
Sokabe, M. and C. S. Fraser (2014). "Human eukaryotic initiation factor 2 (eIF2)-GTP-Met-tRNAi ternary complex and eIF3 stabilize the 43 S preinitiation complex." J Biol Chem **289**(46): 31827-31836.
Southon, E. and L. Tessarollo (2009). "Manipulating mouse embryonic stem cells." Methods Mol Biol **530**: 165-185.
Stark, H., M. V. Rodnina, H.-J. Wieden, M. van Heel and W. Wintermeyer (2000). "Large-Scale Movement of Elongation Factor G and Extensive Conformational Change of the Ribosome during Translocation." Cell **100**(3): 301-309.
Steitz, T. A. (2008). "A structural understanding of the dynamic ribosome machine." Nat Rev Mol Cell Biol **9**(3): 242-253.
Stepanovic, V., D. Wessels, F. D. Goldman, J. Geiger and D. R. Soll (2004). "The chemotaxis defect of Shwachman-Diamond Syndrome leukocytes." Cell Motil Cytoskeleton **57**(3): 158-174.
Sulima, S. O., S. Patchett, V. M. Advani, K. De Keersmaecker, A. W. Johnson and J. D. Dinman (2014). "Bypass of the pre-60S ribosomal quality control as a pathway to oncogenesis." Proc Natl Acad Sci U S A **111**(15): 5640-5645.
Tafforeau, L., C. Zorbas, J.-L. Langhendries, S.-T. Mullineux, V. Stamatopoulou, R. Mullier, L. Wacheul and Denis L. J. Lafontaine (2013). "The Complexity of Human Ribosome Biogenesis Revealed by Systematic Nucleolar Screening of Pre-rRNA Processing Factors." Molecular Cell **51**(4): 539-551.
Thomas, G. (2000). "An encore for ribosome biogenesis in the control of cell proliferation." Nat Cell Biol **2**(5): E71-E72.
Toiviainen-Salo, S., M. K. Mäyränpää, P. R. Durie, N. Richards, M. Grynpas, L. Ellis, S. Ikegawa, W. G. Cole, J. Rommens, E. Marttinen, E. Savilahti and O. Mäkitie (2007). "Shwachman–Diamond syndrome is associated with low-turnover osteoporosis." Bone **41**(6): 965-972.
Tourlakis, M. E., S. Zhang, H. L. Ball, R. Gandhi, H. Liu, J. Zhong, J. S. Yuan, C. J. Guidos, P. R. Durie and J. M. Rommens (2015). "In Vivo Senescence in the Sbds-Deficient Murine Pancreas: Cell-Type Specific Consequences of Translation Insufficiency." PLoS Genet **11**(6): e1005288.
Trainor, P. A. and A. E. Merrill (2014). "Ribosome biogenesis in skeletal development and the pathogenesis of skeletal disorders." Biochim Biophys Acta **1842**(6): 769-778.
Trapman, J., J. Retel and R. J. Planta (1975). "Ribosomal precursor particles from yeast." Exp Cell Res **90**(1): 95-104.
Vetter, I. R. and A. Wittinghofer (2001). "The guanine nucleotide-binding switch in three dimensions." Science **294**(5545): 1299-1304.
Weber, J. S., A. Salinger and M. J. Justice (2000). "Optimal N-Ethyl-N-nitrosourea (ENU) doses for inbred mouse strains." genesis **26**(4): 230-233.
Weis, F., E. Giudice, M. Churcher, L. Jin, C. Hilcenko, C. C. Wong, D. Traynor, R. R. Kay and A. J. Warren (2015). "Mechanism of eIF6 release from the nascent 60S ribosomal subunit." Nat Struct Mol Biol.
Weiss, M. J., P. J. Mason and M. Bessler (2012). "What's in a name?" The Journal of Clinical Investigation **122**(7): 2346-2349.
Wiltgen, B. J., M. J. Sanders, N. S. Behne and M. S. Fanselow (2001). "Sex differences, context preexposure, and the immediate shock deficit in Pavlovian context conditioning with mice." Behav Neurosci **115**(1): 26-32.
Wimberly, B. T., D. E. Brodersen, W. M. Clemons, Jr., R. J. Morgan-Warren, A. P. Carter, C. Vonrhein, T. Hartsch and V. Ramakrishnan (2000). "Structure of the 30S ribosomal subunit." Nature **407**(6802): 327-339.
Wong, C. C., D. Traynor, N. Basse, R. R. Kay and A. J. Warren (2011). "Defective ribosome assembly in Shwachman-Diamond syndrome." Blood **118**(16): 4305-4312.
Xue, S. and M. Barna (2012). "Specialized ribosomes: a new frontier in gene regulation and organismal biology." Nat Rev Mol Cell Biol **13**(6): 355-369.

Yao, W., D. Roser, A. Kohler, B. Bradatsch, J. Bassler and E. Hurt (2007). "Nuclear export of ribosomal 60S subunits by the general mRNA export receptor Mex67-Mtr2." Mol Cell **26**(1): 51-62.
Yelick, P. C. and P. A. Trainor (2015). "Ribosomopathies: Global process, tissue specific defects." Rare Dis **3**(1): e1025185.
Young, S. K., J. A. Willy, C. Wu, M. S. Sachs and R. C. Wek (2015). "Ribosome Reinitiation Directs Gene-specific Translation and Regulates the Integrated Stress Response." J Biol Chem **290**(47): 28257-28271.
Yusupov, M. M., G. Z. Yusupova, A. Baucom, K. Lieberman, T. N. Earnest, J. H. Cate and H. F. Noller (2001). "Crystal structure of the ribosome at 5.5 A resolution." Science **292**(5518): 883-896.
Yusupova, G. and M. Yusupov (2015). "Ribosome biochemistry in crystal structure determination." RNA **21**(4): 771-773.
Zambetti, N. A., E. M. Bindels, P. M. Van Strien, M. G. Valkhof, M. N. Adisty, R. M. Hoogenboezem, M. A. Sanders, J. M. Rommens, I. P. Touw and M. H. Raaijmakers (2015). "Deficiency of the ribosome biogenesis gene Sbds in hematopoietic stem and progenitor cells causes neutropenia in mice by attenuating lineage progression in myelocytes." Haematologica **100**(10): 1285-1293.
Zemp, I. and U. Kutay (2007). "Nuclear export and cytoplasmic maturation of ribosomal subunits." FEBS Lett **581**(15): 2783-2793.
Zemp, I., T. Wild, M. F. O'Donohue, F. Wandrey, B. Widmann, P. E. Gleizes and U. Kutay (2009). "Distinct cytoplasmic maturation steps of 40S ribosomal subunit precursors require hRio2." J Cell Biol **185**(7): 1167-1180.
Zhang, B. (2009). Elucidation of the function of SBDS and the pathobiology of Shwachman-Diamond syndrome with generation of mouse models., U of T Libraries: Univerisity of Toronto. .
Zhang, S. (2009). "Elucidation of the function of SBDS and the pathobiology of Shwachman-Diamond syndrome with generation of mouse models." University of Torronto Libraries.
Zhang, S., M. Shi, C. C. Hui and J. M. Rommens (2006). "Loss of the mouse ortholog of the shwachman-diamond syndrome gene (Sbds) results in early embryonic lethality." Mol Cell Biol **26**(17): 6656-6663.
Zhang, Y. and H. Lu (2009). "Signaling to p53: Ribosomal Proteins Find Their Way." Cancer Cell **16**(5): 369-377.